

POLITECNICO DI TORINO

Department of Mechanical and Aerospace Engineering (DIMEAS)

**Master of Science Course
in Mechanical Engineering**

Thesis of Master of Science

**Optimization of Additive Manufacturing
Parameters Using Single Scan Track
Analysis; Case of Laser Powder Bed Fusion
(LPBF)**



Supervisors

Prof. Matteo Pavese (Polito)

Prof. Mario Guagliano (Polimi)

Dr. Alberta Aversa (Polito)

Candidate

Mehdi Hadi

July 2018

I dedicate this work to the true meaning of my life, Mr. Mahmood Naderi, who always sheds light to gloomy parts of my life.

We hope this work can be a help for those who want to rear their heads in in additive manufacturing field.

Principal Supervisor: Prof. Matteo Pavese

.....

Dr. Alberta Aversa

.....

Candidate: Mehdi Hadi

.....

INDEX

1. INTRODUCTION.....	1
2. ADDITIVE MANUFACTURING.....	3
<i>2.1 Process History.....</i>	<i>3</i>
2.1.1.How AM Was Born?.....	3
2.1.2.Development OF AM.....	4
<i>2.2 Process Methodology.....</i>	<i>5</i>
2.2.1. Conceptualization and CAD.....	6
2.2.2. Conversion to STL.....	7
2.2.3. Transfer and Manipulation of STL file on machine.....	7
2.2.4. Machine Setup.....	8
2.2.5. Build.....	8
2.2.6. Part Removal and Cleanup.....	8
2.2.7. Post Processing of Part.....	8
2.2.8. Application.....	9
<i>2.3 Process Advantages and Disadvantages.....</i>	<i>9</i>
2.3.1. Process Advantages.....	9
2.3.1.1. Design Freedom.....	9
2.3.1.2. Flexibility and Versatility in Manufacturing.....	9
2.3.1.3. Altering Materials to Enhance Workpiece quality.....	10
2.3.1.4. Eco-Design and Eco-Production.....	10
2.3.1.5. Lower Time to Market.....	11
2.3.1.6. Cost Saving.....	11
2.3.2. Process Limitation.....	11

2.4	<i>Process Classification</i>	11
2.4.1.	Material Extrusion.....	12
2.4.2.	Vat Photopolymerization (VP)	13
2.4.3.	Material Jetting.....	14
2.4.4.	Binder Jetting.....	15
2.4.5.	Sheet Lamination.....	16
2.4.6.	Direct Energy Deposition.....	16
2.4.7.	Powder Bed Fusion.....	17
3.	POWDER BED FUSION (PBF) PROCESSES.....	19
3.1.	<i>Principles of PBFs</i>	19
3.1.1.	Electron Beam Melting (EBM).....	20
3.1.2.	Laser Powder Bed Fusion (LPBF) Processes.....	21
3.2.	<i>Different Fusion Mechanisms</i>	22
3.2.1.	Solid State Sintering (SSS)	22
3.2.2.	Liquid Phase Sintering (LPS) and Partial Melting.....	23
3.2.3.	Chemically Induced Melting (CIS)	23
3.2.4.	Full Melting.....	24
3.3.	<i>DMLS/SLM Parameters and Process Issues</i>	24
3.3.1.	DMLS/SLM Process Parameters.....	25
3.3.1.1.	Energy Density.....	25
3.3.1.2.	Scanning Strategies.....	26
3.3.1.3.	Powder Shape, Size, and Distribution.....	26
3.3.1.4.	Bed Temperature and Temperature Uniformity.....	26
3.3.2.	DMLS/SLM Process Issues.....	27
3.3.2.1.	Porosity.....	27

3.3.2.2. Balling.....	28
3.3.2.3. Residual Stress.....	28
3.3.2.4. Cracks.....	28
3.3.2.5. Spattering.....	28
3.3.2.6. Incomplete Melting.....	29
3.4. LPBF of Aluminum Alloys.....	29
3.5. SLM Single Scan Track Study.....	34
4. EXPERIMENTAL SETUP, INSTRUMENTS AND MATERIALS.....	41
4.1 Instruments.....	41
4.1.1. EOSINT M270 SLM/DMLS Machine.....	41
4.1.1.1. Recoating System.....	43
4.1.1.2. Building Platform (or Substrate Plate)	43
4.1.2. Cutting Machine.....	45
4.1.3. Polishing Machine.....	46
4.1.4. Optical Microscope.....	47
4.1.5. Field Emission Scanning Electron Microscope (FESEM)	48
4.2 Powder Material.....	49
4.2.1. Aluminum A357.....	49
4.2.2. AlSi10Mg.....	50
4.2.3. AlSi10Mg+Titanium Diboride (TiB ₂) Composite Nanoparticles.....	52
4.3 Experimental Setup and Sample Preparation.....	53
4.3.1. Single Scan Tracks (SST) and Multi Scan Track (MST) Samples.....	53
4.3.2. Cubic Samples.....	56
4.3.2.1. AlSi10Mg.....	56
4.3.2.2. AlSi10Mg+nTiB ₂	57
5. RESULTS, ANALYSIS AND DISCUSSIONS.....	59
5.1 Single Scan Track Analysis.....	61
5.1.1. On-Top Analysis (Longitudinal)	61
5.1.2. Cross Sectional Analysis.....	74
5.1.2.1. Total Depth of Tracks.....	78

5.1.2.2. Width of Tracks.....	80
5.1.2.3. Upper Depth of Tracks.....	83
5.1.2.4. Lower Depth of Tracks.....	85
5.1.2.5. Angle.....	87
5.1.2.6. Surface Area.....	90
5.2 <i>Multi Scan Track (MST) Analysis</i>	92
5.3 <i>Cubes</i>	97
5.3.1. AlSi10Mg.....	97
5.3.1.1. Archimedean Method.....	98
5.3.1.2. Image Analysis.....	101
5.3.2. Further Discussions.....	104
5.3.3. AlSi10Mg+nTiB ₂	107
6. CONCLUSIONS.....	111
LIST OF SYMBOLS.....	113
REFERENCES.....	115
APPENDICES.....	121
I. <i>Numerical Values of On Top Width (SSTs)</i>	121
II. <i>Numerical Values of Cross Sectional Parameters (SSTs)</i>	125
III. <i>Numerical Values of total Depth (MSTs)</i>	129
IV. <i>Numerical Values of Cubic Samples</i>	130
ACKNOWLEDGEMENTS.....	133

1. INTRODUCTION

The growing necessity to produce various complex parts with special mechanical properties has led engineers to revolve production methods to catch up with changes as quickly as possible. Laser Powder Bed Fusion (LPBF)¹ is a simple example of such revolution that must be able to satisfy market needs in shortest period of time. The production and market atmosphere of today is, what I believe, like a treadmill tournament, in which best players are those who run fastest and stable, while at the same time, any halt can quickly throw them out of the game. Such a statement clarifies that there should be least amount of time tolerance in producing with SLM and delivery to market. This goal becomes a controversial issue especially when the artefact is needed to come out from new powder material, from which no information is in hand. In such conditions, a shortcut to discover process window of new material, rather than doing massive experiments, and find optimal parameters will be of vital importance. This thesis work is organized to target such a requirement.

In this work, the idea of Single and Multi Scan Track analysis will be used to address process window of material, as well as optimal parameters for production of satisfactory parts. To do this, a high number of single scan samples will be produced to define process window of three types of powders, knowing the fact that even high number of samples require very low time and material to produce. The three powder materials will be A357 and AlSi10Mg aluminum alloy, and mixture of AlSi10Mg aluminum alloy powders with TiB₂ nanoparticles. The produced samples will be analyzed from an on-top view and along their cross section and best samples for production will be clarified. Subsequently, multi scan tracks will be studied in order to find effect of hatch distance. Finally, the discovered data from previous parts will be applied in part production to measure their reliability and impose any possible reformation. By far, this methodology will be proven to be a valid way to define SLM table of processability of any powder in shortest period of time.

Designing of structure of this note was done aiming at having a building-up-knowledge reference by which any kind of reader with any level of knowledge about the subject can make use of it; and at the same time, to cover an appropriate range of concepts which are related to the work. This target was achieved by designing the work in six chapters. The following chapter gives a general introduction to Additive Manufacturing, its methodology, benefits and drawbacks and types of processes that exist in this field. The third chapter is devoted to more different subjects. It starts with explanations about different powder bed fusion processes and continues with laser powder bed fusion process, its parameters and draw backs. Following that, a brief history of laser powder bed fusion of aluminum and single scan track strategy will be delivered. Fourth chapter discusses about instruments and materials that were used in experiments with their properties. The set up parameters for sample preparation is also discussed in this chapter. Chapter 5 is totally devoted to results of experiments and discussions about them. And finally, a brief conclusion about findings of the work is represented in chapter 6.

¹ Selective Laser Melting (SLM) and Direct Metal Laser Sintering (DMLS) are other alternative and more common names defined by ASTM standard committee for Laser Powder Bed Fusion (LPBF). Hence, either term will be used interchangeably while holding the same concept.

2. ADDITIVE MANUFACTURING (AM)

Additive Manufacturing (AM) is the first and most important concept of this thesis work we thought is needed to be clarified with reasonable details for the reader, so that to build his/her knowledge up about the process and at the same time, paving the way to understand upcoming concepts about more in-detailed aspects of the work which will be mentioned thereafter. To this aim, this chapter is planned as a general introduction to AM technology and delivers some aspects about process developments, methodologies, terminologies, etc. The chapter is designed in four main sections. The first section notes a brief historical view of emergence of the process and explains how it was developed throughout its age. The second section gives a general view about the process methodology without going into detail. In other words, it provides a basic knowledge about different steps that must be pursued in any AM process to accomplish an artefact. The third section delivers common advantages and disadvantages of general AM technologies. And the final section provides the reader with an idea about different types of AM technology based on ASTM standard classification. For each type of AM technology, a brief explanation will also be delivered about the process apparatus and how it works.

2.1. Process History

All the aspects of life of today is tied to the concept of manufacturing. It plays a vital role from the beginning of system design and organization, to technological logistics, product development, and operational planning and control. Before the mid of the last century, manufacturing was usually termed to production processes in which final part was produced by subtracting material from a blank bloc or part by a mechanical way. The trend changed especially in fifties and sixties due to introduction of new engineering materials and demands for which conventional methods were unable to tackle the necessities. It caused to introduction of a new term called “Unconventional/Non-Traditional Manufacturing” versus the existing Conventional/Traditional ones. It referred to any new process in which other types of energy rather than mechanical are used in any shape in order to produce a part. It opened a window towards new sources like electrical and chemical energy and caused a twist turn in manufacturing processes in terms of used material and fabrication methods. Additive manufacturing (AM) was a single result of this whole that instead of subtracting, works based on adding layer-by-layer principle [1].

In the following subsections, a brief overview of appearance of AM technologies in last century is presented and steps that it proceeded up to now is discussed.

2.1.1. How AM was born?

It was in the late 1960s when for the first time, scientists at Battelle Memorial Institute tried to radiate laser beam to photopolymers to see possibilities of producing solid parts. In their experiment, two laser beams with different wave length were intersecting on the surface of the resin as an attempt to solidify the material at the target point. In 1967, Wyn K. Swainson from Denmark registered a patent with title “Method of producing a 3D Figure by Holography on a

Similar Dual Laser Beam Approach”, but he never proceeded to commercialize his concept [2]. After that, some researches were done on the beam intersection on resins, but it was on beginning of 1980s when Hideo Kodama published his works about a new method of fabricating three dimensional plastic models with photo hardening. In his presented method, A solid model is fabricated by exposing liquid photo-hardening polymer to ultraviolet rays, and stacking the cross-sectional solidified layers. He truly believed that “*solid models of rather complex shapes can be fabricated by this technique. It is a benefit of this technique that the shapes which have internal structure can be fabricated at once*”. [3]. Following that, Hull conceived the idea of modern Stereolithography and patented it in 1986 in a principal way. His work provided basic information for development of a new production technology, the Additive Manufacturing. Finally, one year later at 1987, the first AM apparatus was introduced by 3D System in US known as SLA 1 that stands for Stereolithography Apparatus (SLA). Stereolithography (SL) is a process that solidifies thin layers of Ultra-Violet (UV) light sensitive liquid polymers using a laser. Introducing SLA caused a revolution in manufacturing that later was called with various terms including Material Ingress (MI) or Additive Manufacturing (AM), Freeform Fabrication (FF), Rapid Prototyping (RP), Layer Manufacturing (LM), Rapid Tooling (RP), Rapid Manufacturing (RM) and 3D printing. However, Rapid Prototyping (RP) was the most accepted case for long time since the process was mainly used for preparing prototypes and scaled-plastic models of final part [4,5].

2.1.2. Development of AM

After producing SLA by 3D system, some companies like Sony in Japan and ECO in Germany developed their own versions of Stereolithography with different names, but it was only during 1991 when Laminated Object Manufacturing (LOM), Fused Deposition Modelling (FDM), and Solid Ground Curing (SGC) were introduced as alternative methods of AM that broke down singularity of polymer powders in AM and introduced more types of materials to the field. FDM extrudes thermoplastic materials in filament form to produce parts layer by layer. SGC used a UV-sensitive liquid polymer, solidifying full layers in one pass by flooding UV light through masks created with electrostatic toner on a glass plate. LOM bonds and cuts sheet material using a digitally guided laser. Along with introduction of other sources of energy rather than UV light and other types of powders, in 1992 DMT (now a part of 3D system) introduced Selective Laser Sintering (SLS) in which the heat of a laser sinters powders of materials. At this point, users of technology started to think about producing final parts rather than prototypes or models, so RP was no longer able to carry out the whole meaning of the process and in particular, did not effectively describe more recent applications of the technology. This is why more general phrase like additive manufacturing became more acceptable in which basic principle of the process that is additive approach is also considered [2,5].

The coming years after 1992 became the turning point in which fundamentals and parameters of existing methods were highly analyzed along with introduction of new AM methods with different capabilities. Very high prices associated to the process partially broke down and lots of companies started to commercialize their AM machines and the technology found its way from tables of laboratories to the market. The most substantial move in AM on metals started on 1994, when some companies like EOS in Germany, a current pioneer in the field, commercialized a machine called EOSINT based on laser sintering technology on metal powders. It paved the way for other entrepreneurs to consider Laser Additive Manufacturing (LAM) methods which resulted in

introduction of other laser based AM processes like steel powder-based Selective Laser Melting (SLM) system that was introduced in 1999 by Fockele & Schwarze in Germany [2,6].

The new generations of laser based AM machines for metal powders appeared in 2000 based on Direct Metal Deposition (DMD) by nozzles. It allowed AM technology to enter into repair field besides production because DMD allowed for deposition of powder on the surface by help of a number of nozzles and melting powder at the same time by laser beam. After 2000, introduction of new AM methods almost stopped while the extent of the work done by companies or researchers was focused on optimization of processes, development of new powders, increase building volume, integration of AM methods with other methods of manufacturing like machining and welding to produce net shapes, and trying to produce AM machines with lower prices [2]. In January 2009, about 20 years after introduction of the first AM machine, individuals from around the world met at the ASTM International headquarters near Philadelphia, Pennsylvania to establish ASTM Committee F42 on Additive Manufacturing Technologies. The committee was created to produce standards on testing, processes, materials, design (including file formats), and terminology. Standards were finally published at October of the same year. It provided a unified language for researchers around the globe to talk with in the field of AM [7].

During the same time, the idea of co-creation and co-designing found its way in AM field which allowed customers to participate in concept and design of product. The biggest step in this filed was made by Shapeways company that represented AM technology to a much broader audience by its Shapeway Shops. It allows artists, designers, or anyone to set up “storefronts” and upload 3D models to sell to the public. The products are manufactured on an AM system and shipped directly to the consumer by Shapeways. The audience of AM technology grew drastically in February 2013 when in his state of the union address, US president Barack Obama acknowledged the technology of 3D printing the potential to revolutionize the way almost everything is made [8].

By 2011 and afterwards, several industries, especially medical, biomedical, and aerospace ones were adopting AM as their mean method of manufacturing due to its ability to produce customized parts in low time durations. The direct metal processing technologies garnered significant interest and growth. At the same time, some AM patent licenses expired which caused to introduction and dramatic growth of some lower cost and customized systems to the market. The subsequent years were mainly devoted to AM processes optimizations, and growth of manufacturing units and market places, which more than doubled the market of AM technology from 2012 to 2016, from 2.204 to 5.165 billion dollars, respectively [8,9].

2.2. Process Methodology

Based on ASTM definition, Additive Manufacturing (AM) is *“the process of joining materials to make objects from 3D model data, usually layer upon layer, as opposed to subtractive manufacturing methodologies, such as traditional machining”* [10]. This technology is rapidly developing and integrating to other manufacturing methods and finding its way into our day to day life. AM is an approach in which any free form design in 3D environment can be made directly from CAD file without any needs to specific tools. In this method, one layer at a time is built in X-Y direction and layers are made one on top of the other in Z/third dimension to reach the final shape. Although there are many methods and machines, they generally work using the same principal method which is adding material in layers, each layer being a thin cross section of the

part derived from the original CAD data. There is a sequence of key steps in AM process to convert a CAD file into a part. Gibson et al. [11] defined eight steps in a generic AM process which are shown in figure 2.1 These steps are sequential, which means each step must be accomplished before going to the consecutive one. An overall overview of each step is presented in the following parts.

2.2.1. Conceptualization and CAD

AM technology came about as a result of developments in a variety of different technology sectors, and CAD technology was a very key figure in its foundation. Over the time, CAD systems have evolved from two dimensional to three-dimensional modelers through wire-frame, surfaces and solid-modelling systems, with solid modelling now becoming the norm due to more accuracy. Production of an AM part depends on a 3D software model of the part that fully describes the external geometry. It can involve the use of almost any professional CAD solid modelling software or an integration of them, but the output must be a 3D solid or surface representation and the software package must be able to export STL file out of the built 3D CAD [11,12].

In some cases, 3D CAD file cannot be prepared directly on a software but it should be patterned from an existing object or organism. In such a case, the existing part is scanned by a suitable instrument and acquired points are attached together to have the final shape of the part. Medical section is a very promising sector that uses this method to have 3D models of body parts. In this section, MRI or CT-scan is usually used to acquire cloud of points of real object and points are then manipulated to have 3D shape of the model [13].

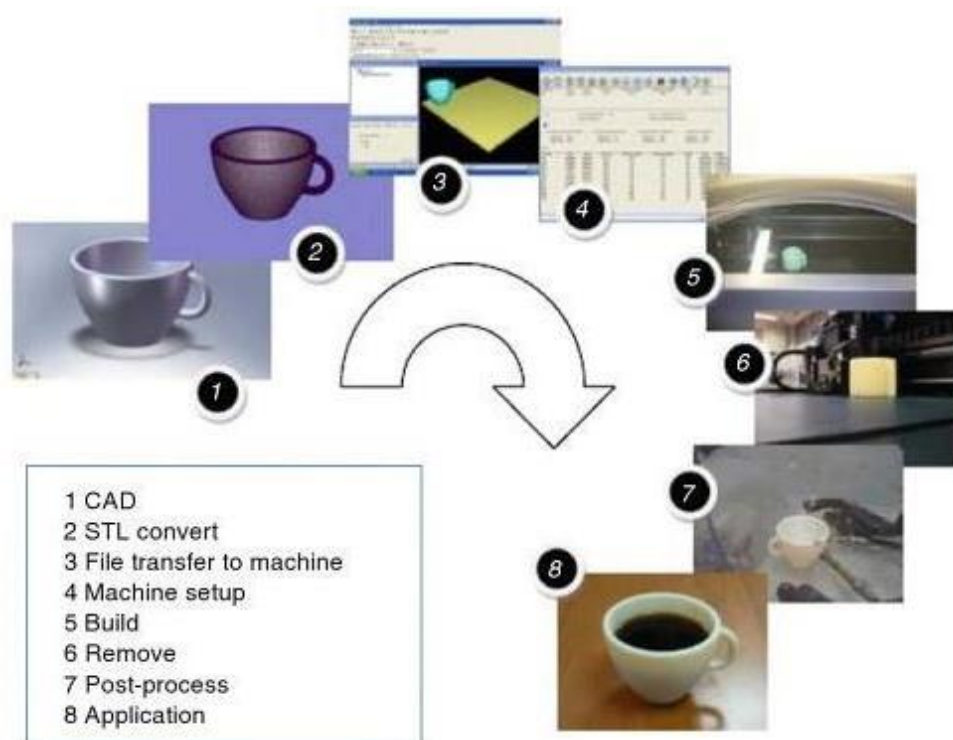


Figure 2.1 Eight sequential steps in AM to convert a CAD part to final product [11]

2.2.2. Conversion to STL

AM machine is able to produce layers on layers based on the final 3D CAD model of the part, but there must be an interference so that the AM machine can recognize the CAD file. To do this, the CAD model should be sliced in 2D contour layers before entering into the AM machine. A good solution is to use a global generic format that is specific for the AM technology. This type of format was developed by 3D Systems in 1987 with the name of “Standard Tessellation Language (STL)”¹ that is an open source format accepted as the standard of AM industry. STL tessellates the surface into a set of oriented triangles, each one describing by a unit outward normal vector and three points of vertices listed in counterclockwise order. The subjected triangles are planar elements which are unable to represent curvatures. However, increasing the number of triangles improve the approximation and accuracy of curvatures at the cost of larger file size which results in more time and process to build. So, the designer should compromise the accuracy with process time and also the type of AM process. For example, if relatively rough processes like FDM are going to be used for CAD model, lower precisions can be used without any problems because the accuracy of the process is so low that covers the problem of meshing deviation [12,14]. Figure 2.2 illustrates the STL file of a general gear made by SOLIDWORKS software along with its original shape.

STL creates an unordered complex of triangles and normal vectors without any unit, color, material and other useful information. Due to these limitations, the international ASTM/ISO adopted “AMF” as a new file format which includes dimensions, color, material and many other features. However, it seems to take a long time for this format to publicize since CAD companies and AM hardware vendors should plan to support AMF in their next software generation [15].

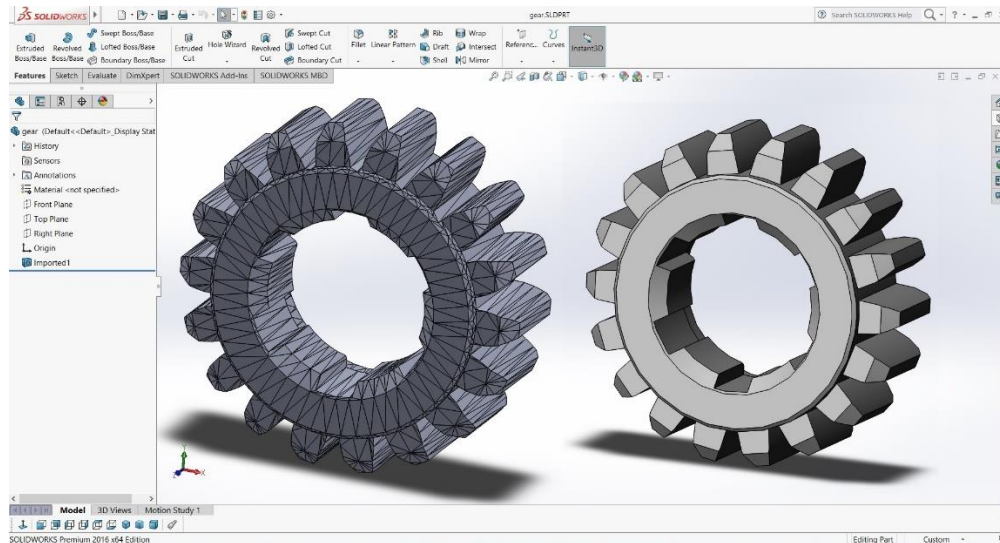


Figure 2.2 A 3D solid gear made in SOLIDWORKS (right) along with its STLed version (left)
(Made by Author)

2.2.3. Transfer and Manipulation of STL File on AM Machine

¹ Some references refer to STL as extracted from Stereolithography which is the first developer of the technique.

At this point the STL file is transferred to the machine and usually handled by a proprietary software on the machine to prepare it for building. The preparation can be orientation change, copying the file to build more than one part at a time, combining with other STL files, or scaling the file to have larger or smaller parts. All in all, the STL file is manipulated before building to assure correctness of the part. In case that AM machine cannot handle preparation processes, a separate STL manipulation software should be used to modify the file before transferring it to the machine [15].

2.2.4. Machine Setup

The AM machine should be properly set up before starting to build. The setup parameters usually include energy source parameters, material constraint (usually for machines that work only with specific materials), layer thickness, etc. that are entered into the preprocessing software of the machine. The machine then cuts the STL file into thin cross sectional layers, parallel to the platform and based on the input thickness. The software usually allows users to have different thicknesses for different areas of the same part for accuracy reasons which is called “adaptive slicing”. In case of necessity, the program also generates an auxiliary support for delicate structures or special shapes like overhangs or internal cavities. The building time can then be calculated based on setting parameters on the machine. In addition to software setups, the machine itself must be physically prepared for the process. The operator should assure sufficient build material loaded into the machine and all the devices especially feeding system work properly. For powder based process, the operator should certify that the feeding system homogeneously distributes powder on the surface. The building platform should also be correctly inserted and levelled based on the machine axes [14,15].

2.2.5. Build

The first four stages of AM process usually require considerable amount of human interaction and controls, but as soon as all the parameters are set up, the AM machine can automatically carry out construction of the part without any human supervision, although sometimes little monitoring of the machine is needed to ensure no errors have taken place like running out of material, powder blockage or software glitches. The three dimensional object is then created by layer-by-layer consolidation of deposited material on platform [15].

2.2.6. Part Removal and Cleanup

When AM machine completes the structure, parts must be removed from the machine chamber. This stage usually needs case specific interactions with machine based on the type of the machine and guidelines that it recommends for safety. For example, in some machines that work with powders and lasers, the user is not allowed to access to the built part until the machine assures that operating temperatures are safe, all parts are stop and chamber is cleaned through a special procedure and evacuated from any powder by the machine evacuator. The as-built AM parts usually cannot be used directly and require an additional amount of cleaning to remove any extra material that is attached to their surface. In all cases, parts must be separated from a building platform on which they were made and then remove any surrounding material especially support structures. For some types especially metallic parts, a wire EDM, bandsaw or milling machine may be required to completely release the part from the platform and its support structures [11,15].

2.2.7. Post Processing of Part

Post processing refers to preparation of produced parts for application. This step is highly dependent on the type of AM process. It may involve abrasive finishing like polishing and sand papering, chemical or thermal treatment of the part, coating, painting, hot isostatic pressing, or machining the part to final dimensions. Some processes result in relatively fragile components that require to use of infiltration with a low melting point material in order to strengthen the final part and find desired densification level and mechanical properties [15,16].

2.2.8. Application

Parts can be used after post processing while considering the fact that AM parts may behave different from what is referred in standard material specifications. It is mainly due to existence of porosity, different microstructures, and anisotropic properties. Porosity is the number one problem in lots of AM processes which can be a source of failure in early stages. The very high temperature gradients and rapid cooling in lots of AM processes causes totally different microstructure than those in conventional processes along with anisotropic properties in different directions. These features must be considered while deciding about application terms of an AM produced part [15].

2.3. *Process Advantages and disadvantages*

AM technology made a revolution in product development and manufacturing and it is even believed that manufacturing as it is known today may not exist if we follow AM to its ultimate conclusion. The world of today is looking at AM as a revolutionary technology that entirely changes the way products are designed and produced as well as the formulas on which business enterprises set their own work. Therefore, one might like to ask about the significance, benefits and effects of AM in industry that causes such statements. The response should be looked for through advantages and limitations of AM that are discussed in the following parts.

2.3.1. Process Advantages

AM provided industry with several advantages in all stages of production, from designing, to product development and application. Although there is a significance change between different classes of AM in terms of used machine, input raw material, and complexity of parts being produced; all of them almost share the same advantages in application. Figure 2.3 depicts the layout of general benefits of AM as well as important effects and changes it brings into a production sector. The layout is discussed in detail hereafter.

2.3.1.1. Design Freedom

The AM technology brings the design and innovation to the forefront. It is able to produce majority of shapes that could not be made before and does not require multiple machines, tools or processes. This brings innovation into design process and gives designer a lot more freedom. A lot of times, an optimal design is not possible to produce due to limitations in manufacturing processes. With AM, there is theoretically no restriction except the size of the part that has to fit inside the machine.

2.3.1.2. Flexibility and Versatility in Manufacturing

Flexibility and versatility in producing different size products with customized features in an economical way is the other benefit of AM. In AM any change to the product due to customization

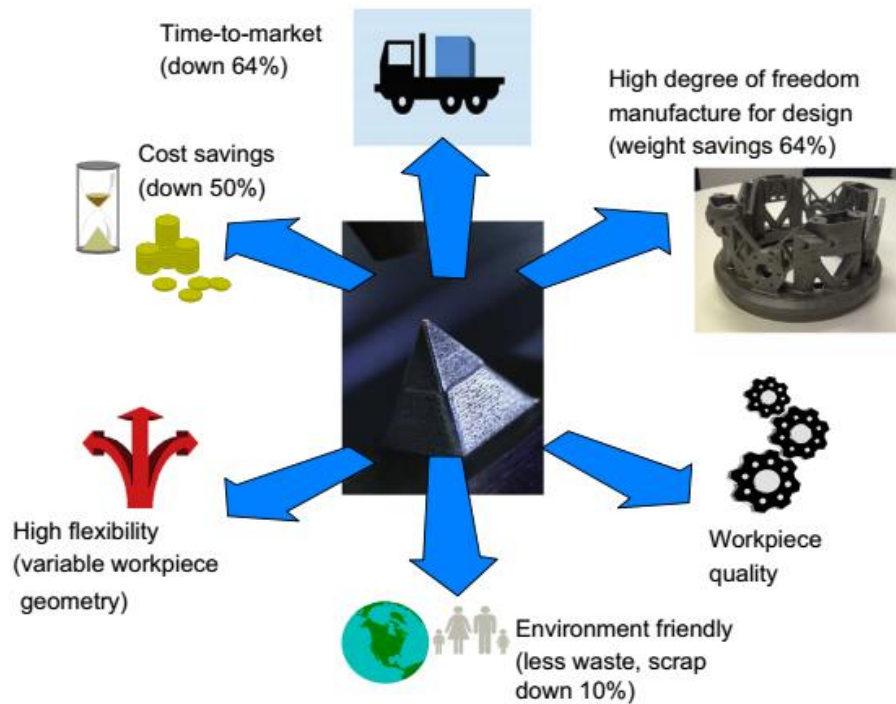


Figure 2.3 Benefits of using AM in production sectors. Numbers in parentheses refer to savings in aerospace and defense sectors [17].

or optimization can be done instantly while it is very difficult in many traditional manufacturing methods. For example, in casting process once an expensive die is made, it can only be used for a special shape and dimension and any possible change in dimension or design needs to produce new die to accommodate alterations. This is not the case in AM where any change in design is welcomed without any effect to fast adjustability of the process.

2.3.1.3. Altering Materials to Enhance Workpiece Quality

AM provides the possibility of using a vast variety of different materials like plastics, metals, composites and ceramics and their combinations. Not only AM can use different materials, but researchers are finding new ways that these processes can be used to alter materials and change their properties. An example is bonding ceramics and metals to increase wear protection, or coating with different material to increase thermal and wear resistance (Like coating metals with ceramics) or corrosion resistance (Like coating medical implants with silver).

2.3.1.4. Eco-Design and Eco-Production

AM decreases the amount of raw material required to produce a part since it has very little amount of waste which is usually recycled. It can reduce the amount of used material up to 75% compared to other manufacturing processes. On the other hand, laser is the most used energy source in AM which is clean, non-pollutant and environmentally friendly. In addition, AM doesn't need any

tooling/retooling which has a large amount of waste in traditional manufacturing and significantly affects environment in a negative way. So it is logical to conclude that AM is a green manufacturing method able to come up with sustainable and green growth.

2.3.1.5. Lower Time-to-Market

AM is able to produce a part in a single stage while other manufacturing processes need considerable setup and process planning, particularly when parts become more complex in geometry. Building a part in an AM machine may only take few hours and multiple parts are often batched together in a single machine, while using even a 5 axis CNC machine, the same process may take weeks with more uncertainty over the completion time. Being a free tooling process, the main concern in AM will only be the CAD model design which leads to a fast process with lower time of production and distribution to market.

2.3.1.6. Cost Saving

Every single benefit mentioned above can result in cost reduction in AM process compared to other type of manufacturing methods. In addition to that, companies can choose a central location for designing and optimization of products, and send results to any AM operating station around the globe through a special network, thereby eliminating the time and cost associated with shipping parts globally. Real-time visibility to production and fast delivery after that also reduces time and cost to some extents [16,17,18].

2.3.2. Process Limitations

Any manufacturing process has a number of limitations in application and AM is therefore no exception. The most striking limitation of AM is related to size of the part. Although AM technology can build shapes that are impossible using conventional methods, it cannot produce parts with very small or large dimensions. The lowest dimension in AM is related to minimum layer thickness that can be adjusted on the machine while largest dimension is related to the chamber size that the machine is able to perform in. The other drawback is related to permissible dimension of internal channels and holes depending on the process. Material can also trap inside internal channels and holes which could be very difficult, or even impossible, to remove. Further, the available input materials for each AM process are very limited and sometimes very expensive. The cost of industrial AM systems is also far more than CNC machines which results in higher costs of production. Some other process limitations are related to build parts and can be specific for each type of process or machine. However, porosity, anisotropy (different microstructure and mechanical properties) in different directions and bad surface finishing are common drawbacks (can also be a privilege in special cases) that usually require post-processing before application [16,19].

2.4. *Process Classification*

A robust method of classification of AM processes has been a key concern for standard communities. There are numerous methods to classify AM technologies based on different criteria like baseline technology (using laser, printer, etc.) and the status of building raw material (powder, liquid, etc.). Figure 2.4 provides a pictorial view of different additive manufacturing processes

based on the state of raw material that is either deposited or laid on surface. The figure shows that building materials in additive manufacturing can be in solid, liquid or powder phase and different ways can be used to bind them in order to produce an artefact.

Some problems raise with this type of classification. For example, some processes group together which are originally different from each other (like Selective Laser Sintering (SLS) being grouped together with 3D Printing), or some processes with similar results land in separated categories (like Stereolithography and material jetting with photopolymers). Given this, it is better not to use a single classification method for AM processes. However, the main classification stands with the definition of ASTM in which a common type of machine architecture and similar material transformation physics are grouped together. For example, processes with a common machine architecture and developed for stacking layers of powder material and a material transformation mechanism using heat to fuse those powders together are all grouped under the name of Powder Bed Fusion (PBF), even though the processes encompasses polymer, metal, ceramic, and composite material, multiple types of energy sources (such as lasers and infrared heaters) and point wise and layer processing approaches. ASTM committee F42 on additive manufacturing classified the existing AM technologies in seven groups which are explained in the following sections [5,20].

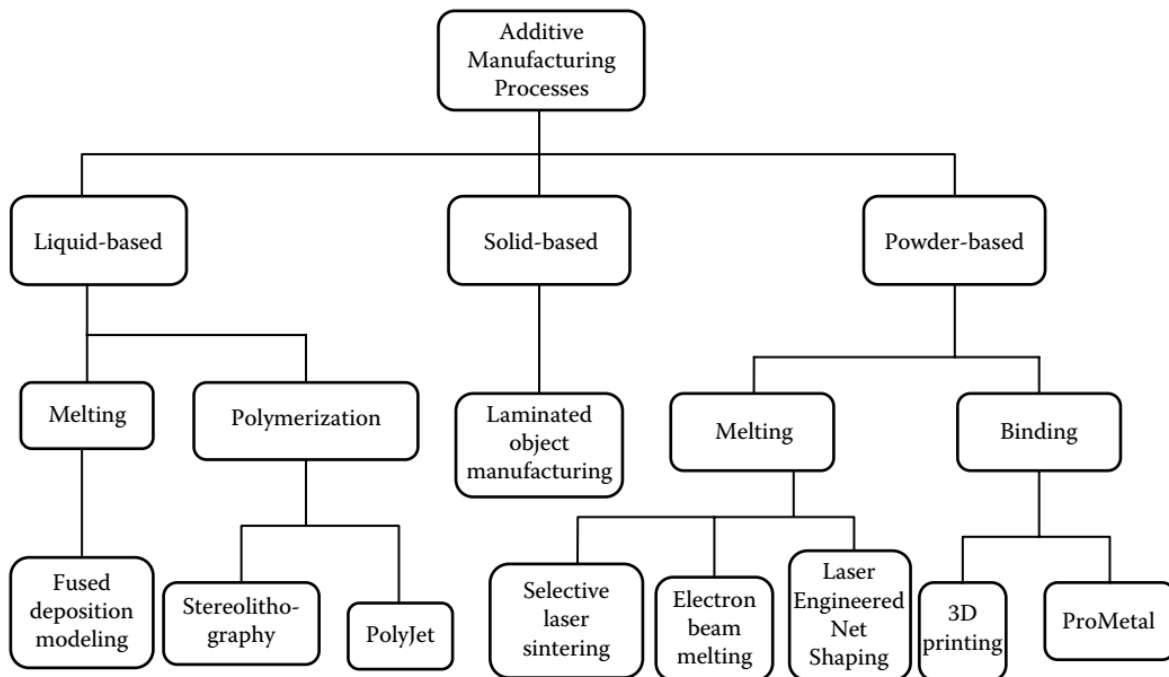


Figure 2.4 Pictorial view of various AM processes base on applied primary material [5].

2.4.1. Material Extrusion

This group of AM contains those processes that work based on principle of extrusion to produce a part, meaning that material contained in a reservoir is extruded through a nozzle which is scanning the surface with a constant speed. Figure 2.5 represents how material extrusion can be employed in AM. To build a part, the material should first be loaded on the machine and then transferred to

a semi-solid state to be able to extruded lately. The raw material can be in solid, pellet, powder or filament form but the most common way is to use filament, because it can be handled and controlled with much simpler mechanism compared to other estates. This is the reason why these set of process are denominated with the commercial name of Fused Deposition Modelling (FDM) that employs crystalline or amorphous thermoplastic filaments.

The filament is heated to reach to a liquid or semi solid phase depending on the type and characteristic of the material. It is then extruded through the nozzle and plots the shape in a controlled manner based on a predefined path. The extruded material often solidifies very fast and binds to underlying layers or support surface to form a coherent solid structure. The support material is usually different than the main structure so that it can be removed easily by mechanical or chemical methods after finishing the part [14,21].

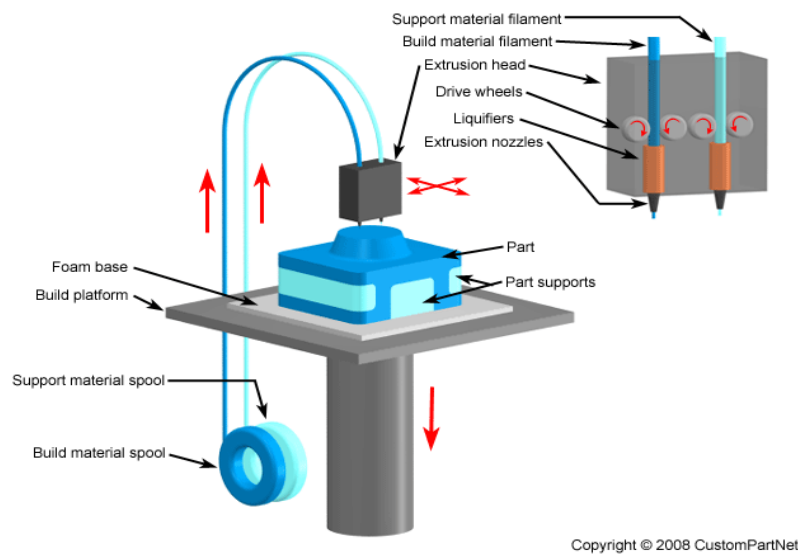


Figure 2.5 Material Extrusion mechanism. The dark blue area is the part and light blue is support with different material [22].

2.4.2. Vat Photopolymerization (VP)

Photopolymers are liquid, radiation-curable resins that react to radiation in different ranges of wavelength and sometimes to visible light systems as well. These materials undergo a chemical reaction as soon as they are exposed to radiation and become solid. So it is called Photopolymerization which is the key figure in lots of AM processes. The most famous process of this group is Stereolithography (SL) which refers to macroscale, laser scan vat photopolymerization that uses Ultraviolet (UV) laser to affect photopolymers. Gama rays, X rays and visible light are the alternative sources of energy used in the other VP methods. Based on the scanning principles, this group of processes are divided to vector scan, two photon approaches, and mask projection. Figure 2.6 shows how a vector scan vat photopolymerization machine looks like in which scanning takes place along vectors on the cross section. This method is typical of Stereolithography process. The principle is the same for mask projection and two photons in sense that a photo sensitive resin solidifies.

However, in mask projection the entire layer is irradiated at one time while unwanted parts are masked with a photo-resistant resin, and in two photon scanning the resin solidifies in intersection of two laser beams. The process starts with a CAD model and the model is then translated to a STL

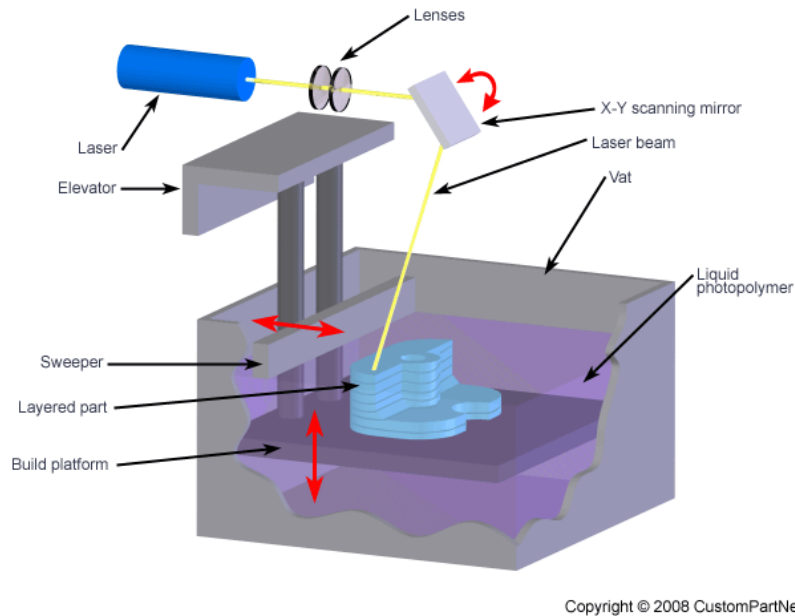


Figure 2.6 Vector Scan Vat photopolymerization process [24]

file in which the pieces are cut into slices with each slice containing the information required for each layer. STL file is manipulated on machine and a platform is created to hold the piece and support any overhanging structure. Then the laser selectively solidifies a layer of cross section by tracing 2D contours of the CAD model. The part being built rests on a platform that is dipped into the vat of liquid photopolymer as shown in figure 2.6. After the platform is lowered, the surface of vat is recoated and laser starts to scan the next layer building the part from bottom up [23].

2.4.3. Material Jetting

Material jetting is similar to inkjet printing documents, but instead of printing ink drops on paper, building material is dropped onto the build platform using either a continuous or drop on demand approach. The drops of material then solidify using heat, UV light (for photo-sensitive materials), or any alternative approach depending on type of input material. Further layers are built up on top of the others to form the final shape. Figure 2.7 shows the mechanism of this process in which printing head is able to use two different materials for support and main part. The process can be used on a wide variety of materials including polymers, ceramics and metals [25].

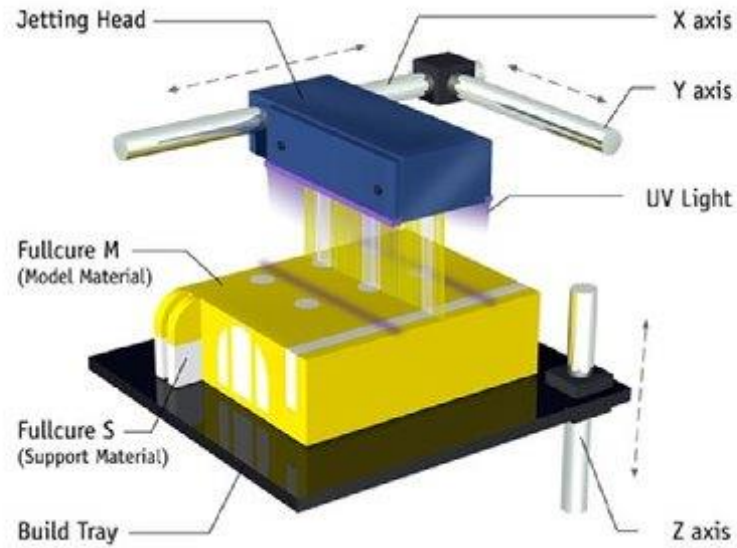


Figure 2.7 Material Jetting apparatus [26]

2.4.4. Binder Jetting

The original name for binder jetting is three dimensional printing (3DP) that later on, became the name of a pioneer company in the field.

Figure 2.8 illustrates how binder jet machine works to build a part. In this process powder is supplied on the build chamber and distributes all around the surface by means of a levelling roller to form a thin layer. The binder is then applied to target regions and glues powders together.

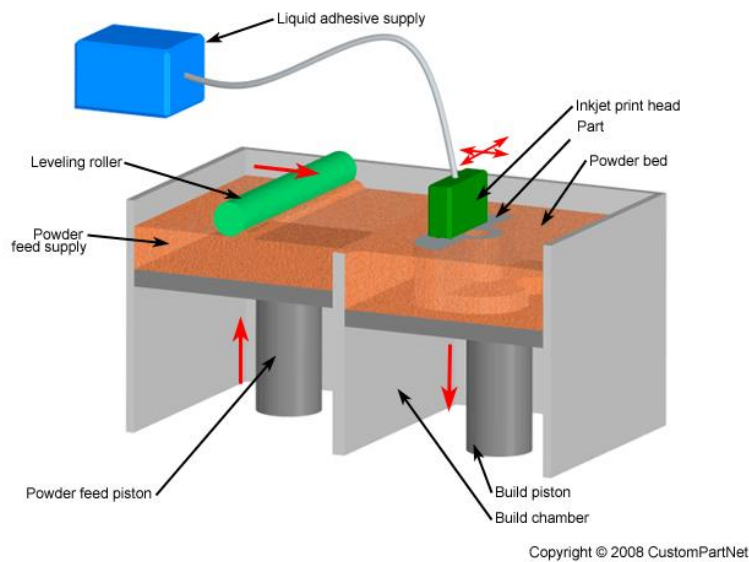


Figure 2.8 Binder Jetting mechanism [28].

Hence in binder jet only a small portion of part material is delivered by printer head compared to material jetting in which all of material is delivered by the head. Once a layer is completed, the power piston raises to feed new powder for next layer. The existing powder on the plate self-supports the part which eliminates the need for support structures in lots of cases. After completing the fabrication, parts are usually heated at high temperatures or infiltrated to increase mechanical properties.

The process can be scaled economically by simply increasing the number of printing nozzles. It enables the process to produce colorful parts and parts with different coloring. Such features along with the lack of high power energy source in binder jetting process turns it into a relatively high speed low cost AM process [27].

2.4.5. Sheet Lamination

The first additive manufacturing processes in this group was Laminated Object Manufacturing (LOM) that involves layer by layer lamination and gluing of paper material sheet and cutting it with CO_2 laser in which each sheet represents one cross sectional layer of the part. A schematic of this process is represented in figure 2.9. After that, a number of similar processes have been developed based on other type of materials and cutting strategies and type of bonding layers. In some other processes especially for metals, sheets are first cut in form of cross section and then stacked together. Despite other types of AM technologies, this group of process produces lots of waste due to existence of subtractive method in the heart of process [29].

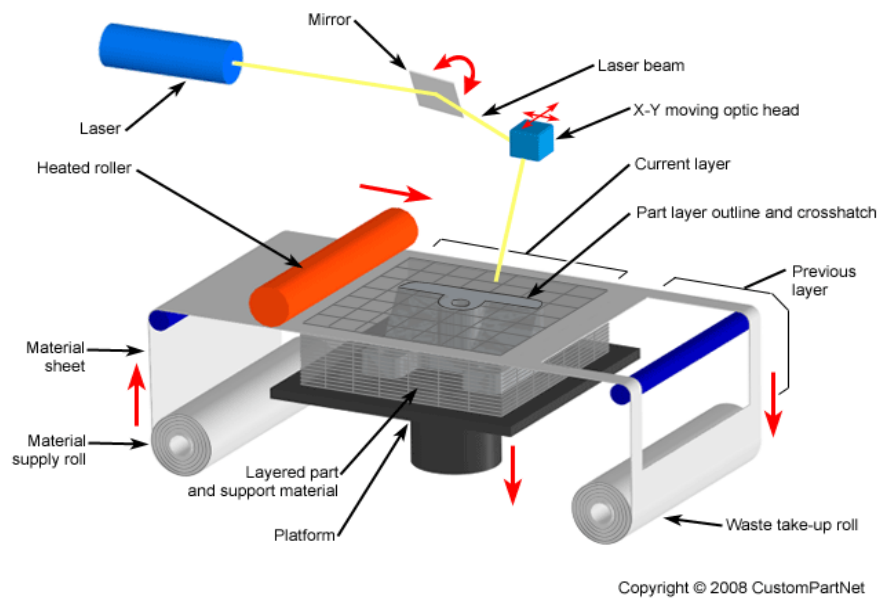


Figure 2.9 Sheet lamination Mechanism [30]

2.4.6. Directed Energy Deposition

Directed Energy Deposition (DED) processes enable creation of parts by melting material as it is deposited. As it is shown in figure 2.10, powder or wire is fed directly into the focal point of an energy beam to create a molten pool with the aid of a robotic multi-axis system. A shielding gas

protects the melt pool from oxidation while the nozzle continuously scans the whole cross section based on shape and strategy that is given to it. When cross section of a layer is complete, table of the machine moves down a distance equal to layer thickness and the subsequent layer of cross section is built. This process is repeated until the total shape of part is completed.

In summary, these processes are essentially three dimensional welding machines that can also be used to repair a part where the damage portion is reconstructed selectively. There is a number of studies to use this process for repairing because heat and material source are delivered from the same side and therefore molten material can be straightly directed towards damaged area. Although this basic approach can work for polymers, ceramics, and metal matrix composites, it is predominantly used for metal powders. Thus, the technology is often referred to “Metal Deposition” [31].

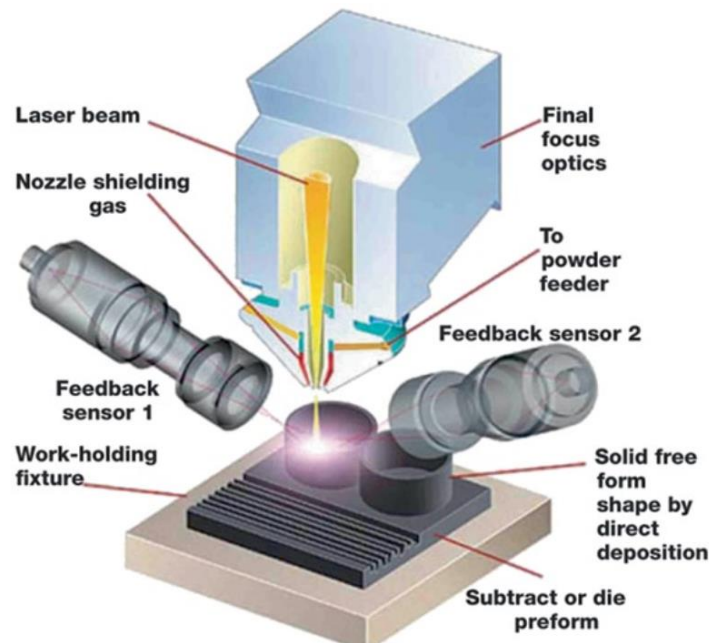


Figure 2.10 Directed Energy Deposition [16]

2.4.7. Powder Bed Fusion

This group of AM is the core topic of the thesis work, so we will study it in detail in the following chapter.

3. POWDER BED FUSION (PBF) PROCESSES

This chapter is specifically planned to briefly cover variety of subjects which are related to topic of the thesis and provide the reader with a platform to better understanding different parts of the experimental work. It is tried to be planned as a transition point to connect the reader to the subject and at the same time, be a useful source for different aspects of the work. The discussions will be held around Powder Bed Fusion (PBF) mechanisms and different issues related to it since it is the main subject of the thesis which is used in experimental procedures. Following that, some technical notes related to thesis will be discussed from literature to inform the reader about developments that have been done so far. Given all the above, the chapter is drafted in five main sections. The first part discusses about Electron Beam Melting (EBM). From the second section forward, subjects are specialized to Laser Powder Bed Fusion (LPBF)¹ processes which are the case in experimental schemes. The second section talks about different fusion mechanisms that can happen during LPBF processes. The third section discusses about important parameters of this process in detail and provides information about how these parameters affect the process. It is then followed by defects and issues that are possible to rise during the process and must be eliminated. The fourth part of the chapter gives a wide review from literature about LPBF of aluminum alloys to provide the reader with a historical view as well as a basic knowledge about what has been done in this regard. Finally, the chapter will be closed in fifth section by the concept of single scan tracks that is the core intention of experimental works of the thesis.

3.1. Principles of PBFs

Powder Bed Fusion (PBF) processes were among the first introduced and commercialized AM processes. The basic characteristics in PBF is one or more thermal sources to fuse powder particles together, a procedure to control scanning of each layer in order to fuse powders in prescribed regions, and feeding and re-coater mechanisms to uniformly distribute fresh powders on surface when needed. The working principles of PBF machines is rather simple. The powder is first placed in feeder where it then distributes it on the surface of the platform. Once an appropriate thickness of powder on layer has been certified, a focused beam is directed onto the powder bed and is moved with special mechanism depending on the source of the beam. The exposed powder to the beam is thermally fused and a single slice of cross section is formed, while the non-exposed powder remains intact and serves as support for subsequent layers. When a layer is completed, the building platform is lowered down by one-layer thickness and a new layer of powder is added and levelled using a counter rotating roller and then the beam scans the subsequent cross section. The process repeats until building the part is completed. The type of applied thermal energy source makes the key difference between PBF processes. Electron beam and laser beam are the two types of energy

¹ As it was mentioned before, selective Laser Melting (SLM) and Direct Metal Laser Sintering (DMLS) are other alternatives for Laser Powder Bed Fusion (LPBF) that can be used interchangeably. As a matter of fact, SLM and DMLS are more common terms while LPBF is a more general case.

sources used in PBF resulting in Electron Beam Melting (EBM) and different Laser Powder Bed Fusion (LPBF) processes which are explained here [32,33].

3.1.1. Electron Beam Melting (EBM)

EBM is a relatively new AM process that uses a high energy electron beam to impose fusion between metal powder particles. As it is represented in figure 3.1, EBM working mechanism is similar to any other PBF processes with some modifications. The beam direction is controlled by magnetic coils which provides the process with instant movements of the beam, the case that lacks in LPBF processes. It gives process the capability to keep multiple melt pools moving simultaneously for part contour scanning which also increases the build speed. The electron beam is also used to preheat the platform in addition to melting powders, which leads to very high preheating temperatures. This is why individual scan lines in EBM are usually indistinguishable compared to their LPBF counterpart. Higher platform temperature also leads to coarser and continuous grain structures with less porosity than LPBF processes.

The powder bed in EBM process must be highly conductive to direct negative (Electron) charges that strike its surface. Thus EBM can only be used for conductive materials while its LPBF counterpart can be used for any material that absorbs energy at the laser wavelength. The electron beam is powered by a very high voltage of 30 to 60 kV to eliminate or minimize environmental reactions such as oxidation. However, high energy beam is not enough to eliminate interactions and the process has to be handled in a high vacuum chamber. This is why EBM is mentioned as a potential future technology to manufacture parts in outer space due to vacuum conditions there [5,33].

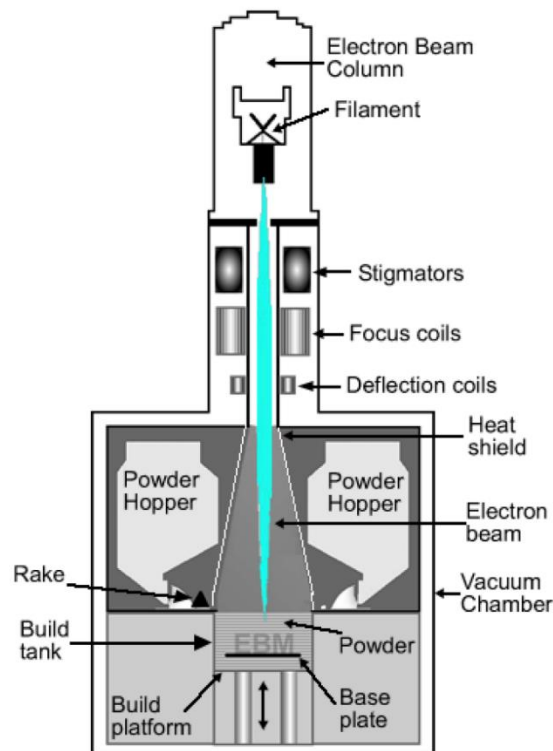


Figure 3.1 Schematic of Electron Beam Melting (EBM) Apparatus [34]

3.1.2. Laser Powder Bed Fusion (LPBF) processes

LPBF are those set of powder bed fusion processes in which a laser beam is used as the source of energy to diffuse powders together. Properties of the chosen laser defines classes of materials that can be handled with the process. Carbon dioxide (CO_2) and doped Yttrium-Aluminum-Garnet (YAG) lasers are the most extensively used lasers in LPBF processes which are specific for polymers and metals powder processing, respectively. Figure 3.2 illustrates a LPBF system with YAG laser that is specific for metals due to high absorptivity at the specific laser wavelength. As the figure represents, the mechanism of process is pretty much like EBM, but here energy source is a laser that is controlled across the surface by means of galvanometric mirrors.

The LPBF process should take place inside an enclosed chamber filled with a shielding gas to eliminate any harmful effect of atmosphere like oxidation of powder and melting pool. The other benefit of chamber is to provide a steady and uniform cooling period after a part is built. If after finishing, parts and powder bed are directly exposed to ambient temperature and atmosphere, the parts can distort due to uneven thermal gradients and powders may oxidize. In order to decrease laser beam power requirements and uniform thermal expansion and extraction during the build process, the temperature of powder and build platform should be preserved at a value below melting point and glass transition temperature of the powder. The chamber again helps in keeping temperature high and reduces energy consumption [33,35].

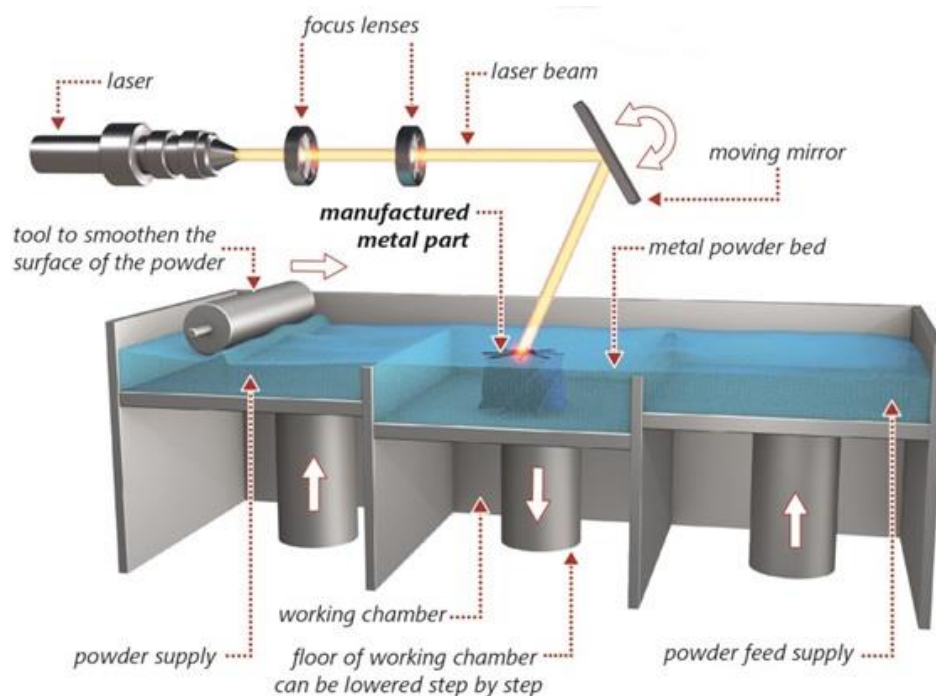


Figure 3.2 Schematic of Laser Powder Bed Fusion (LPBF) machine specific for metals [36]

When built parts are cold enough, they can be removed from the powder bed and cleaned from loose powders. Usually, a finishing process is needed for LPBF parts because whenever the beam scans borders of cross sections, some of the neighboring powder particles stick or partially diffuse to the part and make a relatively rough surface. Hence, they are removed and surface quality is improved by a finishing process before sending the part for final application [35].

There are few major providers in the world that produce systems for LPBF technologies. They use different phrases to describe their systems such as selective laser melting (SLM Solutions®), laser cusing (Concept Laser®), laser sintering (PhenixSystems®/3D- systems®), direct metal laser sintering (EOS GmbH®), and laser melting (Renishaw®). The difference in these processes usually originates from patent issues and trademarks, but processes are also distinguishable based on the dominant fusion process and state of the powders while receiving laser energy. In another word, the class of processes change based on the fusion mechanism that happens during the process and its value [37]. In the following section, all the possible fusion mechanisms in LPBF along with their existing processes are represented.

3.2. Different Fusion Mechanisms

There are four types of fusion mechanisms that can happen in different LPBF machines. These mechanisms are:

- Solid state sintering
- Liquid phase sintering
- Chemically induced binding
- Full melting

Following subsections clarify the differences between these mechanisms along with explanation of the processes that develop them.

3.2.1. Solid State Sintering (SSS)

Sintering process in solid state is a thermal process that occurs at temperatures between one half of the absolute melting temperature and the melting temperature ($T_{Melt}/2 < T_{SSS} < T_{Melt}$), which is usually termed as fusion of powder particles without melting. The main driving force for this process is minimization of total surface energy which involves neck formation between neighboring powder particles. Figure 3.3 illustrates neck formation during sintering process. As it is clear from the figure, powder material between two ends of neck diffuse together and form a unit structure.

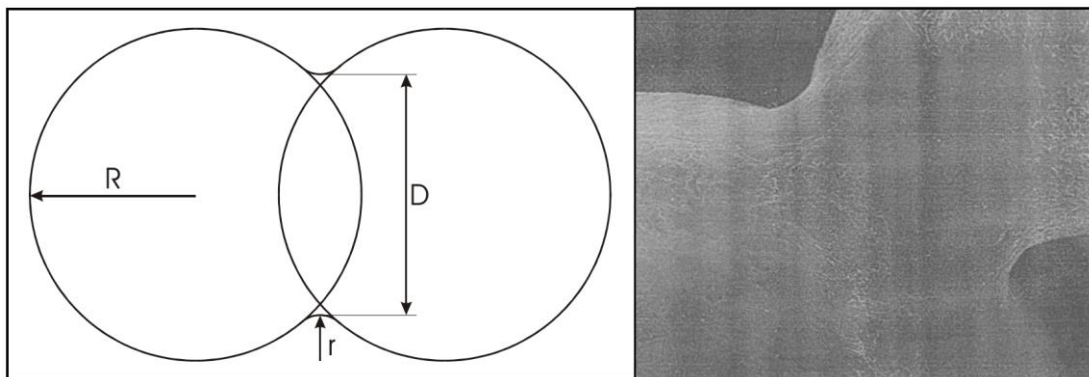


Figure 3.3 Schematic of neck formation mechanism in Solid State Sintering (left) and neck formation between two stainless steel powder particles (right) [38].

Total surface energy is directly related to surface area, thus smaller powder particles have lower surface energy and initiate sintering at lower temperatures and sinter more rapidly with respect to their bigger counterparts. On the other hand, sintering exponentially increases versus temperature, so approaching to melting temperature increases sintering rapidly.

Solid State Sintering is the process that happens in Selective Laser Sintering (SLS) machines. In these type of machines, laser is able to increase temperature of powder on bed to a value below melting point temperature to impose diffusion between particles. However, speed of diffusion is highly temperature-dependent and becomes very fast at melting temperature or very close to that. It is also powder dependent and changes from one type of powder to the other. This is the reason why only few AM machine producers use sintering as a primary diffusion mechanism [33,38].

3.2.2. Liquid Phase Sintering (LPS) and Partial Melting

Liquid phase Sintering (LPS) is a well-known term in powder processing industry that refers to fusion of powder particles when a portion of particles become molten while others remain solid. In such a case, the molten part plays the role of glue to bind solid particles together. As a result, high melting point powders can be glued together with lower powers due to partial (and not full) melting of binder. A clear example of this group is to use stainless steel powder as structural material mixed with Cu particles as binder. Usually there is a clear distinction between binder and structural material and they can be combined in three different ways as below:

- Mixture of binder and structural powders, with binder having lower melting temperature.
- Composite particles, in which each powder article is a composite combination of binder and structural material.
- Coated particles, in which structural particles are coated with binder material.

In some cases, only structural material is used without binder but the heat supplied to a powder particle is insufficient to melt the whole particle thus only a portion of it becomes molten and acts as binder while the other remains solid. It is also possible for non-eutectic alloy compositions, where partial melting occurs between liquidus and solidus temperature of the alloy. The term Direct Metal Laser Sintering (DMLS) was first developed for in-eutectic partial-melting of alloys. Instead, non- alloy compositions were preferred to be called with full melting [33,38].

3.2.3. Chemically Induced Sintering (CIS)

Chemically induced binding uses special types of thermally activated chemical reactions between two types of powders or between atmospheric gases and powders to bind products together. In these types of processes, no binder elements are used and the laser material interaction time is very short to eliminate diffusion process that happens in solid state sintering. But instead, in high temperatures, materials in powder particles start to react with each other or with gases in atmosphere to form new compositions that binds particles together. Hence, the composition of final part will have new materials inside due to chemical reactions. It is worth noticing that temperature in these processes never reaches to melting point, so these powders are usually compatible with SLS machines that work below melting point. A very first powder for this process is SiC that disintegrates into Si and C in high temperatures. The free Si then reacts with oxygen in atmosphere

to form SiO_2 that reacts as a binder between SiC particles. So the final parts will be composed of a mixture of SiC and SiO_2 [33,38].

3.2.4. Full Melting

Laser full melting is one of the most commonly used mechanisms in LPBF processes of engineering metals and alloys. In this method, laser energy is so high that it can easily melt all the scanned powder and re-melt a portion of previously solidified structure which creates a well-bonded high-density structure from the initial powder. Selective Laser Melting (SLM) is the accepted term for this type of process. It shares the same process apparatus and procedures with the other sintering methods, and the only difference is in the idea of full melting mechanism [39]. Figure 3.4 clarifies the differences between all fusion mechanisms that exist in LPBF processes.

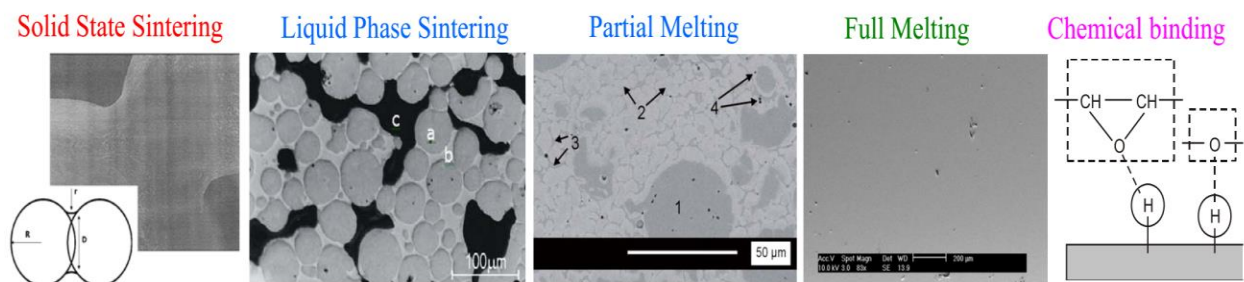


Figure 3.4 Possible fusion mechanisms in LPBF processes [39]

The reason for existing different terms for LPBF processes is related to continuous developments in laser processing conditions such as laser power, focused spot size and layer thickness. In fact, first versions of laser tools had low power with large focal size that resulted in low ability of laser to melt powder. Hence, first LPBF machines were usually based on sintering or partial melting of powder which resulted in parts with no ideal density and often required post processing to increase density. However, developments in all the fields of laser technology resulted in high power lasers with very small focal spot size that could practically melt any material. This is why SLS is almost disappearing from LPBF technologies and the other processes, i.e. SLM and DMLS, are used interchangeably for full melting of powder. These two AM techniques have both been used as synonyms for LPBF process by ASTM international, although they had different meanings at first [10,40]. In this thesis work, we respect to ASTM terminology for additive manufacturing, so SLM and DMLS will be used interchangeably hereafter, and will refer to full melting of powder at scanning spots.

3.3. SLM/DMLS Parameters and Process Issues

As it was mentioned before, SLM/DMLS is associated with complete melting of the powder material which leads to high density and strength of built parts. Working principles in SLM is similar to other PBF processes. A laser beam is used to selectively scan locations on the bed and fuses the powder to the underneath solid material by fully melting it. The laser scanning path for each layer is defined based on part geometry at the corresponding z direction and the selected scanning strategy. The bed is lowered down by the defined layer thickness and a fresh layer of powder is uniformly spread after laser scanning in one layer is completed. This procedure repeats

until the entire part is built. During the entire process, the SLM build chamber must be protected with homogeneous gas flow to prevent oxidations [33]. Almost all metals can be processed by SLM, but their process window can vary because of difference in material composition.

The final properties of processed materials are defined by laser-material interaction conditions. Regardless of the type of input raw materials, near full density components can be fabricated under the optimized process parameters. Any inclination from these optimal parameters can lead to technical defects like porosity, balling, and cracks. In the following parts, the effective parameters in SLM technology and typical defects that can be detected in the part will be discussed.

3.3.1. SLM/DMLS Process Parameters

The processing parameters in SLM originate from four key aspects of process, namely, laser, scanning, powder and temperature. As figure 3.5 represents, there are a set of different parameters linked to four aspects of SLM process that contribute to final properties of parts. However, each set has some parameters with primary importance that are set before starting the process, and some others with secondary importance that are usually constant for all types of materials. Laser scan speed and power are examples of primary parameters and pulse duration and frequency are usually considered as secondary importance. In the following parts, the primary parameters will be represented and their effect on properties of SLMed parts will be discussed.

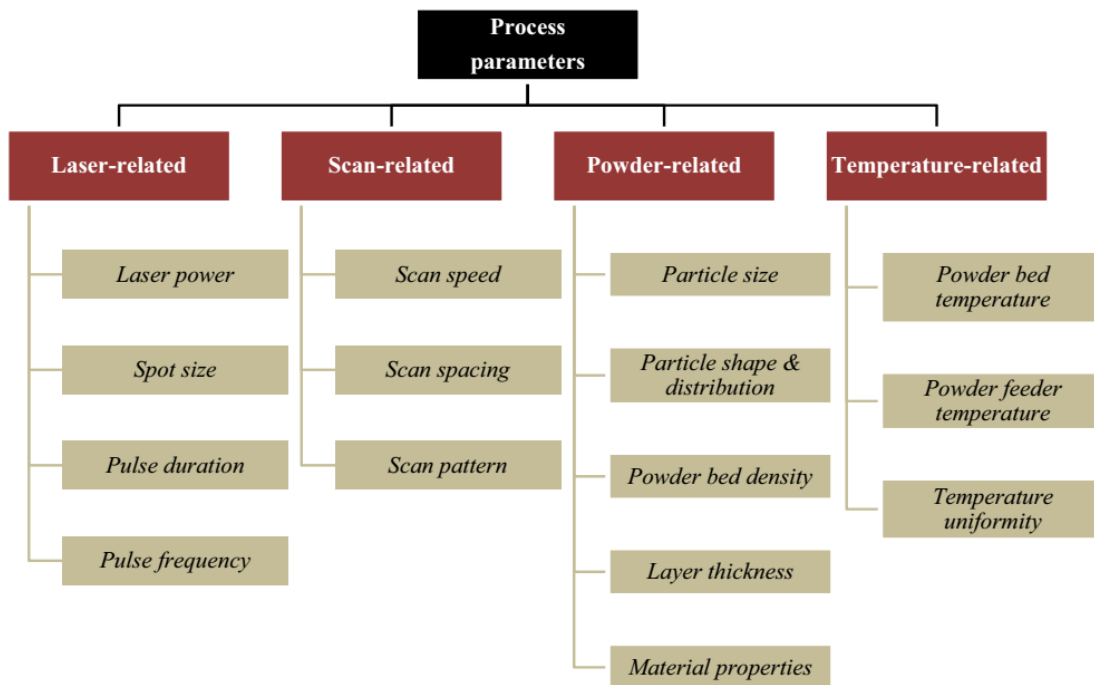


Figure 3.5 Classification of parameters in SLM [41]

3.3.1.1. Energy Density

Laser power, scanning speed, layer thickness and line spacing (hatch distance) are the most important input parameters in SLM that define final results. An optimal value for each one of these parameters is required to set on the machine before starting. However, effect of these parameters

can be combined and presented as (Volumetric) Energy Density (ED/VED), which is an engineering parameter to show the energy delivered to a unit volume of powder on the bed. Equation 3.1 shows how these parameters are related to each other in VED definition.

$$VED = \frac{P}{vth} \left(\frac{J}{mm^3} \right) \quad (\text{Eq. 3.1})$$

Where P (W) is laser power, v (mm/s) is scanning speed, and t and h (mm) are layer thickness and hatch distance, respectively. It should be noted that parameters in VED are strongly interdependent and also mutually interact with other parameters in SLM. For instance, the required laser power is usually defined by melting point of powder material, but also is affected by bed temperature, absorptivity characteristics of the powder which by itself is influenced by material type and powder shape, size, and density on the bed [33,35,41].

3.3.1.2. Scanning Strategies

Scanning strategy is related to the path that laser travels while scanning a layer and whether its direction changes or remains constant for subsequent layer. This parameter is very important in SLM since it highly affects thermal history during the process. Figure 3.6 that is taken from the literature illustrates a wide range of scanning strategies that can be depicted in building layers. In reference of this figure, researchers revealed that scanning strategy highly affects thermal gradients and temperature distribution in the part, thus also affecting any temperature dependent property like density, thermal and residual stress, consolidation, melt pool characteristics, microstructure and deformation of the part.

Studying the literature shows that an optimal scanning strategy should be depicted aimed at uniformity of thermal gradient. It has been reported that altering scanning strategies (rotating the scanning direction in each layer) improves temperature gradients and thermal features of the part. This is why 45° and 67° rotate scanning are usually adopted for SLM parts. however, 67° rotating is by far the most used one because it leaves very small directional stress which can be due to non-repeated scan vector feature [35,42].

3.3.1.3. Powder Shape, Size, and Distribution

Powder morphology, size and distribution highly affects absorptivity of the laser as well as thermal conductivity, powder flowability and spreading. Finer particles can absorb more laser energy and provide a better surface area. The packing density of powder on the bed is also affected by powder shape, size and distribution. A wide range of powder size helps for a higher powder bed pack density since the gap between large particles can be filled with smaller ones. About the powder morphology, it should be noted that a spherical shape improves flowability of powder and the packing density. When packing density of powder is higher, thermal conductivity of powder bed and mechanical properties of the part will be better [33,43].

3.3.1.4. Bed Temperature and Temperature Uniformity

Powder bed temperature is a parameter that is highly related to laser power, scan speed and hatch distance and must be balanced based on these parameters. Having high temperatures in the chamber (High laser power and high bed temperatures) results in high density parts, but can lead to poor

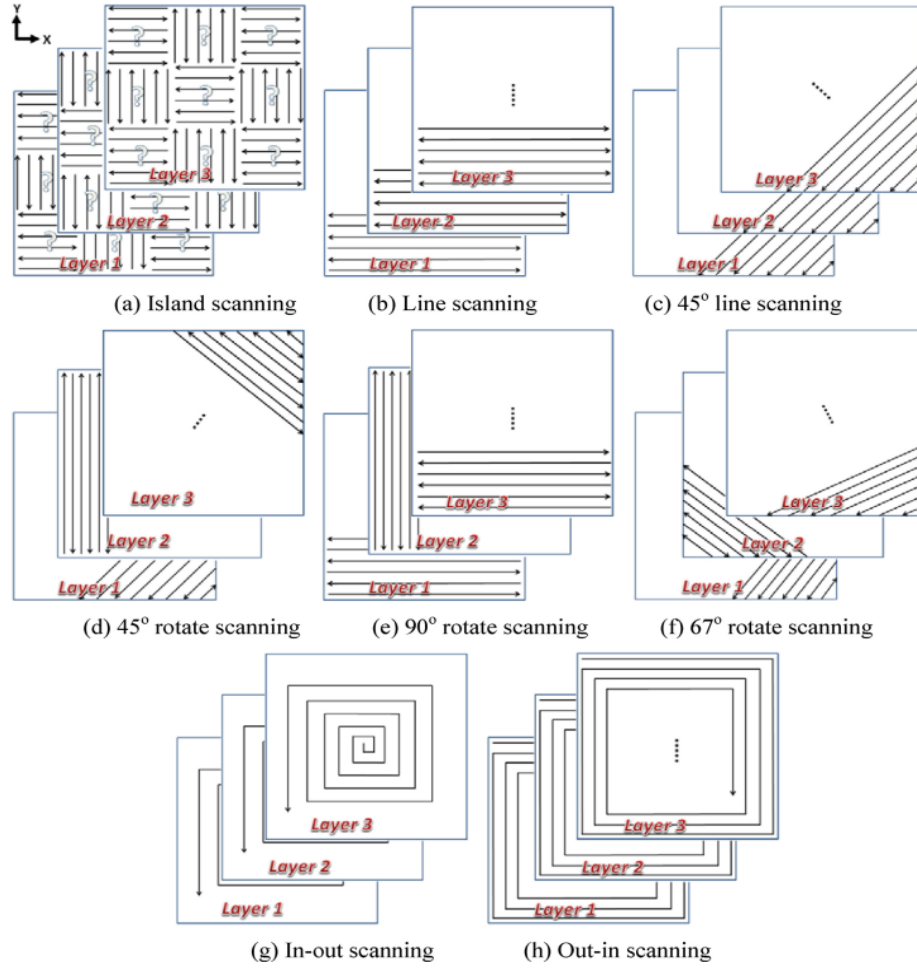


Figure 3.6 Schematic of some scanning strategies that can be depicted in SLM [42]

accuracy and difficulty in cleaning. On the other hand, uniformity of powder bed temperature should be assured to achieve homogeneous properties across the part [33].

3.3.2. SLM/DMLS Process Issues

3.3.2.1. Porosity

Porosity is the most common defect in SLM products which is formed by gas filled areas during the process. It can be found as large irregular pores due to incomplete melting, shrinkage micro-pores due to a lack of feeding within inter-dendritic zones, spherical pores caused by trapped gas, etc. Optimal selection of process parameters is the only way to reduce porosity in final products and produce near full dense parts. For a single scan line, these parameters usually include laser power and speed which determine the melt pool stability. If the melt pool is unstable, it results in irregular or discontinuous tracks which is a potential source for porosity. In fact, for a given laser power there is a range of scanning speed for which the pool is stable and the range increases with an increase in laser power. However, increasing laser power brings about the so called hydrodynamic instability which is driven by Marangoni effect and increases porosity. Hatch distance and layer thickness are the other important parameters in defining porosity level that

should be determined considering their interrelation with speed and power of laser. Porosity increases as these parameters increase above a threshold [35,41,43].

3.3.2.2. Balling

Balling is one of the most substantial problems in SLM. It happens when a molten pool takes the shape of a circular or segmental cylinder due to effect of surface tension and makes a fragmented scan track rather than a continuous one, which is known as balling. Balling phenomenon is detrimental to quality of produced SLM parts and hinder the further developments of SLM process. Since SLM is a layer by layer process, balling phenomenon in one layer can affect lots of subsequent layers or even the entire body. If it happens in one layer, it will act as a severe obstacle to the uniform deposition of powder for next layer and tends to cause porosity and delamination due to poor inter-layer connections. In cases of severe balling, the balls on the surface can hinder or even stop the movement of paving roller and stop powder deposition. This phenomenon highly increases the surface roughness and demolishes mechanical properties of the product [44,45].

3.3.2.3. Residual Stress

Laser based processes are known to introduce massive amount of residual stresses as a result of high thermal gradients, large thermal expansion and shrinkage due to rapid heating and cooling, and non-uniform plastic deformation during heating and cooling cycle. Part of the residual stress is introduced due to cooling and shrinkage of molten material and part of it originates from strain-induced stresses in previously built layer or substrate. Residual stress can cause other types of defects in part like deformation and cracking. It can also cause anisotropic effects in SLMed parts and demolish mechanical properties in one or all directions. There are some subsequent defects in SLM that originate from the pair of residual stress and thermal gradients, like shrinkage, deformation and delamination. The built parts are usually heat treated to relieve their residual stress after the process. However, some techniques like preheating the platform and choosing a suitable strategy for scanning like island scanning (case a in figure 3.6) can be used during production to decrease residual stresses and eliminate its harmful effects [35,43].

3.3.2.4. Cracks

High temperature gradients between melt pool and its surrounding environment can cause excessive thermal stresses and cracks. In addition to thermal gradients, existence of some alloys in composition of the powder can intensify cracking, the property which makes difficult the SLM of such powders. Crack can happen between neighboring layers as a result of tensile residual stress between two layers or along the grain boundaries (intergranular cracks) during solidification. Reducing crack density can be done by reducing laser power which leads to decrease steepness of thermal stresses and fracture during solidification [35,43].

3.3.2.5. Spattering

Sputtering is termed to injection of liquid droplets and non-molten powders around the melt pool due to high pressure and plasma caused by melt evaporation. The spatter caused by non-molten powder particles can be designated by its microstructure which is similar to that of powder alloy, while researches show spatters originated from liquid droplets have significantly different chemical composition compared to initial feed stock. The generated spatter around the scan line is usually

spherical and much larger than the size of the used powder. Spattering intensifies when the melt pool is overheated above a threshold and highly increases when energy density increases. In case of massive spatter, the recoater can be stopped by solidified spatter droplets during paving the next layer [43,46].

3.3.2.6. Incomplete Melting

If the imposed energy density is insufficient to melt all the powders at the laser spot, some non-molten particles remain which can be trapped and make pores inside the part. In some cases, the applied hatch distance is higher than optimal value which causes a line of non-molten powder along the scanned layers known as elongated pore [43].

3.4. LPBF of Aluminum Alloys

Aluminum alloys are the second most used metal after steel which are categorized into heat treatable, non-heat treatable and casting alloys. They are increasingly employed in automotive, aerospace, and aircraft applications thanks to their recyclability, excellent strength-to-weight ratio, thermal and electrical conductivity, corrosion resistance, formability, and attractive appearance. However, advances in new technologies call for alloys with higher mechanical properties and customized details that is not attainable by traditional manufacturing processes. AM and specially SLM/ DMLS along with post processing treatments has become a promising manufacturing tool for such necessities. In this part of the thesis we try to bring and discuss about part of the literature of SLM of aluminum alloys to provide the reader with an idea about different alloying compositions that are used in SLM together with history of these alloys in SLM.

Referring to the literature reveals that researchers divide AM processes of aluminum alloys/composites into two different groups, namely (direct/indirect) Selective Laser Sintering (SLS) and Selective Laser Melting (SLM).

In SLS of Al powders, the base Al alloy/composite is mixed with a polymeric binder or secondary metal, knowing the fact that they must have a significant difference in melting point temperature with respect to Al material. So a low energy laser can be used to (partially or totally) melt and join them together without hardly affecting Al powder. The green part produced in this way may need post processing like burning the binder and infiltration with a low melting alloy to increase mechanical properties. The key difference between direct/indirect SLS refers back to the ways that base powder is prepared. In indirect SLS, the base metal powder (here is Al alloy) is mixed with a polymeric powder and laser selectively melts polymer which then acts as a binder to glue Al powders together. The polymer binder is then burnt in a furnace and green part is infiltrated with a low melting point alloy in order to increase density. However, in direct SLS, the base Al powder is coated, mixed, or composited with two or more immiscible alloys with significant difference of melting point with respect to Al. The secondary part of powder partially or totally melts and sticks the base powders together to make a dense part. Whatever is the type of SLS process, it partially sinters the powder and can be done with low energy lasers [47].

However, as it was mentioned in previous section, SLM is referred to the cases in which Al powder is directly melted by high energy laser beam to achieve 100% density in a single step. SLM appeared after a cutting edge innovation in laser technology that provided the possibility to produce

high power lasers to directly melt any material, rather than using low power ones to sinter low melting point powders.

There are some difficulties in handling SLM of Al alloy powders which is the reason why available Alloys for process is limited and the number of publications is not very much in this regard. The very high reflectivity (higher than 91%) and striking thermal conductivity of Al significantly increases laser power required for treating the powder. The other obstacle is high delicacy of Al based alloys to oxidation that causes problems during melting and solidification. The oxide layer on the upper surface of the pool evaporates under the energy of laser beam. It is believed that Marangoni forces that stir the pool are the most likely mechanism to disrupt this oxide layer which allows the beam to more fuse to underlying layer. At the same time, oxides at the sides of pool remain intact and create region of weakness and porosity which are important issues in processing Al based alloys [39].

The available literature of SLM on aluminum powder shows that it needs careful process control to avoid defects like distortion, layer delamination, balling and oxidation. SLM of aluminum is described as a very complicated process because there are a lot of parameters that influence densification mechanism, microstructural feature, and quality of final parts. These parameters which were represented in figure 3.5 show that SLM/SLS process on aluminum is controlled on one side by properties that are related to powders, and on the other side, by parameters that are set or related to the used machine. This is why the whole literature in this area is focused on effect of these parameters on one or more special aspect of produced parts like porosity, balling, distortion etc. [47]. It led to definition of process window for different compositions and alloys based on input parameters, using either the single scan track strategy or making cubic samples directly. The studies showed similar process windows for all types of powders which was consist of no melting, partial melting, good consolidation and excessive balling regions, although there were differences in the location of boundaries which were separating various regions for different types of powders. A more thorough discussion about the process window will be delivered when we talk about single scan strategy in SLM. Also part of the literature about SLM of Al-based alloys will be delivered there since some researches were performed based on single scan tracks. Nevertheless, in the following we discuss about some aspects in SLM of Al-based alloys and the role played by each parameter.

From all types of aluminum alloys, Al-Si based alloys and their composites are by far the most used and studied alloys in the SLM technology, followed by few researches on other alloys. In addition to Si, other elements like Mg and Cu are added to the composition aimed at improving mechanical properties. AlSi10Mg has the highest demand in SLM researches amongst all aluminum alloys mainly because of its special solidification characteristics that makes it less prone to cracking, delamination and deformation. A vast majority of the literature about this alloy is about laser and scan related parameters, especially laser power and energy density, and their effect on porosity and properties of final product [48]. An extensive study of different parameters was done by Olakanmi (2013) where he studied effects of processing and powder material parameters of SLMed pure Al, Al-Mg and Al-Si alloys on the process window, densification and microstructure of parts. His work showed that laser power and scan speed (energy density) mostly affect flow and solidification of single scan layers while an optimum selection of them decreases temperature gradients in melt pool and surface tension which is a help to stability of melt pool. He defined four combinations for energy density, namely no marking, partial marking, good consolidation and

excessive balling, from which only the range of “good consolidation” is the optimum range of energy density to have dense parts. This range was defined from 12 J/mm² to less than 30 J/mm² for all alloys in his work. On the other hand, his work on powder properties showed that addition of alloying elements (Mg and Si) has no significant effect on processing window, but rather affect the nature of the evolved surface morphology of processed powders from a top view. He finally concluded that powders must have spherical shape and their oxide thickness must distribute uniformly in order to prevent agglomeration and having a more homogeneous dense part [49].

The parameters studied by Olakanmi were also investigated separately by other researchers on other Al-based alloys. For example, Buchbinder et al. (2011) used a 1kW laser in their work to increase building rates and argued that scan velocity in SLM of Al based alloys including AlMg3, AlMgSi0.5, AlSi12 and AlSi10Mg is power dependent, meaning that in order to have dense SLM parts, the scanning speed should increase while power increases and vice versa, which leads to higher build rates and better performances of SLM process. In terms of energy density, their results stand close with the work by Olakanmi (2013). They also measured mechanical properties of AlSi10Mg, and showed that despite results of other researchers, hardness is not hardly affected by velocity, power and hatch distance and remains constant for a large range, if the combination of the three gives a dense part. They argued that hardness is highly dependent on cooling rate and due to having very high cooling rate in SLM with any input parameter, hardness will remain very high, at about 200% higher than die cast parts. About the tensile strength, their study showed that tensile strength of SLM part in 0 and 90 degrees with respect to building direction were 420 and 360 MPa, respectively, which was considerably higher than die cast metal AlSi10Mg (240MPa) [50].

In a similar work, Louvis et al. (2011) studied effect of laser power and scan speed on density of aluminum 6061 and AlSi12 Alloys. They defined a narrow process parameter based on energy density with minimum balling, while any increase in speed or hatch distance led to breakage of molten track and delamination which demolish density. On the other hand, the authors observed that higher powers increase density of parts and suggested to use high powers for SLM of aluminum alloys. However, they found that even in case of optimum building parameters, existing oxygen in the building chamber and oxidation is the key problem in SLM process of aluminum alloys that restricts having full density parts. In fact, when the melt pool is formed, the oxide layer on the upper surface of melt pool evaporates under laser beam while oxide films on both sides of melt pool remain still. Stirring the melt pool due to Marangoni force breaks the oxide layer at the bottom allowing diffusion to underlying tracks while side-oxide-walls remain intact. These walls of oxide create regions of weakness and porosity and stop melt pool from wetting the surrounding [51]. Oxidation is a common problem in SLM of aluminum alloys and specializes part of the literature to itself. It is so common subject that there is a quotation about it even in lots of publications that do not straightly address its issue. However, all the publications about oxidations in SLM of aluminum alloys conclude that oxide layers have indeed the tendency to lower the wetting of the substrate and thus induce balling of the molten material, affect the fluid flow in the melt pool, and consequently the absorption of the laser energy; and impede uniform melting of the top deposited layer to the solid substrate below [57].

In addition to machine processing parameters, a small section of literature in SLM of Al alloys are devoted to effect of powder morphology, size and distribution. For example, Abulkhair et al. (2015) studied effect of powder properties like size distribution, morphology, composition, flowability and apparent density on quality of AlSi10Mg SLM parts. In terms of morphology, spherical

powders demonstrated better in terms of flowability and density with respect to irregular or non-spherical shapes. In terms of composition, authors showed that having higher amount of Si in composition enhances laser absorption, fluidity, and wettability; but for values close to eutectic composition (which is the case for this alloy), Si will be an assistant for formation of platelets which are potential sites for crack nucleation under cyclic loading and destroying fatigue life. Finally, authors concluded that a more uniform distribution of powders and higher apparent density leads to better qualities in final parts. All in all, they showed that powder properties should be considered in SLM process of Al alloy since they affect porosity in the final part [52].

The other part of relevant literature is related to scanning strategy and temperature field. There are a bunch of publications about scanning strategies in SLM which talk about non-aluminum alloys. A complete survey about scanning strategies and their effect on stress and deformation of SLMed Inconel 718 has been done by Cheng et al. (2016) which can be used as a reference for majority of alloys. There are a bunch of other works done on scanning strategies such as the one by Jhabvala et al. (2010) which was done on WC-steel coated and 18-carat alloyed gold powder. Their report is not as complete as the one done by Cheng et al. (2016) in sense that they only investigated four strategies. However, what all these publications have in common is that in scanning a single layer, it is better to divide the surface in smaller regions (named islands) and change scanning path for each island so that every two neighboring island have different scanning paths; and for building the next layer, it is better to change the angle of scanning line to distribute thermal stresses. This work is correctly done by Read et al. (2015) when they aimed at optimizing process parameters of AlSi10Mg [42,53,54].

Investigation of mechanical properties of final parts and optimization of process parameters are the other part of history. In terms of mechanical properties, Mower and Long (2016) studied mechanical properties of AlSi10Mg produced by SLM (after thermal stress relieving) and compared them with similar alloy of Al6061 produced by conventional methods (wrought alloy). They showed that while stiffness of SLM AlSi10Mg is almost equal for both SLM and conventional cases, its fatigue behavior is considerably lower than conventional one (Al6061), i.e. the lifetime of SLM type in any cyclic stress amplitude was approximately an order of magnitude lower than the wrought one, and for any lifetime, the stress tolerated by SLM was 30% lower. The authors also compared yield stress of Al6061 (293Mpa) with SLM AlSi10Mg which was about 227 Mpa and 172 Mpa for measurements aligned parallel and perpendicular to AM layers, respectively, with almost double deformability for parallel with respect to perpendicular case [40]. In another work, Kempen et al (2012) studied mechanical properties of SLMed AlSi10Mg alloy. However, their results are not quite comparable with the ones of Mover and Long in the sense that they found almost equal tensile strength in both of XY and Z direction of samples with values of 391 and 396, respectively. The authors also investigated hardness of SLMed AlSi10Mg alloy and found that it is equal to hardness of high pressure die casted of the same alloy. The Charpy impact energy of as built SLM samples was also higher than conventionally casted AlSi10Mg alloy. They finally concluded that mechanical properties of SLMed AlSi10Mg is in any case higher or at least comparable to the casted material thanks to its very fine microstructure and fine distribution of Si phase [55]. A more completed scheme of tensile strength of SLMed AlSi10Mg is presented by Herzog et al. (2016). The authors gathered all literatures of mechanical properties of SLMed AlSi10Mg and showed that ultimate tensile strength is reported between 315 to 396 MPa which is always comparable or higher than conventional casted and high pressure die casted, while heat treatments usually decrease the strength at the expense of hardenability [56]. In terms of process

optimization of SLMed AlSi10Mg, researchers try to investigate combined effects of parameters and analyze the results on porosity of final artefact. Two works done by Abulkhair et al. (2014) and Read et al. (2015) on AlSi10Mg alloy are good examples in this case. In the first one, authors investigated effects of hatch distance, scanning speed and scanning strategy. They showed that for a special speed, porosity remains constant as long as there is an optimal value of hatch distance that provides enough overlap for layers. It was also concluded in this work (and some other publications) that scanning twice the same area with different laser powers tend to reduce porosity to a great level [41]. However, in the second work authors used design of experiment methods (Response surface methodology) to find optimal parameters of SLMed AlSi10Mg. They studied effects of interaction of laser power, scanning speed, hatch distance and island size on porosity and mechanical properties of the built parts. They showed that island size is ineffective on porosity while laser power, speed and interaction of speed and hatch distance are highly effective on porosity (similar to results of Abulkhair et al. (2014)). Finally, they showed that building direction doesn't have any meaningful effect on tensile and creep resistance of this alloy [54].

Finally, the newest trend in SLM of aluminum is to reinforce the metallic matrix with small size ceramic particles to improve specific strength, stiffness, wear, fatigue and creep properties, while it often severely degrades the plasticity and machinability of the matrix. The ductility and toughness of so called Metal Matrix Composites (MMCs) can be kept constant or even improved with a simultaneous increase in strength by reducing the particle size to the nanometer range which is given the term "nanocomposites". Titanium diboride (TiB_2) and silicon carbide (SiC) are the most famous candidates for aluminum alloy reinforcements, especially for AlSi10Mg. Some researches in the literature used reinforcements by mixing it with aluminum powders directly, and then used it for SLM part preparation. Lorusso et al. (2016) and Manfredi et al. (2014) used this technique where they directly mixed TiB_2 and SiC with AlSi10Mg and AlSiMg alloy powders, respectively. In the first work, Lorusso et al. (2016) studied tribological effects of MMCs by mechanically mixing micro-sized and nano-sized TiB_2 with AlSi10Mg and use them to build SLM samples. They showed that wear rate for micro-size TiB_2 reinforcement is higher than nano-size reinforcement and aluminum alloy. This property was explained by interfacial bond between metal matrix and ceramic particles (TiB_2) where the lower stress at the interface between nanoparticles and the alloy helps for a stronger interface in the nanocomposite with respect to its microcomposite counterpart. Authors also argued that presence of reinforcement decreases friction coefficient with respect to pure alloy, with a more significant reduction for microcomposite [58]. In the other work, Manfredi et al. (2014) studied microstructures of AlSiMg reinforced by SiC micro-ceramics after being processed by SLM. They showed that due to very high temperature in SLM, silicon carbide is totally disappeared and aluminum carbide is formed which usually demolishes mechanical properties. However, authors showed that hardness measurements for composites containing SiC is 70% higher than pure AlSiMg processed by SLM [59].

Another method used by other authors is to prepare composite powders for SLM by in situ reaction and gas atomization solidification process instead of mechanical mixing, which is believed to prepare a uniform distribution for high fractions of nanoparticles in aluminum matrix and eliminates effects of particle agglomeration during SLM process (authors rejected their idea about agglomeration in their next publication!). The other benefit of this method is that morphology of powder doesn't change in case of having larger dimension reinforcements and therefore flowability will not demolish due to powder shape [60]. A fresh work in this area is the one done by Li et al. (2017) where they produced nanocomposite of AlSi10Mg and TiB_2 by the above mentioned

technique and used it in SLM to investigate properties of new powder. The authors showed that addition of TiB_2 to the metal matrix improves SLM processability of powder and helps to formation of a much finer microstructure compared to pure alloy; while TiB_2 chemically stays stable and doesn't react with the metallic elements. Further, they could produce completely dense and crack-free samples which resulted in a tensile strength higher than most conventionally fabricated wrought and tempered Al alloys, and previously reported SLMed Al-Si alloys [61].

3.5. SLM Single Scan Track Study

Selective laser melting of a powder happens when a laser beam selectively scans over the surfaces of a deposited powder on platform, each surface being a cut of the part in z direction. Each surface (layer) is formed by longitudinal lines (tracks) of molten powders which superimpose one on the other. Hence, final properties of the built part are strongly affected by properties of single scan tracks and the connection between them, as well as properties of each single layer. It led to a more efficient procedure to explore characteristics of the built part by investigating melt pool parameters instead of building whole samples. In this method, the powder is distributed on the surface and only a single line is scanned by laser with preset parameters. When a laser beam scans the surface of a metallic powder bed, the resulting track may be continuous with a crescent shape cross-section, continuous with an elliptical section, discontinuously irregularly broken, discontinuously balled or only partially melted [62]. The single scan track is usually analyzed based on the following factors to evaluate the quality of work.

- Continuous, uninterrupted and rather symmetrical scan line to prevent pores and irregularities in shape.
- Accepted level of penetration into the layer below to prove adequate wetting and bonding to the previous layer.
- Accepted level of height to be used as bed for subsequent building layers.
- Optimum connection angle between the melt pool wall and the surface of substrate which is a sign for dimensional accuracy and density and minimizes required overlap between neighboring tracks.

Although it seems that process window acquired by single scan can be used for any optimization, it needs elaborated analysis on melting pool parameters. On the other hand, scan spacing/hatch distance is a key factor in AM that is neglected in single scans but will anyhow be included in the final production. It should be chosen with extreme care in order to ensure enough overlap between adjacent scan lines [35]. Given this, Multi Scan Track analysis is also developed by some authors to have a more completed study on processability and optimization of different powder elements.

The number of publications in the field of single and multi scan track strategies is very limited especially about multi scan track analysis. In addition, there is very few works on studying these strategies on SLM of aluminum alloys which leads us to cover different types of powder materials in this section, rather than specifying for aluminum. However, literature shows these strategies can be used for different purposes. In this section of thesis work, the reader is addressed to some literatures in the field in order to get an idea about history and developments of these theories as well as possible methodologies which are suggested by various researchers.

Majority of the work in area of single and multi scan track is devoted to defining process window for special powder materials. Childs et al (2004) were the first pioneers who applied single scan theory to study effect of laser power and scan speed on melt pool geometry, continuity of tracks and process window of two types of steel. They concluded that geometrical analysis of single scan tracks can be used as a benchmark for best combination of speed and power of machine [62]. In another work, the same authors conducted a more elaborated study on same powder materials to investigate process window based on single and multi scan tracks and supported their results with simulation analysis. They found five different qualitative forms of tracks for different power and speed combinations. The authors translated their results on process map and found that there is a continuous region on process map for each type of scan track in which all tracks share similar geometrical properties along their length. Furthermore, results were quite similar for different types of alloying powders. About multi scan tracks, the authors failed to deeply study effect of hatch distance and tried to still correlate porosity of final part to speed and power of laser without any relevance to scan spacing (or energy density) [63]. These works established essential benchmarks for single and multi scan strategies and addressed other authors to expand the idea for other types of powder materials. A good example is the work done by Wang et al. (2012) where they used single and multi-track strategies to study effect of input energy density on SLM process stability of 316L stainless steel, being the single track at the core of the study. They classified all tracks in four groups, including regular and thick shape, regular and thin shape, regular but occasionally broken shape, irregular and pre-balling shape, and represented it in a process window showed in figure 3.7 which again strengthens the idea of having scan tracks with similar properties in close regions based on power and speed of scanning, and not scattered throughout the range of parameters.

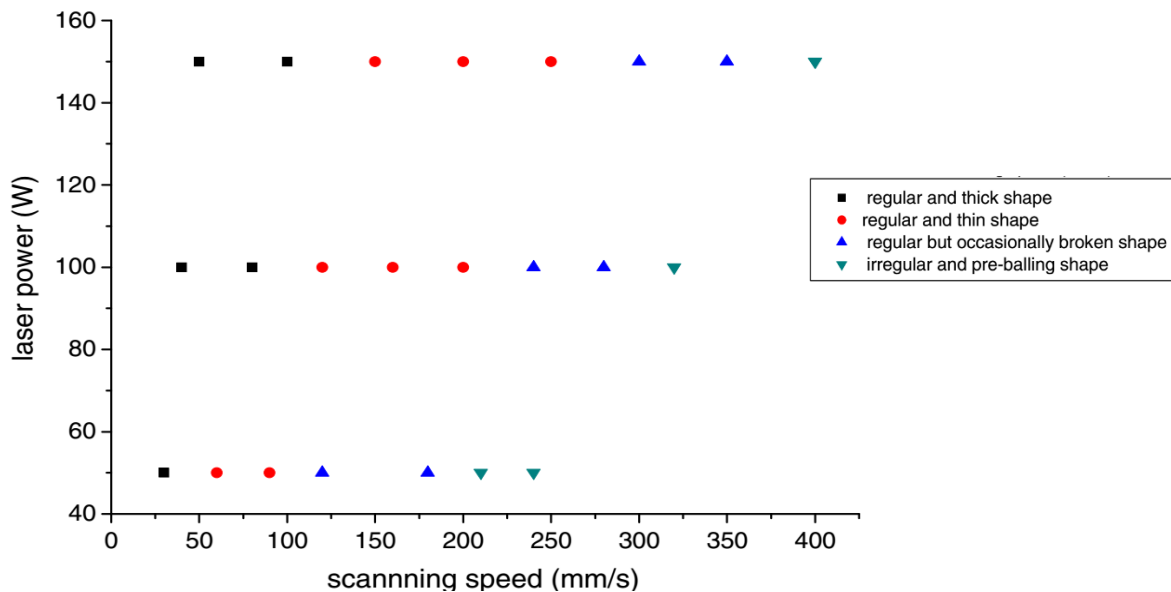


Figure 3.7 Process map of 316L stainless steel defined by Wang et al. (2012) using single scan track strategy [64].

The other interesting thing they showed was that for different groups of tracks, different overlapping values can be adopted to reach desired properties. For example, for regular and thick shape tracks, low (10%) overlapping is adequate while for thin shape tracks a higher overlapping

(30%) is required. So, they basically used the shape of tracks as a reference for hatch distance, despite previous authors who used width of tracks which was mentioned before [64].

A similar work but on different material was done by Ciurana et al (2013), where they studied optimization of selective laser melting parameters of CoCrMo by means of single scan track analysis. They adjusted power and speed of scanning for each scan track and found three different regions to host scan tracks based on energy density including continuous tracks, irregular and the ones with balling effect. Their study supports the idea of having separated regions for tracks with optimum shape and geometrical parameters. However, these areas are case specific and not constant for different types of powders. The important thing pointed out by authors is that borders of these zones is not only dependent on power and scan speed, but also highly affected by thickness of the layer. For example, a set of power and scan speed for a single scan track with a special layer thickness may fall in continuous region, while changing layer thickness makes it to move towards irregular or balling one [65].

single scan strategy also found its way in phenomenological studies in SLM thanks to its simplicity and fast speed in making final conclusions. Balling is one of the most important phenomenon in SLM which was studied with single scan strategy by few authors like Gu and Shen (2009). These authors studied effect of SLM process parameters and powder characteristics on balling phenomenon of stainless steel and finally reached to graph shown in figure 3.8 which is a representation of scan track characteristics based on laser power and scanning speed. In this portrayal, I, II, III, and IV regions were representative of tracks without consolidation, tracks with significantly coarsened balls, tracks with small-sized balls and/or cracks, and continuous and smooth tracks, respectively. This technique enables them to carefully see and analyze balling formation, growth, diminishing, and disappearing while adjusting a wide range of process parameters. The authors argued that this map can be used as a key reference to eliminate balling effect by smart controlling on power and speed [66].

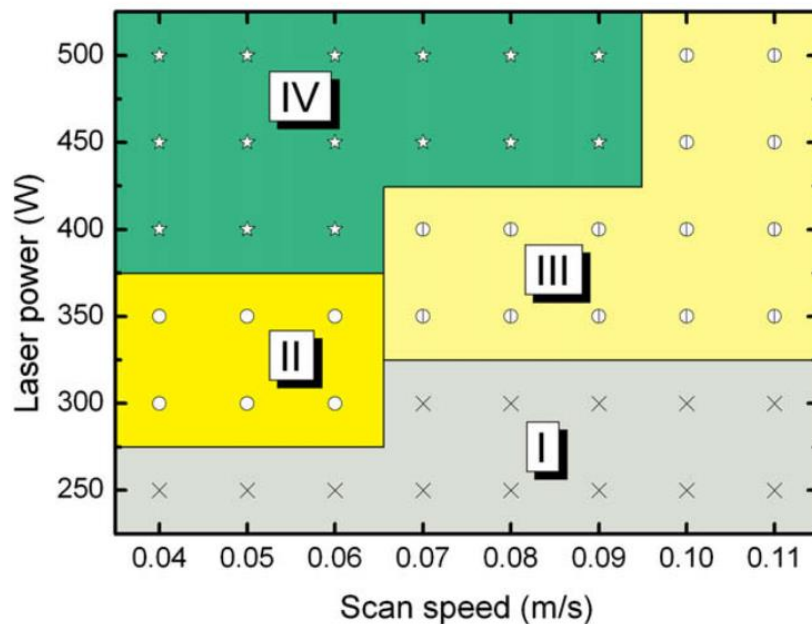


Figure 3.8 Process window of 316L stainless steel defined by Gu and Shen (2009) aimed at studying balling phenomenon [66]

During developments of strategic method of single scans, some authors insisted on considering the very important aspects of interactions of scan lines parallel to focusing on analyzing single tracks in order to get a brighter view of properties of final products. Beal et al. (2006) were among those who discussed about variation of single track dimensions while applying subsequent tracks. Their proposed scheme is represented in figure 3.9. The figure explains that sequentially scanning any single layer from distributed power decreases the amount of available powder in the vicinity for the subsequent scan tracks which causes a sequential decrease in their size. The reduction in powder is due to melting and densification which imposes contraction on track's cross section and leaves a free space at surrounding of scan line due to reduction in its dimensions. Further, part of the available powder is missed in spattering. Hence, the available powder for next scan line will be lower which leads to smaller dimensions and increases porosity. This phenomenon can be repeated for alternated scanning because the missed powder is not substituted at any stage. Given this, the authors showed if after each scan track the bed is refilled with fresh powder, the shortage of powder is compensated and the size of all tracks will be identical, which can be a help in porosity reduction.

However, since refilling the bed after each scan track heralds for very high expenses and incredible process time, there should be a compensation between quality and expenses at the first step. This study shows that not only properties of single scan tracks are of vital importance in defining the level of porosity of the built part, but also any interaction between scan lines and powder on the bed can be of key importance [67].

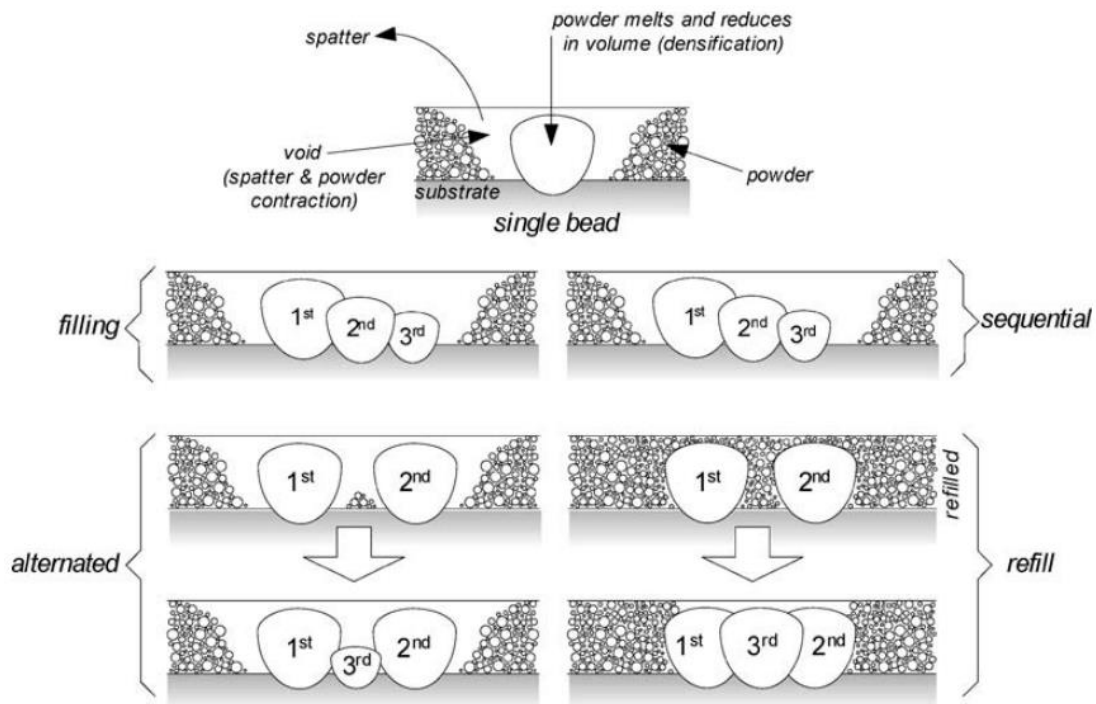


Figure 3.8 Effect of sequential scanning on dimensions of scan tracks [67]

In order to get a clear view about single and multi scan track strategy on SLM of metallic powders, the reader can refer to various works done by Yadroitsev and his colleagues who are outstanding pioneers in SLM field. Researches mentioned in Ref. 44 and ref. 68 to 71 represent some of the

key studies by these authors which provide the reader with basic necessities. In reference 44, the authors studied effect of laser power, scanning speed and layer thickness on single track geometry of several types of powders. They used single track strategy to analyze instability of SLM process and showed that there is a threshold of process stability for all types of powders that is determined by process parameters and can be predicted by the shape of single scan tracks. The authors classified single tracks in two groups referring to stability and instability zones, where the molten track is continuous and broken, respectively. They separately studied effect of scanning speed, laser power and layer thickness on shape of tracks and their stability and then considered effect of interaction of parameters. In addition to studying parameters, the research includes a broader context from optimal scanning parameters, to effect of scanning strategies and mechanical properties of SLMed samples [44]. In a parallel work, they studied instability of molten pool with more details and concluded on the range of optimal scanning speed based on the laser power and argued that this range increases by increasing power and becomes narrow with increasing thermal conductivity [68].

In the other study Yadroitsive et al. (2011) analyzed the effect of hatch distance on single scans and morphology of the surface. They showed how width of scan layers can be a help in choosing correct hatch distance in order to have adequate overlapping between layers and eliminate non-synthesized powders in between the tracks. They defined the first scan width as a benchmark for hatch distance and showed any hatch distance lower than first layer thickness leads to a reduction in size of subsequent layers and molten material with respect to the first one, while any value higher than that leads to non-synthesized powders to remain in between two subsequent layers. As a matter of fact, the maximum value for hatch distance should not exceed the average width of continuous track in order to manufacture a smooth surface. Furthermore, if hatch distance is lower than scan track width, the height of tracks at the beginning and the end of sequence will be higher due to interaction of laser and reduction of available powder after building each layer, which can lead to excessive porosity if not eliminated [69]. In a following work Yadroitsev et al (2012) establish links between the principal SLM parameters (laser power density, scanning speed, layer thickness), properties of the powder and geometrical characteristics of single tracks. They used statistical analysis to determine a sequential order for parameters of SLM of stainless steel powders based on their level of significance, with laser power as the most important factor in correct shaping of scan tracks, followed by layer thickness, scanning speed, and particle size, respectively [70]. In the final reference, Yadroitsv et al (2013) used the single scan strategy to investigate the role of two affective energy input factors in SLM of 316L stainless steel on track formation and its geometrical parameters, in order to predict the effect on final product. The two input factors which are preheating temperature and scanning speed were adjusted while power of the laser was fixed. The authors showed that several problems rise while increasing preheating value from a threshold, including powder agglomeration due to sintering, increasing satellites around the pool, and increasing spatter due to higher melting pool temperature. About the geometrical characteristics of scan tracks, they concluded that preheating controlled the contact angle and height of the track, while scanning speed governed track width and contact zone characteristics [71].

We close this section of the thesis by the work done by Abulkhair et al. (2016), where they studied effect of changing the scan speed on the melting and solidification of AlSi10Mg upon irradiation with a laser beam, in order to investigate the fundamental origin of porosity in SLM parts of relevant alloy and analyze the response of the SLM material at a level below the size of the melt pool. They chose 50 and 40 micrometers as the best hatch distance and thickness layer,

respectively, and showed that the height above the substrate increases with increasing scan speed, whereas the opposite trend is seen with the re-melted depth (depth of penetration into substrate material). In addition, the height of scan track on the substrate surface is always lower than the height of deposited powder layer thickness. In the range of their process parameters, they didn't observe any balling effect and explained it by good wettability of powder with substrate material which is a crucial factor affecting the bonding of a layer to the one below (wetting in SLM means that molten metal has spread over the substrate or the previous layer rather than balling). Finally, they concluded that any type of porosity is developed during layer accumulation in multi-layer processing since cross section of individual scan tracks didn't show any porosity. In other words, pores do not form in single tracks or layers using a pre-defined set of parameters but they do form in multi-layered samples [72].

4. EXPERIMENTAL SETUP; INSTRUMENTS AND MATERIALS

This chapter is devoted to technical aspects of the thesis work and discusses about experimentations. Technical aspects of the work can be classified in three groups based on their nature in the work. As a result, the chapter is organized in three subsections to discuss each class in detail. The first section is related to instruments in which all equipment used in the experiments will be discussed. The discussions will include machine type and setup, while working principle and procedure of the machine will also be explained wherever it seems to be of importance. The second section covers material issues and talks about type of powders that were used to produce samples as well as their properties. The chapter will close by third section, in which experimental set up and sample preparation is represented. It explains all aspects of sample preparation including setup parameters, sample type, and geometry.

4.1. instruments

4.1.1. EOSINT M270 SLM/DMLS Machine

The SLM machine utilized to produce samples for this thesis work was EOSINT M270 Dual mode which is presented in figure 4.1. The dual mode refers to Standard and Xtended cases which refers to switching the operating inert gas between Nitrogen and Argon, respectively, each one allowing to use various qualified materials based on their properties. We utilized Xtended mode with argon as inert gas for all the experiments.



Figure 4.1 Eosint M270 Dual mode SLM machine utilized for the thesis

The machine comprises a process chamber with recoating system, elevating system and platform heating module, an optical system with laser, a process gas management system, a process computer with process control software, and a set of standard accessories. A list of nominal properties of the machine are reported in table 4.1.

Table 4.1 Properties of SLM machine used in thesis

Property	Value
Effective Building Volume (including building platform)	$250 \times 250 \times 215$ [mm]
Building Speed (Material Dependent)	$2 - 20$ [mm ³ /s]
Layer Thickness (Material Dependent)	$20 - 100$ [μ m]
Laser Type & Maximum Power	Yb (Ytterbium)-Fiber Laser, 200 [W]
Scan Speed	Up to 7000 [mm/s]
Variable Focus Diameter	$100 - 500$ [μ m]

During operation the process chamber is secured by interlock while the 200 W Ytterbium fiber laser fully melts the powder at the focusing point on platform. Figure 4.2 shows the working chamber of the machine during laser scanning process and after finishing a set of samples.

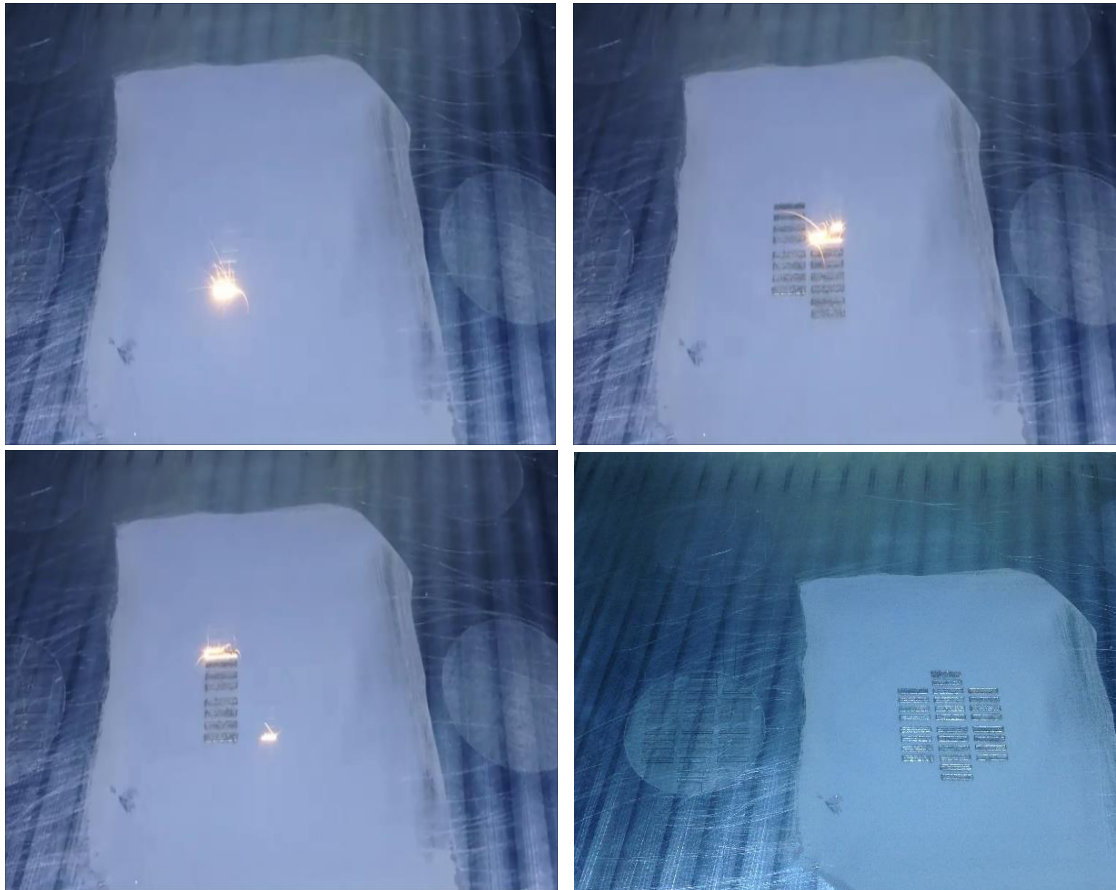


Figure 4.2 Image of inside working chamber of SLM machine during and after processing a set of samples

In addition to setting parameters on machine as key figures to define properties of final products, the building platform and recoating system should be wisely chosen or modified based on type of the powder. The following subsections explain the modification of the two, based on the used powders.

4.1.1.1. Recoating System

The recoating system which creates the layer of powders is comprised of a recoating element, a recoater arm, and a linear drive which moves the recoater arm in the horizontal direction. The system remains intact for utilizing any type of powder while recoating element is changed or modified to become compatible with powder. Due to non-homogeneity of distributed powder on surface after using recoating element of the machine (High speed steel blade) as well as existing free-of-power regions, it was decided to use another type of film applicator that was made in the faculty being geometrically similar to SH1107/60/1 model of SHEEN© Instruments. The schematic of this applicator is represented in figure 4.3. As the figure illustrates, the four sided film applicator makes the possibility of having four different layer thickness by having four gap sizes in one unit, while at the same time, the cylindrical shape provides excellent homogeneity of distributed powder and smooth surface. The four gap sizes of four sides are 30, 50, 60, and 80 micrometers where by simply rotating the cylinder through 90° the next gap size is placed onto the test surface and a new layer thickness is adjusted.

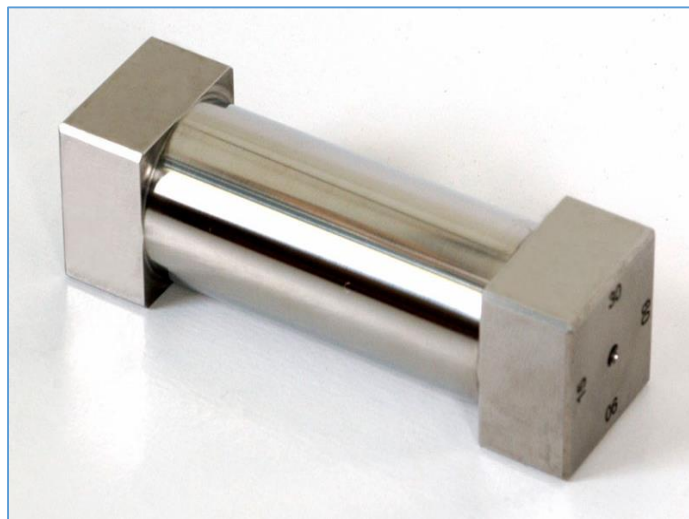


Figure 4.3 Four sided film applicator used in thesis

In addition to modification on recoater, the powder was mixed with 50% weight of ethyl alcohol (EtOH) which together with recoater solved all problems related to powder distribution.

4.1.1.2. Building Platform (or Substrate Plate)

The parts are built on a building platform, which can either be integrated into the part (e.g. for tooling inserts) or separated from the parts after the building process. In latter case which was our type in experiments, the platform can normally be reused many times after few post processing (like machining and stress relieving) on it. They were direct-base building platform with standard

size of $250 \times 250 \text{ mm}^2$ to perfectly match the build area and were attached to the career plate in process chamber by four corner screws.

Two types of platforms were used in experiments. The first type which is shown in figures 4.4.a to c consists of the base plate made of Al-Mg alloy and nine casted disks of AlSi10Mg with 40 mm in diameter which are screwed to negative holes in main plate with similar diameter. This type which was used to prepare single (and multi) scan samples had proved to be very advantageous, because each disk can host a different set of samples and once a set is prepared, its disk can be removed for further analysis while the rest of platform (and therefore disks) can yet be utilized to produce new samples. This property is clear in figures 4.4.a to c. Furthermore, the substrate (disk) can be chosen with same chemical composition of powder to eliminate any risk of unwanted chemical reactions.

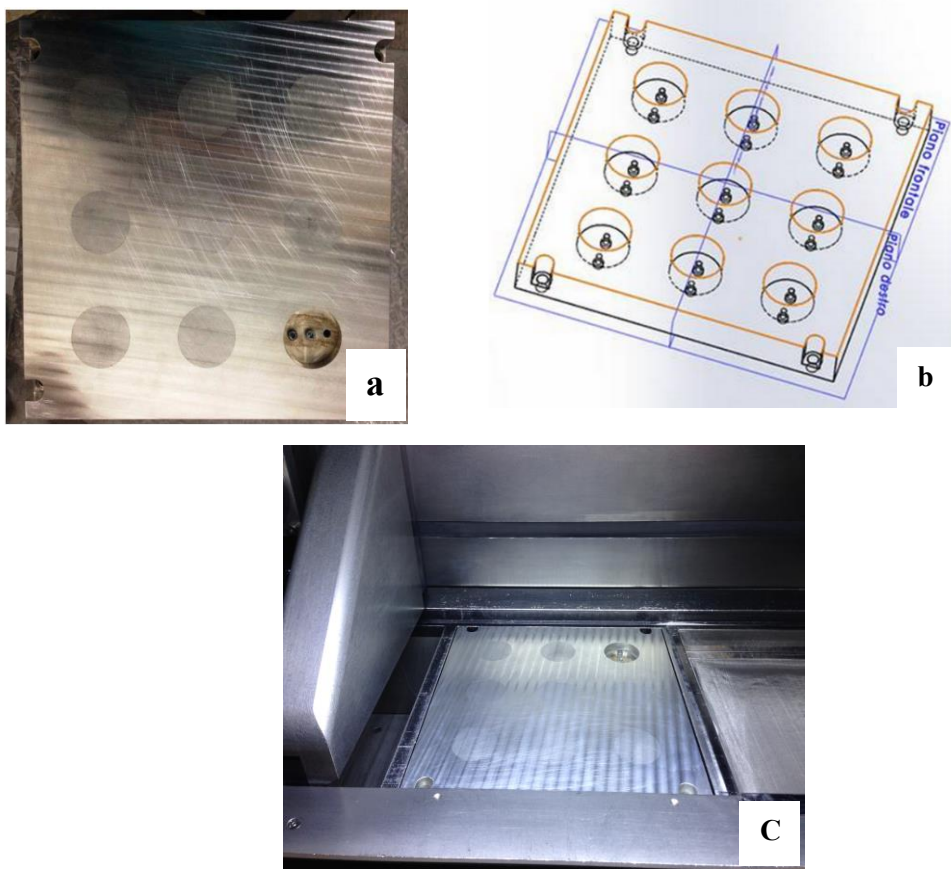


Figure 4.4 Used platform to prepare single and multi scan samples

The second type of platform which is shown in figures 4.5.a and b was used to host cubic samples. This type of substrate was the simple one of Al-Mg material without any hole for discs. So the plate could be used for one round of samples at a time and must be post processed before reusing for further works.

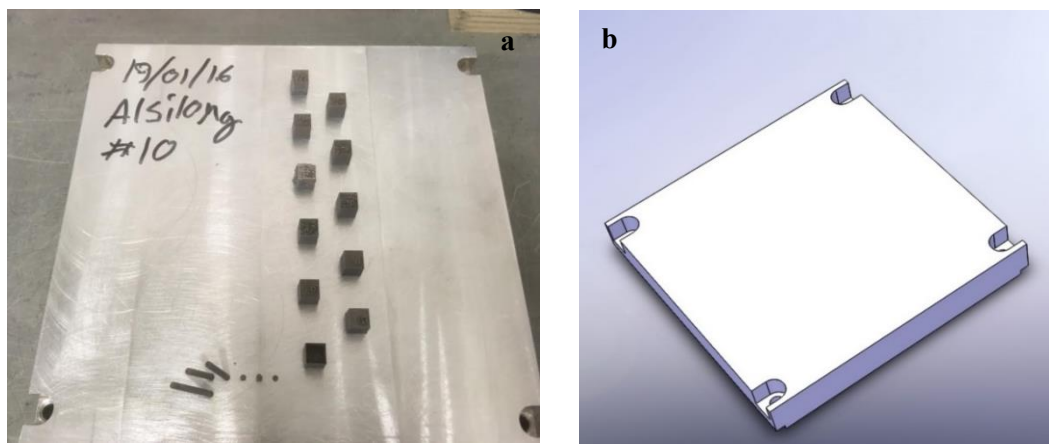


Figure 4.5 Used platform to prepare cubic samples

4.1.2. Cutting Machine

As depicted in figure 4.6.a, Isomet 4000 precision cutting machine was utilized to cut built samples and prepare them for further analysis. This type of machine was a very good candidate for our cases because it applies very low cutting forces during the process and causes no/least damages to delicate samples. The machine was equipped with a diamond or cermet blade for all the cases and cutting speed and feed rate were set at 2900 rpm and 1.5-2 mm/min respectively.

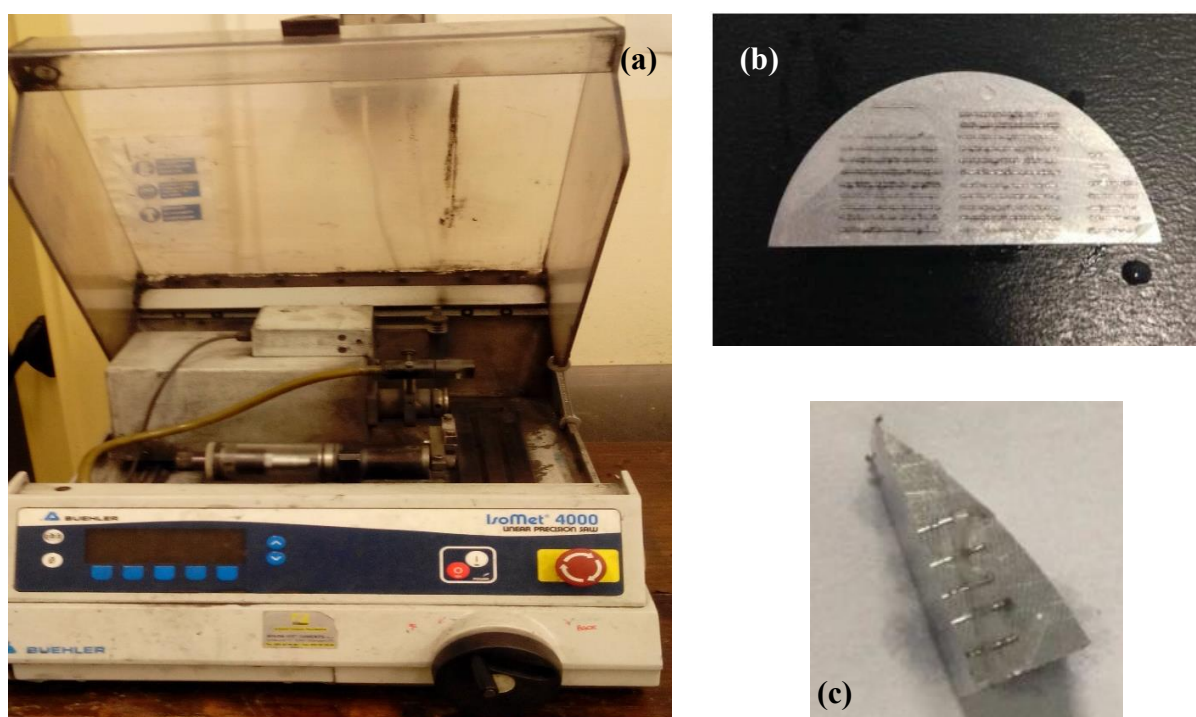


Figure 4.6 Isomet 4000 precision cutting saw utilized in thesis work (a) along with steps of sample preparation from bulk material (b and c)

Soap water was pumped at the cutting section all along the processes aimed at preventing high temperatures and subsequent damages on cutting blade and samples. All the samples were cut at the middle to eliminate any interfering effects around the borders during future analysis. Figures 4.6. b and c illustrate sample preparation steps from the built parts. Samples were placed in conductive resins before polishing for easier handling parallel to be applicable to the automatic polishing machine.

4.1.3. Polishing Machine

A Presi polishing machine modeled Mecatech 234, which is an automatic model, was applied in this thesis work to make sample surfaces crystal clear for analysis. The Schematic of this machine is depicted in figure 4.7. Various handbooks and references suggest slightly different procedures to polish aluminum alloys. However, a more conservative method was used in this thesis work to prevent excessive forces on samples due to their delicacy, especially for single and multi scan samples. In this method, single and multi-scan samples were polished with #500 sand papers until they were plain and then flatted with #800 and #1200 respectively for 3 minutes. The bed's rotational speed was kept at 300 rpm and a force of 30 N was applied on each sample. The head's rotational speed was kept at 40 rpm in the same direction of the bed. In addition, pure water was sprayed at the polishing location all along the process in order to wash any removed material from polishing spot as well as lubrication and eliminating any friction.



Figure 4.7 Image of the polishing machine utilized to prepare samples.

The prepared samples in previous step were further burnished for 3 minutes by 6, 3 and 1 micrometers diamond suspension on polishing cloths, respectively. At this step, rotational speed of bed and head was reduced to 150 and 30 rpm respectively. The applied force on each sample was reduced to 25 N for 6 and 3 micrometers diamond suspensions, while for 1 micrometer it was

further reduced to 20 N to eliminate any scratch on the surface which easily originate due to soft nature of aluminum alloys. Figure 4.8. a and b illustrate surface of typical single scan and cubic samples after tracing all steps of polishing process.

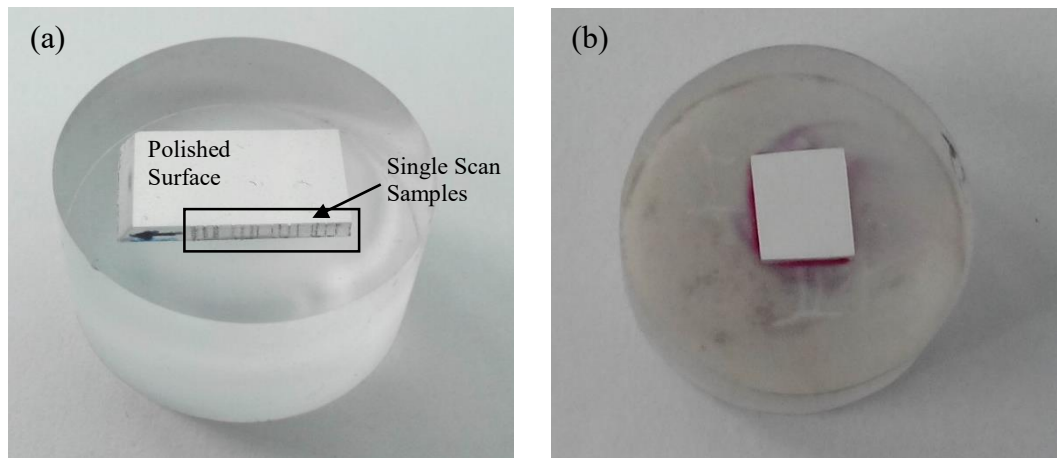


Figure 4.8 Crystal clear surface of a typical single scan (a) and cubic (b) sample after polishing process

4.1.4. Optical Microscope

Two types of Leica Fluorescence Optical Microscopes produced by Leica© Microsystems were used to observe surface of samples and take images where needed. The model of used equipment was LEICA EZ4W and LEICA DMI 5000M, the latter one being mostly use in this thesis work with the schematic represented in figure 4.9. Different magnifications on microscopes were adopted for various images which will be separately represented on each image where needed. All the adjustments of the optical microscope as well as image capturing was managed by a special software on a connected personal computer which is offered by Leica corporation for the case specific microscope.

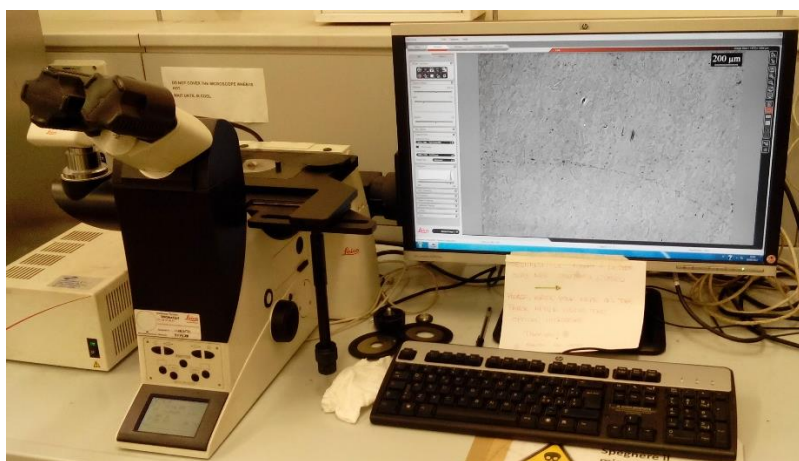


Figure 4.9 Optical microscope modelled LEICA DMI 5000M used in the thesis work

At this point of the work, it is useful to introduce principal procedure of performance of the optical microscope which was used in the thesis work. In this type of microscope, the light is radiated

towards a mirror where the mirror then reflects it towards the specimen. The reflected light through the specimen is then passed through powerful objective lenses which produces the first magnification. The magnification of these lenses is determined and it is possible to exchange between different lenses through the software to achieve different magnifications. The image through the objective lens is then magnified again by the eyepiece lens and forms the final image. The magnification of eyepiece lens is constant with value of 10x which should be multiplied with magnification of objective lens to give a total value.

4.1.5. Field Emission Scanning Electron Microscope (FESEM)

A FESEM Zeiss SupraTM 40 with the schematic depicted in figure 4.10.a was used to take images from powders before SLM process to determine their technical properties. At this point, it is beneficial to briefly introduce working principles of a FESEM equipment. The usual concept of electron microscope is similar to optical ones, with the difference of beams of electrons being used instead of light beams, as it is simply represented in figure 4.10.b. In a common surface electron microscope, electrons are liberated from a field emission source and accelerated in a high electrical field with very high voltage. Within the high vacuum column these so-called primary electrons are focused and deflected by electronic lenses to produce a narrow scan beam that bombards the object according to a scanning pattern. The strike of these electrons on sample surface results in secondary electrons to emit from each spot of the sample surface with different angles and velocities which depends on surface structure of the object. A detector attracts these secondary electrons and strikes them to a scintillator disc which contains a substance that can convert the energy of striking electrons into photons or light. The more secondary electrons reach the scintillator, the brighter the signal is at that point. This signal is amplified and transformed to a video scan-image that can be seen on a monitor or to a digital image and can be saved and processed further. All the process is performed in vacuum condition to assure that electrons are not affected by any atmospheric elements.

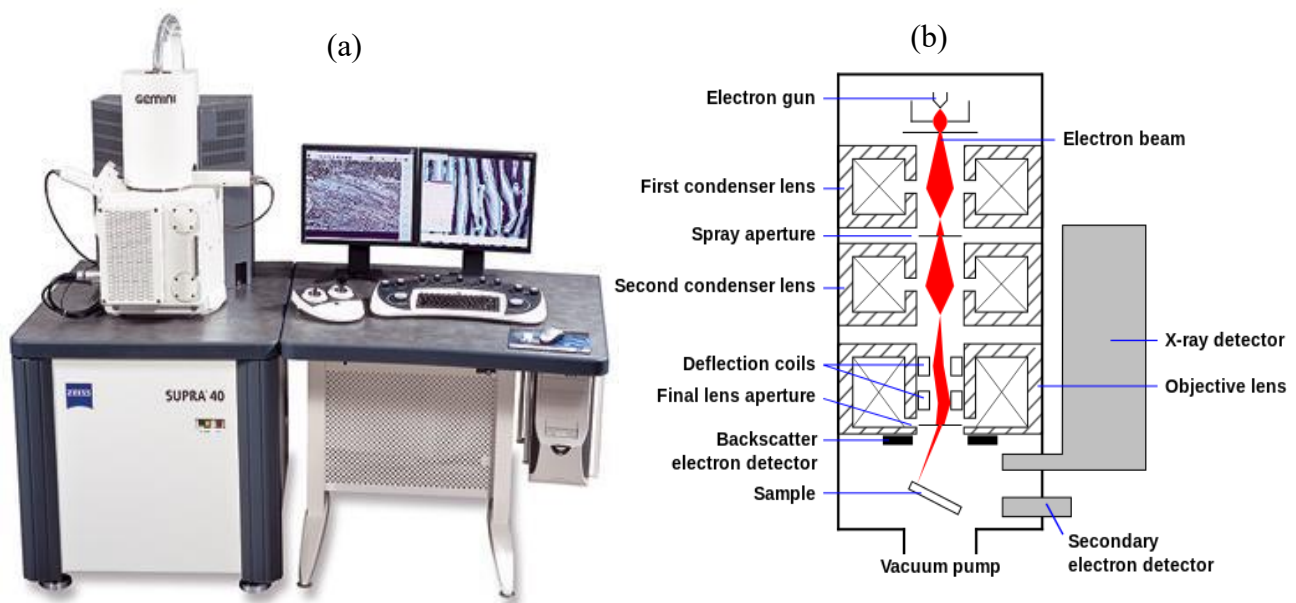


Figure 4.10 Schematic of FESEM Zeiss SupraTM 40 used in the thesis (a) and simplified working principle of this type of machine (b).

A number of common laboratory equipment was also utilized during experiments which are not explained here due to their publicity and simplicity. Precision scale, delicate handling tools, and cleaning equipment are some examples. However, we may briefly explain their application in following sections in case it is needed for better understanding the concept.

4.2. Powder Materials

4.2.1. Aluminum A357

A357 (Al-7Si-Mg) aluminum alloy (DIN designation), also known as A13570 in UNS, was the first alloy to utilize for single and multi-scan samples. This typical cast alloy is suitable for lightweight structures, especially in aerospace and automotive industries, and at the same time meets requirements for structural durability and corrosion resistance. It is usually heat treated to improve its strength characteristics, after which becomes one of the strongest sand cast aluminum alloys. A357 aluminum alloy is a good candidate to process by SLM thanks to its relatively small difference between liquidus and solidus temperature compared to other high strength aluminum alloys. It is due to the fact that its composition is close to the eutectic composition of the phase diagram Al-Si, while the presence of magnesium allows the possibility of hardening by natural or artificial aging. Existence of magnesium in Al-Si alloys enables the precipitation of Mg_2Si which will strengthen the matrix to a significant extent without compromising the other mechanical properties. The other benefit is that high thermal gradient in SLM can affect eutectic Si particles which have an undesired needle-like shape and modify them to a fibrous morphology. This transition is beneficial since existence of needle-like eutectic silicon in the Al matrix speeds up cracking and failure of the part, especially under high tensile stresses [72].

The employed A357 powder was produced by EOS GmbH company through gas atomization technique. Table 4.2 shows general composition of the powder as given by the company datasheets.

Table 4.2 General composition of A357 powder

A357 Element	Weight percent %
Si	6.5-7.5
Fe	≤ 0.1
Cu	≤ 0.05
Mn	< 0.03
Mg	0.45-0.6
Ti	0.04-0.2
Zn	< 0.05
O	< 0.2
N	< 0.2
Al	Remaining

In addition to powder composition, the shape and size of powders is very important in defining final properties of built parts. Aimed at getting idea about powder morphology, the as-received powder was scanned by Field Emission Scanning Electron Microscope (FESEM) Zeiss SupraTM 40, and result is represented in figure 4.11. As the figure shows, A357 powders have both spherical

and irregular shapes with a wide variety of dimensions. In fact, general dimension of powders starts from some microns and goes up to 50 in total, but the average remains between 30 to 35 micrometers.

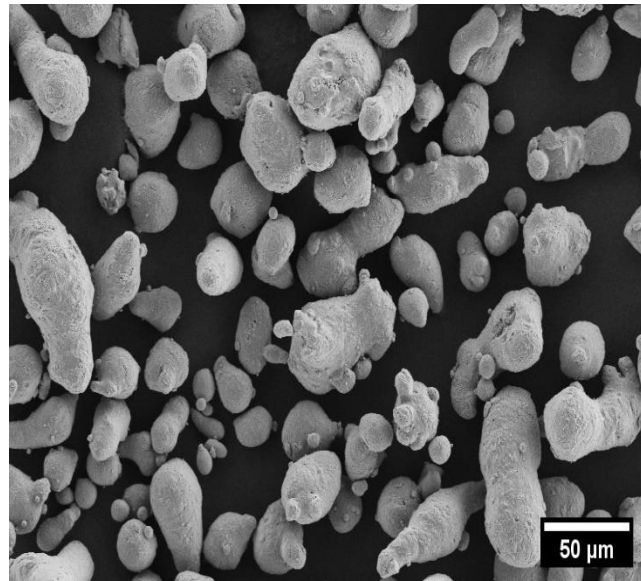


Figure 4.11 FESEM image of A357 powders

4.2.2. AlSi10Mg

AlSi10Mg aluminum alloy, known as A03600 in UNS designation, was the second alloy used in experiments to produce single and multi scan samples as well as cubic ones. This alloy offers good strength, hardness and dynamic properties and is therefore used for parts with thin walls and complex geometry subjected to high loads, like in the aerospace and automotive industries. The specific powder used in the experiments was provided by EOS GmbH company (Germany) through gas atomization process. Table 4.3 shows material composition of this alloy which is mentioned in the company datasheets.

Table 4.3 General composition of AlSi10Mg Powders

AlSi10Mg Element	Weight percent %
Si	9-11
Fe	≤0.55
Cu	≤0.05
Mn	<0.45
Mg	0.2-0.45
Ti	0.15
Zn	≤0.1
Al	Remaining

Figure 4.12 depicts the Al-Si phase diagram with the Si content of A357 and AlSi10Mg alloys hosted on it. As indicated in figure, the composition of AlSi10Mg alloy is closer to eutectic

composition in Al-Si phase diagram compared to A357, thus making it even better for SLM due to small difference between liquidus and solidus temperature.

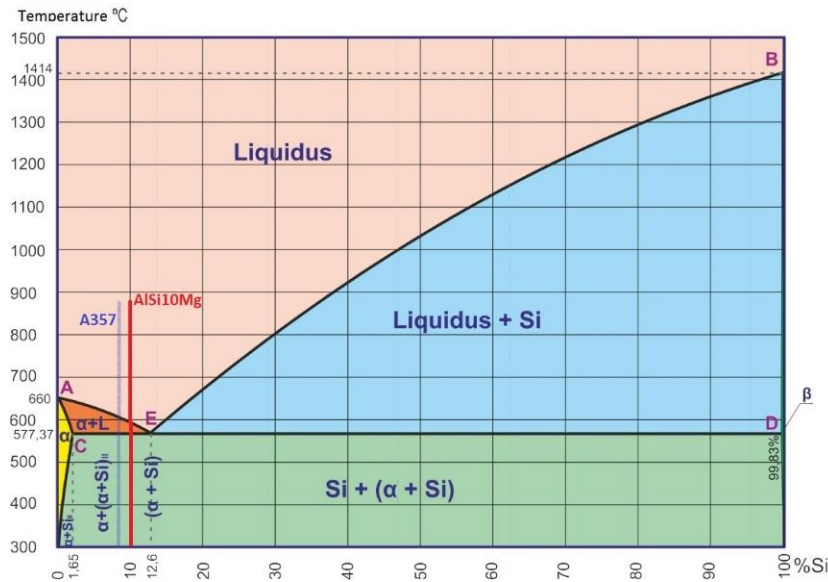


Figure 4.12 Al-Si phase diagram with designation of A357 and AlSi10Mg Si content [73]

The SLM process is characterized by extremely rapid melting and re-solidification which promises improved mechanical properties without any need for excessive heat treatments (Stress relieving is usually needed). In fact, AlSi10Mg alloy is by far the most studied and used aluminum alloy in the field of SLM. A357 is farther from the eutectic point compared to AlSi10Mg which is a sign of higher need to heat treatment for natural or artificial aging. This situation is compromised by higher percentage of magnesium as it is clear from the two tables, which is a key inscription to induce aging.

The AlSi10Mg powder morphology was depicted by abovementioned apparatus and results is shown in figure 4.13.

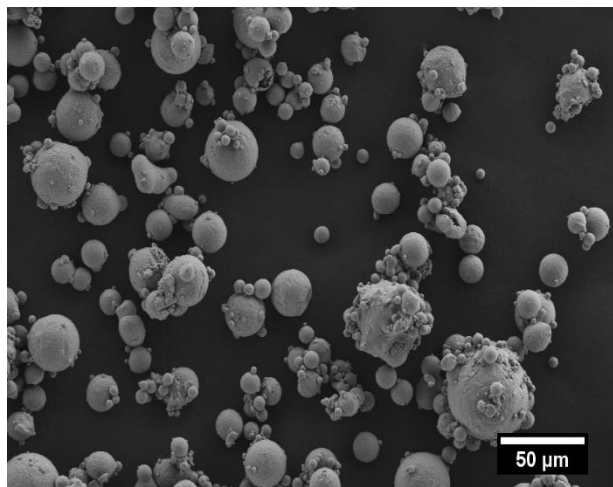


Figure 4.13 FESEM image of AlSi10Mg powders

This figure shows as received AlSi10Mg powder particles are spherical with quite regular shapes, with a wide dimension range from 1 to 45 micrometers. However, the average size of powder particles remains around 21 to 27 micrometers. The same figure shows that numerous small particles tend to agglomerate on the surface of bigger ones creating some clusters with size of 60 to 80 micrometers. This property should be considered when dealing with explanations about SLMed powder with a specific contribution to the layer thickness.

4.2.3. AlSi10Mg alloy+ Titanium diboride (TiB₂) composite nanoparticles

The third type of powder was achieved by reinforcing former alloy with nanoparticles of TiB₂. TiB₂ benefits from high elastic modulus, hardness and thermal and chemical stability and has a good wettability during SLM of aluminum alloy without any undesired chemical reaction with alloying elements. These properties have turned it to one of the most used reinforcements with aluminum matrix composites (AMCs) to improve mechanical properties. In fact, TiB₂ tends to improve laser absorptivity in SLM as well as acting as nucleus during solidification which causes finer microstructure and improves ductility [58,60].

In order to produce third group of single and multi scan samples, the AlSi10Mg aluminum alloy was mixed with 1 weight percent of nanoparticles of TiB₂ with the average particle size of 58 nanometers. The blend was dry-mixed in a ceramic jar for 24 hours to assure homogeneous distribution of nanoparticles throughout the mixture. Hence, the new composite included AlSi10Mg with exact properties explained in section 4.2.2 with composition of table 4.3, plus 1% of nanoparticles of TiB₂.

The FESEM image of selected powder is given in figure 4.14. The figure shows that TiB₂ nanoparticles are uniformly distributed on the surface of spherical aluminum alloy powders. Although it is scarcely observable that nanoparticles tend to slightly agglomerate with each other, the total grid of dispersion can still be considered uniform and without significant effect on properties of final part.

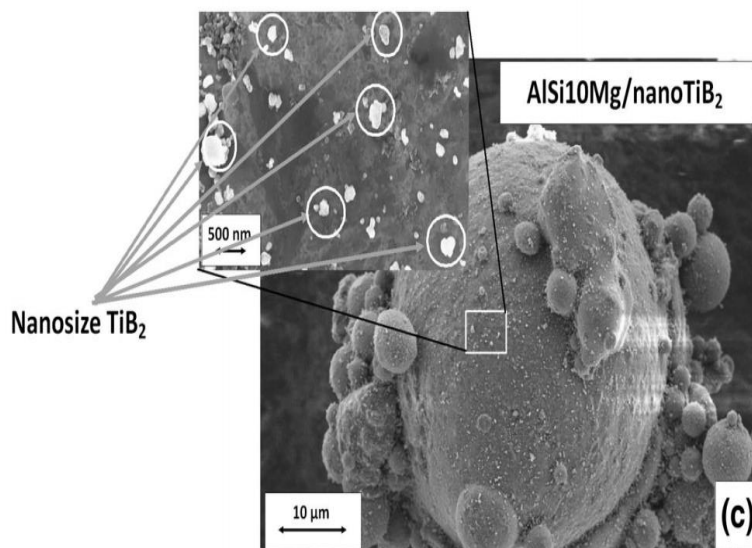


Figure 4.14 FESEM image of AlSi10Mg+ TiB₂ composite nanoparticles

4.3. Experimental Setup and sample preparation

The main goal of this study was to use analysis (mainly geometrical) on single (and multi) scan tracks in order to predict the best sets of parameters to have a final part with best possible quality, and then try to establish a correlation between quality of single scan tracks and final product. To this aim two classes of samples were required to build for analysis and any further comparison, the first class being single and multi scan samples from aforementioned three alloys and the second class being cubic samples as parts being close enough to a SLMed final product, which can be used as a reference later on. In the following, the experimental setups related to each class of samples in discussed.

4.3.1. Single Scan Track (SST) and Multi Scan Track (MST) Samples

SST samples were the ones for which the laser only scans a single straight line of the deposited powder on platform with an individual set of input parameters. On the other hand, MST samples are multi SSTs with a special hatch distance. Any modification in input parameters leads to noticeable change in SSTs and thus final parts. The input parameters we considered in this thesis work were the following:

- 1) powder material (A357, AlSi10Mg, and AlSi10Mg+nano TiB₂),
- 2) laser power
- 3) laser scanning speed
- 4) layer thickness
- 5) hatch distance
- 6) shielding inert gas in chamber
- 7) preheating temperature of platform

The first three parameters were modified for SSTs while for MSTs hatch distance was also modified. The rest of parameters were kept constant with values reported in table 4.4.

Table 4.4 Adjusting parameters on SLM machine for SST and MST samples

Parameter	Layer thickness	Adjoining Distance	Shielding Gas	Platform Temperature
Value/type	50 [μm]	0.7 [mm]*	Argon	100 [$^{\circ}\text{C}$]

* Its concept will be explained later.

Experimental setup for SST and MST of all alloys was performed in totally equal condition. To this aim, laser power and scanning speed were changed through a special applicable ranges which is represented in table 4.5.

Table 4.5 Adjustable range of laser power and scanning speed on SLM machine

Range limits	P [W]	v [mm/s]
Minimum value	60	50
Maximum value	195	5000

Design of experiments was performed based on values of table 4.5. It led to 42 different combinations of input parameters and same number of SST samples for each alloy. These combinations are represented in table 4.6.

Table 4.6 Combination of input parameters for SST samples

P [W]	v [mm/s]	P [W]	v [mm/s]	P [W]	v [mm/s]	P [W]	v [mm/s]	P [W]	v [mm/s]	P [W]	v [mm/s]
60	50	100	50	130	50	160	50	180	50	195	50
	300		300		300		300		300		300
	800		800		800		800		800		800
	1200		1200		1200		1200		1200		1200
	1900		1900		1900		1900		1900		1900
	3000		3000		3000		3000		3000		3000
	5000		5000		5000		5000		5000		5000

The table shows that power and speed of SLM machine are subsequently adjusted in six and seven values, respectively, in order to cover a wide range of these parameters and their effect on geometry of SSTs based on machine's table of parameters. As mentioned earlier in 4.1.1.2, SST and MST samples were printed on casted discs placed in negative holes on platform. The surface of disc was divided with 3mm×8mm contours to host SST and MST samples. For SST samples, two scan tracks were built inside each rectangular contour with 0.7mm distance from each other which is mentioned as adjoining distance in table 4.4. Border lines of host contour was built with equal input parameters for all samples, just for simplicity of sample designation at the end. Figure 4.15 illustrates characteristics of SST sample and rectangular contour along with an image of built sample.

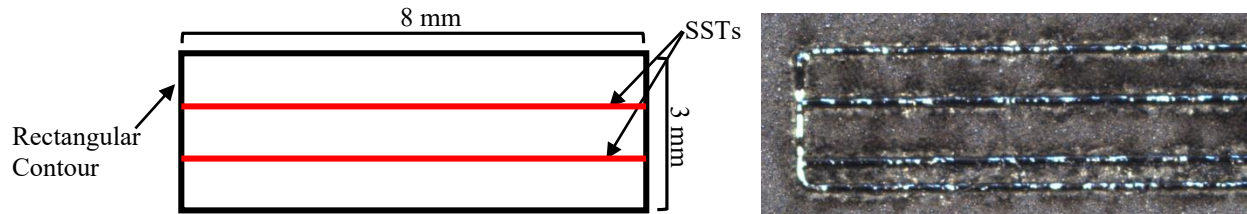


Figure 4.15 Geometrical designation of SST samples on SLM machine (left) and a typical produced sample (right).

On the other hand, for MST samples the entire contours were scanned with 12 different sets of input parameters to get a single layer of SLMed powder. However, the main focus was on hatch distance since its effect was totally neglected in preparation of SST samples. Table 4.7 reports these parameters in detail.

The number of passes that laser should take until a rectangular contour is fully scanned and a MST sample is produced depends on the hatch distance. For low values of hatch distance, the laser should travel much more passes to build a single layer, thus increasing time of process.

Table 4.7 Combination of input parameters for MST samples

P [w]	v [mm/s]	h [mm]	P [W]	v [mm/s]	h [mm]
180	300	0.07	195	800	0.17
		0.12			0.22
		0.17			0.07
		0.22			0.12
195	800	0.07	1200		0.17
		0.12			0.22

Figure 4.16 shows how hatch distance can affect number of passes of laser in a fixed area. The figure which is taken from equal surface areas inside contours shows how hatch distance can affect number of passes of laser while power and speed are kept constant. In fact, for hatch distance of 0.22mm few number of passes are enough to scan all the contour and powders in some areas remain intact and don't melt, while for hatch distance of 0.07mm numerous numbers of scans are required with considerable amount of overlapping between SSTs.

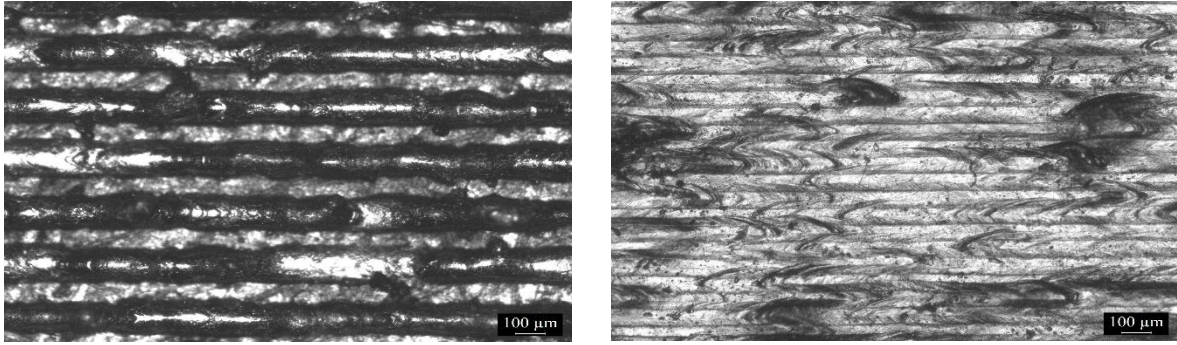


Figure 4.16 Effect of hatch distance on number of passes and time of process. Figures are for power=195 W and speed =1200 mm/s and hatch distance =0.7mm (right) and 0.22mm (left).

In order to have an efficient way of sample preparation and build all the SST and MST samples of same powder at once, the relevant rectangular contours were designed in a way to cover the area of platform discs as much as possible. Given this, all the 54 set of samples (SSTs+MSTs) for each powder were separately produced on two discs (6 discs in total for three powders). Figures 4.17 a to d show arrangement of all SST and MST samples on platform discs for a typical powder, along with their built discs in the machine.

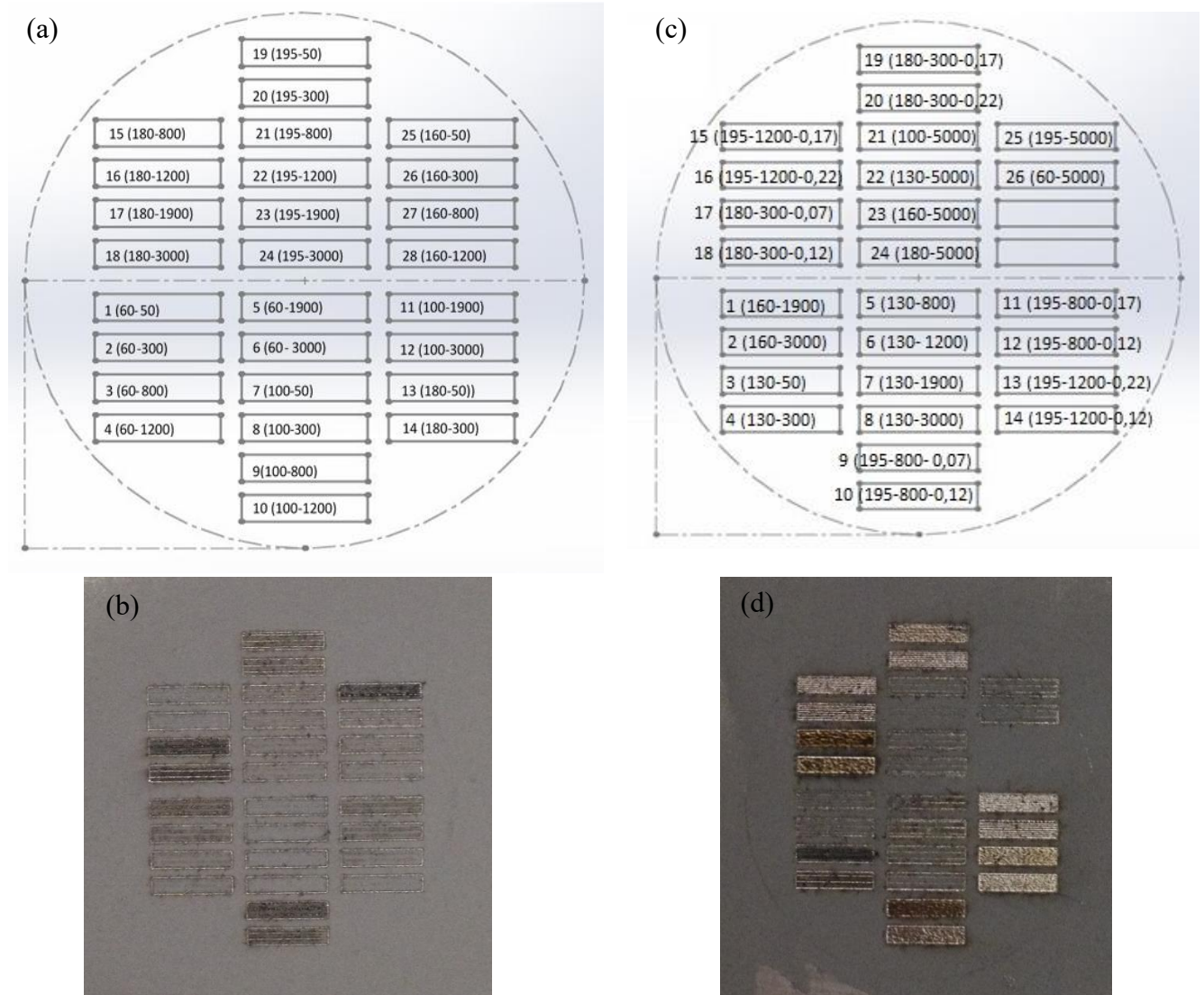


Figure 4.17 Arrangement of SSTs on first disc (a) and its built version on machine (b), arrangement of combination of SSTs and MSTs on second disc (c) and its built version on machine (d).

4.3.2. Cubic Samples

4.3.2.1. AlSi10Mg

Cubic samples were prepared in order to have a reference for comparing acquired data from SST and MST samples. The cubes were built from AlSi10Mg alloy with $1 \times 1 \times 1 \text{ mm}^3$ in dimension by setting selective parameters represented in table 4.8. Power and speed of scanning are selected in a way to cover an acceptable range of P-v diagram of AlSi10Mg alloy. The rest of parameters are kept constant for all samples which are reported in the same table alongside their values. A total number of 11 cubic samples were built for AlSi10Mg alloy on the same platform. Due to extensive range of input parameters for cubic samples, it was most likely to have some samples without any powder consolidation.

Table 4.7 Combination of input parameters for cubic samples (AlSi10Mg)

Sample Number	11	6	4	8	9	3	7	5	10	2	1
P [W]	60	100	100	100	100	130	160	195	1	195	10
v [mm/s]	1900	50	300	1200	1900	1200	50	50	300	1200	3000
Layer Thickness	50 [μm]										
Hatch Distance	0.17 [mm]										
Shielding Gas	Argon										
Platform Temperature	100 [$^{\circ}\text{C}$]										

Given this, it was decided to scan the border and number of all samples with fixed parameters in order to have simpler sample designation at the end as well as preventing deformation or destruction of fragile samples. Figure 4.18 shows produced samples on platform just after production and cleaning. As it is clear in the figure, sample 11 didn't have any powder consolidation and only borders are printed on the platform.



Figure 4.18 Cubic samples of AlSi10Mg powder after production

The focused of this thesis work was on studying effect of properties of SSTs and MSTs on quality of final part. This is why the simple scan strategy was chosen to build cubic samples of AlSi10Mg which is the most similar case to single scan tracks. The simple scan strategy includes scanning a layer with parallel tracks without any change in angle or direction of scanning in the layer and at the same time, continue scanning consecutive layers with same conditions, without any change in direction or angle of scanning path.

4.3.2.2. AlSi10Mg+nTiB₂

The other set of cubic samples were produced by AlSi10Mg+nTiB₂ MMC. The setting parameters for this group was modified with respect to its mother alloy and the main focus was driven to hatch distance changing. Table 4.8 shows sets of parameters which are used for this case. Hatch distance and thickness of layer are mentioned in the table with “h” and “t”, respectively. The rest of the parameters which are not mentioned in the table are similar to case of AlSi0Mg.

Table 4.7 Combination of input parameters for cubic samples (AlSi10Mg+nTiB₂)

P [W]	v [mm/s]	h [mm]	t [mm]
160	300	0.12	0.03
160	800	0.12	0.03
160	1200	0.15	0.03
195	800	0.17	0.03
180	800	0.15	0.03
180	1200	0.12	0.03
195	800	0.17	0.03
195	1200	0.1	0.03
195	800	0.1	0.03

Scanning strategy for this case was 67° rotating scan. It means that to scan each new layer, the scanning direction is rotated for 67°, while scanning direction will remain constant for all tracks in every single layer.

5. RESULTS, ANALYSIS AND DISCUSSIONS

As we know, engineering applications are always facing new materials with a wide range of adjustable properties. Selective Laser Melting (SLM) is therefore no exception in facing new challenges due to introduction of new powders with different compositions into machine in order to produce engineering parts. At this point of the game, the need for a very robust decision making process is revealed to produce the final part with lowest cost, wastes, powder consumption, and in the shortest period of time. Hence, the decision maker should be able to find the best matched parameters of SLM machine for the new powder while respecting lowest cost and time duration. At the moment, the common effort in handling new powder composition for SLM is to design a set of experiments based on different setting parameters of the machine and then try to produce small parts (Cubes or Cylinders), each one with a special bunch of input parameters. The produced parts are then cut from the substrate and sent for further analysis. At the final stage, the acquired data are analyzed in order to choose the best ones to be set on the machine for final part production. Although the acquired data that an engineer decides to analyze usually depends on the process and requirements of final product, porosity is always an influential factor needed to be considered. At this point, if the acquired data is not satisfactory and much weaker than directing the engineer to a final decision, the input parameters will be expanded in numbers and/or ranges to expand the effective area on the process and all the work is subsequently repeated. Such a strategy is by far the accepted one by industrial and academic centers to produce a final part with optimized properties. However, it is not a free of cost issue and one can argue on following disadvantages that rises during applying this method:

1) Duration of the work: it is clear that SLM processes take a long time to produce a set of samples due to the nature of the process especially necessity of feeding very thin layer in each sequence in order to let it diffuse to previously built structure. This problem is highly empowered when it is needed to produce lots of samples due to the extent of number and range of input parameters. For example, if we consider the “Factorial Design” as the method of experiment for a process of two effective parameters, namely power of the machine and scanning speed with two different values each, the total number of $2^2=4$ samples should be produced by SLM machine and then analyzed at the next steps. However, if analysis revealed no satisfaction and the designer decides to add two other values to scanning speed and power (now with 4 values for each), the number of samples to be produced increases dramatically to $2^4=16$. Knowing the fact that it is not strange to have a bunch of parameters on the machine and a big variety of them, one concludes that production time (that is already high enough) increases exponentially in case of any reformation in experiments.

2) Cost of the work: It is enough to talk in the engineering way to say that “Time is money”, so when time duration of process is longer, the process would become more expensive. Nevertheless, one can still argue about the fact that when a number of cubic samples are to be produced for analysis, a special amount of powder should be fed to the machine in order to make samples. The more the number of samples, the more it becomes the needed powder and cost of preparation. It may not be the vital case for the cheap and disposable materials. But when it comes to more advanced cases where price is not negligible, any attempt is welcomed in order to reduce powder

consumption. In some cases, having expensive powders may direct decision maker to try to confine some parameters or their range of variety with the purpose of having lower number of samples to produce. It can also happen when the attempt is focused on time duration and the final part is needed to be produced as quickly as possible.

Cost and time limitation may also direct decision maker to restrict some parameters or their range of variety with the purpose of getting the results as quickly as possible. Although this settlement may lead to some results, there is the risk of losing interesting information about the nature of process and material in neglected regions. Other case specific problems may also rise while facing new materials. All in all, the so called “Rapid Manufacturing” method may no longer remain rapid.

Given all the above mentioned, Single and Multi Scan Track (SST and MST) Analysis is introduced as a useful way to eliminate the two problems of cost and time to a reasonable extent. In this method, the designer is free to design experiment with any number of parameters, because eventually there is no need to make a cube for a set of them but instead, only a single line or layer on the substrate is scanned for each set of parameters. In such a case, even if the number of classified parameters is too high, the time and cost of optimization still remains very low.

It is logical to claim about low time and cost of this method, because producing a single line on the surface of substrate for each set of parameters only needs a single pass of laser beam on that line. So the time of sample production can be considered negligible compared to the case of cubes. On the other side of the coin, not only the process has lower expenses due to less time duration, but also the amount of powder needed to produce single and multi scans is also negligible. However, discussion about benefits of this process cannot last forever and sooner or later, some vital questions start to rise in the mind about effectiveness and uncertainties of the method. Some vital cases of these questions are:

Knowing the fact that the cross section of single scan lines is very small, what parameters can be studied instead of density or porosity of the samples?

Does this method really work? Considering that thermal effects that are highly effective in SLM are almost negligible in this case? And some others.

In this chapter of the thesis work, we are going to answer to such questions in detail and draw a benchmark for future investigations, as well as plotting a process window for each type of powder. This goal is achieved by means of analysis of results of detailed experiments on three different aluminum alloys (as represented in previous chapter), discussing results based on phenomenological facts, and support or compare them where needed. However, before going into details it is worth mentioning that since we had three types of powder alloys, it was decided to represent all data and discuss them in a comparative way between three powder types so that the reader faces a more organized template for massive amount of data, and at the same time compare different results for each alloy and its counterparts. Meanwhile, due to high number of samples for each alloy and in total, there will be a massive amount of numerical data for all alloys that should be truly represented. Otherwise, the reader will be misled into enormous amount of numbers without getting a clear idea about behavior of alloy (s) and effect of parameters. So it was decided to eliminate mentioning numerical values in this chapter and all trends will only be explained

through relative graphs in a comparative way. However, all of the numerical values will be cited in case specific tables in appendix so that the reader could refer to them where needed.

This chapter is divided in three sections based on three main group samples that are to be discussed. The first section covers all data related to Single Scan Track (SST) samples. It includes two main parts which are related to on-top and cross sectional analysis of SSTs. In order to study any aspect of SSTs, all findings related to the three alloying powders are mentioned and compared together so that the reader keeps pace with the text. The second section is related to Multi Scan Track (MST) samples in which all experimental results related to MSTs of three alloying powders are represented. And the final chapter is devoted to cubic samples, where all findings related to two groups of cubes are separately represented and discussed.

5.1. Single Scan Track (SST) Analysis

5.1.1. On Top Analysis (Longitudinal)

Considering a SST sample reveals that there are two geometrical aspects that can be studied in order to define stability of SLM process. The first one is longitudinal properties which refers to shape and stability of scanning track along its length (on top), and the other one is properties of cross section of the track when it is cut in the middle (melt pool). In majority of literatures, researchers study only one geometrical aspect of scan tracks without any considerations to the other one that leads to non-completed results which cannot be used with enough assurance. Since the two aspects need totally different analysis and considerations, we discuss about the first one in this part and leave the latter one to be addressed in next part.

At a very first step of the work, it was tried to use visual inspection on top of SST samples to determine stability of their track line. Observing the top of SST samples of different alloying powders by naked eye didn't reveal too much information since it is very small in dimension to be watched in details. However, looking at all samples under the optical microscope with 50x magnification showed there is a meaningful similarity between some groups of samples in term of dimensional properties, regardless of the type of aluminum alloy powder which was used for it. Given this, five different groups of samples were recognized based on the shape of the track line. Figure 5.1 illustrates typical shape of a scan line which is expected in each group. It shows that scanning a line of aluminum powder with predefined parameters produces a shape similar to one of figures a to e which refer to no powder deposition, balling, thin and stable, irregular shape, and too thick tracks, respectively. As it is obvious from images and definitions, parameters that result in thin and stable track lines are supposed to be the preferred ones to produce parts with least level of porosity.

The general concept of (volumetric) energy density in figure 5.1 has already been defined in section 3.3.1.1. However, it is repeated here again by equation 5.1 for sake of simplicity:

$$VED = \frac{P}{vth} \left(\frac{J}{mm^3} \right) \quad (\text{Eq. 5.1})$$

Where P (W) is laser power, v (mm/s) is scanning speed, and t and h (mm) are layer thickness and hatch distance, respectively.

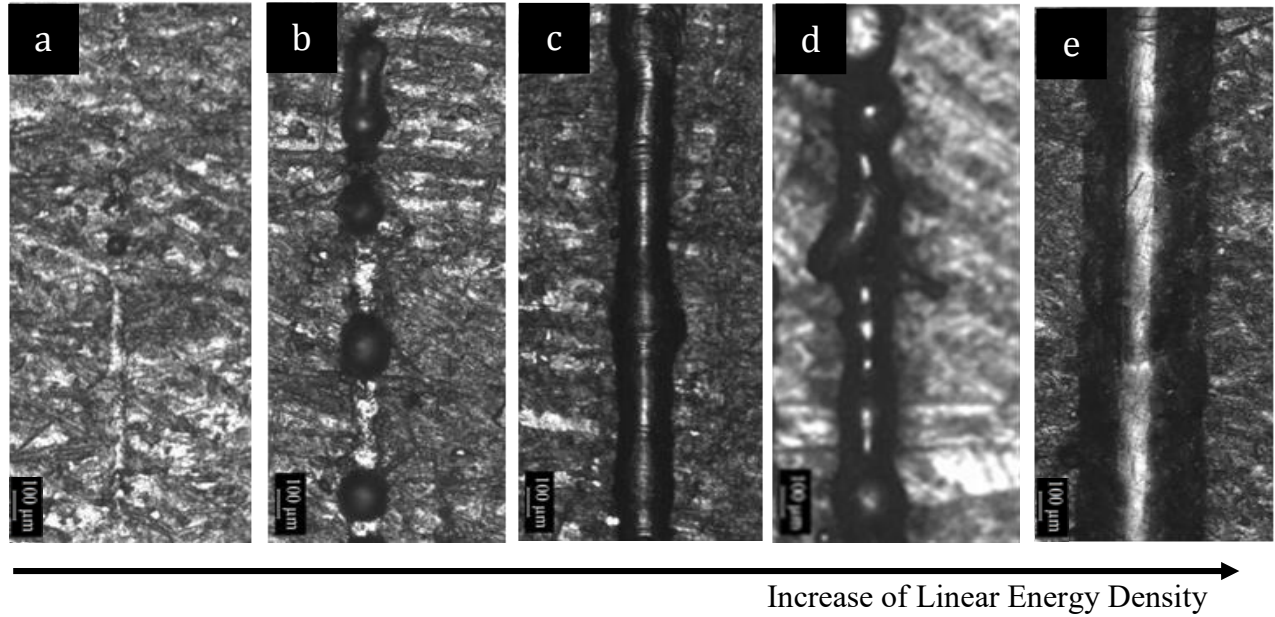


Figure 5.1 Classification of typical SST samples based on the shape of their track lines. a: Not Enough Deposition, b: Balling, c: Thin & Stable, d: Irregular, and e: Too Thick

Nevertheless, layer thickness was considered constant for all SST samples of this thesis and therefor can be eliminated due to comparative nature of study. Further, speaking about hatch distance is meaningless in single scan strategy which leads to elimination of this parameter from equation and defining a compatible factor known as Linear Energy Density (LED). It can be defined as follows:

$$LED = \frac{P}{v} \left(\frac{J}{mm} \right) \quad (\text{Eq. 5.2})$$

Where its building parameters have already been introduced. LED/VED is by far the most important parameter in SLM which increases by increasing power or decreasing scanning speed. Turning back to figure 5.1 shows how increasing this parameter affects powder consolidation and enhances the amount of molten powder. It shows that when amount of input LED is low, it is not enough to melt powders and only a slight sign of scanning (or nothing) appears on surface, while with increasing LED the amount of powder consolidation increases until at some points, a thin and stable track is formed which is consider as appropriate shape of track in SLM process. Any further increases in LED leads to instability of melt pool or over-dimensioned tracks which are of no interests.

All on top images of SST samples of the three aluminum powders were taken by optical microscope and grouped on a parametric graph based on classification of figure 5.1. The two parameters of LED, namely power and speed, were considered as key figures which led to graphs represented in figures 5.2 to 5.4 for A357, AlSi10Mg, and AlSi10Mg+nTiB₂, respectively (Nanoparticles of TiB₂ will be called nTiB₂ from now on). These graphs provide a good reference as process window of the material in which the reader can see and compare different shapes of scan tracks and their changes with respect to LED parameters. As previously noted in table 4.6, seven different values of scanning speed are studied for SST samples while graphs 5.2 to 5.4 only host six values. It is

due to the fact that in all three types of powders, scan speed of 5000 mm/s resulted in no powder deposition and so it was decided to be eliminated from all graphs which doesn't make any inconveniences.

It is worth mentioning that data related to AlSi10Mg alloying powder was taken from a parallel thesis work done by Moshiri (2016) which is represented in reference 74 (except for data related to cubic samples which are done in this thesis and do not exist in reference 74). These data are mentioned here for comparative reasons and are used in two types. The first type which is mentioned by its reference number (74) is pure data, meaning that all data are exactly inserted here without any modification or changes, while for the second type, data are mentioned without the reference number which means modification, changes, or extra analysis is done on pure data of reference 74 which cannot be found in its mother reference. This policy is performed to clearly address the reader to concept and extent of each study.

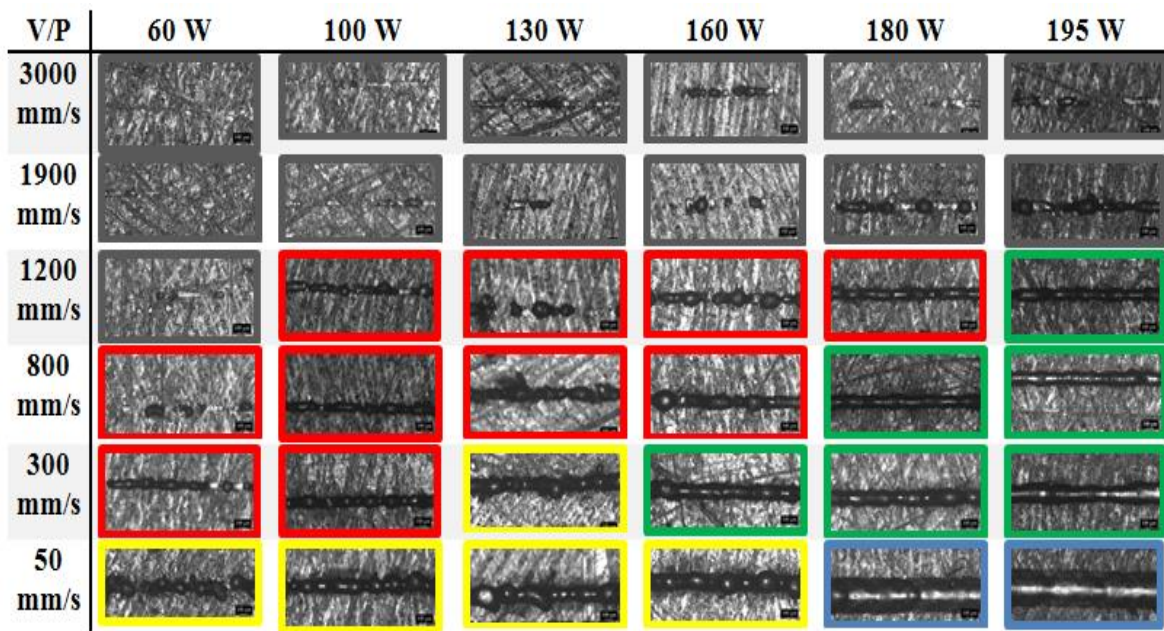


Figure 5.2 Classification of SST samples based on stability, case of A357 alloying powder. Black: not enough deposition, Red: balling, Green: thin and stable, Yellow: irregular, Blue: too thick

Figure 5.2 illustrates different classes of SST samples of A357 alloying powders versus changes in laser power and scanning speed, i.e. LED. LED increases from top-left of graphs to bottom-right which causes a striking increase in consolidated powder. The graph shows that increasing scanning speed above a threshold for any power value deteriorates stability of process and increases balling and discontinuous tracks, while increasing power usually moves the process towards stability and continuous tracks. The bottom of the chart shows that very high LEDs is also not suitable for process since accumulation of excessive thermal in the melt pool causes instability and irregular shapes. Further, the graph shows that range of stability of process to produce thin and stable tracks (green color) for A357 alloy is very limited compared to total range of parameters (6 out of 36 setting parameters). This is a sign of delicate or hard SLM processability of this alloying powder.

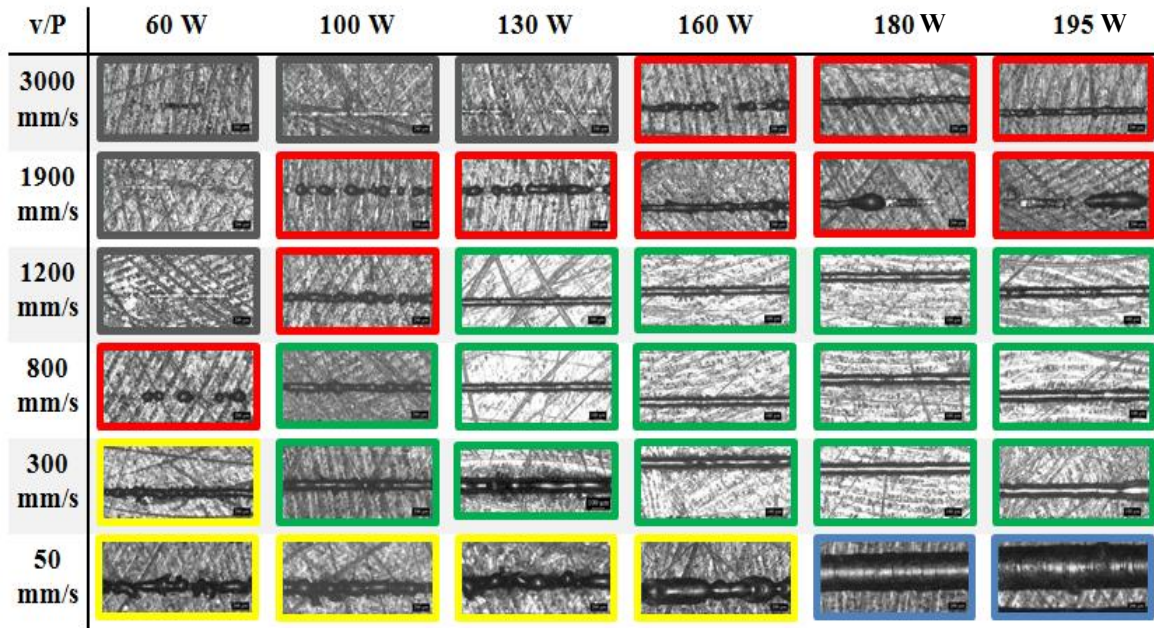


Figure 5.3 Classification of SST samples based on stability, case of AlSi10Mg alloying powder [74]. Black: not enough deposition, Red: balling, Green: thin and stable, Yellow: irregular, Blue: too thick

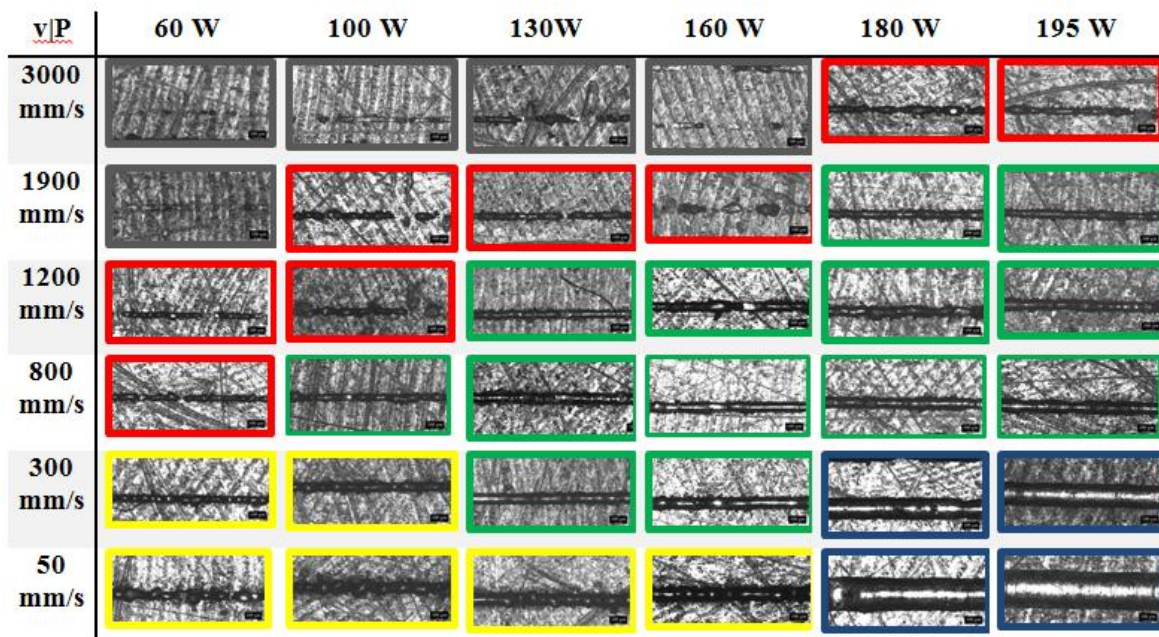


Figure 5.4 Classification of SST samples based on stability, case of AlSi10Mg+nTiB₂ alloying powder. Black: not enough deposition, Red: balling, Green: thin and stable, Yellow: irregular, Blue: too thick

Figure 5.3 shows process window of AlSi10Mg alloying powders with respect to power and scanning speed. It shows similar behaviors as A357 with respect to energy density, but with striking changes in borders of regions. In fact, powder consolidation is much higher than A357 which resulted in much broader area for balling and thin and stable tracks, along with a tiny area for no deposited powders. The extensive region for thin and stable tracks (14 out of 36 setting parameters)

can be a sign for incredible SLM processability of this aluminum alloy and the reason for it as being the most used aluminum alloy in SLM.

The last figure of the group (5.4) illustrates process window of AlSi10Mg+nTiB₂ alloying powders with respect to LED. It shows similar results to its mother aluminum alloy with some slight changes in borders of regions. In fact, borders of thin and stable tracks extended to broader scanning speed values and the number of too thick tracks has increased as well. It is usually due to improved absorptivity of laser which is proven to happen by Chen et al (2017) as a result of addition of TiB₂ nanoparticles [60]. As a matter of fact, increasing absorptivity causes more energy to be inserted into the melt pool which results in more powder consolidation for any range of speeds. Comparing graph 5.4 with 5.3 also shows the new metal matrix composite is a very good candidate for SLM due to its ability to produce thin and stable tracks in a wide variety of power and speed ranges.

A more compact representation of figures 5.2 to 5.4 is illustrated in graphs 5.5 to 5.7 (left) in order to have a clearer view of process window of each alloy. The borders of each class of sample is also plotted to distinguish abrupt changes in geometry alongside the length of tracks. These graphs are far more simple to understand process window of three aluminum powders and provide a robust way to compare results with each other. On the right side of same images, different classes of samples are represented with respect to combination of power and speed, i.e. LED (in logarithmic scale). The above mentioned deductions which were driven from figure 5.2 to 5.4 can be seen in these graphs with more clarity. However, having classifications based on energy density reveals new aspects of process which are of high importance.

Figure 5.5 right represents classes of different samples of A357 alloy based on LED. The most striking deduction from this graph is that although LED is the most important factor in SLM of different powders, it cannot always guarantee the best results if individual parameters and interaction between them is neglected. For example, the same values of LED close to 0.1 J/mm can result in no deposition or balling, or values close to 0.4 J/mm can produce either irregular or thin and stable tracks. So LED cannot lonely determine optimal conditions of SLM process and is only a criterion to show the amount of energy that is received by a unit length of a single scan track. However, a range of LED should be determined in which the process is mostly probable to produce thin and stable tracks (range of LED for green line). Given all the above mentioned, optimal LED selection is a necessity in SLM process in order to produce best-shaped tracks, but it's not sufficient. It means that in order to assure thin and stable tracks, effect of power and scanning speed should be considered separately parallel to their role in LED.

Referring to case of A357 in figure 5.5, results shows that usually high range powers (more than 160 W) along with medium range speeds (between 300 to 1200 mm/s) can produce stable tracks, provided that the fraction P/v falls in optimal range of LED (green line in right graph). The same conclusions can be used for the other two alloys due to similarity of trends. Nevertheless, a broader range of power (100 to 195 W) with respect to A357 case can also be used while the range of speed is the same. It can be a sign of better processability and absorptivity of AlSi10Mg and its reinforced composite with respect to the other alloy.

The final point to translate from graphs is about having an estimate of the level of significance of power and scanning speed in SLM of the three alloys. Considering figures 5.5 to 5.7 (left) one can

conclude that throughout a wide range of power, the machine tends to produce similar shape tracks while increasing speed significantly changes classes of tracks.

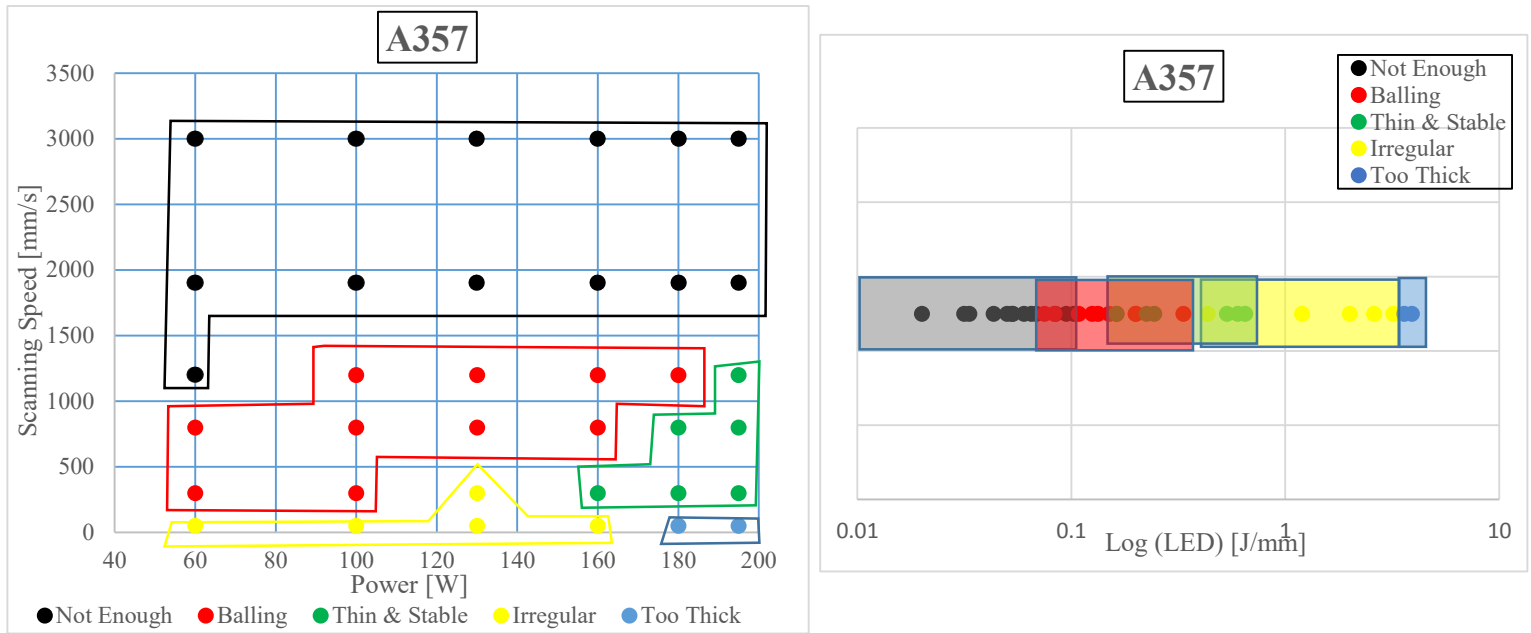


Figure 5.5 SLM Process window of A357 aluminum alloy (left) and Scan track classification based on Linear Energy Density (LED) for the same alloy (Right)

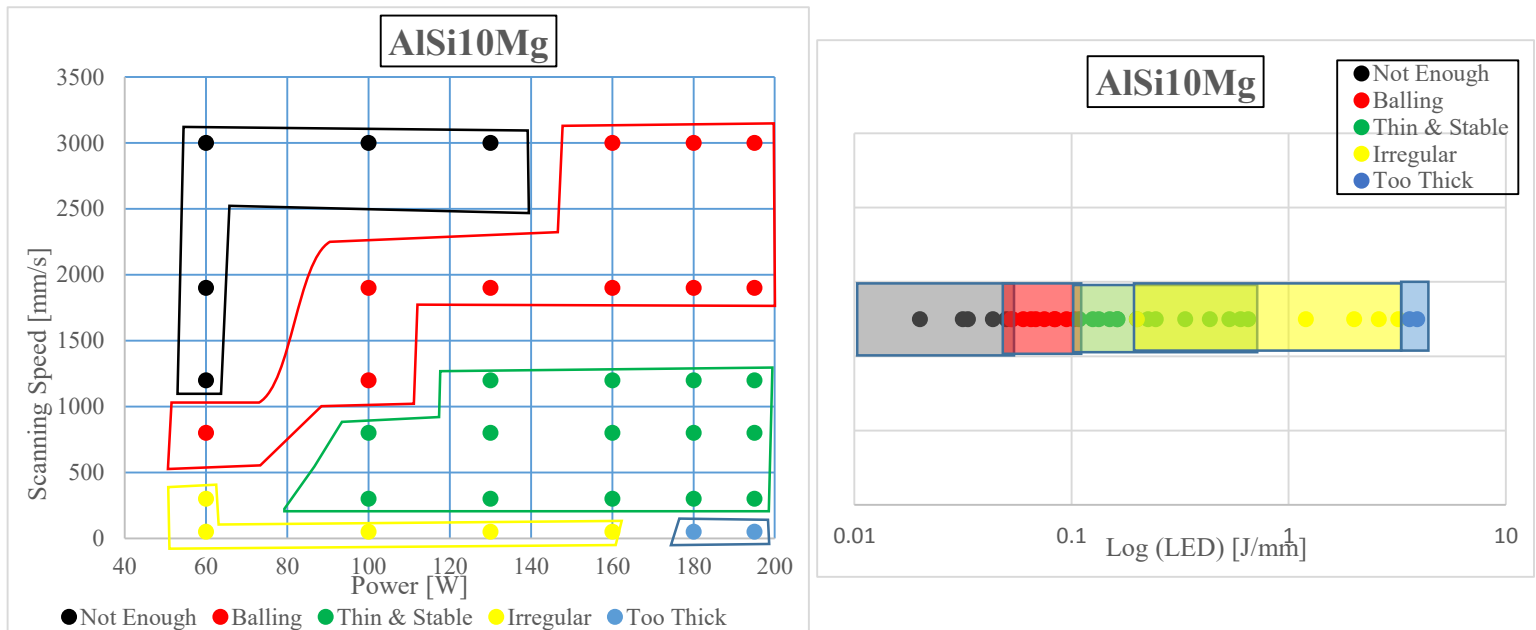


Figure 5.6 SLM Process window of AlSi10Mg aluminum alloy (left) and Scan track classification based on Linear Energy Density (LED) for the same alloy (Right)

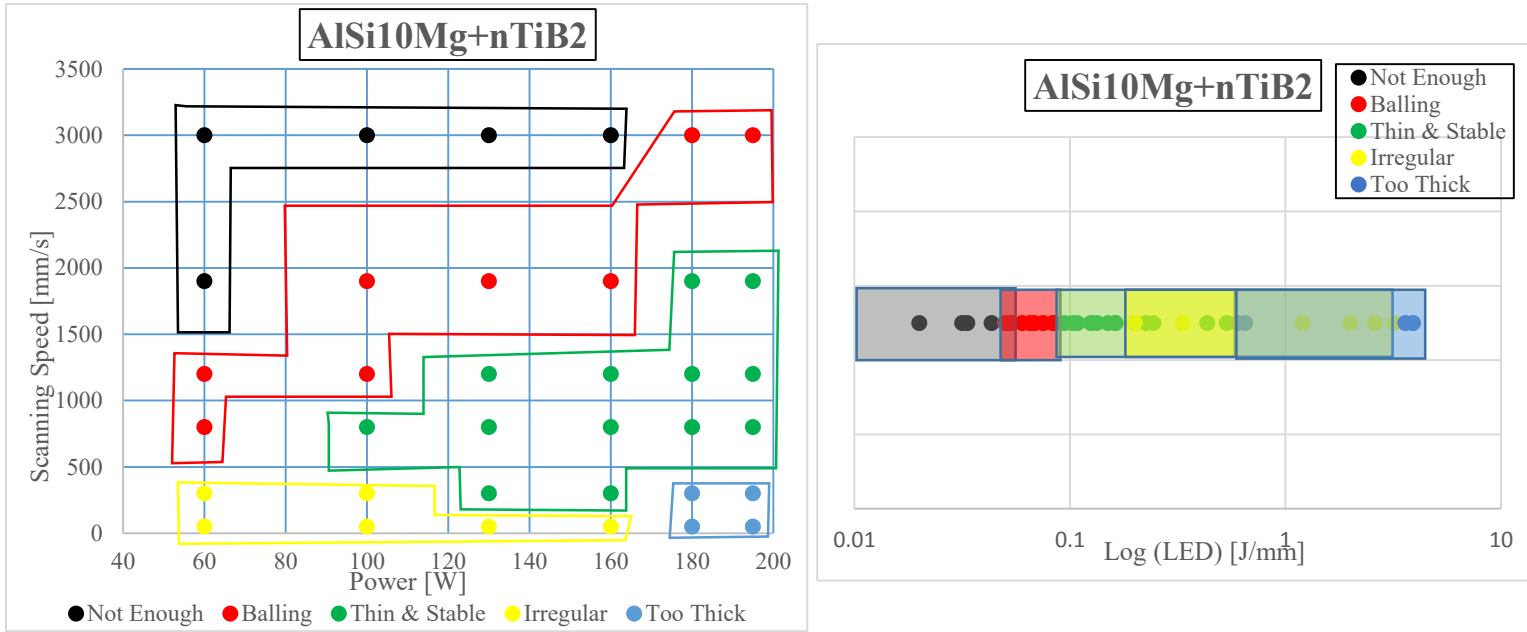


Figure 5.7 SLM Process window of AlSi10Mg+nTiB₂ aluminum alloy (left) and Scan track classification based on Linear Energy Density (LED) for the same alloy (Right)

It can be seen by the fact that drawn borders for groups of samples are more stretched in direction of power axis rather than scanning speed. It means that laser power earns more significance in producing stable tracks which stands with findings by Yadroitsev et al (2012). Meanwhile, regions of thin and stable tracks (with green borders) tend to extend by increasing power and shrink by increasing speed. For example, the stable region in figure 5.5 shows that increasing power from 160 W to 195 W extends stability from one value of speed to three values, while in the same region increasing speed from 300 to 1200 mm/s compresses stability from three values of power to one value. Such a trend shows that increasing laser power extends the stability range for different values of speed which is compatible to results mentioned by authors of reference 68.

Visual inspection used in abovementioned classification was proven to be a useful tool to investigate stability of scan track along its length. However, engineers prefer to mention and analyze results with numerical values since visual inspection can lead to slightly different values if it is done in different conditions (different people, different microscope magnifications, etc.). In other words, it can be used to have a general overview of the process window but any detailed analysis on results is required to be done with more precise methods of measurements. A number of various methods could be used to specify numerical values to on-top images of single scan tracks, but it is preferred to use a simple method which hosts aspects of visual inspection and at the same time, provides an effective and complete vision of track shapes. Aimed at this, on-top width of each scan track was measured in different points and acquired values were used for further analysis.

In order to have the same condition of measurements for all tracks, an equal grid was allocated to all tracks using the Open Source ImageJ software. and width of tracks was measured at intersection of tracks and grids using the same image processing software. This method is illustrated in figure 5.8.

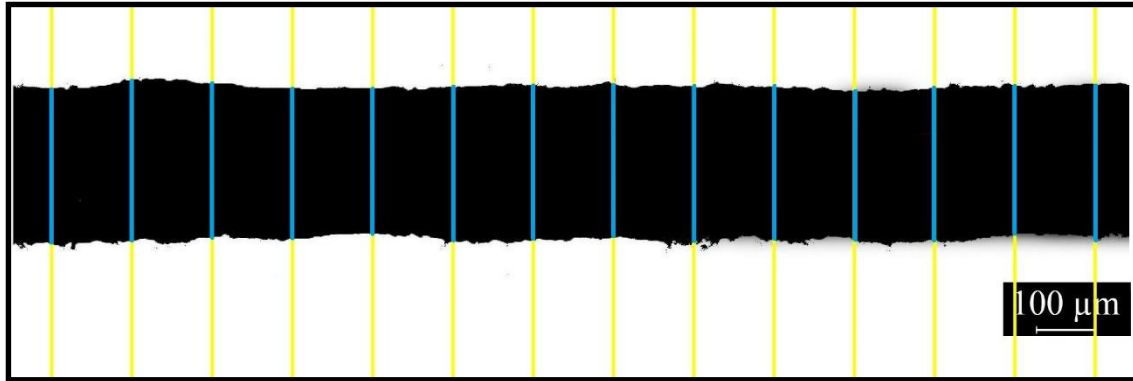


Figure 5.8 Preparation of an on-top image of a typical SST sample for measurements. Blue lines are measured as on-top width.

Figure 5.8 which is typical shape of a “too thick” sample shows how an image is prepared for on-top image measurements. Having equal grids for all samples assures equal conditions for all of them while stretching grid along the scan line imports any effect of instability into measurements. Length of blue lines was measured for all samples and average value of measurements as well as standard deviation was calculated. The length of blue lines for regions of samples with no powders deposition (like in not enough deposition and balling samples) was defined equal to zero which implies a high value to standard deviation and shows high instability. Using this method, standard deviation of samples with no powder deposition will be equal to zero which is a sign of something unusual in results. This strategy also affects mean value and will be discussed in detail in the following.

Figures 5.9 to 5.15 illustrates graphs of average width size and standard deviation of on-top width measurements for SST samples which are plotted based on increasing order of energy density for three types of alloying powders. The five classes of samples mentioned in graphs, namely, not enough, balling, thin and stable, irregular, and too thick, are taken from classification in graphs 5.2 to 5.4 since the main goal here was to specify numerical values to previous graphs.

Figure 5.9 represents graph of on top average width of SST samples of A357 alloying powder versus logarithmic scale of LED. As the graph shows, there is a usual increasing trend for average width versus LED while some irregularities are seen especially for irregular and balling classes. Also the left side of graph shows that there is a threshold of LED before which the laser is unable to melt any powder on platform. However, the most interesting point about this graph is that thin and sable tracks show a regular increasing trend versus LED compared to other types. In addition, there is a narrow band of 120 μm to 175 μm track width in which tracks could be thin and stable while tracks out of this band loose their stability. A better interpretation of this graph could be done by considering standard deviation of measurements which is illustrated in figure 5.10.

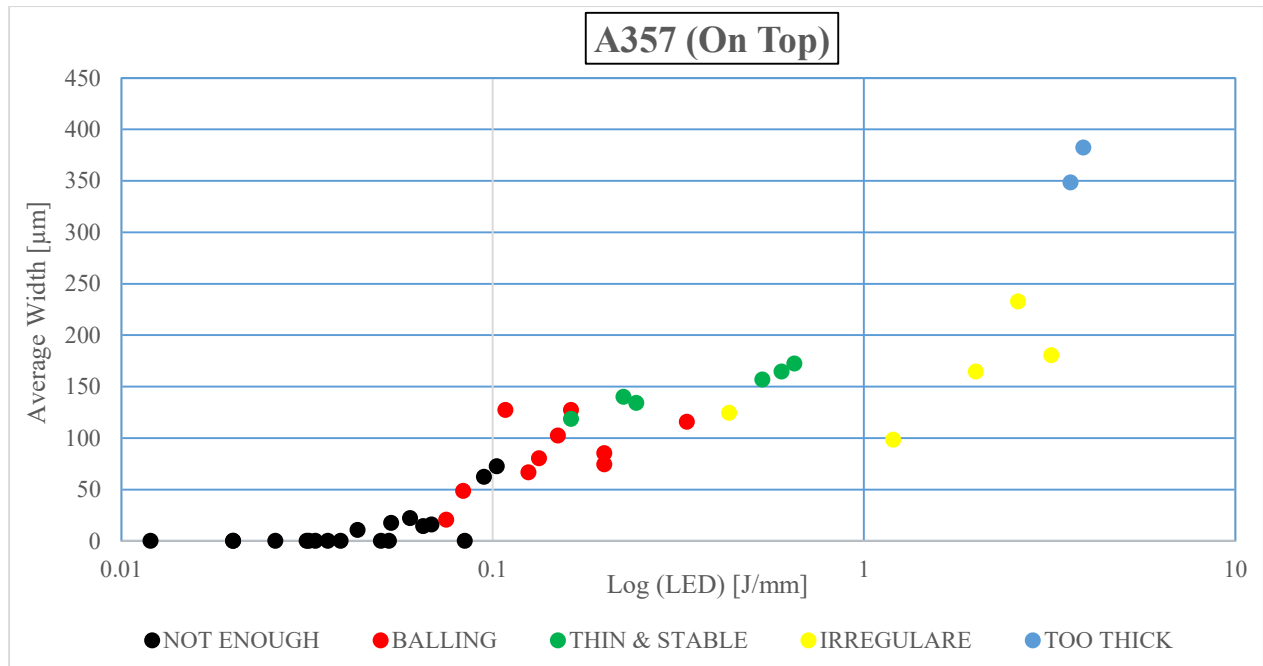


Figure 5.9 On top average width of SST samples versus LED, case of A357 alloying powder

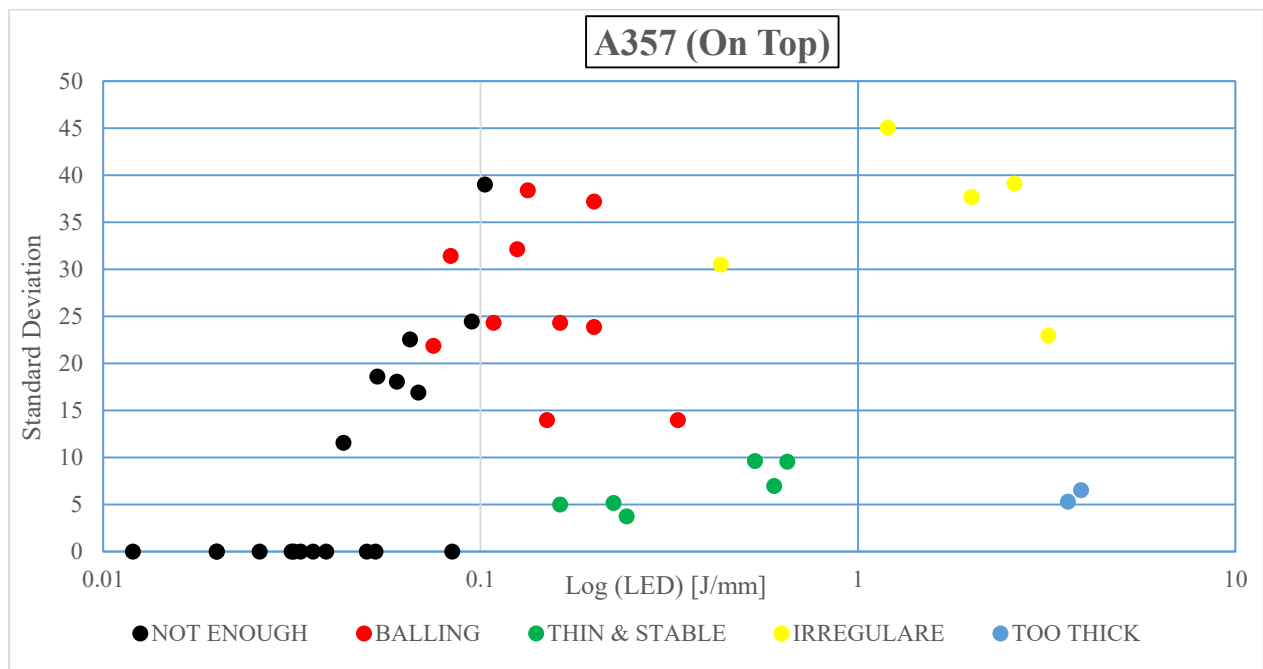


Figure 5.10 Standard deviation of on top measurements versus LED, Case of A357 alloying powder

The concept of standard deviation here shows stability of process, because it logically shows how typical measurements along blue lines in figure 5.8 are different from mean width value. Hence, a high standard deviation is a sign of instability of scan tracks which results in different width dimensions along length of track, while zero standard deviation shows no powder deposition. Referring to figure 5.10 shows that standard deviation ranges for thin and stable tracks as well as

too thick tracks is very low which shows stability of tracks. On the other hand, the other three classes have very high standard deviations with dramatic fluctuations in their values. At this point it becomes clear that although figure 5.9 shows almost similar scan width for thin and stable and irregular tracks, figure 5.10 shows that irregular tracks cannot be used to produce a perfect part since the stability along this type of tracks is brutal.

Similar graphs for second alloying powders, i.e. AlSi10Mg, are portrayed in figure 5.11 and 5.12. figure 5.11 illustrates the graph of on top average width of SST samples versus LED for different classes of samples of AlSi10Mg. The graph shows that there is an increasing trend for average width with respect to LED which is similar to A357. However, the range of average width for thin and stable samples has increased between 100 μm to 245 μm which shows better processability of the powder with respect to A357. Figure 5.11 should be analyzed parallel to figure 5.12 which shows standard deviation of measurements versus LED for the same alloy. As figure 5.12 represents, standard deviation of thin and stable tracks as well as too thick tracks is very low (between 5 to 15) while it hardly increases for other types of samples. This figure shows that irregular samples have very high standard deviation which makes them unsuitable for production purposes, although their average width is similar to thin and stable tracks in figure 5.11. On the other hand, too thick tracks show very low standard deviation for both alloys, as well as very high average width. However, this type of track is not appropriate for production and the reason will be discussed in following sections when dealing with cross section analysis.

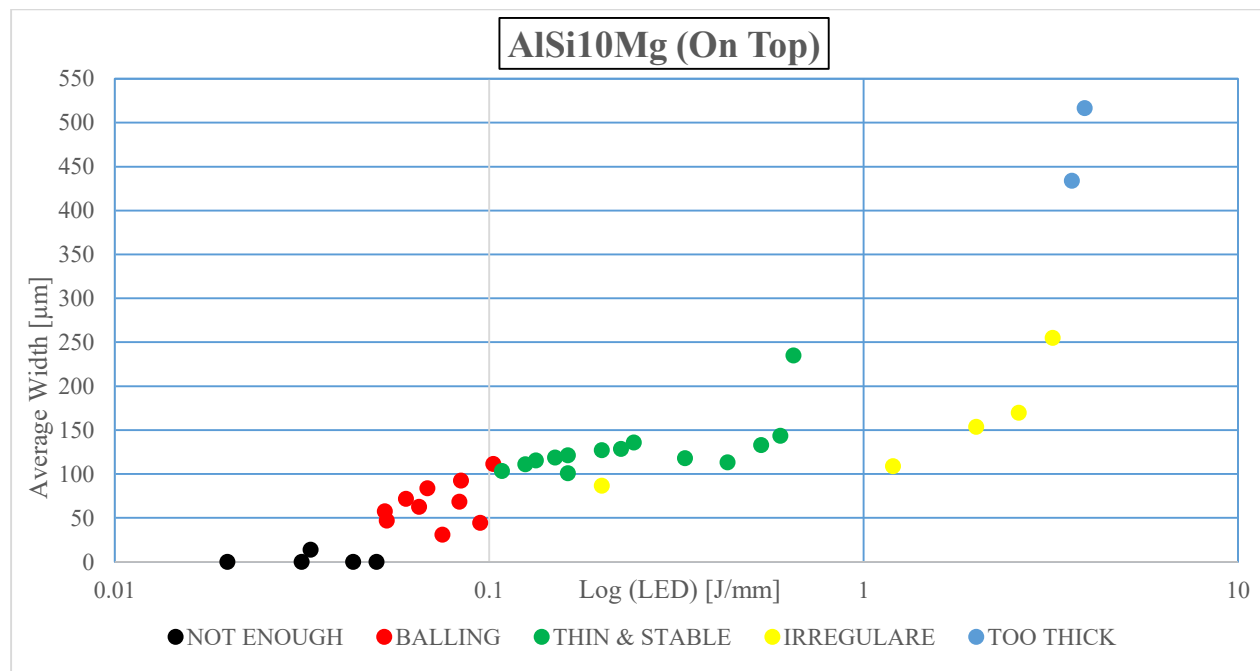


Figure 5.11 On top average width of SST samples versus LED, case of AlSi10Mg alloying powder

The final interesting point in graphs of the two alloys is that tracks with balling show highest level of fluctuations in their trend versus LED with respect to other tracks. It could be due to nature of balling which happens by formation of spherical shapes out of molten powder which highly affects the measurements. Having a look at numerical values reveals that for a special value of power balling increases with increasing speed. It shows that scanning speed is a very important factor in

formation of this type of tracks, and it should be chosen with extreme care in order to eliminate this phenomenon along every single scan.

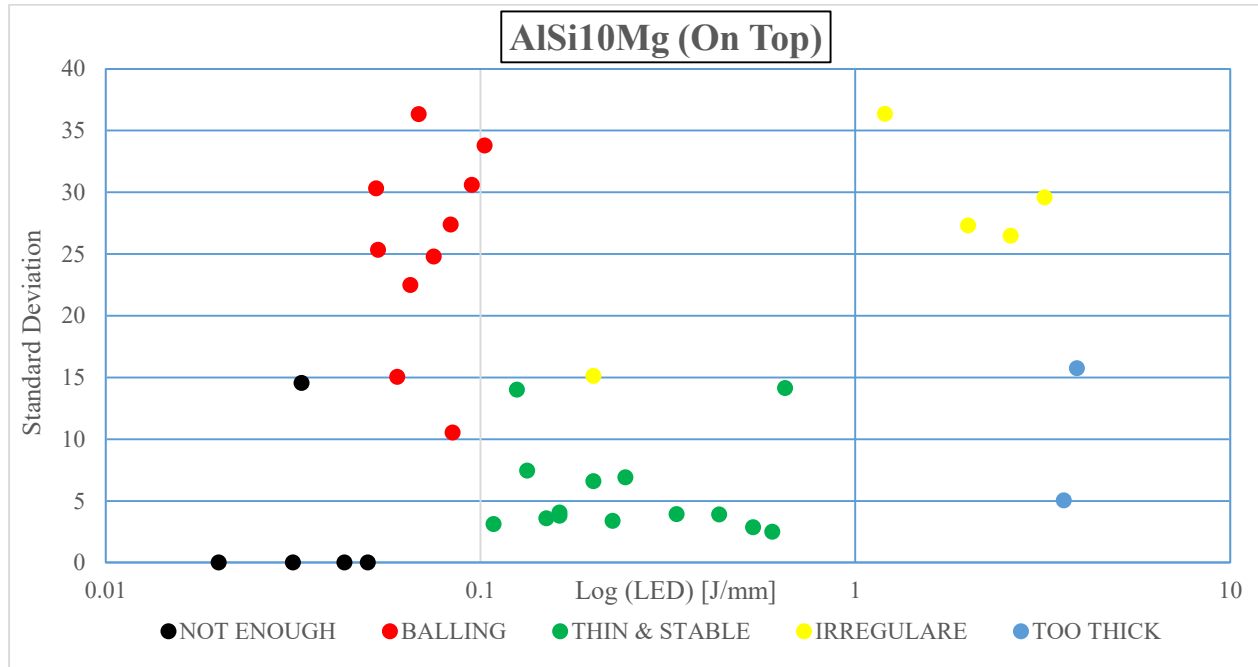


Figure 5.12 Standard deviation of on top measurements versus LED, Case of AlSi10Mg alloying powder

The same graphs for the last powder are plotted in figure 5.13 and 5.14. Figure 5.13 shows average width of scan tracks versus LED for AlSi10Mg+nTiB₂. The graph shows that range of average width for this metal matrix composite is slightly higher than other alloys in some areas of thin and stable tracks, while it becomes slightly lower than AlSi10Mg for irregular and balling tracks. However, more samples are entered into too thick group which can be due to increased absorptivity thanks to addition of TiB₂. Standard deviation of the same alloy versus LED is represented in figure 5.14. The figure shows that standard deviation of thin and stable samples is between 2 to 12 which is very close to values for other two alloys and at the same time meets requirements for stability of scan line. On the other side of the coin, too thick tracks show very low standard deviation (about 3) with almost no fluctuation which is a sign of perfect stability. The wild fluctuations which was clear for balling tracks of other two alloys is not the case here but rather, balling tracks show a smoother trend with respect to LED. Comparing graphs of 5.11 and 5.13 shows that each two graph have very similar behaviors with respect to LED with slight changes in numerical values. In the meantime, comparing graphs of standard deviation for the alloy and composite (i.e. 5.12 and 5.14) shows that addition of TiB₂ nanoparticles slightly decreases instability of tracks along their length which can be seen in decreasing standard deviation values.

We close this part by a short comparison of on top measurements for all three alloys based on LED. To this aim, a combination of average width graphs based on LED for three alloys as well as standard deviations are made which are represented in figures 5.15 and 5.16, respectively. Figure 5.15 which is related to average width shows that ascending behavior of three alloys versus LED is quite similar. However, lots of time width of scan tracks for A357 is lower than its other counterparts which can be due to weaker processability of this alloy.

Recalling figure 4.12 from previous chapter shows that A357 has lower silicon content which makes its viscosity higher and also decreases laser absorption. It results in lower melt pool temperature and smaller dimensions.

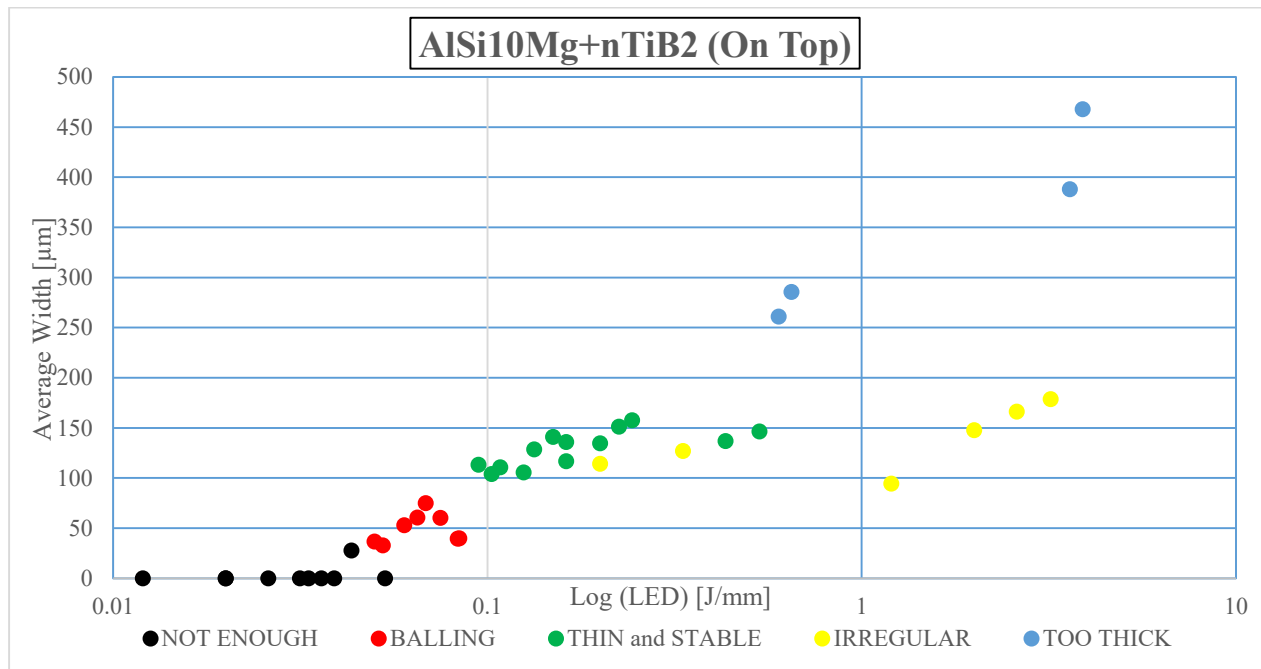


Figure 5.13 On top average width of SST samples versus LED, case of AlSi10Mg+nTiB₂ alloying powder

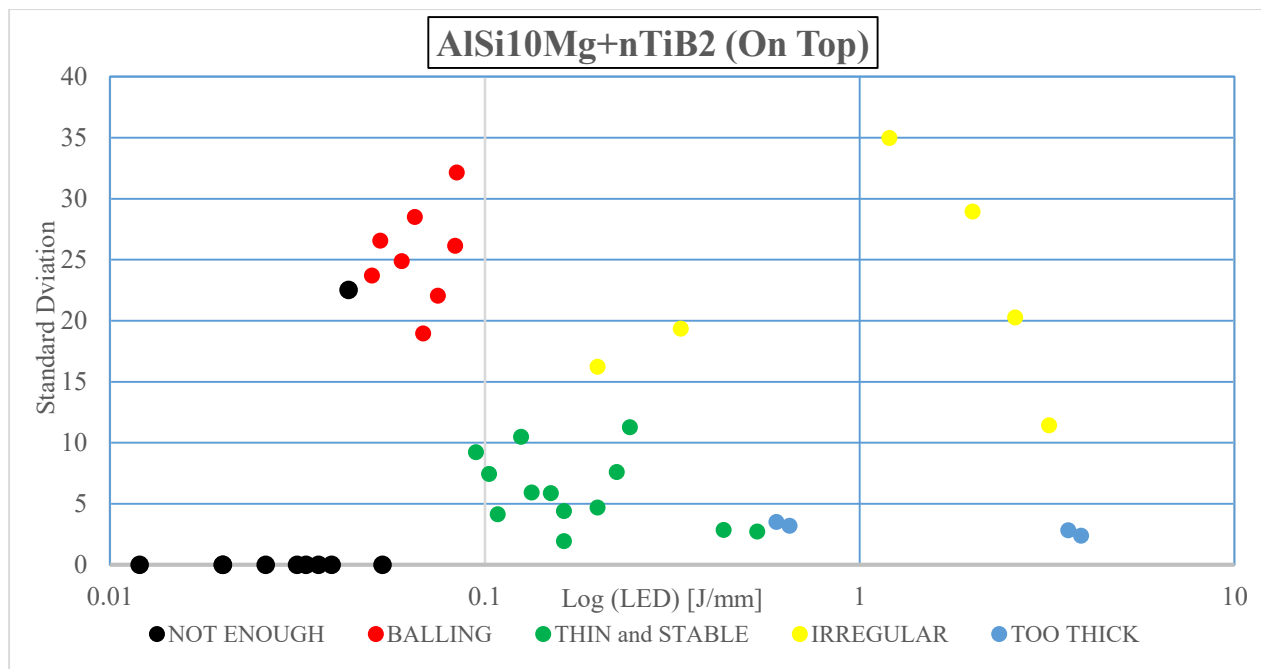


Figure 5.14 Standard deviation of on top measurements versus LED, Case of AlSi10Mg+nTiB₂ alloying powder

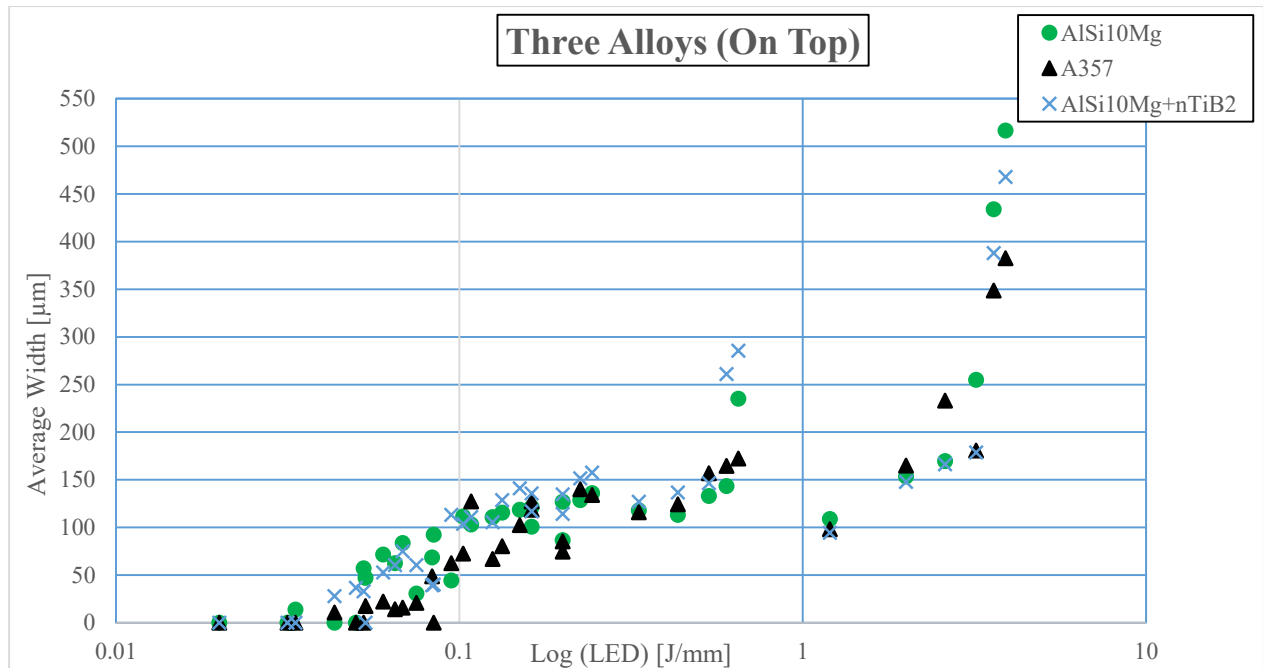


Figure 5.15 On top average width of three aluminum alloys based on Linear Energy Density (LED)

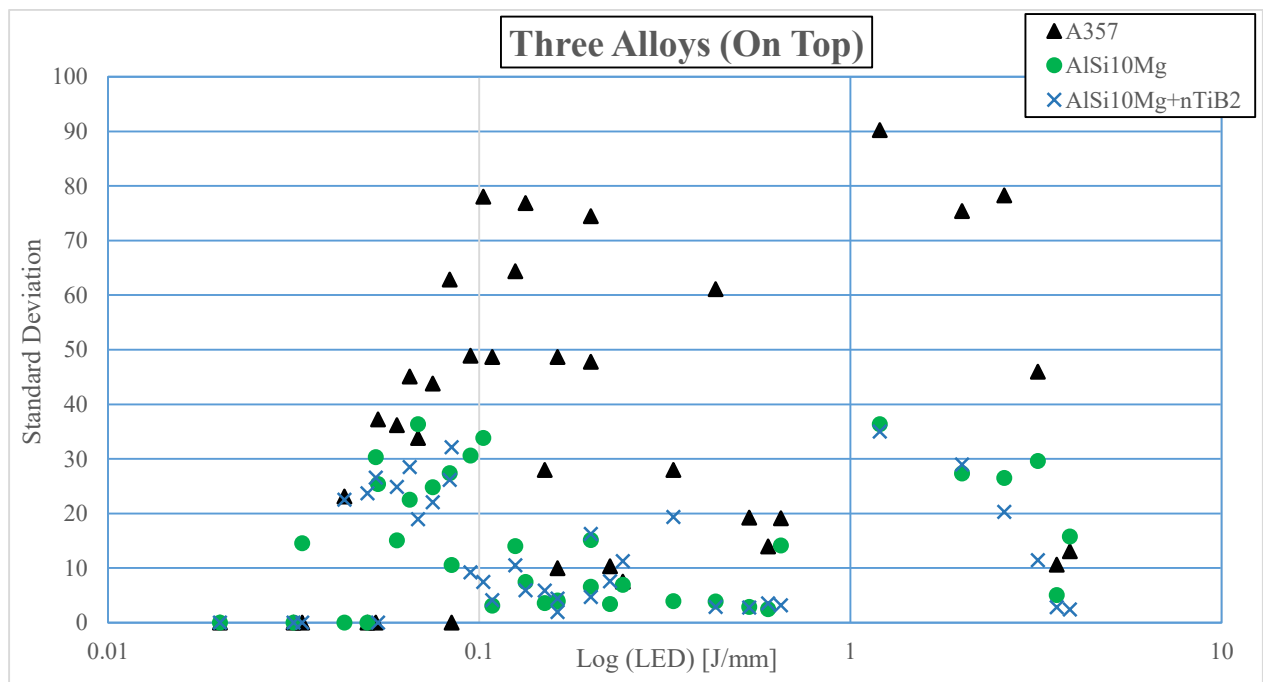


Figure 5.16 Standard deviation of on top measurements for three aluminum alloys based on Linear Energy Density (LED)

It is logical to consider that values of LED between 0.1 to 1 J/mm are most possible to lead thin and stable tracks (this supposition is true based on previous graphs for three alloys, figures 5.9 to 5.14), we can see that in this area AlSi10Mg+nTiB₂ tracks have the highest track width, while before and after these values AlSi10Mg is the foremost. It means that addition of TiB₂ composites

can lead to lower energy consumption or reducing process time while having desired tracks. The subsequent graph which is designed based on standard deviation illustrates that A357 samples always tend to have much larger values for standard deviation. It means that SLM process of this alloy leads to much more unstable tracks and process planning and control for this alloy will be very difficult compared to the other alloys. On the other hand, AlSi10Mg and AlSi10Mg+nTiB₂ keep the pace with each other with minor tolerances which were briefly discussed in previous graphs.

5.1.2. Cross Sectional Analysis

Cross sectional analysis of scan tracks refers to measurements of geometrical aspects of a single scan track when it is cut in the middle. In other words, the geometrical aspects of the melt pool at the point of cutting are measured and analyzed in this section. In order to be able to see the melt pool geometry, all samples were polished carefully to very high surface quality and observed under the optical microscope. Figure 5.17 a shows how cross section of a typical scan track seems under the microscope and geometrical parameters that can be measured on it, and case b in same figure shows a real image of melt pool with 200x magnification.

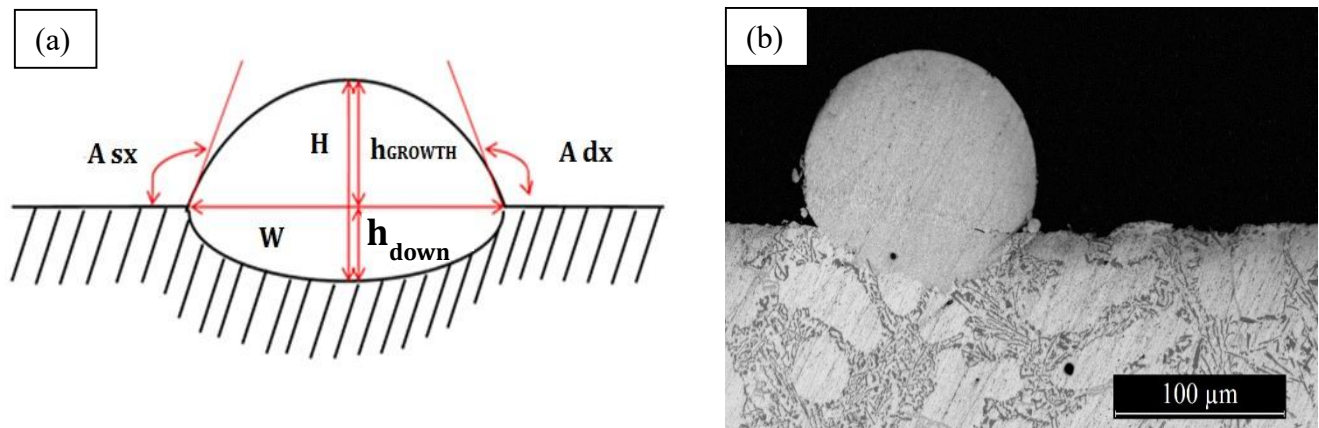


Figure 5.17 Expected shape of cross section of a single scan track under the microscope with its geometrical parameters (a), and a typical real shape under the microscope (b).

As figure 5.17.a represents, a typical scan track in total can have seven geometrical values to measure which are as following:

- H : Total depth of fusion of track
- W : Width of track at points of intersection with substrate surface
- h Growth/Upper Depth/Wetting distance: Vertical distance between track head and substrate surface
- h Down/Depth/Lower Depth: Vertical distance between substrate surface and bottom of melt pool.
- A_{sx} & A_{dx} : Left and right angle with respect to surface substrate. An average of the both will be used later.

- Area: Total area of the melt pool.

Before going to geometrical measurements, a pictorial graph similar to ones for on top images was made in order to get an overview about cross sectional shape trends based on input parameters. These graphs are illustrated in figures 5.18 to 5.20 for A357, AlSi10Mg and AlSi10Mg+nTiB₂, respectively. For samples with not enough deposition, there could either be nothing on substrate or very small deposition which is not enough to be considered as a track. Hence, for this type of sample the cross section may be seen with no effect (in case that cutting point is not at deposited area) or very small powder consolidation (in case that cutting section is at deposited area) in some rare points. We left an empty space for the first cases since only the substrate surface was observed under the microscope.

Figure 5.18 illustrates the pictorial graph of cross sections for A357 based on power and scanning speed. The graph shows that increasing power results in larger cross sections as well as more diffusion into substrate, while increasing speed reduces size of tracks and causes lower diffusion into substrate.

P/V	60 W	100 W	130 W	160 W	180 W	195 W
3000 [mm/s]						
1900 [mm/s]						
1200 [mm/s]						
800 [mm/s]						
300 [mm/s]						
50 [mm/s]						

Figure 5.18 Cross sectional view of SST samples based on input parameters, Case of A357. Black: not enough deposition, Red: balling, Green: thin and stable, Yellow: irregular, Blue: too thick

A quick view to the same graph shows that thin and stable tracks are those in which there is a reasonable diffusion of track into substrate while at the same time, the amount of consolidated

powder above the substrate is sufficient, too. Meanwhile, balling and too thick tracks are two ends of ruler where in the first one there is lots of powder consolidation above the substrate with negligible diffusion into it, while in the latter case majority of molten powder is diffused into substrate creating an oversized track. Irregular tracks can have reasonable shapes in some cases which is pretty much like thin and stables. However, it must be pointed out that from what is recalled from on top analysis, this type of track cannot hold a property along its length and the perfect cross section is only at the point of cutting. This issue reveals the importance of studying scan tracks along length and cross sections, since only studying one dimensional aspect can lead to uncertain results.

A similar graph for case of AlSi10Mg is plotted in figure 5.19. While this graph holds all general details explained for A357 case, cross sections seem to be more regulated in shape. The most striking feature of this graph is that a slight increase in diffusion into substrate is observed with respect to previous alloy. It can be mentioned as a key reason for the fact that a number of setting parameters for A357 which lead to balling tracks result in quite thin and stable ones for AlSi10Mg, because the latter powder is able to diffuse more amount of deposited powder into substrate and make thin and stable tracks instead of balling.

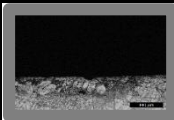
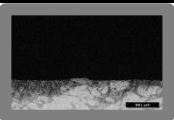
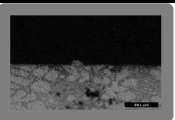

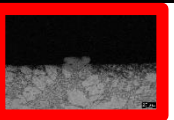


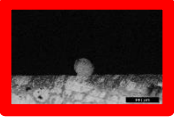
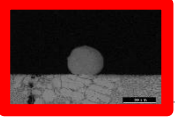

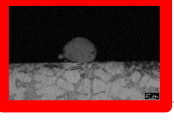
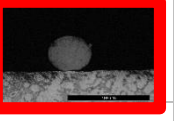

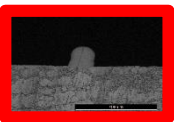
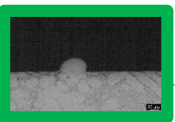
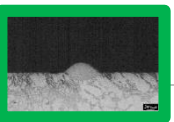
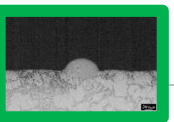
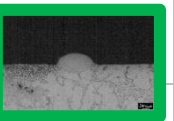
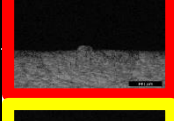
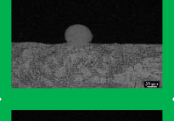
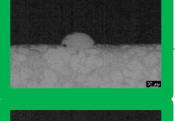



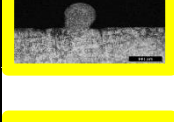


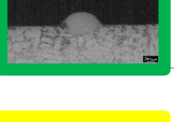
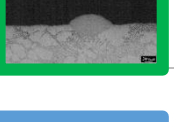
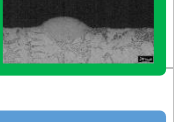


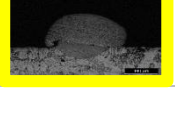
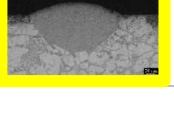
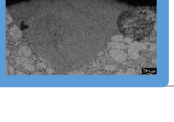

P/V	60 W	100 W	130 W	160 W	180 W	195 W
3000 [mm/s]						
1900 [mm/s]						
1200 [mm/s]						
800 [mm/s]						
300 [mm/s]						
50 [mm/s]						

Figure 5.19 Cross sectional view of SST samples based on input parameters, Case of AlSi10Mg. Black: not enough deposition, Red: balling, Green: thin and stable, Yellow: irregular, Blue: too thick. Images are taken from [74].

The schematic of final pictorial graph for AlSi10Mg+nTiB₂ is illustrated in figure 5.20. while the graph holds general details discussed for other alloying powders, it represents slightly higher diffusion into bed which especially at the final end of power axis. It is interesting to note that for each alloy, the cross sectional shape of thin and stable tracks is similar while it changes for other track types from case to case.

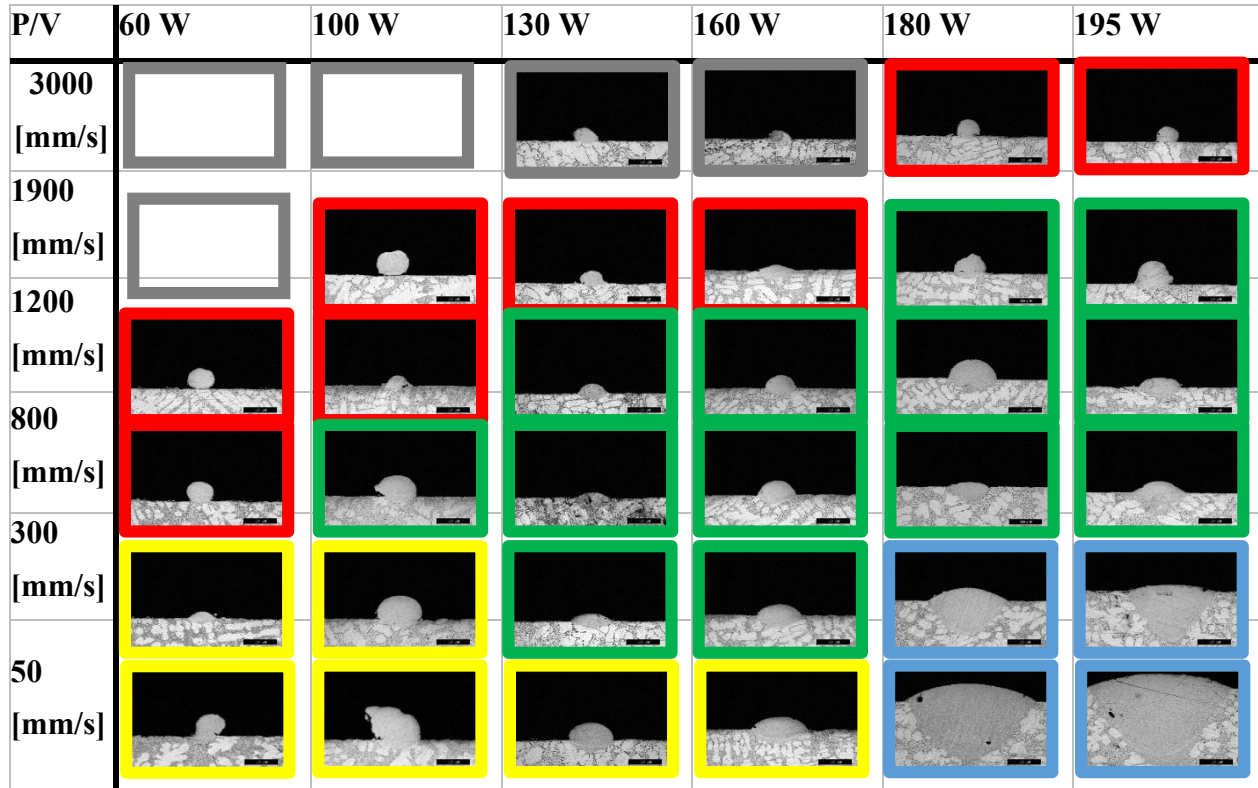


Figure 5.20 Cross sectional view of SST samples based on input parameters, Case of AlSi10Mg+nTiB₂. Black: not enough deposition, Red: balling, Green: thin and stable, Yellow: irregular, Blue: too thick.

Here we stop any further explanations about cross sections since it will be studied in full details during following parts. In fact, every single geometrical parameter introduced in figure 5.17.a follows a special behavior for each type of powder. It is important to investigate these parametric behaviors for every group of scan tracks in order to choose best tracks for production or optimization purposes.

For all samples of three alloying powders, the cross section/melt pool images were captured using optical microscope with 200x magnification. The acquired images were then analyzed using Open Source ImageJ software to attain the seven geometrical aspects of melt pools. Out of seven parameters, the right and left angle were combined together to introduce an average value of the both, since it was found useless to mention them in separate ways. It led to a total number of six geometrical numbers for every single SST sample. Having this in mind, it becomes clear that a massive amount of numerical data was attained for three alloys which needs a proper way of representation, otherwise, the reader will be misled in tracking results. Given this, the best way to discuss about results while keeping general concept in a straight line was found to be discussing each geometrical parameter for three alloys in a separate subsection. Hence, in each subsection the

reader is directed to a general view of geometrical aspect of each alloy as well as comparison between them. The classification expressed in on top image analysis will be used for cross sectional analysis in order to keep coherency between two sections and easily make contributions where needed. The following parts address these results in detail.

5.1.2.1. Total Depth of Tracks

Total depth is one of the most important geometrical factors of melt pool that is defined as the total height of the pool including the fused depth inside substrate/previous layer. Its value is highly dependent on input parameters and it turns out to be very important to understand its behavior in different classes of samples of different alloys, as well as its behavior with respect to input parameters. The following figures are built based on total depth measurements for three alloys versus increasing order of LED for each class of SSTs.

Figures 5.21 to 5.23 illustrate graph of LED versus total depth of the melt pool for different classes of samples of A357, AlSi10Mg, and AlSi10Mg+nTiB₂, respectively. A comparison between them shows that there is an increasing trend for total depth versus LED in all alloys. However, the trend in A357 is more erratic compared to other alloys in sense that depth values are more scattered especially for balling tracks. Total depth for thin and stable tracks of three alloys are very close to each other. In fact, this value is almost in ranges of (75-130), (60-140), and (50-120) micrometers for A357, AlSi10Mg, and AlSi10Mg+nTiB₂ which are very similar to each other and can be used as a reference to define suitable tracks parallel to other benchmarks. It happens while for too thick tracks, difference in values is about 100 units for A357 and the other two. The interesting detail is that total depth of thin and stable tracks of A357 clearly increases with LED, while the composite powder has an attempt to keep it constant with increasing LED. A key point seen in these graphs and will also be clear in other following graphs is that too thick tracks show a very sharp difference in their behavior compared to others. It happens while steadiness of changes in LED doesn't change so much. Hence, the reason should be pursuit through phenomenological aspects of melting which will be explained here based on the literature and will be true for similar phenomenon in other graphs.

Usually the dimension of molten pool is controlled by conduction of heat from intersection of laser spot and powder to other areas. Stirring the melt pool during scanning also plays a role in heat delivering and distribution. But in certain parameters, the conductive mechanism of melting can have a transition and become the so called “keyhole Mode”. In such a case, evaporation of metal increases to a high extent which causes to dramatic increase in pool dimension compared to conductive case. One of the problems of this melting mechanism is that the formed cavity due to metal evaporation can collapse or remain in melt pool and cause porosity [75]. This case is clearly distinguishable for too thick samples in figure 5.2 where pores remained in the pool. Too thick tracks are not suitable cases for production purposes because beside porosity problems, thermal gradients, residual stresses, and deformation are much higher due to deep diffusion of track into underlying layer. The consumed energy is also high due to having high power.

Similar to on top analysis, a graph was prepared for all three alloys without any representation of tracks classifications which is illustrated in figure 5.24. The graph which depicts total depth versus LED shows that three alloys have totally similar behavior and responses with respect to LED. Results of the three alloys form a narrow band on graph which means that geometrical parameters

A357

Y-axis: Total Depth [μm]

X-axis: Log (LED) [J/mm]

Legend:

- NOT ENOUGH
- BALLING
- THIN and STABLE
- IRREGULAR
- TOO THICK

AlSi10Mg

Total Depth [μm]

Log (LED) [J/mm]

● NOT ENOUGH ● BALLING ● THIN and STABLE ● IRREGULAR ● TOO THICK

Log (LED) [J/mm]	Total Depth [μm]	Category
0.02	0	NOT ENOUGH
0.03	0	NOT ENOUGH
0.03	10	NOT ENOUGH
0.04	10	NOT ENOUGH
0.04	0	NOT ENOUGH
0.05	40	BALLING
0.06	95	BALLING
0.07	30	BALLING
0.08	70	BALLING
0.09	70	BALLING
0.10	85	BALLING
0.12	140	BALLING
0.15	60	THIN and STABLE
0.18	75	THIN and STABLE
0.20	80	THIN and STABLE
0.25	80	THIN and STABLE
0.30	90	THIN and STABLE
0.35	70	THIN and STABLE
0.40	90	THIN and STABLE
0.50	125	THIN and STABLE
0.60	100	THIN and STABLE
0.80	90	THIN and STABLE
1.00	90	THIN and STABLE
1.20	100	IRREGULAR
2.00	110	IRREGULAR
3.00	145	IRREGULAR
4.00	180	IRREGULAR
5.00	275	TOO THICK
5.00	355	TOO THICK

79

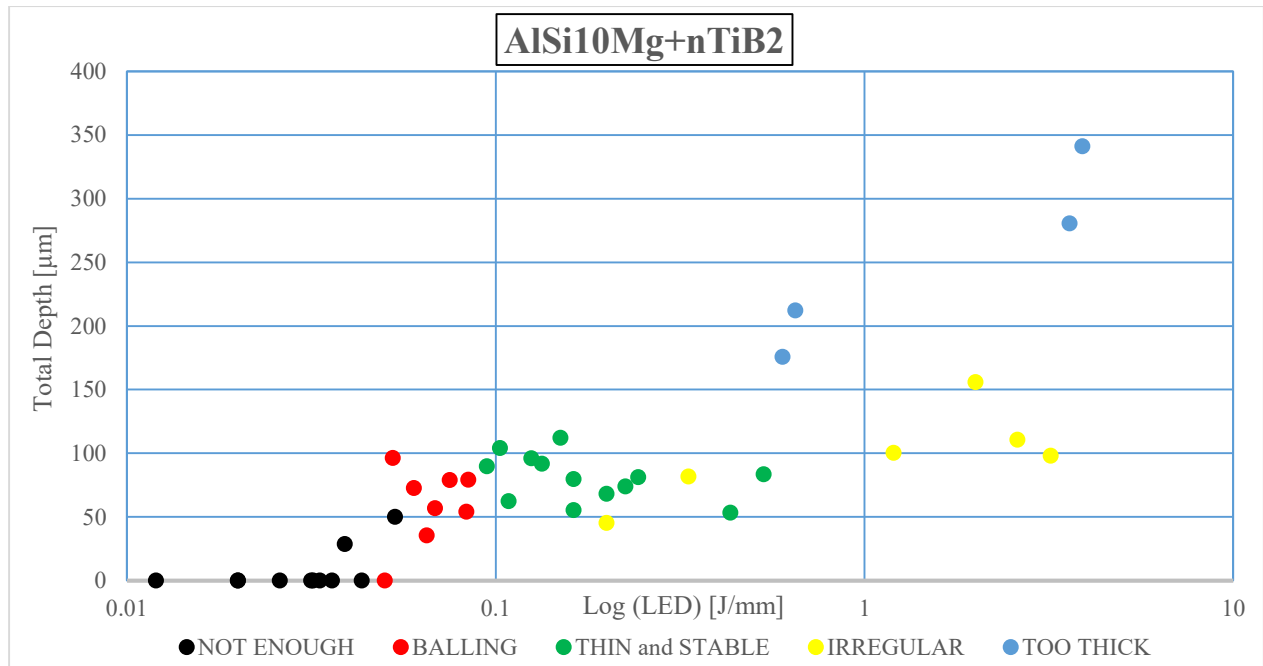


Figure 5.23 Total depth of melt pool versus Linear Energy Density (LED), case of AlSi10Mg+nTiB₂

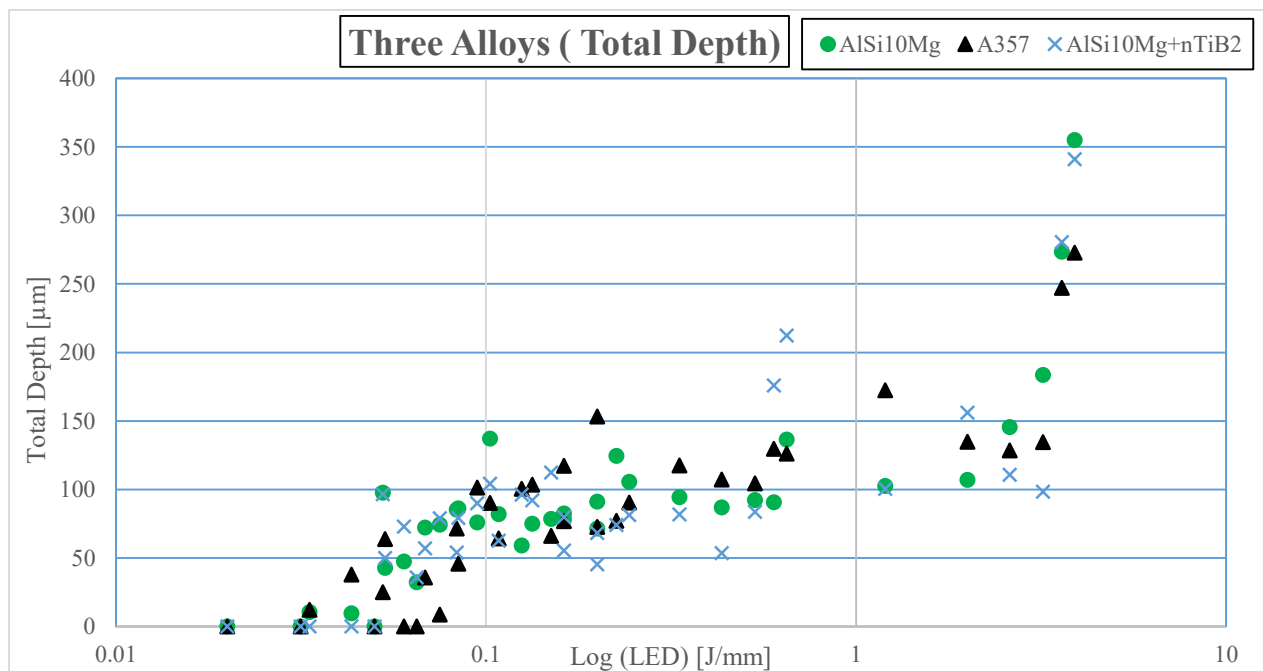


Figure 5.24 Total depth of melt pool versus Linear Energy Density (LED) for all alloys

5.1.2.2. Width of Tracks

Figures 5.25 to 5.27 represents graph of LED versus width of the melt pool for different classes of samples of A357, AlSi10Mg, and AlSi10Mg+nTiB₂, respectively. The graphs show an increasing tendency versus LED and at the same time, values are less scattered for three alloys compared to

total depth. The thin and stable tracks have a width value almost in ranges of (110-200), (90-220), and (90-160), for A357, AlSi10Mg, and AlSi10Mg+nTiB₂, respectively. It doesn't confirm results of on top analyses according to which A357 scans results thinner with respect to the others which can be related to on-top measurements that doesn't allow for a completely perfect measurement.

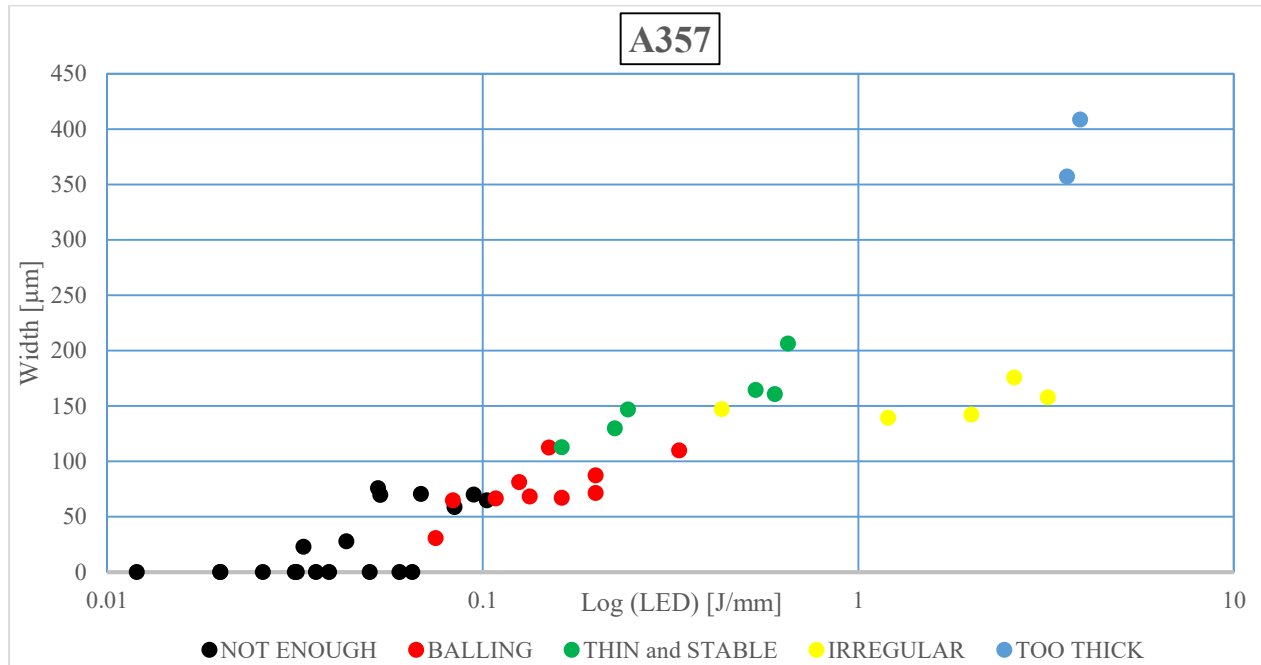


Figure 5.25 Width of melt pool versus Linear Energy Density (LED), case of A357 alloy

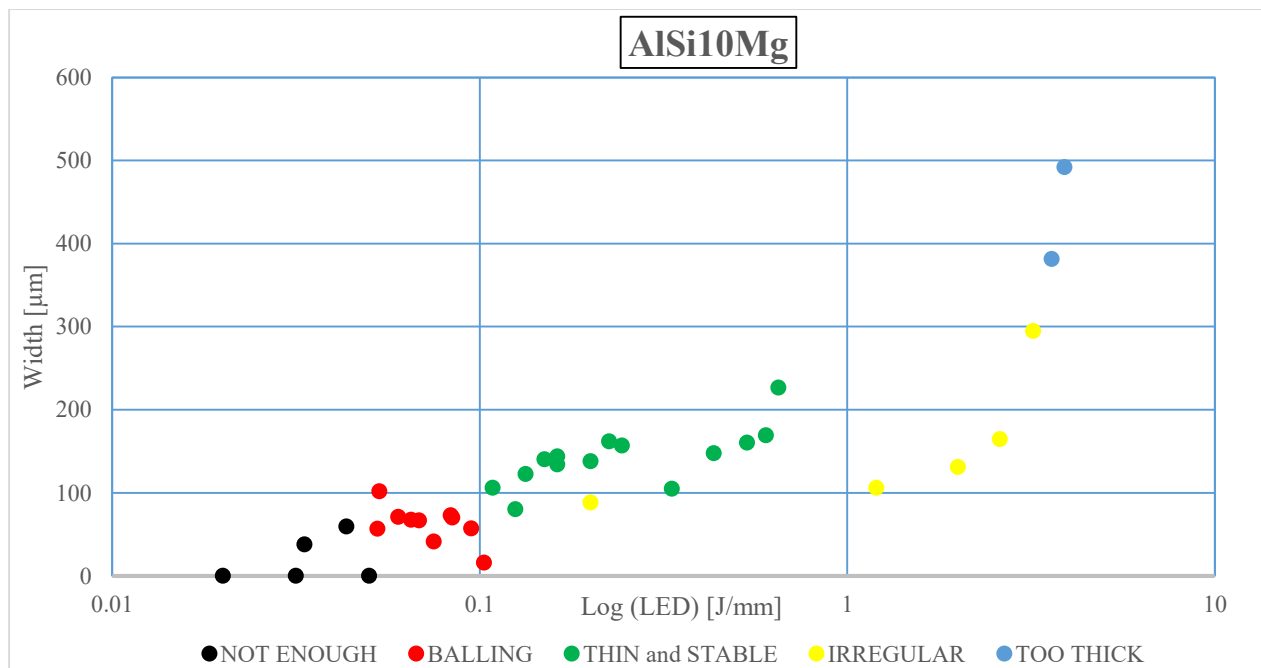


Figure 5.26 Width of melt pool versus Linear Energy Density (LED), case of AlSi10Mg alloy. Pure numerical data are taken from reference 74 to build the graph.

Similar to total depth, the values of width for thin and stable tracks of three alloys share a wide range which can be translated to the fact that regardless of the type of alloys, it is necessary (but not sufficient) for total depth and width of tracks to be in a special range to be considered as thin and stable ones.

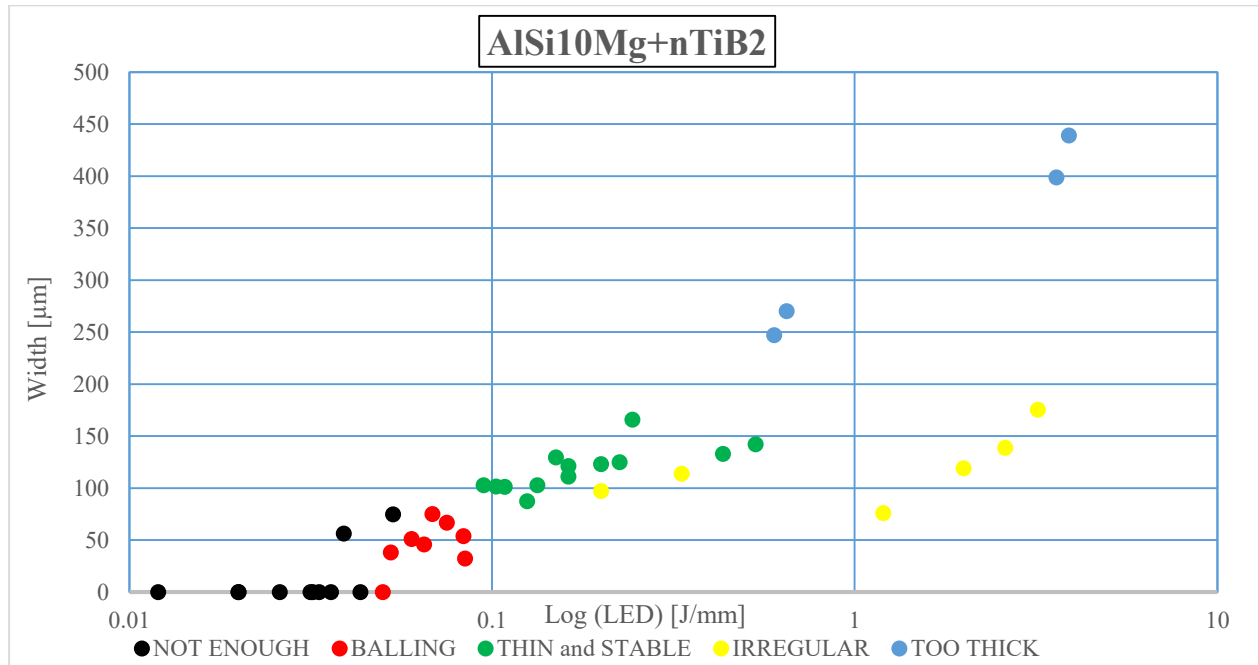


Figure 5.27 Width of melt pool versus Linear Energy Density (LED), case of AlSi10Mg+nTiB₂

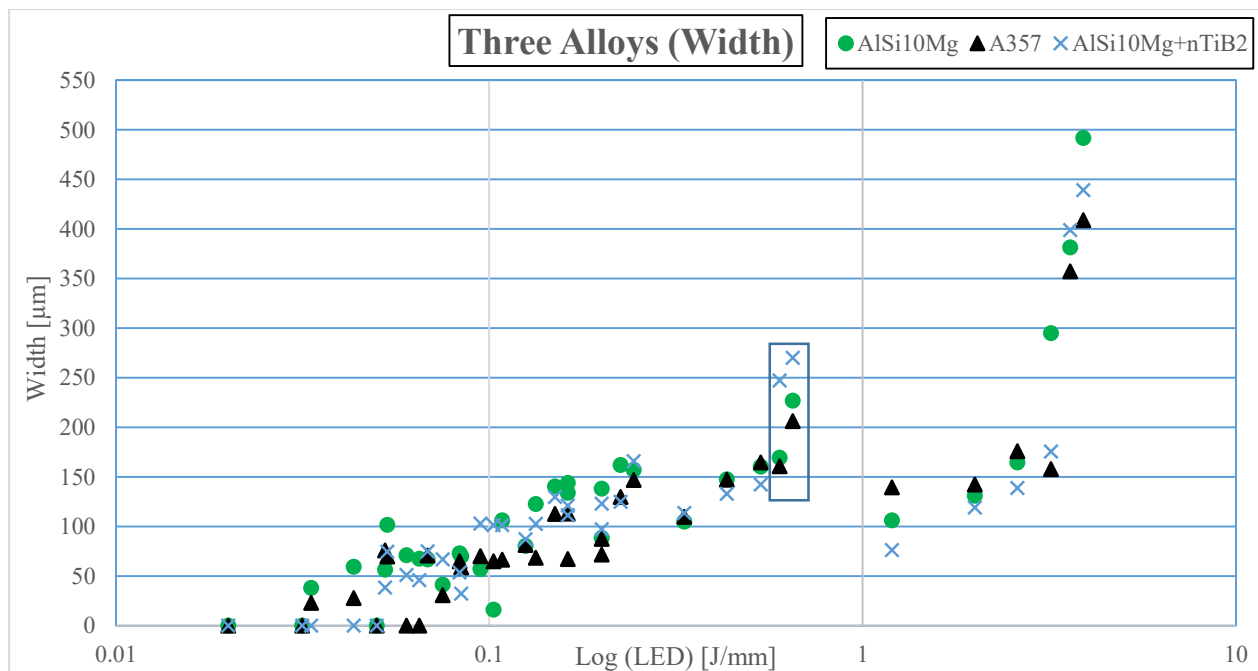


Figure 5.28 Width of melt pool versus Linear Energy Density (LED) for all alloys

A further comparison between these values with similar ones in total depth shows that thin and stable tracks are the ones which are fatter in intersection with substrate. In other words, the heat is more spread horizontally than vertical. About too thick values, the rocketing behavior in values is observed which shows that keyhole transition extends melt pool dimensions in all direction.

Figure 5.28 illustrates width of tracks with respect to LED for three alloys. It shows that similar to total depth, width of tracks for three alloys have a very similar behavior with respect to LED. It is interesting to see that all alloys rocket, smooth, or descend the graph quite similar together. If we consider three parts of graph which was introduced in previous part, the graph shows increasing behavior in all of them. However, if we neglect two values which are inside triangle, the behavior of remaining will be quite similar to what was explained for total depth values.

5.1.2.3. h growth of Tracks

Figure 5.29 to 5.31 represent graphs of LED versus growth of melt pool for different classes of samples of A357, AlSi10Mg, and AlSi10Mg+nTiB₂, respectively. The graphs show that melt pool dimensions above the substrate surface show very strange behavior during facing different LEDs. However, the key point is that for three types of alloys, balling and irregular samples spread along a wide range of values while thin and stables tend to keep their dimensions in narrower bands. In fact, the range of growth are almost (35-80), (40-80), and (20-85) for A357, AlSi10Mg, and AlSi10Mg+nTiB₂, respectively, which have a wide range in common similar to abovementioned dimensional parameters. It strengthens the hypothesis which was made before and complete it, say, regardless of the type of alloys, it is necessary (but not sufficient) for total depth, width, and growth of tracks to be in special ranges to be considered as thin and stable ones. When it comes about too thick tracks, they show very low growth compared to previous geometrical parameters which means a small amount of massive molten powder remains above substrate and majority of it is either evaporated or diffused into the substrate/previous layer.

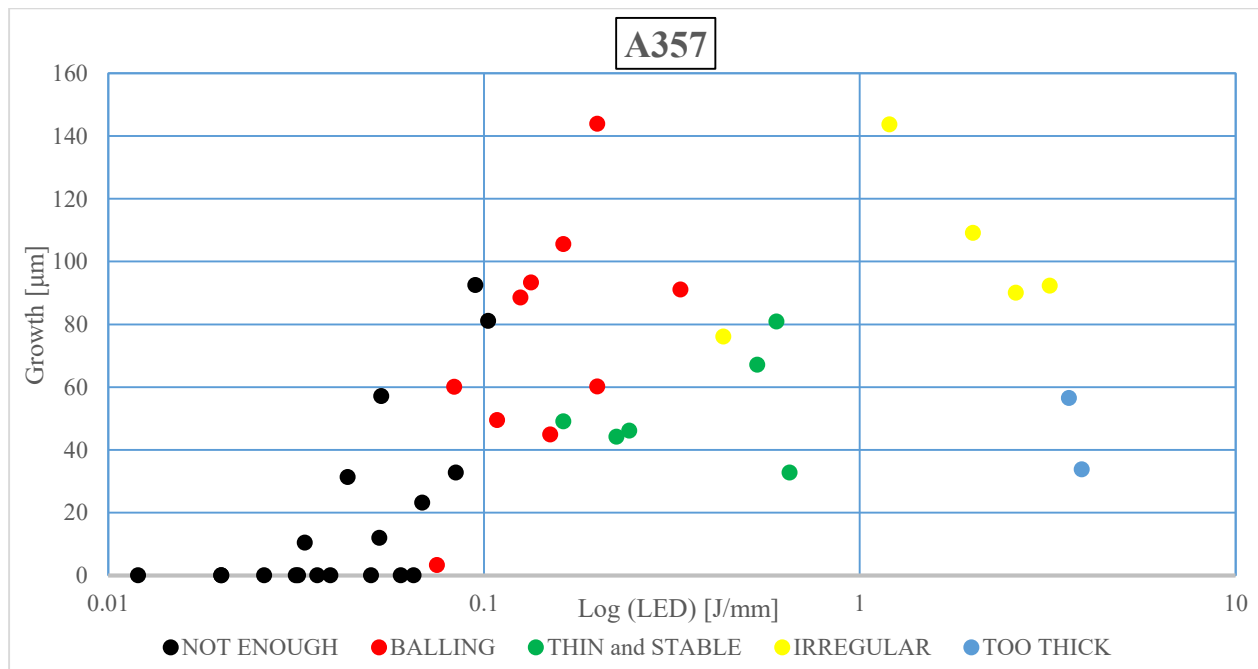


Figure 5.29 Growth of melt pool versus Linear Energy Density (LED), case of A357 alloy

It can be mentioned as another reason that shows this type of track is not suitable for production purposes because it has kind of “over penetration” into previous layer which leaves the part with lots of thermal stresses, possible cracks, and deformation, and makes the chamber dirty due to metal evaporation which can also affect chemical composition.

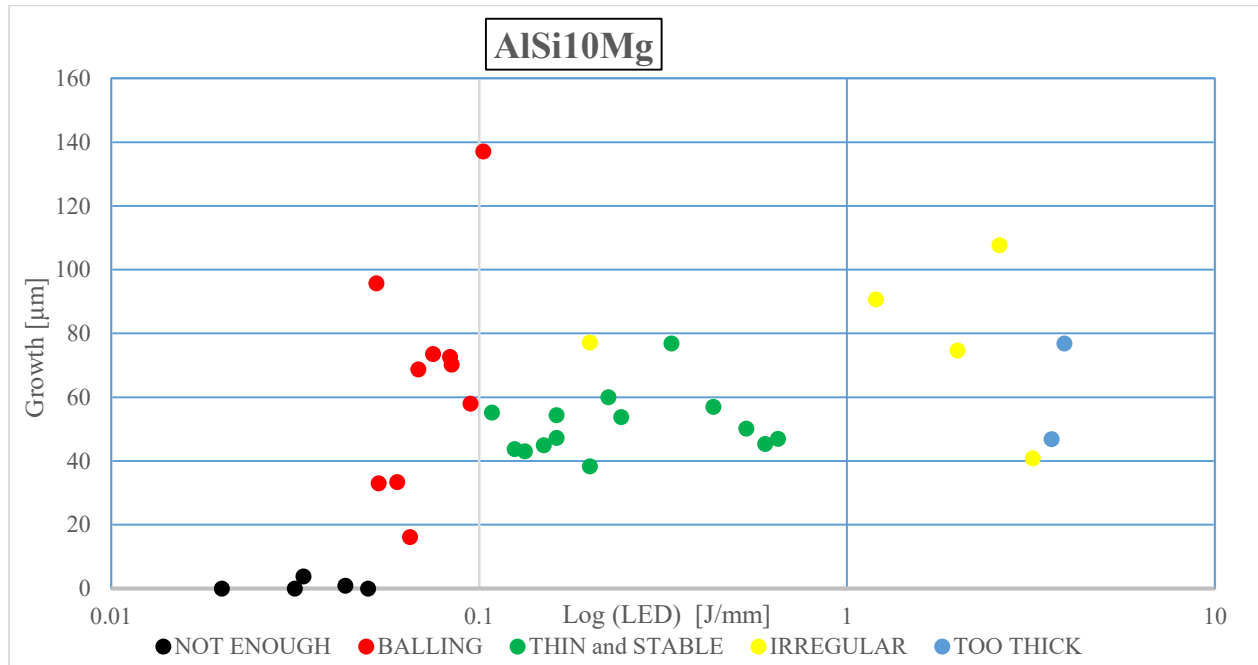


Figure 5.30 Growth of melt pool versus Linear Energy Density (LED), case of AlSi10Mg alloy. Pure numerical data are taken from reference 74 to build the graph.

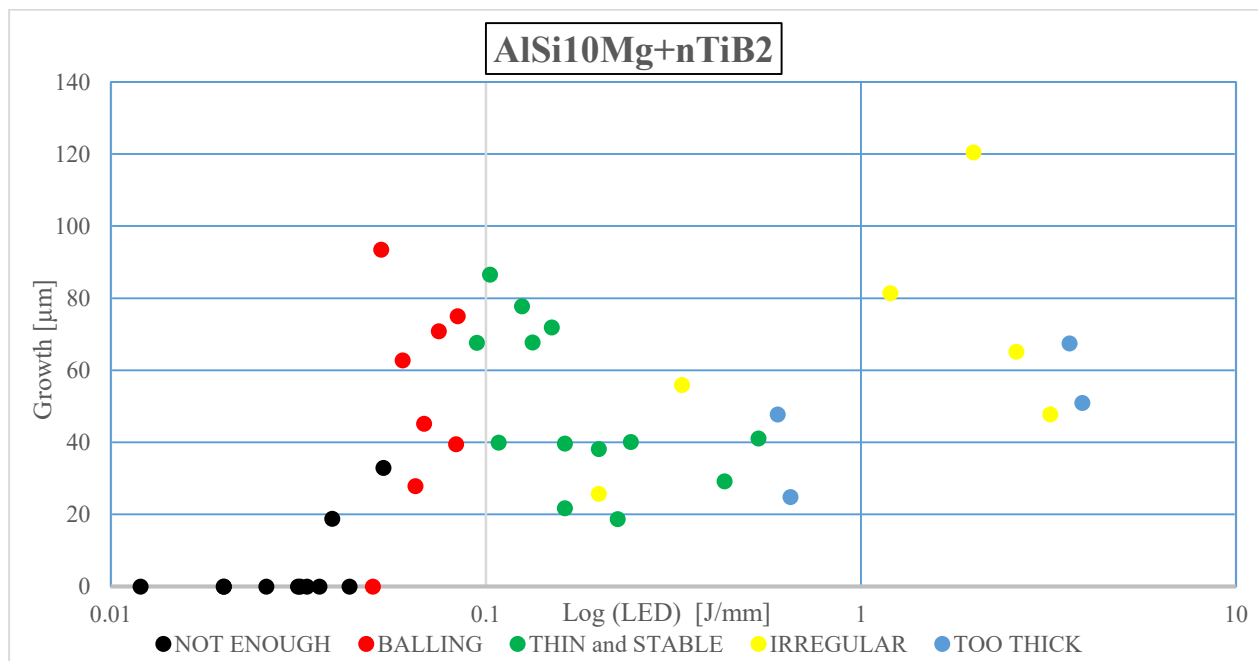


Figure 5.31 Growth of melt pool versus Linear Energy Density (LED), case of AlSi10Mg+nTiB₂

Figure 5.32 depicts graph of results of growth measurements for all alloys in one place. It shows that three alloys show less similar behavior in growth compared to abovementioned parameters, but yet they tend to react in the same way. The interesting point is that in second part of graph (LED between 0.1 to 1), A357 has obviously higher values than others. It results in lower depth of fusion into underneath which is expected to be seen in subsequent graphs.

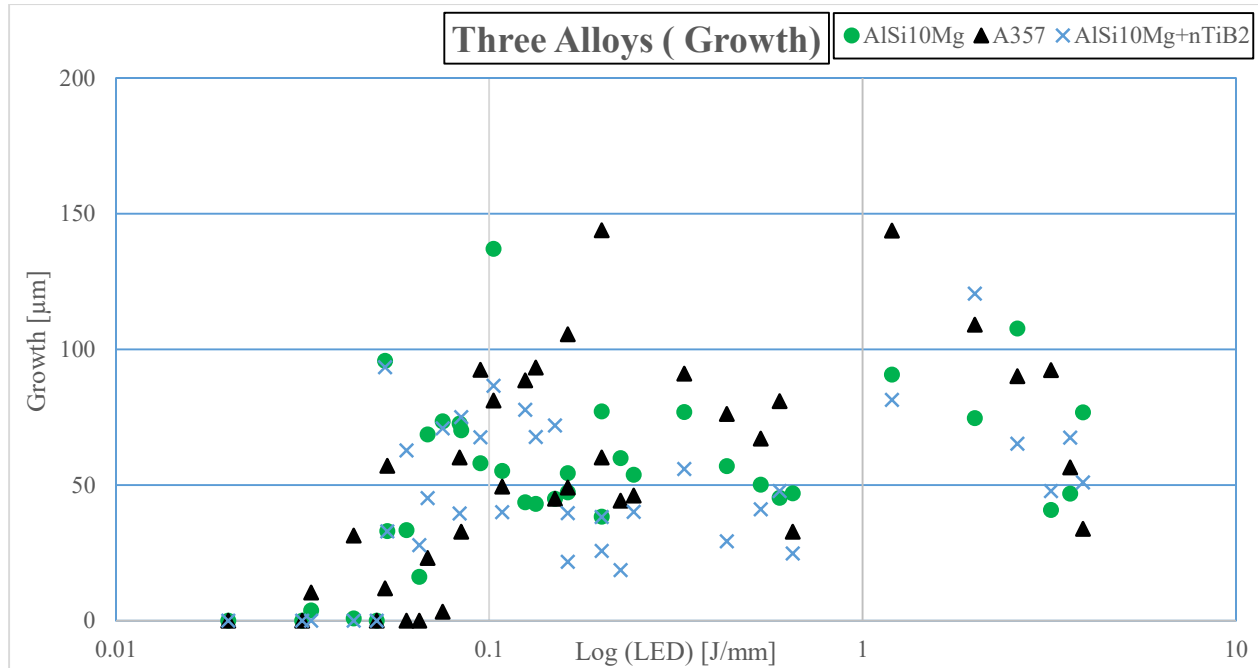


Figure 5.32 Growth of melt pool versus Linear Energy Density (LED) for all alloys

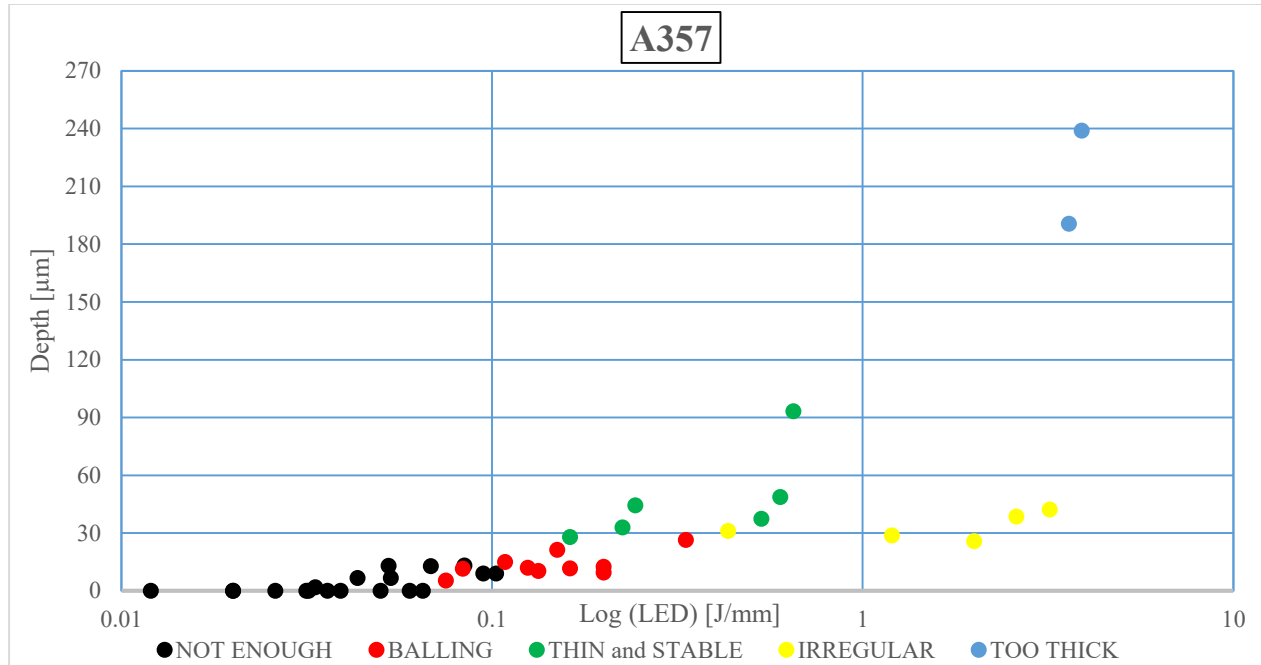
A very important thing about growth graphs of all alloys is that growth of scan tracks should always be lower than two times of layer thickness, i.e. lower than 80 μm . Otherwise the distributor arm can be misled or even stopped by extra dimension when spreading the next layer. the graphs above show than no one of thin and stable tracks of three alloys cause such problem, but it can easily happen with some balling or irregular tracks.

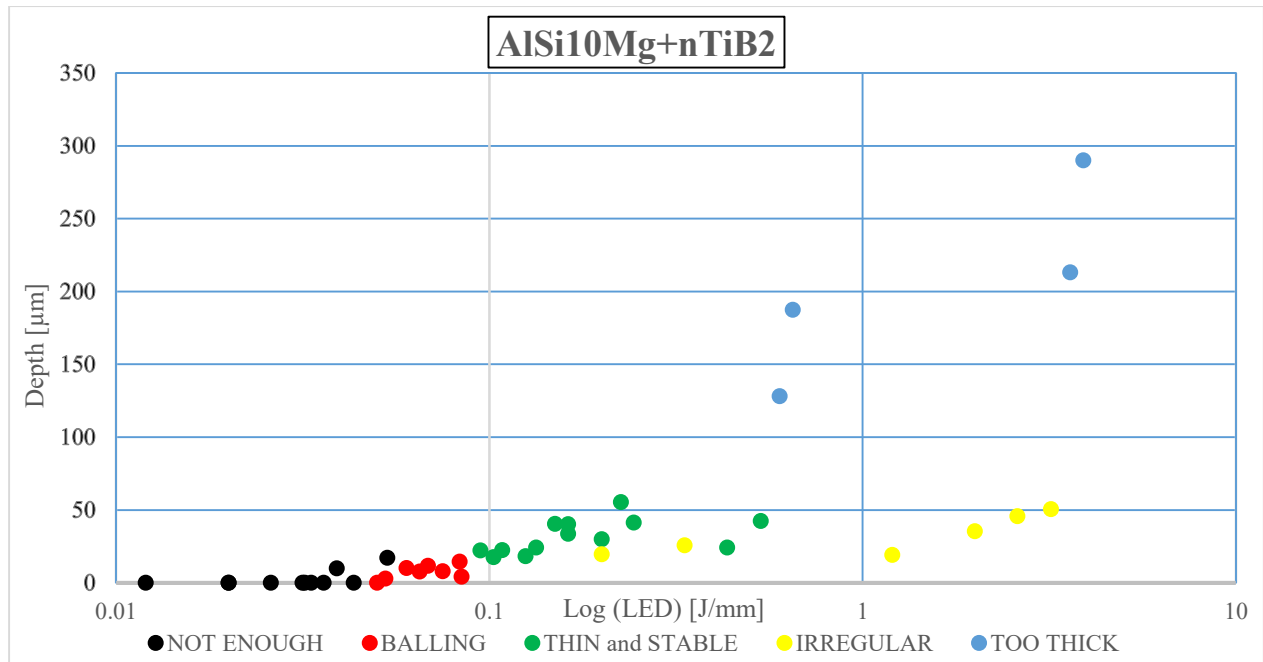
5.1.2.4. Lower Depth of Tracks

Figure 5.33 to 5.35 represent graphs of LED versus lower depth of melt pool for different classes of samples of A357, AlSi10Mg, and AlSi10Mg+nTiB₂, respectively. Lower depth which is a module to show diffusion into substrate/previous layer shows a very slight increases versus LED with similar erratic behaviors for irregular samples of three alloys. Its range of variation is (30-90), (20-100), and (20-50), for A357, AlSi10Mg, and AlSi10Mg+nTiB₂, respectively. It shows that the range is very limited for the composite compared to other powders, although all of them share a specific range.

The most striking point of all of graphs is that balling samples have very low depth into the surface which means their limited diffusion weakens any bond between them and the underneath layer. Therefore, this type of track must be eliminated in production to have acceptable mechanical properties. As it is expected for too thick tracks, they have very high depth of fusion into previous layer for all three powders.

The combination of all graphs is represented in figure 5.36. It shows that also in terms of depth, the three alloys form a very narrow band in graph which is a result of quite similar trends. As it was expected, the values for A357 in second part of graph is lower than others which is a sign of lower ability of this type of powder to penetrate into previous layers.





A357

Angle [Degree]

Log (LED) [J/mm]

● NOT ENOUGH ● BALLING ● THIN and STABLE ● IRREGULAR ● TOO THICK

Log (LED) [J/mm]	Angle [Degree]	Defect Type
0.015	0	NOT ENOUGH
0.025	0	NOT ENOUGH
0.03	0	NOT ENOUGH
0.04	0	NOT ENOUGH
0.045	0	NOT ENOUGH
0.05	0	NOT ENOUGH
0.055	0	NOT ENOUGH
0.06	0	NOT ENOUGH
0.07	0	NOT ENOUGH
0.08	0	NOT ENOUGH
0.09	0	NOT ENOUGH
0.1	52	NOT ENOUGH
0.12	62	NOT ENOUGH
0.15	76	NOT ENOUGH
0.18	122	NOT ENOUGH
0.2	148	NOT ENOUGH
0.04	26	NOT ENOUGH
0.05	45	NOT ENOUGH
0.06	75	NOT ENOUGH
0.08	81	NOT ENOUGH
0.1	76	NOT ENOUGH
0.12	97	NOT ENOUGH
0.15	122	NOT ENOUGH
0.18	148	NOT ENOUGH
0.2	162	NOT ENOUGH
0.1	48	BALLING
0.12	62	BALLING
0.15	87	BALLING
0.18	90	BALLING
0.2	30	BALLING
0.1	97	BALLING
0.12	128	BALLING
0.15	130	BALLING
0.18	83	BALLING
0.2	107	BALLING
0.1	52	BALLING
0.12	62	BALLING
0.15	87	BALLING
0.18	90	BALLING
0.2	30	BALLING
0.1	97	BALLING
0.12	128	BALLING
0.15	130	BALLING
0.18	83	BALLING
0.2	107	BALLING
0.1	52	BALLING
0.12	62	BALLING
0.15	87	BALLING
0.18	90	BALLING
0.2	30	BALLING
0.1	97	BALLING
0.12	128	BALLING
0.15	130	BALLING
0.18	83	BALLING
0.2	107	BALLING
0.1	52	BALLING
0.12	62	BALLING
0.15	87	BALLING
0.18	90	BALLING
0.2	30	BALLING
0.1	97	BALLING
0.12	128	BALLING
0.15	130	BALLING
0.18	83	BALLING
0.2	107	BALLING
0.1	52	BALLING
0.12	62	BALLING
0.15	87	BALLING
0.18	90	BALLING
0.2	30	BALLING
0.1	97	BALLING
0.12	128	BALLING
0.15	130	BALLING
0.18	83	BALLING
0.2	107	BALLING
0.1	52	BALLING
0.12	62	BALLING
0.15	87	BALLING
0.18	90	BALLING
0.2	30	BALLING
0.1	97	BALLING
0.12	128	BALLING
0.15	130	BALLING
0.18	83	BALLING
0.2	107	BALLING
0.1	52	BALLING
0.12	62	BALLING
0.15	87	BALLING
0.18	90	BALLING
0.2	30	BALLING
0.1	97	BALLING
0.12	128	BALLING
0.15	130	BALLING
0.18	83	BALLING
0.2	107	BALLING
0.1	52	BALLING
0.12	62	BALLING
0.15	87	BALLING
0.18	90	BALLING
0.2	30	BALLING
0.1	97	BALLING
0.12	128	BALLING
0.15	130	BALLING
0.18	83	BALLING
0.2	107	BALLING
0.1	52	BALLING
0.12	62	BALLING
0.15	87	BALLING
0.18	90	BALLING
0.2	30	BALLING
0.1	97	BALLING
0.12	128	BALLING
0.15	130	BALLING
0.18	83	BALLING
0.2	107	BALLING
0.1	52	BALLING
0.12	62	BALLING
0.15	87	BALLING
0.18	90	BALLING
0.2	30	BALLING
0.1	97	BALLING
0.12	128	BALLING
0.15	130	BALLING
0.18	83	BALLING
0.2	107	BALLING
0.1	52	BALLING
0.12	62	BALLING
0.15	87	BALLING
0.18	90	BALLING
0.2	30	BALLING
0.1	97	BALLING
0.12	128	BALLING
0.15	130	BALLING
0.18	83	BALLING
0.2	107	BALLING
0.1	52	BALLING
0.12	62	BALLING
0.15	87	BALLING
0.18	90	BALLING
0.2	30	BALLING
0.		

AlSi10Mg

Log (LED) [J/mm]	Angle [Degree]	Category
0.02	0	NOT ENOUGH
0.03	0	NOT ENOUGH
0.04	0	NOT ENOUGH
0.03	145	NOT ENOUGH
0.04	172	NOT ENOUGH
0.05	64	BALLING
0.05	128	BALLING
0.06	143	BALLING
0.07	95	BALLING
0.08	123	BALLING
0.09	72	BALLING
0.10	25	BALLING
0.10	76	BALLING
0.12	108	THIN and STABLE
0.13	124	THIN and STABLE
0.15	132	THIN and STABLE
0.18	129	THIN and STABLE
0.20	83	THIN and STABLE
0.25	129	THIN and STABLE
0.30	132	THIN and STABLE
0.40	115	THIN and STABLE
0.50	132	THIN and STABLE
0.60	145	THIN and STABLE
1.2	95	IRREGULAR
2.5	88	IRREGULAR
3.5	70	IRREGULAR
4.0	153	IRREGULAR
4.5	158	TOO THICK
4.8	150	TOO THICK

88

A spherical melt pool above surface with low diffusion into beneath tends to have acute angles, while it moves toward orthogonal and obtuse values when part of spherical shape penetrates into substrate. Given this, it is concluded that in order to have thin and stable samples (orthogonal and obtuse angles), energy density should be set in a way to have about 50% diffusion into underneath surface.

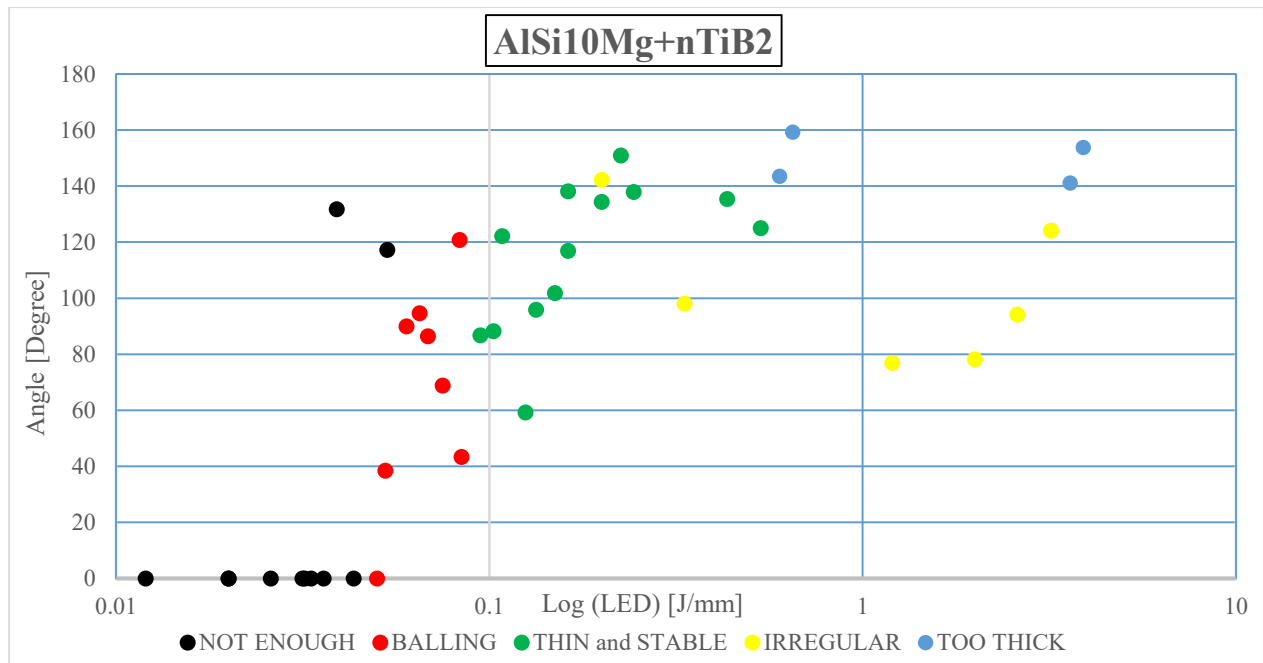


Figure 5.39 Horizontal angle of melt pool versus Linear Energy Density (LED), case of AlSi10Mg+nTiB₂

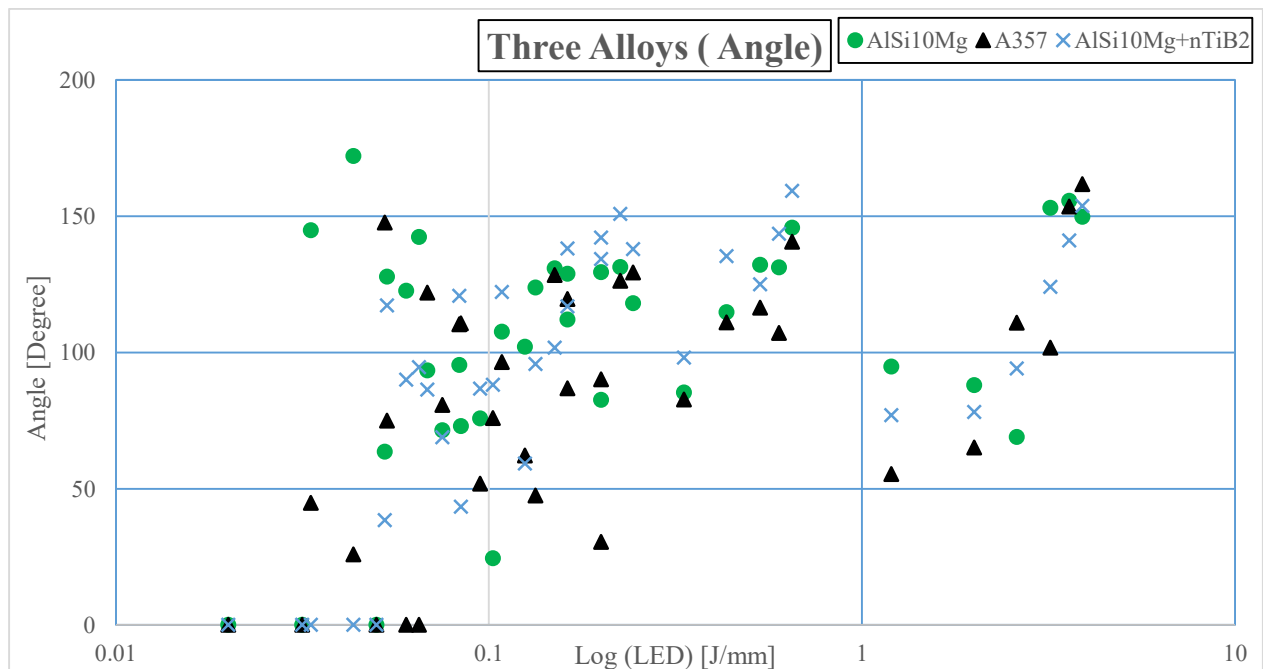


Figure 5.40 Horizontal angle of melt pool versus Linear Energy Density (LED) for all alloys

Energies far beyond normal case leads to too thick tracks where very high percentage of supposed spherical shape penetrates into underneath layer leaving a small arc on the surface. It results in very high angles which is obvious in graphs of three alloys.

The graph for angles of three alloys is depicted in figure 5.40. It shows that unlike other geometrical parameters, the three alloys show different behaviors in angle and cover a wide region. Meanwhile, the values become much closer to each other for LEDs higher than 1 J/mm. Moreover, it is interesting to see that majority of AlSi10Mg+nTiB₂ samples have high angles for second part of graph, i.e. LED between 0.1 to 1 J/mm which is translated as lower growth and arc-shape-pools above surface. This result is compatible with graph 5.32 which shows majority of the mentioned alloy samples have low growths in the same part of graph.

5.1.2.6. Melt Pool Area

Figure 5.41 to 5.43 represent graphs of LED versus surface area of melt pool for different classes of samples of A357, AlSi10Mg, and AlSi10Mg+nTiB₂, respectively. It is logical to see an increasing trend for area of the melt pool versus LED. Meanwhile, the most striking features of graphs is very high value of area for too thick tracks. It shows that transition of melting mechanism to keyhole can suddenly triple size of the melt pool without any striking changes in input parameters. However, similar to other parameters, area for thin and stable tracks tends to stay in narrow ranges which are almost (6000-19000), (5000-24000), and (5000-11000) μm^2 for A357, AlSi10Mg, and AlSi10Mg+nTiB₂, respectively.

Figure 5.44 plots surface area of all alloy samples with respect to LED. It shows a very narrow band especially for LEDs lower than 1 J/mm which translates to similarities in behavior, but it hardly changes for higher values of LED.

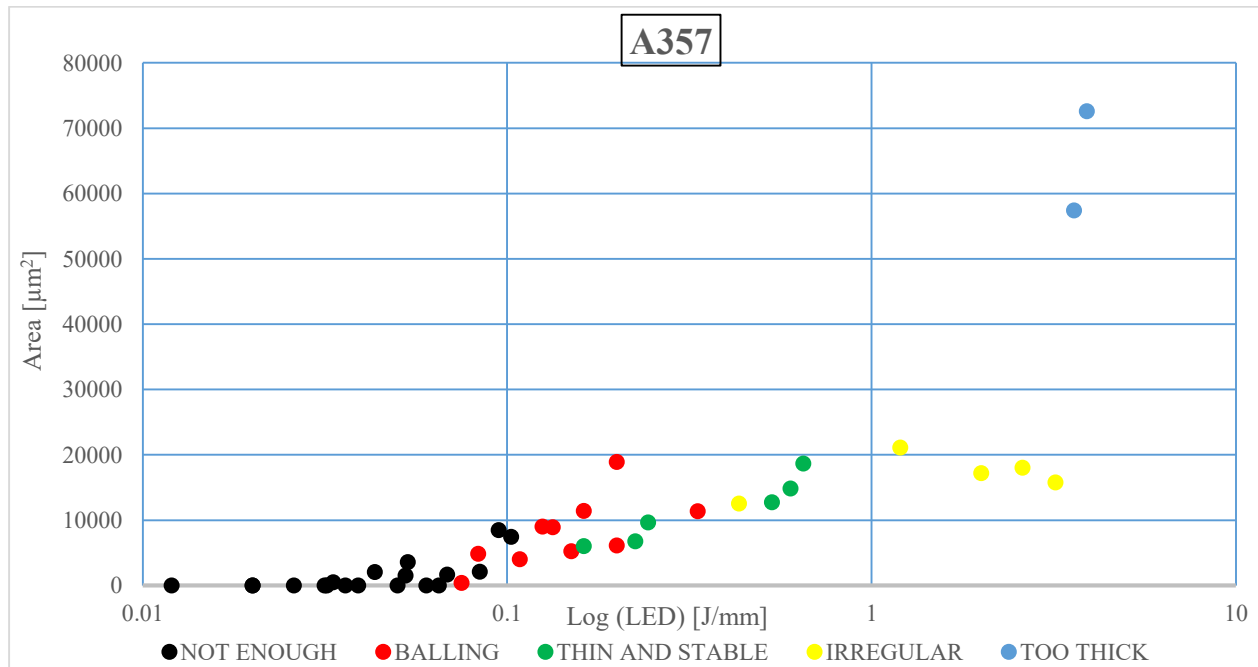


Figure 5.41 Surface area of melt pool versus Linear Energy Density (LED), case of A357 alloy

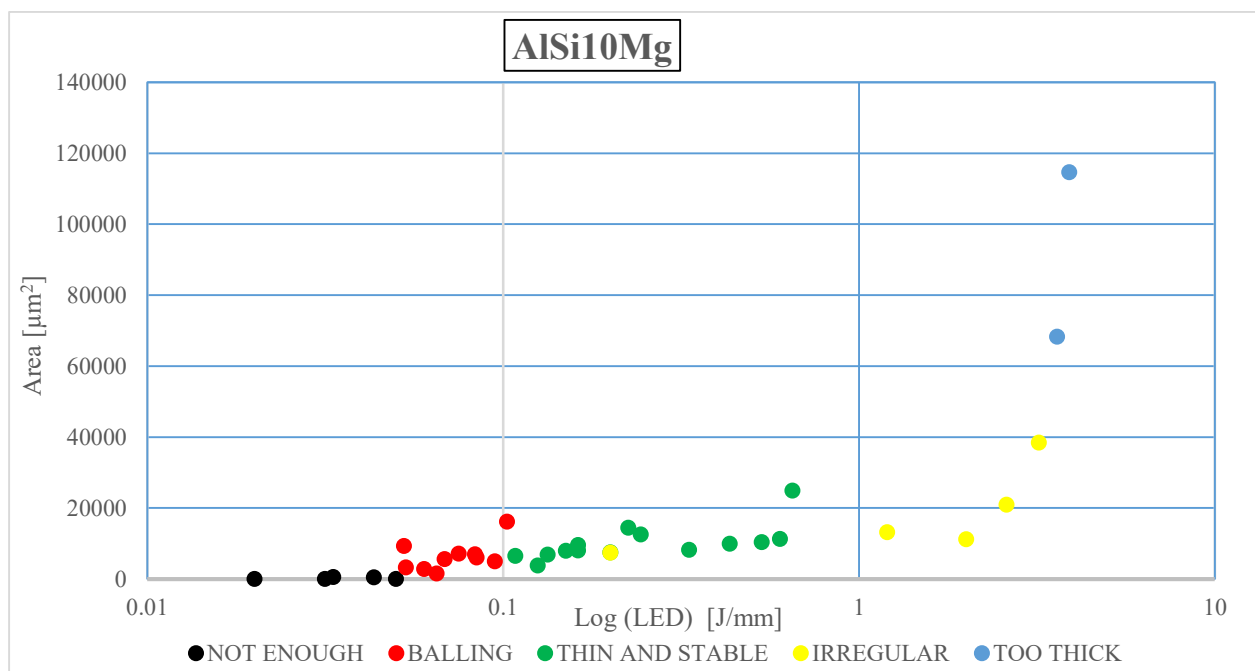


Figure 5.42 Surface area of melt pool versus Linear Energy Density (LED), case of AlSi10Mg alloy. Pure numerical data are taken from reference 74 to build the graph.

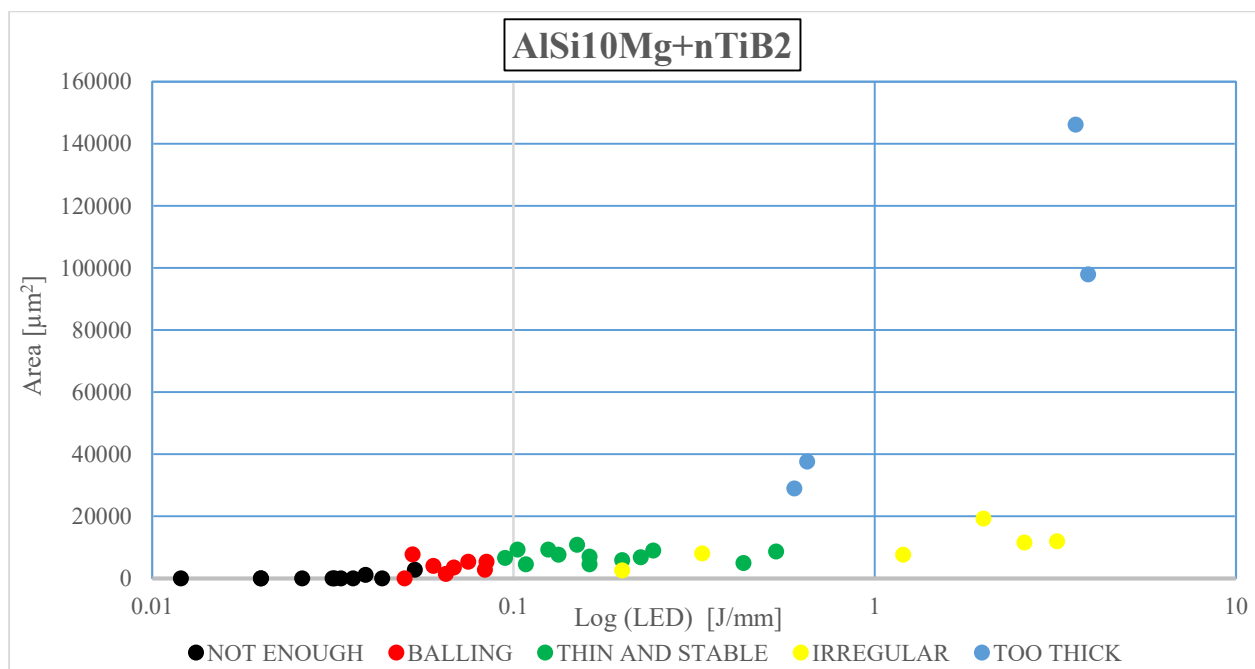


Figure 5.43 Surface area of melt pool versus Linear Energy Density (LED), case of AlSi10Mg+nTiB₂

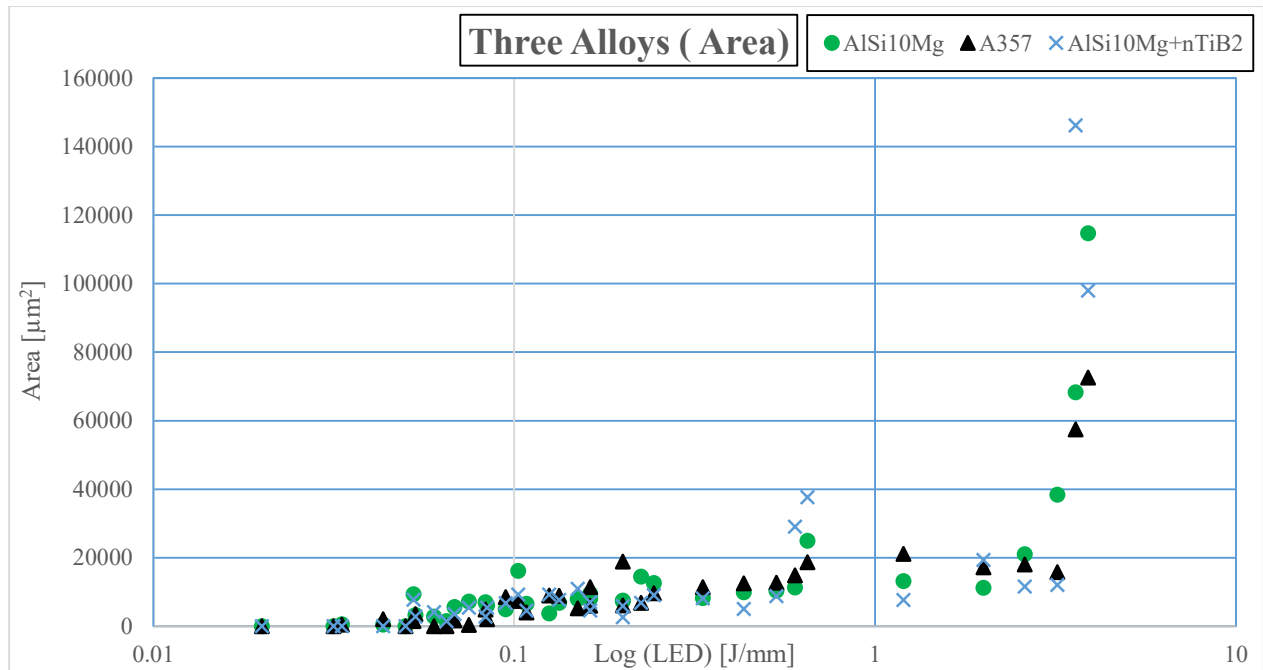


Figure 5.44 Surface area of melt pool versus Linear Energy Density (LED) for all alloys

5.2. Multi Scan Track (MST) Analysis

Studying only about single scan tracks of a powder sheds remarkable lights to process window of the material but cannot manifest everything, because it only considers single lines without any regard to interaction between them. In fact, when the laser scans parallel lines to finish a layer, there will be a special amount of overlapping between them. It means that part of the energy laser is consumed to re-melt overlapping section which makes the resulted track slightly different in shape and geometry compared to SSTs. The amount of overlapping depends on size of tracks and hatch distance and reduces by increasing hatch distance. The interaction between various numbers of tracks is studied in this part of thesis under the concept of Multi Scan Track (MST) analysis. However, a limited number of parameters was studied because the main goal was to define appropriate hatch distance for each alloy with no further discussion about interaction of parameters. Having a reciprocating scanning strategy to build a layer resulted in a shape similar to schematic of figure 5.45, in which cross section to study is perpendicular to scanning direction. The on-top analysis for MST samples only gives a common view about track interactions, instability along their length, and processing time. We simply skip this step because its analysis can be found either in SST section or cross sectional analysis of MSTs.

The cross section of MSTs for two alloys was polished up to high finishes and observed under the optical microscope. Figure 5.46 which is prepared only for AlSi10Mg+nTiB₂ gives a general view about how cross section of MST samples changes with respect to input parameters. As the figure shows, increasing scanning speed (which reduces volumetric energy density) causes a reduction in geometrical parameters of MSTs. On the other hand, increasing hatch distance up to a threshold keeps continuity of tracks while higher than that breaks down them into separated ones which results in non-molten powder and increases porosity. So, the first conclusion of this section is that visual inspection can be used to detect the threshold of hatch distance in MST samples.

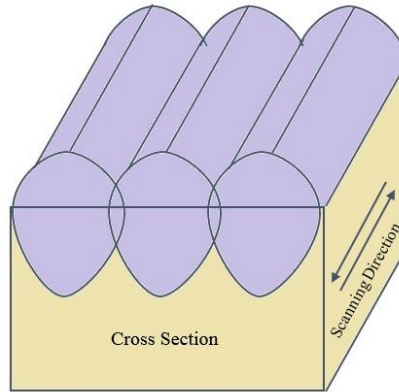


Figure 5.45 Schematic of a Multi Scan Track (MST) Sample

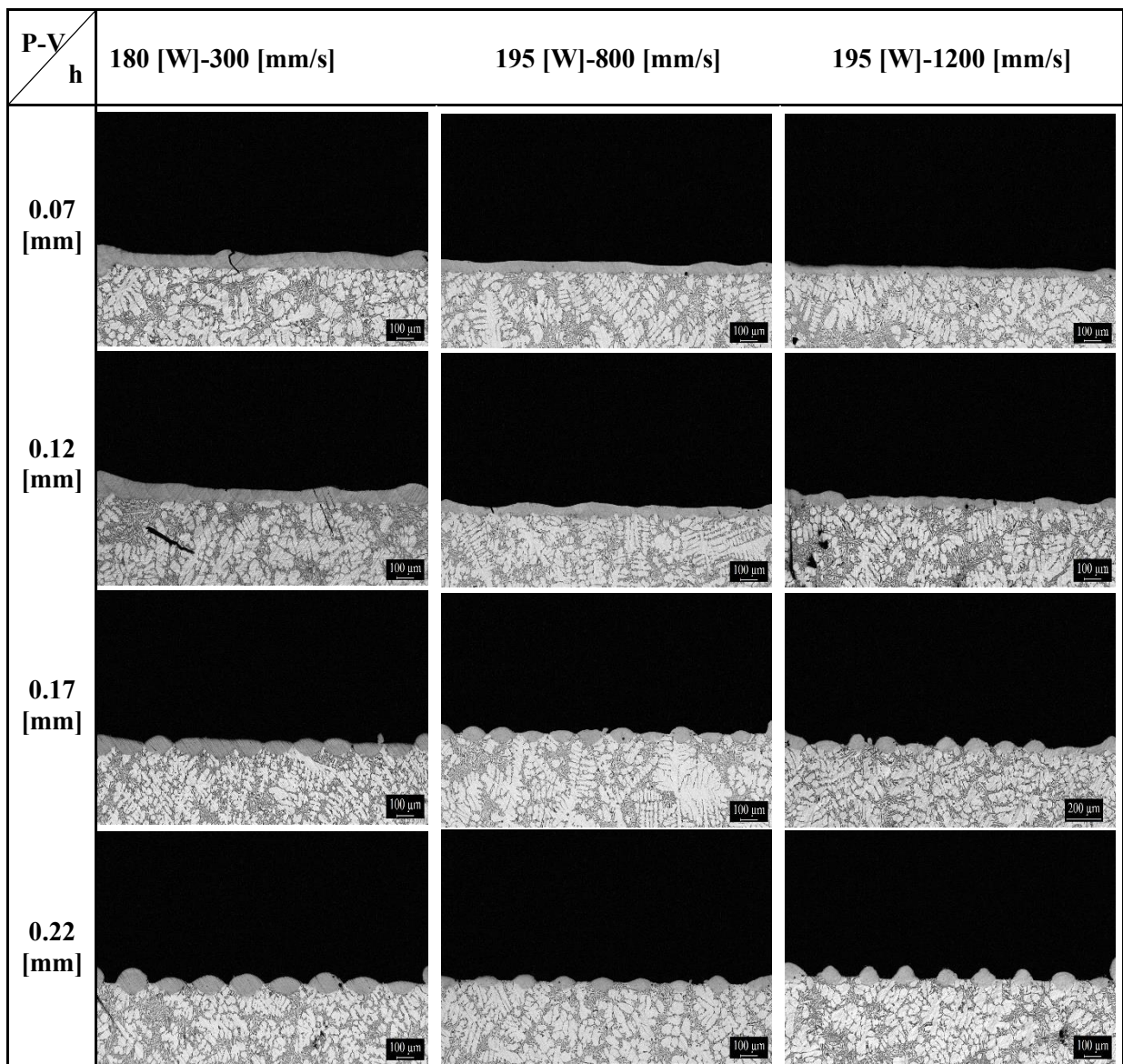


Figure 5.46 Schematic of cross sections of MST samples, case of AlSi10Mg+nTiB₂

The total depth of melt pools was measured in cross section of samples for two alloys and an average value was devoted to each case along with standard deviation of measurements. Different graphs can be devoted to total depth measurements based on various parameters such as VED, laser power, scanning speed, and hatch distance. A number of these graphs was chosen to discuss behaviors of input parameters while being compatible to specific range of input parameters. At this point we tend to discuss separately about graphs of each alloy rather than comparing them with each other because comparisons in previous section gives enough hints to know behavior of each alloy. Hence, results will be discussed for A357 and AlSi10Mg+nTiB₂, respectively.

Figures 5.47 to 5.49 illustrate the acquired results for A357 alloying powder. Figure 5.47 which is plotted based on VED and hatch distance, shows that for a special hatch distance increasing VED increases total depth and at the same time, increasing hatch distance with same VED also increases the total depth. However, for hatch distances of 0.17 and 0.22, μm the trends become irregular which is a sign of not having the right values. The reason behind increasing total depth by hatch distance is that higher hatch distance leads to lower overlapping, which means lower amount of energy is consumed to re-melt previous line. Therefore, more powder gets molten and the size of pool will be larger.

Figure 5.48 and 5.49 represent graphs of total depth versus scanning speed and laser power, respectively, while hatch distance changes. As graph 5.48 shows, any increase in scanning speed while keeping constant hatch distance reduces the total depth. It is because the laser spot finds lower time to dwell at a point while speed increases which results in reduction of layer depth. However, the behavior in graph 5.49 seems weird in sense that 195 W power almost always results in lower depth values. It is due to fact that 195 W power samples are all done with much higher speeds (800 and 1200 mm/s) compared to 180 W (300 mm/s) that in total, results in lower VED for this power and reduces depth of layer.

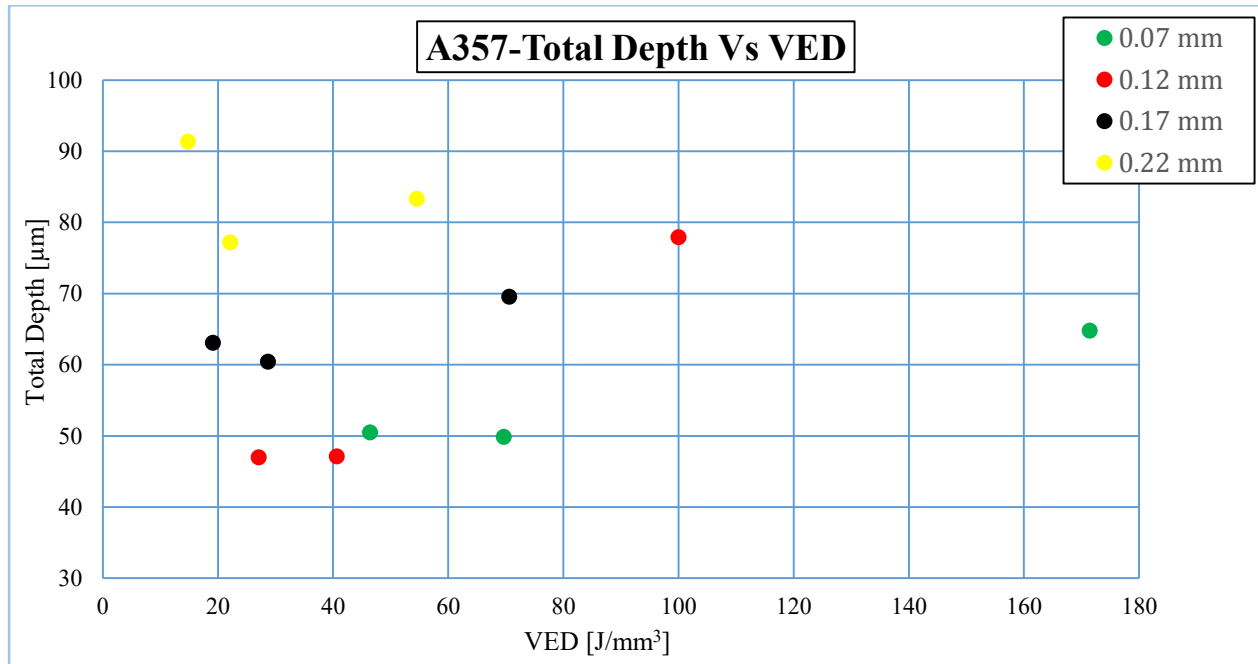


Figure 5.47 Graph of VED versus total depth based on hatch distance changing, case of A357

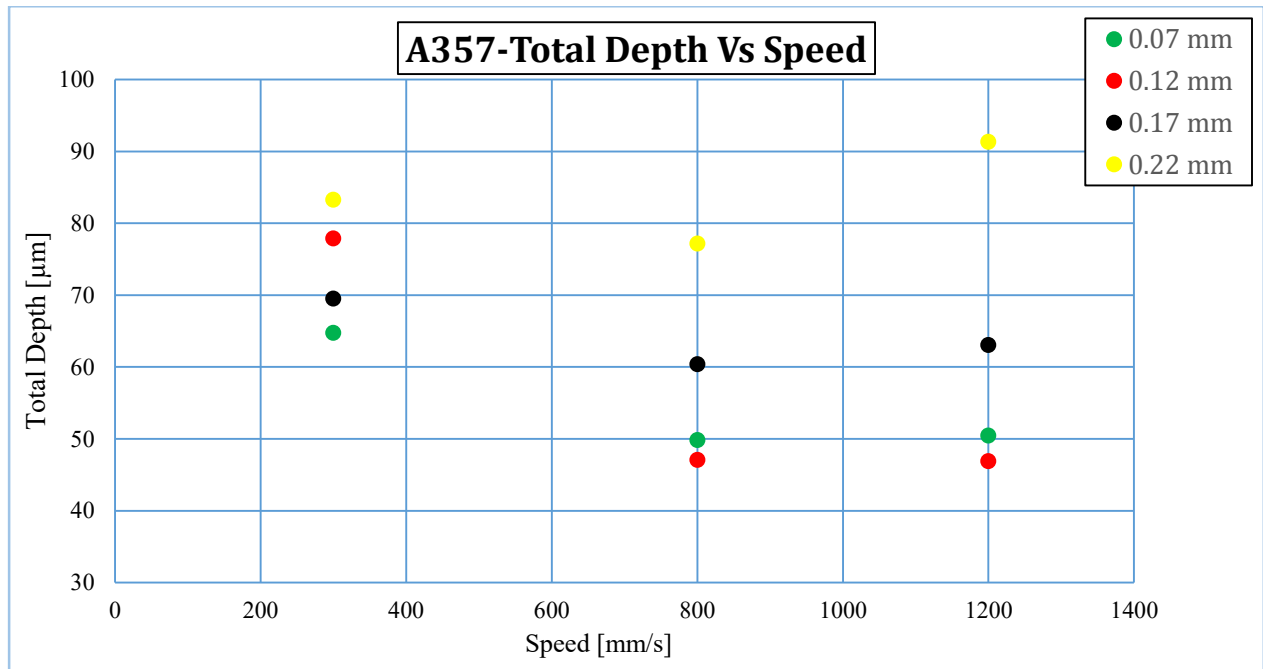


Figure 5.48 Graph of scanning speed versus total depth based on hatch distance changing, case of A357

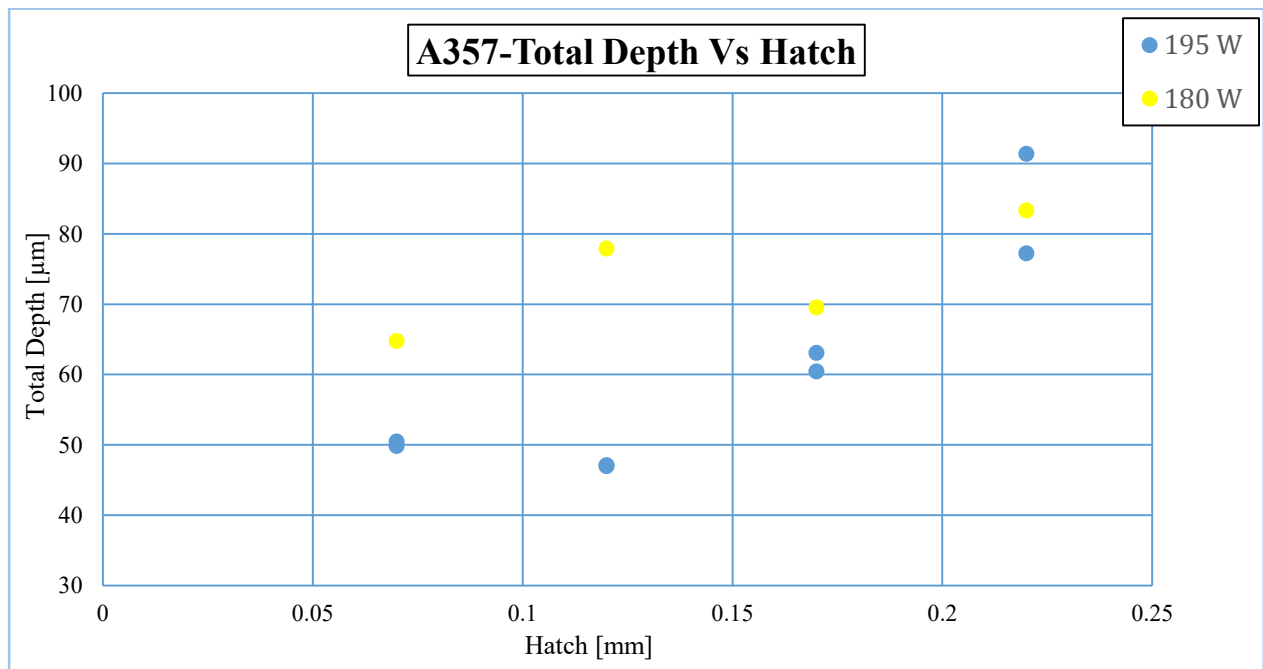


Figure 5.49 Graph of Hatch versus total depth based on power changing, case of A357

The main point that can be driven from images and graphs of MSTs is that hatch distance which usually depends on spot size of laser beam can be increased up to a threshold. Any value above that threshold leads to discontinuous tracks and non-molten powder.

Similar graphs for MST samples of AlSi10Mg+nTiB₂ MMC were obtained which are depicted in figures 5.50 to 5.52. Figure 5.50 that plots VED versus total depth shows increasing both of hatch distance and VED result in higher depth which is similar to A357. The other graphs also show very similar behaviors to A357, so all explanations for it will stand here, too.

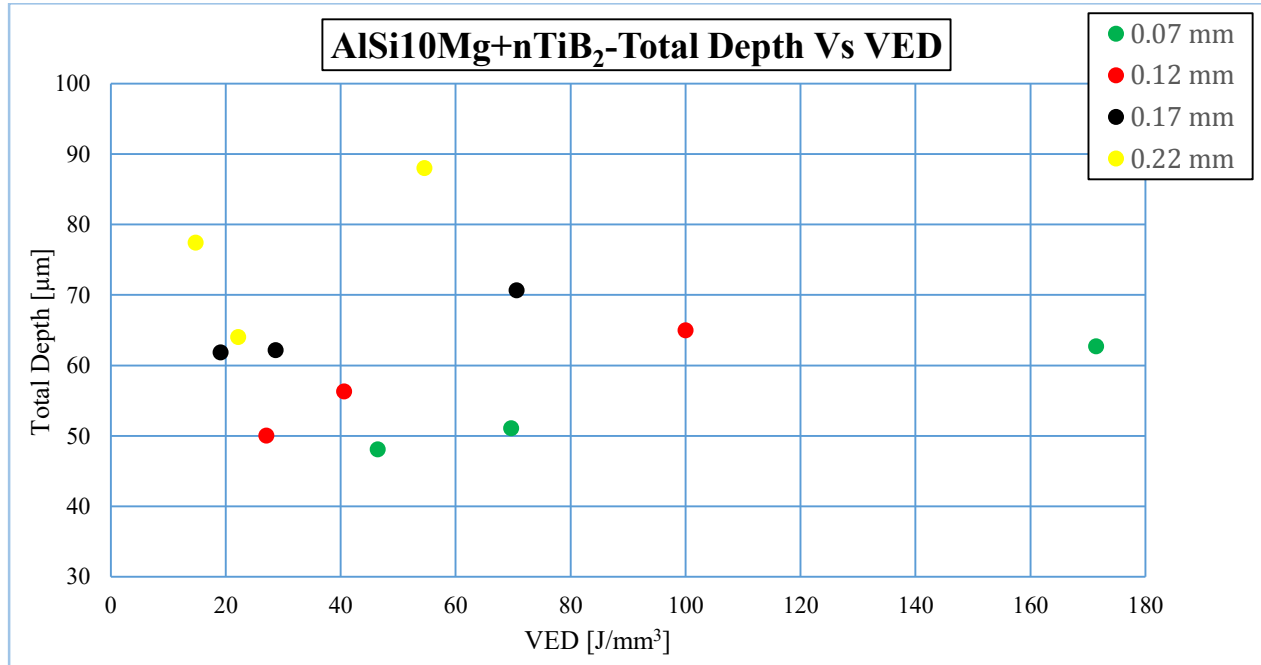


Figure 5.50 Graph of VED versus total depth based on hatch distance changing, case of AlSi10Mg+nTiB₂

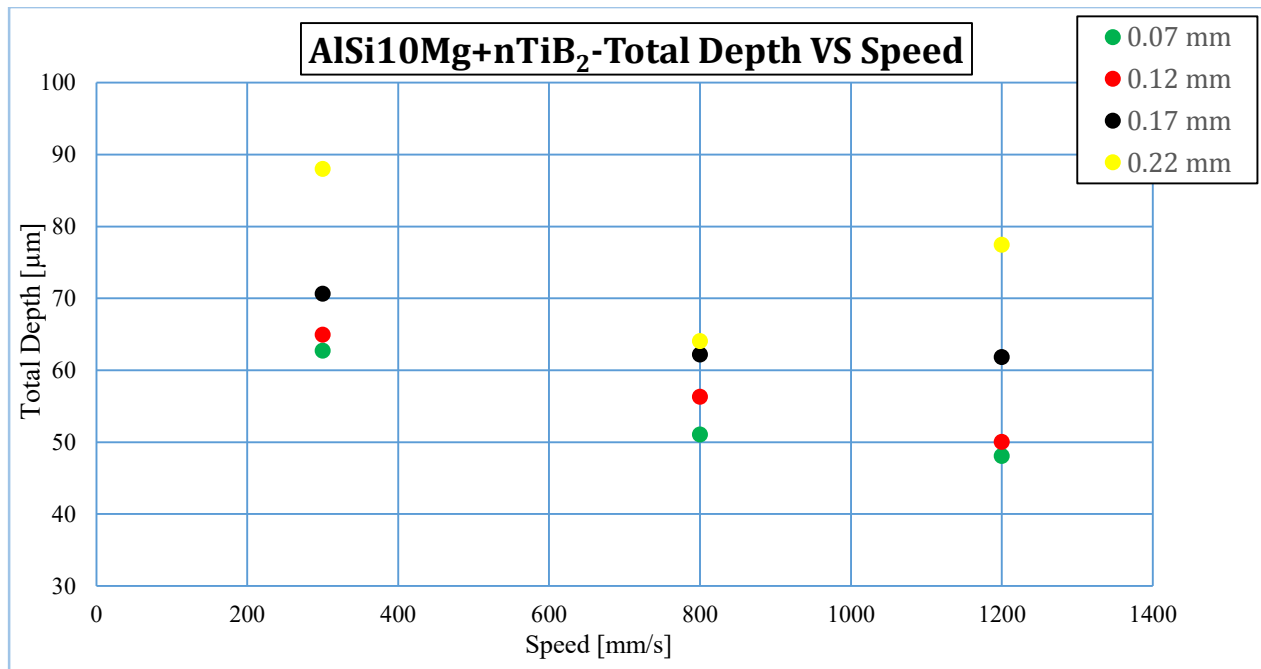


Figure 5.51 Graph of scanning speed versus total depth based on hatch distance changing, case of AlSi10Mg+nTiB₂

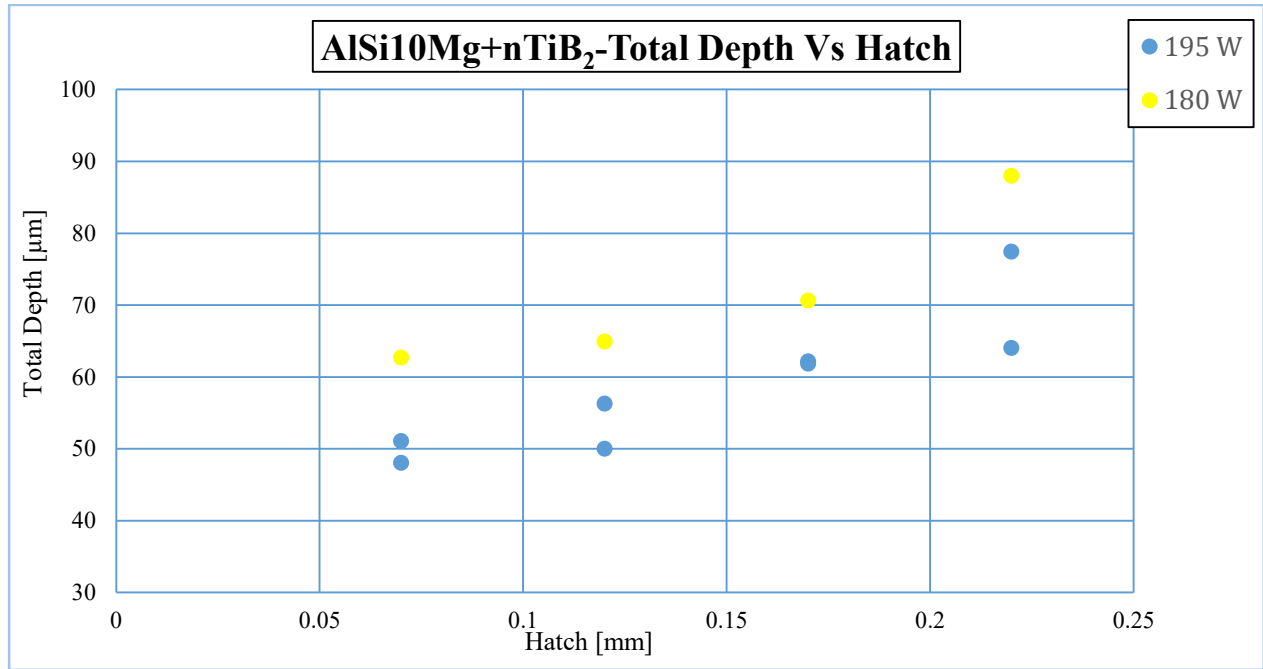


Figure 5.52 Graph of Hatch versus total depth based on power changing, case of AlSi10Mg+nTiB₂

5.3. Cubes

The final step of this thesis work was to investigate single scan tracks behavior in cubes. In other words, we wanted to see how SSTs interact with each other in a complex, when they are overlapped with each other in a layer, and join together in stacked layers one on top of the other. Cubic samples were produced in two groups for AlSi10Mg and AlSi10Mg+nTiB₂ and each one will be explained separately in the following.

5.3.1 AlSi10Mg

Cubic samples of AlSi10Mg were produced with parameters mentioned before. Parameters were chosen based on classifications of SST samples which was mentioned in section 5.1. In fact, more number of parameters were chosen inside thin and stable area and around its borders, while it was assured that parameters were chosen from all groups of SSTs.

It was interesting to see that the only built sample in group of not enough deposition powder in SSTs had not any powder deposition also in cubes. It was built with 60 W and 1900 mm/s for scanning and speed, respectively. Figure 5.53.a shows this sample after cleaning. As the figure shows, borders of cube are correctly made because they are built with standard parameters for all cubic samples, while inside of cube is totally empty which means LED was so low to deposit any powder (borders are made with 195 W power and 1200 mm/s speed). On the opposite side, there was the other sample made with very high energy density which is shown in figure 5.53.b. It was built with 50 mm/s and 150 W in speed and power, respectively. The image shows that energy density of this sample is so high that it totally re-melted the border and extrude molten powder out of it.

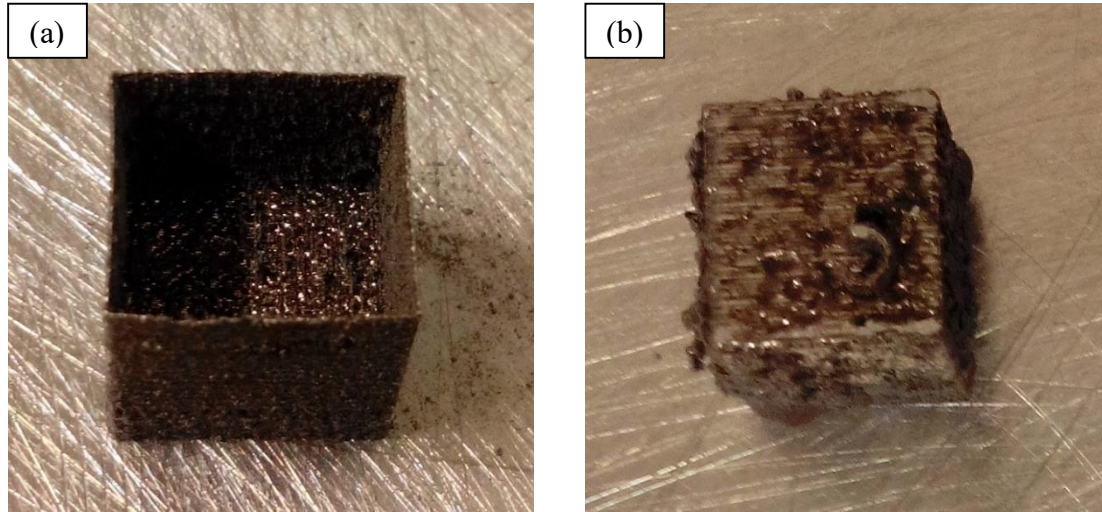


Figure 5.53 Schematic of samples built at two ends of energy density. (a) is built with lowest and (b) is built with highest amount of VED.

Figure 5.53 clearly declares that borders of samples can affect final measurements. Hence, all surfaces of samples were polished to some distance to assure any effect of borders is eliminated. Density (and hence porosity) of samples were measured with Archimedeian method, as well as image analysis of polished cross sections. The two methods are discussed in detail in separate sections.

5.3.1.1. Archimedeian Method

The first methodology relies on the Archimedeian principle that says a solid immersed in a liquid is exposed to the force of buoyancy. The value of the force is the same as that of the weight of the liquid displaced by the volume of the solid. So, by measuring the weight of the specimen both in air and liquid (water), it is possible to determine the density of the specimen using Eq. 5.3, for known density of the liquid (water density was considered equal to 1 g/cm³).

$$\rho_a = \frac{W_{air}\rho_{liquid}}{W_{air}-W_{liquid}} \quad (\text{Eq. 5.3})$$

Where W_{air} , W_{liquid} , ρ_{liquid} are the weight of sample in air, the weight of sample in water, and density of water, respectively. Archimedeian method is able to measure pure density and doesn't give any idea about surface condition or open porosities (porosity=1-Density). However, it can be elaborated to another type of density, known as "Geometrical", by which one is able to distinguish open and close porosity percentages. This parameter can be calculated using Eq. 5.4.

$$\rho_G = \frac{W_{air}\rho_{liquid}}{W_{Wet}-W_{liquid}} \quad (\text{Eq. 5.4})$$

Where W_{Wet} is weight of specimen outside of liquid while it is totally wet. The logic behind this formula is that weight of a wet sample includes weight of liquid inside open porosities on the surface which in any case, will be more than a dry one. The two values of density were measured for all samples and relative porosities was then calculated. Here we still follow the policy of not mentioning numerical values like previous sections and only bring different graphs. As it is already mentioned, the reader can find numerical results of all experiments in relative tables in appendix.

Figures 5.54 and 5.55 illustrates results of both densities plotted with respect to volumetric energy density in logarithmic scale. The first figure represents pure values of densities while the second one shows relative densities in percentage. For relative densities, the density of AlSi10Mg alloy in standard conditions was considered as 2.71 g/cm^3 . The two graphs have somehow the same concept and trend and are just represented in different scales.

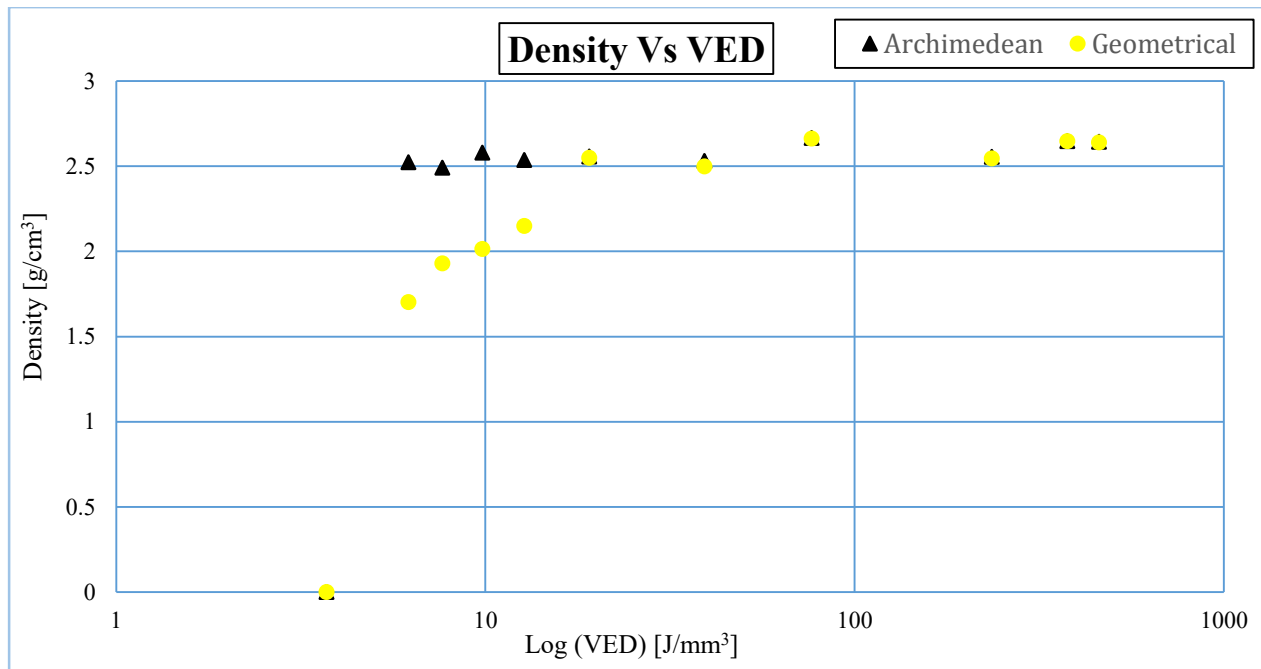


Figure 5.54 Values of Archimedean and Geometrical density of cubes of AlSi10Mg versus VED.

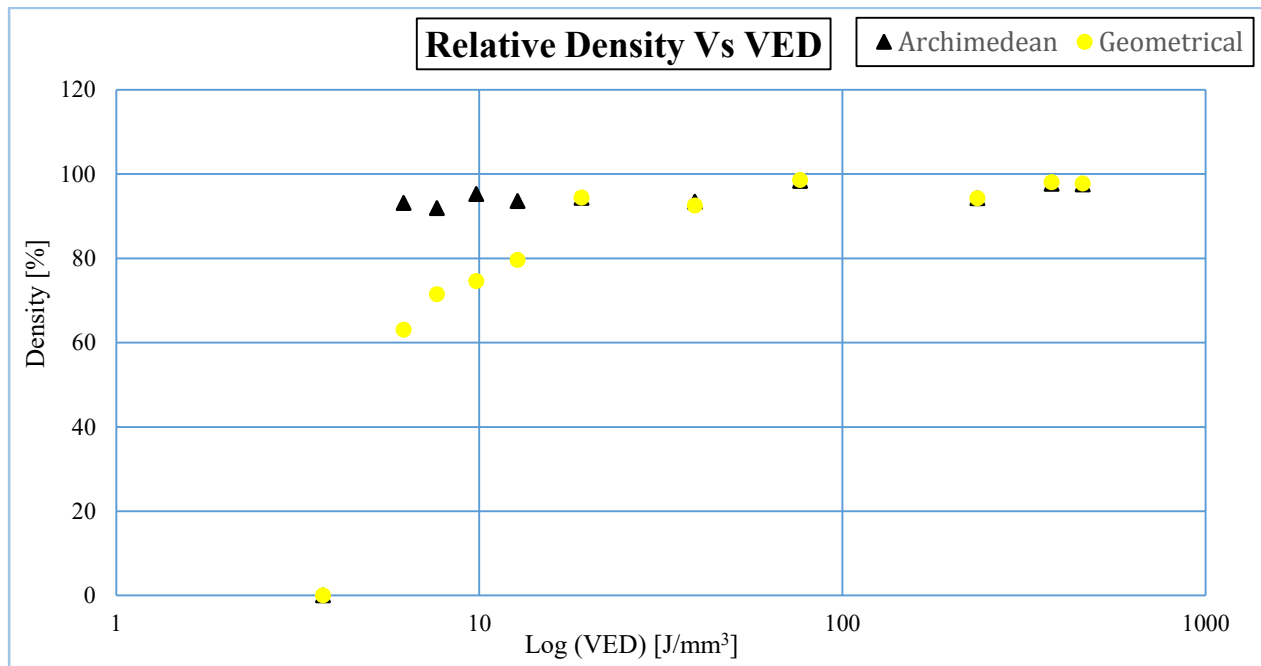


Figure 5.55 Relative values of Archimedean and Geometrical density of cubes of AlSi10Mg versus VED.

Figures 5.54 and 5.55 show that Geometrical and Archimedean density almost coincide each other for high VEDs while for low VEDs, Archimedean density exceeds its counterpart. It means that amount of open porosities is higher for lower VED and reduces with increasing VED. This effect is expected to be seen when talking about porosity graphs. On the other hand, increasing VED up to a certain point rapidly increases density to very high values close to 100% and keeps it high for further increase. Zero value for density is related to the sample with no powder deposition.

Density and porosity of surface indicate the same concept in two different ways and having one can lead to the other. However, we found it useful to also have graph of porosities here because it is the parameter that is usually used in AM to address quality of the work, rather than density. Archimedean and Geometrical density direct to two types of porosities known as open and close porosity. The first one refers to type of porosities that have access to the surface of specimen, and the latter refers to those porosities that are in the core, without any access to the surrounding. A sum of the two gives total porosity of the sample. Figure 5.56 illustrates diagram of the three types of porosity versus VED. The figure shows that open porosity receives very high values for low VEDs but it shows a very sharp reduction with growing VED. For very high VEDs, open porosity plays almost a negligible role in total porosity. On the other hand, close porosity tries to keep a stable value for high and low VEDs, but it shows a slight reduction by increasing VED. In terms of total porosity, the graph can be divided in two parts. The first one is for low VEDs in which open porosity is very high and total porosity trend capitulates to opens, and the second one for higher VEDs in which close porosity dominates and total porosity shows a trend similar to it. All in all, any type of porosity decreases with increasing VED. It is important to point out that data (100% porous) for sample with no deposition (60 W power and 1900 mm/s speed) were eliminated from the graph in order to have a more stretched graph along porosity axis and being able to see small quantities with more clarity.

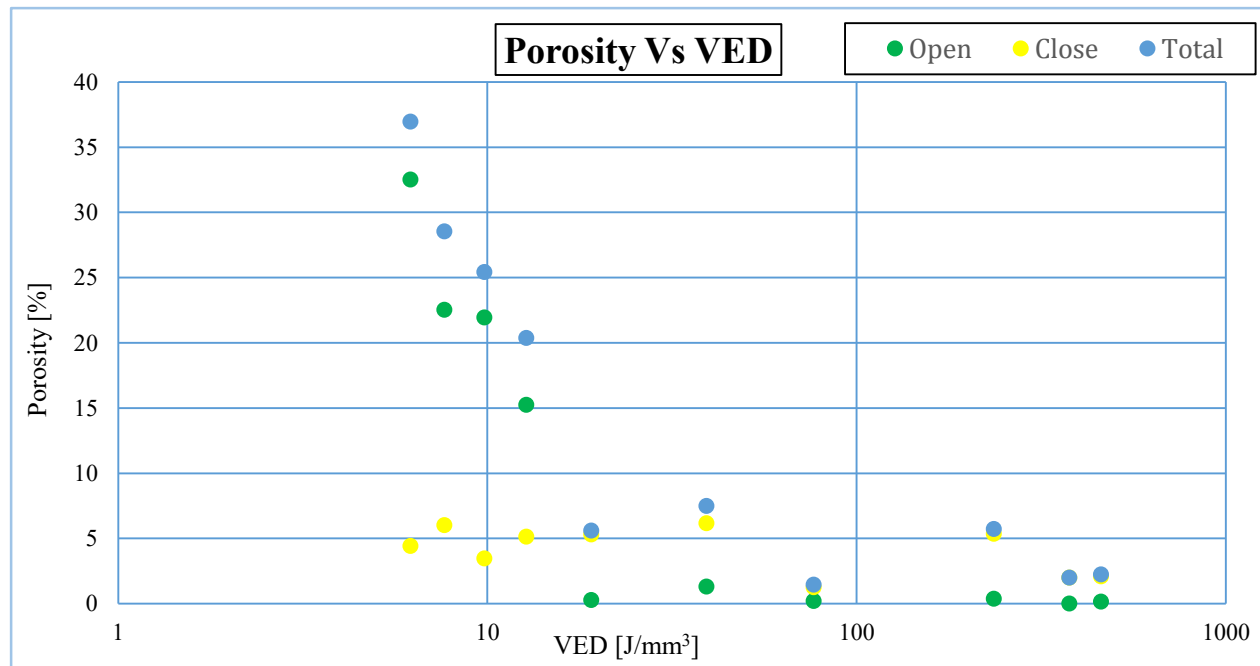


Figure 5.56 Graph of porosity of cubes of AlSi10Mg versus VED.

There should be a reason why open porosities for these types of samples are so much higher than close ones for low VEDs which will be discussed using information from image analysis.

5.3.1.2. Image Analysis

The other version of porosity analysis is to look at the glossy cross section of specimen with a magnification lens and perform image analysis on it. In another word, the cross section image is analyzed to see how much of the area of cross section is occupied by pores of any kind. Pores are designated based on changes in image color.

Cross section of cubic specimens was pictured after being finished to very fine degrees. Visual inspection of images gives a general view about correctness of input parameters. The acquired images from cross sections are represented in figure 5.57. They are prepared in a way to clearly see pores and designate their shape and trends. Based on previous declarations, each scan line direction has been in horizontal direction and perpendicular to the page. Black color is related to pores because when the light sent by optical microscope delivers to non-flat section on surface, its reflection deviates from original path and cannot reach the eye of observer, leaving a black spot instead. White color is representative of a flat background.

As we know, round shape porosities are usually representative of gas bubbles trapped inside the part while stretched shapes are related to inappropriate parameter interactions that results in non-molten powders remaining between tracks. Figure 5.57 shows that for the hatch distance considered, the best set of parameters are 195 W power and 300 mm/s for speed which results in lowest amount of porosity. It shows that for a special power (like 100 or 195 w) by increasing speed above a threshold, the dimension of tracks reduces and the set hatch distance will no longer be enough to make proper overlap between layers. So there will be lots of un-molten powder between tracks. This type of porosity which is caused due to excessive hatch distance is called “elongated Porosity” in the literature. The situation is also intensified due to not having any type of scanning strategies.

Figure 5.57 manifests very high importance of interaction of parameters in SLM to have a qualified part. It shows that although some set of power and speeds can have perfectly thin and stable tracks, putting an undesired hatch distance can ruin all principles of the game. There will remain no doubt that porosities are results of undesired hatch distance, by measuring central distance between them (by considering 200 μm scale as reference) which leads to values very close to considered hatch distance for these samples. In terms of layer thickness, it is clear that it has been chosen wisely since the amount of porosity inside consolidated sections is very limited.

Using these images one can explain why for low values of VED, values of open porosities are higher than close ones as it was mentioned in figure 5.56. The reason is because porosities for low VED are formed due to high hatch distance, there will be a high amount of un-molten powder which is exposed to air. For a better understanding, consider a porous case in figure 5.57 (like case 10). If we try to cover a porous line in shape of a rectangle, the rectangle will form a rectangular cube by going into depth. This rectangular cube is most possibly filled all with un-molten powder due to fixed hatch distance and not having any scanning strategies. So the majority of porosities inside have access to the surface which makes them open.

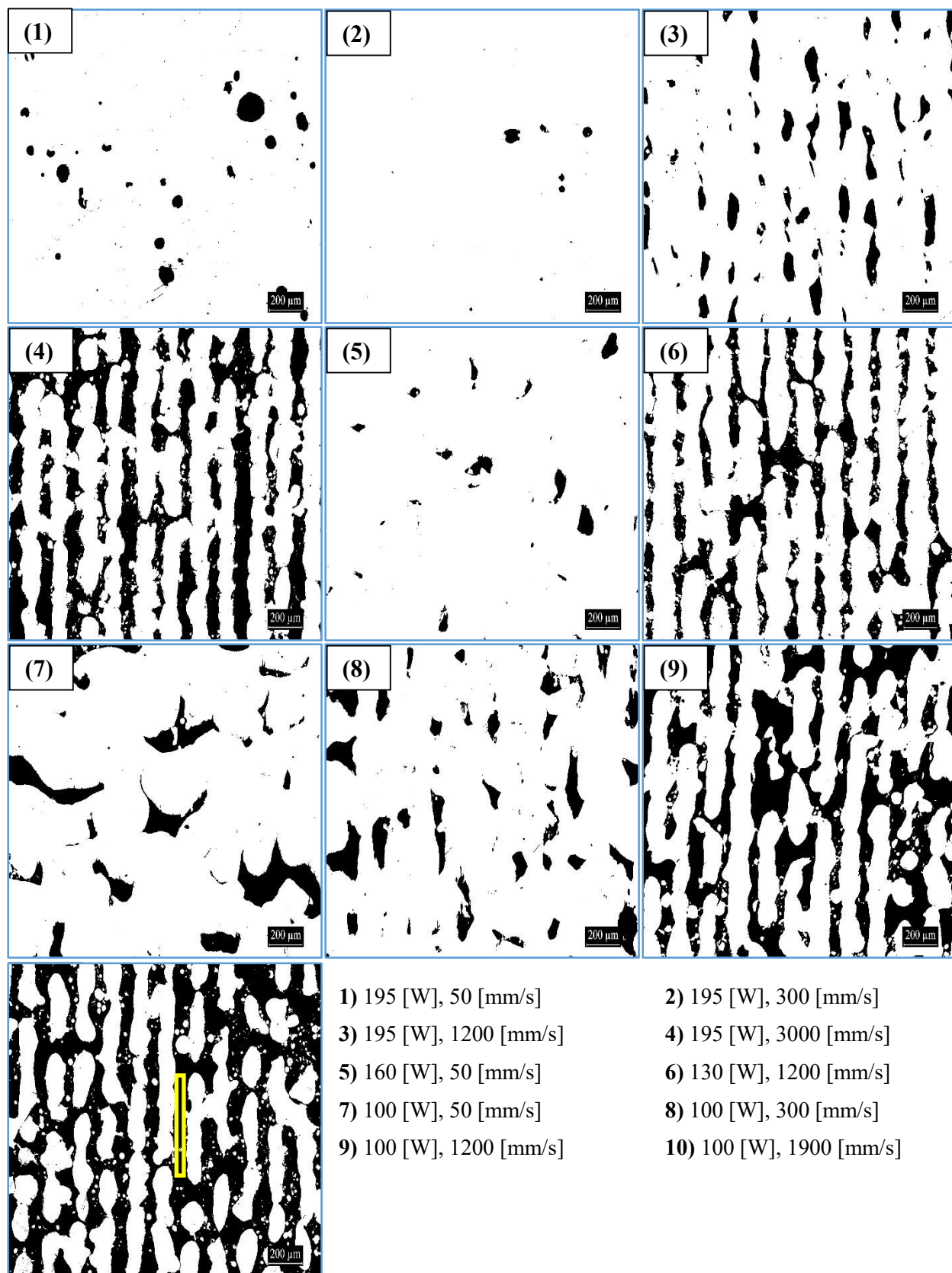


Figure 5.57 Cross sections of cubic samples of AlSi10Mg prepared for porosity analysis

The acquired images were analyzed to get percentage of porosity. We suppose the reader is informed that images without scale bar should be used to measure porosity since it highly affects the measurements. Results of the measurements are plotted in figure 5.58. The figure shows that there is a striking difference between measured values of porosity with respect to other methods. The difference is very high for high porosities (Low VED) and reduces for lower porosities where it becomes almost negligible for least porous ones. Meanwhile, the trend of porosities of image analysis is in compatible pace with total porosity of Archimedean. The reason behind higher values of image analysis than Archimedean should be discussed with regard to open porosity due to similarity of trends. The most possible reasoning behind it will be discussed in the following.

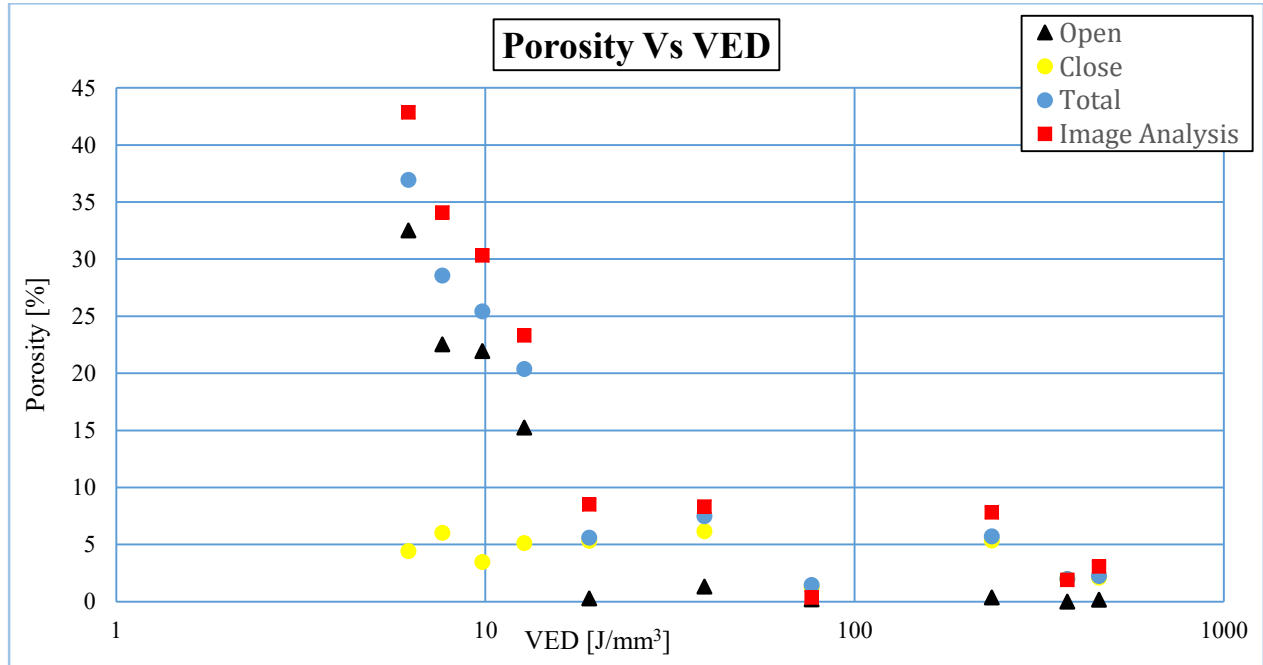


Figure 5.58 graph of VED versus all types of measured porosities of cubic samples, case of AlSi10Mg

We said that it is possible to measure open porosity by means of Archimedean method if the weight of wet sample is available. As it is obvious in figure 5.57, majority of powders in very porous parts are in shape of non molten and only exist between layers. The truth is that measuring weight of wet sample for Archimedean doesn't exactly give the "weight of sample+weight of water inside open pores", but instead, it gives "weight of sample+weight of water which is able to penetrate between unmolten powders". To explain more, it is better to refer to figure 5.59 for more clarity. The figure illustrates a typical shape of open porosity for very porous samples of figure 5.57. White circles are remaining powders which are not melt.

When water pours on the surface, it can only penetrate in spaces between powders and not into them. Such a fact causes powders to be calculated as part of the specimen in Archimedean principle. It could be true that density of powders in an area is lower than density of the same area filled with molten material, but anyhow non molten powders contribute an effective role in density. They also contribute to dry weight of specimens which results in higher density again. So it is a tricky behavior that should be considered in Archimedean method.

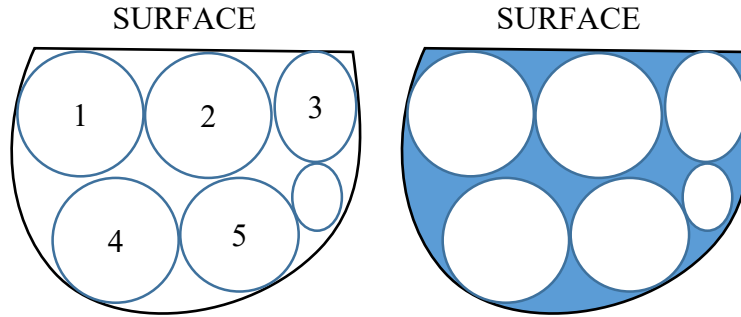


Figure 5.59 Typical shape of an open pore before (left) and after (right) wetting by water

On the other side of the coin, pictures for image analysis are taken by optical microscope that works based on light reflection from shiny surface. Referring to figure 5.59 left, powders on surface (1,2,3) may be lost during polishing, but remaining powders on bottom (4,5) don't affect measurements because microscope delivers a black spot wherever there a change in height.

The other important point is that even un-molten powders inside open porosities contribute in Archimedean density, while they are totally neglected in image analysis. These effects reduce by decreasing porosity and tend to zero for cases in which there isn't any un-molten powder remained. This behavior can be clearly seen in graph of figure 5.58. Given all what mentioned, one can conclude that porosities calculated by image analysis method are more reliable.

5.3.2 Further Discussions

The main goal of this part of thesis work is to try to establish links with previous parts in which discussions was driven about scan tracks characteristics. To do this, porosity results will be linked with those aspects of previous sections that are supposed to be more influential than the others. Both porosities attained by Archimedean and image analysis can be used in discussions, but we prefer to use one term in all cases to maintain coherency of the text. So results acquired by image analysis will be used which are by far more reliable.

As a very first step, we prepared figure 5.60 that provides a useful visual perspective about results of image analysis on process window of AlSi10Mg. The most important point to drive from the graph is that set of parameters that are close to borders of balling have considerably higher porosity compared to the ones that are closer to too thick borders. It is also quite clear that for thin and stable samples, increasing power sharply reduces level of porosity and at the same time, reducing speed can be a help for thin and stable samples to reach lower level of porosities. It is worth mentioning that samples with balling tend to show similar shape of porosity (elongated porosity), regardless of their setting parameters. In other words, samples with balling have similar (and almost equal) porosity structure whether they are produced by low or high laser powers (and speeds).

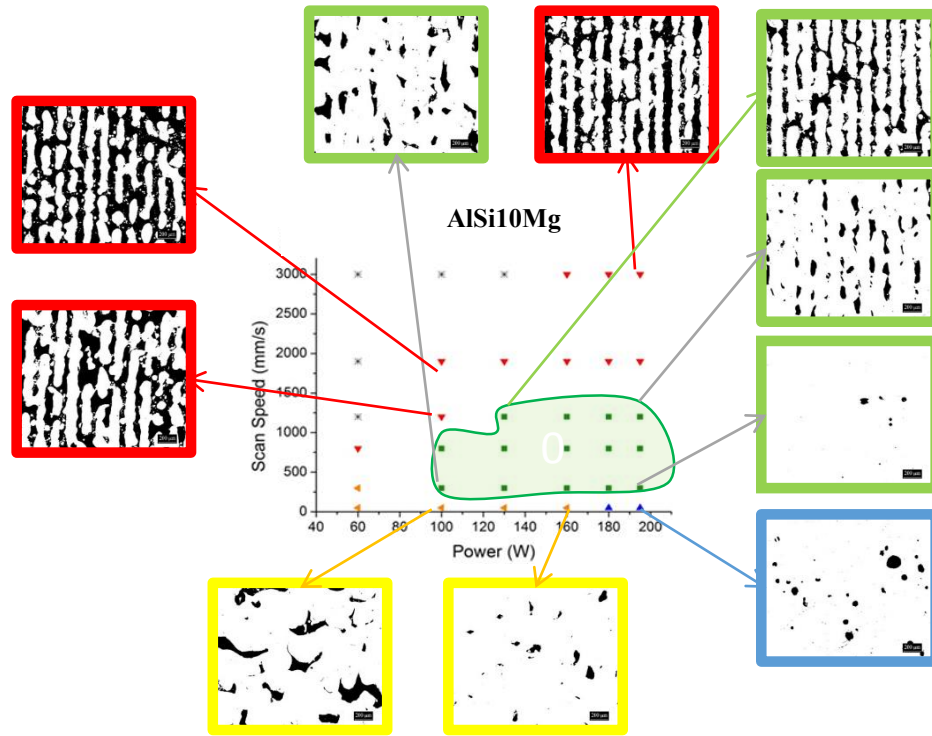


Figure 5.60 Representation of results of image analysis on process map of AlSi10Mg.

Another type of representation of figure 5.60 is illustrated in figure 5.61 that holds the same concept with addition of exact numerical values. The figure shows that best specimen in terms of porosity is number 2 which falls in groups of thin and stable tracks. It shows that the introduced method in SSTs is successful to determine optimal parameters. However, figures 3, 6, and 8 which are also in thin and stable group have not acceptable porosity which is due to unsuitable hatch distance. The reason is that all porosities are stretched along hatch path and not inside tracks. In other words, tracks are continuous wherever they are overlapped. On the opposite side, there are balling tracks which are discontinuous not only along hatch path distance, but also in lots of places where they have overlap.

Irregular tracks have a different story in this figure. The two samples have relatively low porosities compared to others. However, their porosity is not along hatch path but also in opposite direction. This condition is more obvious in figure 7. To strengthen this idea, one can compare figures 7 and 8 together which have the same power, but the first one has lower speed than latter. It is clear that although figure 8 has higher speed (which can lead to higher porosities), its porosities are more longitudinal than case 7.

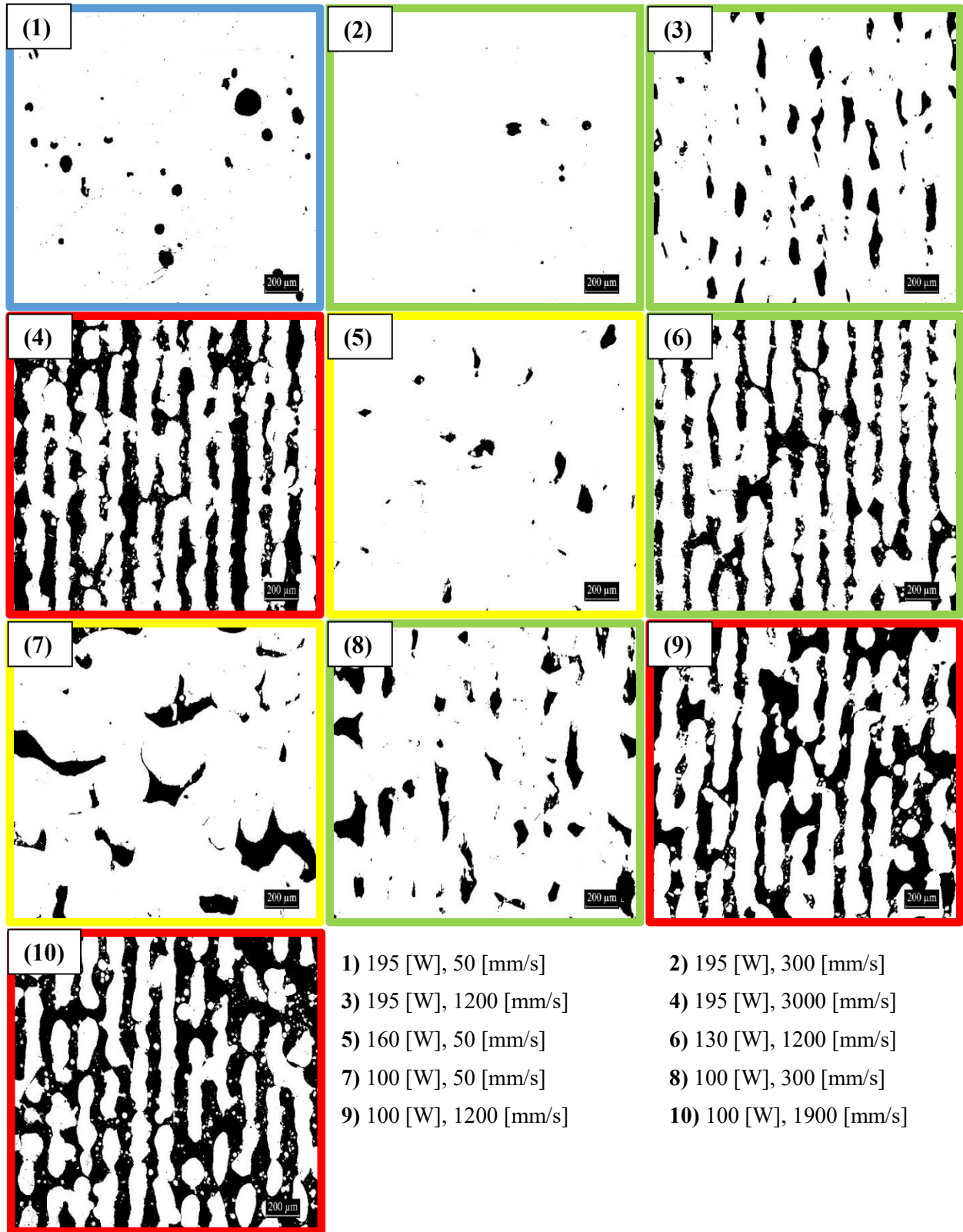


Figure 5.61 Cross sections of cubic samples of AlSi10Mg classified based on SST sample classifications. Red: Balling tracks, Green: Thin and Stable, Yellow: Irregular, Blue: Too Thick

The other point is that cases 5 and 7 are made with lowest speeds amongst all irregular samples (50 mm/s) which means laser have had enough time to dwell in a point and melt all surrounding powders. Furthermore, having high densities even for thin and stable tracks was not strange for these cases with 0.17 mm hatch distance, because it was declared in section of MSTs that this hatch can hardly give continuous structure with different sets of parameters.

In a geometrical view, overlapping of two scan tracks depends on width of them and the hatch distance between them. Given this, we recalled the measured parameters of SSTs for cases of cubic samples and plotted a graph for porosity versus “Width of track/hatch distance”. Figure 5.62 illustrates the results.

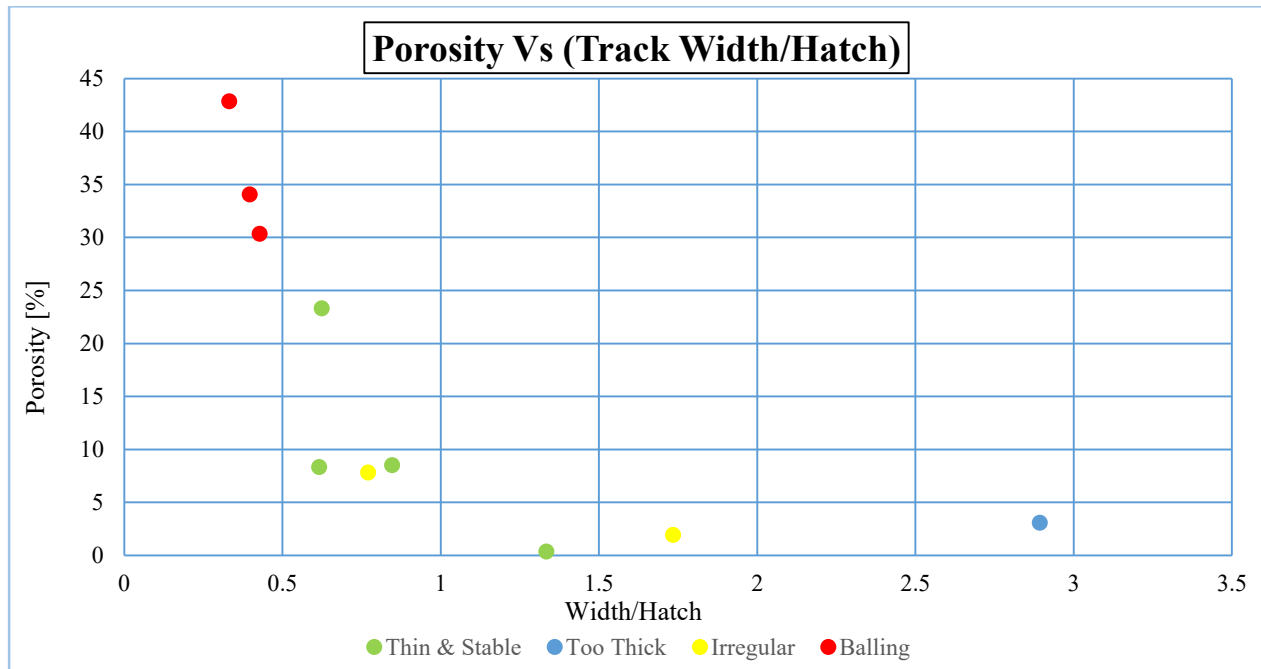


Figure 5.62 Graph of porosity of cubes versus ratio of width of tracks to hatch distance

As figure 5.62 shows, all types of SSTs in a cubic complex tend to have lower porosities when ratio of width to hatch distance is about 1.4. It can be seen by decreasing trend of porosities at both sides of the mentioned point, regardless of the type of track. So it is not by accident to see that the best point with lowest porosity (number 2 in figure 5.57) sits exactly at this point, because on one side it has all geometrical advantages in its tracks and on the other side, it has proper amount of overlap with its neighboring tracks. When hatch distance is higher than width ($\text{width/Hatch} < 1$), it gives the powder between tracks a strong potential to remain intact and demolish the part. We can conclude that in order to have dense parts out of thin and stable tracks, width of tracks should be measured and then hatch distance should be set in a way that width/hatch ratio is equal to 1.4 (we believe we can say between 1.3 to 1.4, from what is seen from graph). However, we don't have any information for behavior of this material between 0.80 and 1.4 which means it is better to do a study in this area for more details.

5.3.3. AlSi10Mg+nTiB₂

Pure results of experiments for this alloy was taken from a parallel work that was conducted in the faculty. Scanning speed and power in this study was chosen in a way to have thin and stable tracks in most of cases, while hatch distance was adjusted. Such a case provided a better strategy to study effect of hatch distance.

Density analysis of the test was performed only by Archimedeian method and geometrical density was also attained following that. The key difference between these set of tests with previous case was that it was done by changing hatch distance parallel to speed and power justifications. The other point to drive is that adjusted hatch distances were tried to be chosen in a way that always assures overlap between layers. So it was expected to see different results with respect to previous alloy. It provided a platform to see effect of wider parameters on porosity of final specimen. As a first step, the graph of relative Archimedeian and Geometrical density versus VED is represented in figure 5.63. The graph shows that Archimedeian density is always higher than Geometrical, but their difference is higher for lowest VEDs. It is due to the fact that lower VEDs cause to produce more open porosities in the part that will affect difference between the two densities. It is interesting to see that majority of samples have high densities which is a result of choosing thin and stable tracks with appropriate hatch distance. This graph can be used as a reference to say that “single scan strategy is certified to be a useful way to represent process window of a material and at the same time, help to choose best parameters and optimize the process”. However, those set of parameters (power and speed) should always be chosen that lead to thin and stable tracks and besides, hatch distance should be chosen based on the layer width to assure enough overlap between layers.

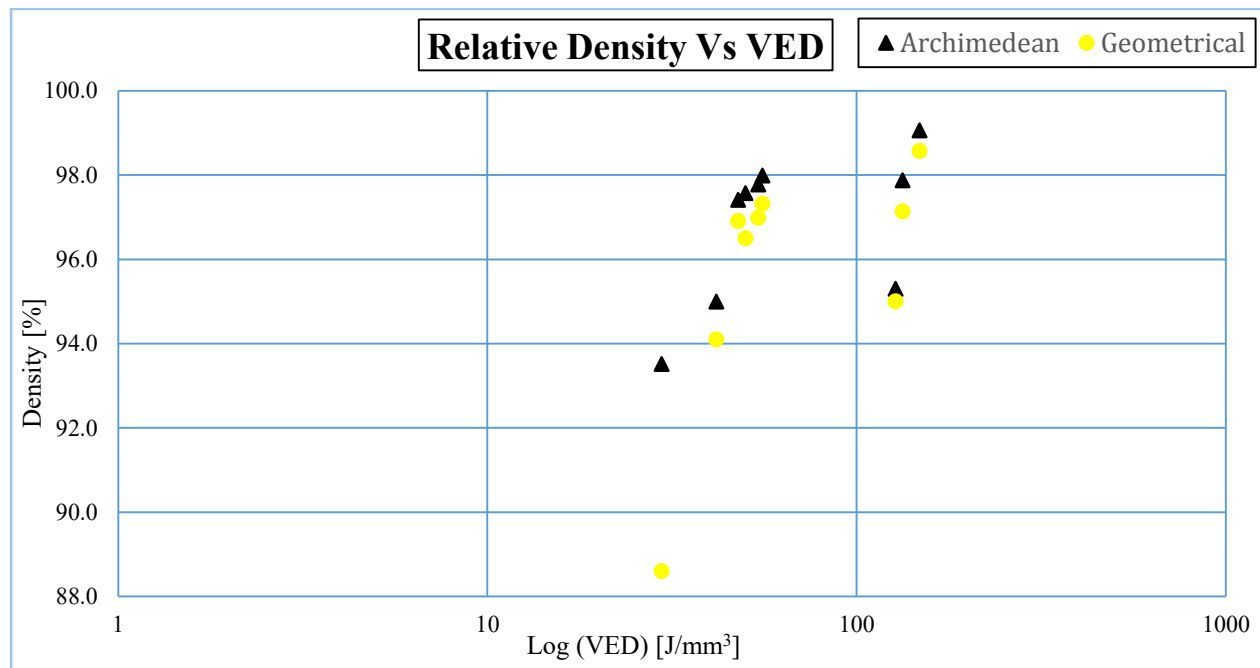


Figure 5.63 Relative Archimedeian and Geometrical density of cubic samples versus volumetric energy density, case of AlSi10Mg+nTiB₂

A short comparison between results of this MMC and AlSi10Mg (Figure 5.63 and 5.55) can be interesting. In figure 5.55 that was related to AlSi10Mg, the difference between two densities was

very high for low VEDs, but it became negligible for higher values. However, figure 5.63 shows that there is a steady difference between the two densities of MMC. It is due to the fact that setting parameters for majority of samples were amongst optimal ones which led to steady values of density. Hence, the sharp trend that was observed for the alloy is not valid here.

Different porosity levels of samples were calculated based on densities. Figure 5.64 illustrates the graph of open, close and total porosity of this material with respect to VED. The graph shows a decreasing tendency for three types of open, close and total porosity with respect to VED which is similar to AlSi10Mg cases. However, open porosities always keep lower values than close ones which is opposite of previous case. It happens thanks to adjusted hatch distance and scanning strategy that provided enough overlap between scan lines and eliminates non-molten powders in structure.

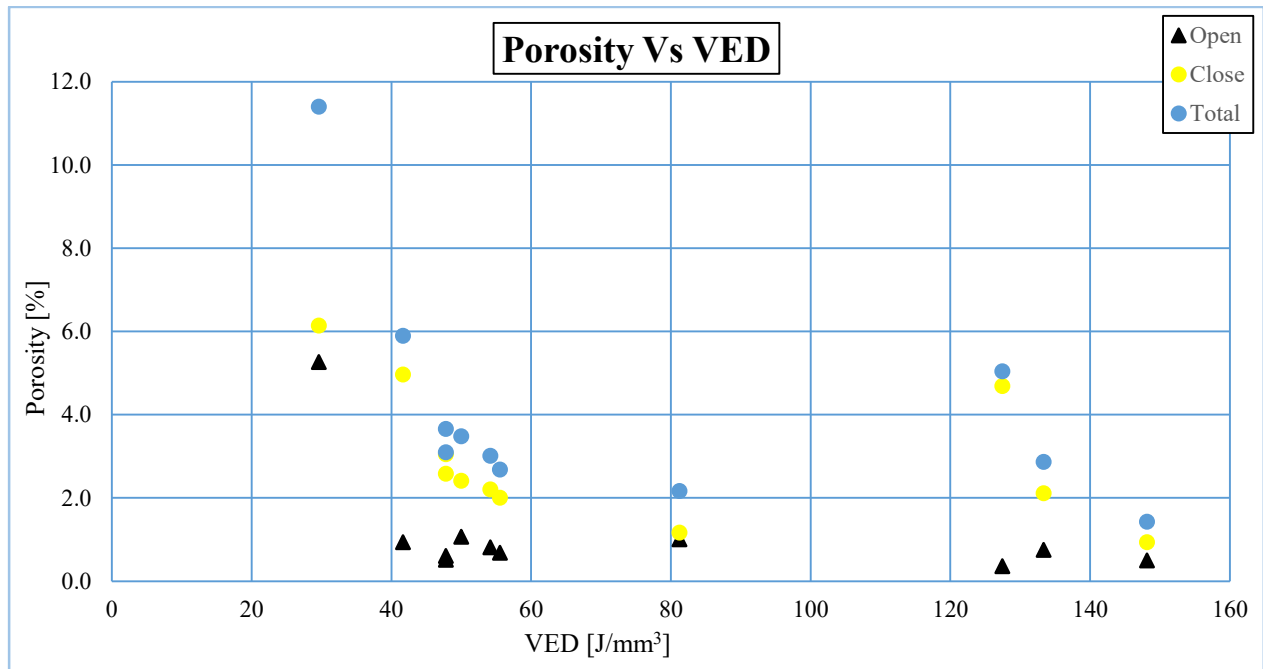


Figure 5.64 Graph of open, close and total porosities of AlSi10Mg+nTiB₂ with respect to VED.

In order to link acquired results with previous sections, we plotted the graph of Width of tracks/hatch versus porosity for cubes. The result graph is illustrated in figure 5.65. The mentioned graph shows slightly similar results to AlSi10Mg case in sense that as the width-hatch ratios decreases to values lower than one, porosity increases to very high values. If we only consider thin and stable track, there is a tendency to very low values of porosity when the ratio reaches 1.3 to 1.4. We did it by linear regression of data of thin and stable tracks which resulted in 1.33 for width/hatch distance ratio. This result is compatible with what was driven for the case of AlSi10Mg and mentions that thin and stable tracks can lead to parts with least amount of porosity only if there is acceptable overlap between them. This acceptable value of overlap should be in a way that ratio of width/hatch distance is between 1.3 to 1.4.

As a general rule to make, we can say that for any process selection or optimization, thin and stable tracks should be chosen based on what was explained in SST section, and then hatch distance

should be set in a way to assure that scan lines overlap with each other in a way that width/hatch distance is between 1.3 to 1.4, based on what is measured for width of tracks.

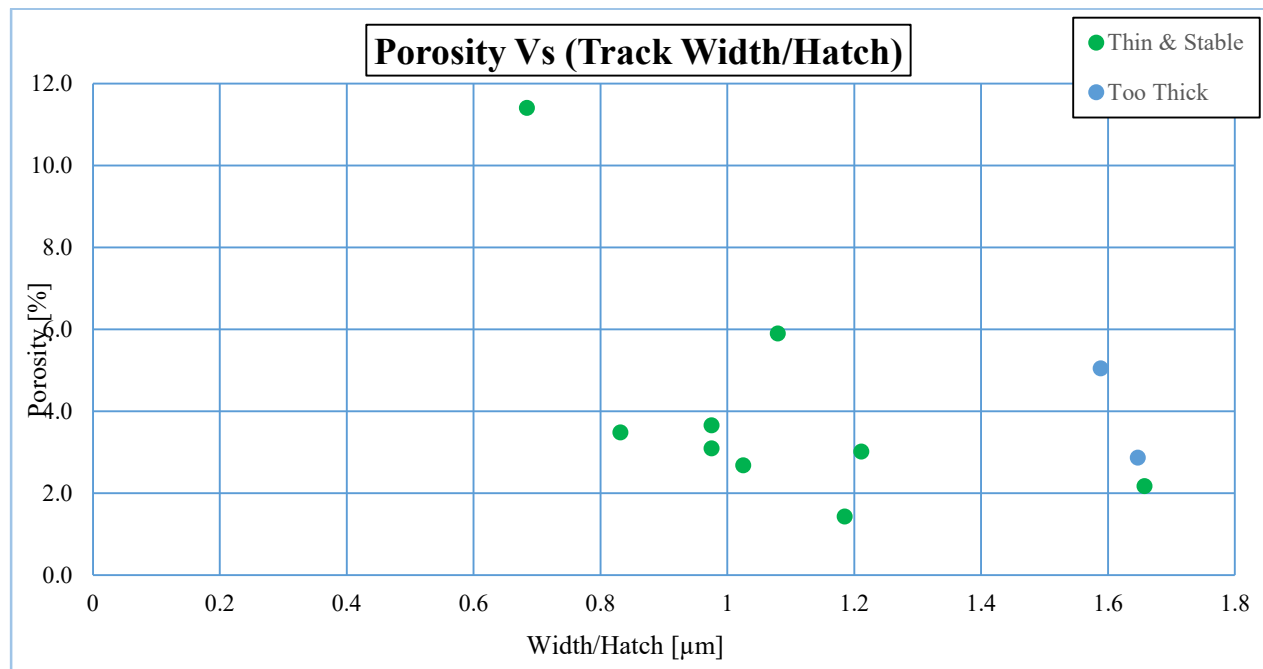


Figure 5.65 Graph of ratio of width of SST samples to hatch distance with respect to porosity

6. CONCLUSIONS

This study was devoted to investigate possibility of using SST strategy to draw SLM process window of a powder and use it for new production or optimization of existing process. The goal was achieved by designing experiments in three classes. The first two classes included studying SST and MST strategies to define process parameter setup, and the last class was putting those parameters in action to produce cubes and check if strategies succeeded. A357, AlSi10Mg, and AlSi10Mg+nTiB₂ were used as powder materials.

At the very first step, the process window of each alloy was defined based on on-top and cross sectional analysis of scan tracks. It was showed that there are five close regions in each graph, each one including scan tracks that are pretty much similar to each other. The regions were called based on their track shape to “Not Enough Deposition”, “Balling”, “Thin and Stable”, “Irregular”, and “Too thick”, among which only thin and stable is of importance in production. These regions were considered as references for further analysis. It was shown that all types of powder materials have these regions in their process window and the only difference between them is related to border of each region. Based on same classification, it was concluded that A357 has most difficult processability, while the other two materials keep pace with each other. However, addition of TiB₂ increases powder absorptivity that was evident in graphs. The results of three materials showed that increasing scan speed above a threshold causes instability, while increasing power always directs the process towards stable regions.

In order to have a brighter view of process window, all geometrical aspects of SSTs were studied from on-top and cross sectional view. The results showed that studying a SST only from one side can easily lead to wrong results, so both longitudinal and cross sectional aspects must be considered. The on-top analysis showed that there is a medium range for on top width for which standard deviation of measurements (instability of SST) is very low and can lead to thin and stable tracks. Any step out of this range deteriorates the track shape and makes it of no interest for production purposes. On the other hand, six parameters were defined and studied in full detail for cross section of a SST. These parameters were Total depth, Width, h growth, lower depth, angle, and area of the melt pool. The study showed regardless of type of the powder material, it is necessary for each geometrical parameter to be in special range to have thin and stable tracks. For example, the value of angle for any type of powder should be near perpendicular or slightly obtuse, and very small or large angles are not acceptable. In terms of energy density, it was concluded that total depth, width, lower depth, and area of pool increases by energy density while h growth and angle show different behaviors. Optimal energy density for the thin and stable tracks were found to be between 0.1 and 1 [J/mm, in logarithmic scale]. However, it was proven that it is necessary for energy density to be in a special range to have thin and stable tracks, but not enough. It means that interaction of parameters should also be considered. Too thick tracks showed very sharp changes almost in all graphs and their strange behavior was explained with keyhole transition.

The second part of experiments which was done on MSTs showed that in order to have continuous layer, the hatch distance must be chosen with extreme care. It was proven that increasing hatch

distance to a threshold keeps continuity of tracks, whereas any value above that threshold breaks down continuity of tracks and deteriorates final properties by causing elongated porosities.

The information acquired from SSTs and MSTs was used to perform third part of experiments which was producing and analyzing cubic samples out of AlSi10Mg and its metal matrix composite. The results showed that regardless of powder material, increasing VED for samples increases all types of open, close, and total porosities. The most important conclusion in this part was that in order to have final parts with acceptable porosity, an appropriate amount of overlap between tracks should be assured besides having parameters for thin and stable tracks. The proper overlap for AlSi10Mg and its MMC was proven to be in a way that width/hatch distance ratio is between 1.3 to 1.4 (about 1.33), which gives parts with near full density. However, for width/hatch distance of aluminum alloy between 0.80 to 1.3, we didn't have enough points to see behavior and we think it is better to study the alloy also in this area. Given all the works above, a simple methodology was concluded to pursue in order to have parts with optimized parameters. This methodology is represented in the following:

The first work to deal with new powder in SLM is to define process window based on range of power and scanning speed of the machine. A design of experiment method can be used for this purpose. Layer thickness can change or remain constant at this stage. The produced samples out of designed data are then analyzed on top and in cross section to define different groups of samples. Then MST samples can be produced to investigate effect of different hatch distances based on the rule of overlapping mentioned above. At this point, it is possible to produce some few cubic samples if there are any dark points about data. If the data are derived with enough certainty, they can be used for final production purposes.

LIST OF SYMBOLS

Acronym	Explanation
3DP	Three Dimensional Printing
AM	Additive Manufacturing
Al	Aluminum
AMCs	Aluminum Matrix Composites
Co ₂	Carbon Dioxide
CIS	Chemically Induced Sintering
CAD	Computer Aided Design
DEP	Direct Energy Deposition
DMD	Direct Metal Deposition
DMLS	Direct Metal Laser Sintering
EBM	Electron Beam Melting
FESEM	Field Emission Scanning Electron Microscope
FF	Freeform Fabrication
FDM	Fused Deposition Modelling
h	Hatch Distance
HIP	Hot Isostatic Pressing
LOM	Laminated Object Manufacturing
LAM	Laser Additive Manufacturing
LPBF	Laser Powder Bed Fusion
LM	Layer Manufacturing
LED	Linear Energy Density
LPS	Liquid Phase Sintering
MI	Material Ingress
MST	Multi Scan Track
MMC	Metal Matrix Composite
P	Power

PBF	Powder Bed Fusion
RM	Rapid Manufacturing
RP	Rapid Prototyping
RT	Rapid Tooling
SLM	Selective Laser Melting
SLS	Selective Laser Sintering
SST	Single Scan Tracks
STL	Standard Tessellation Language
SL	Stereolithography
SLA	Stereolithography Apparatus
SGC	Solid Ground Curing
SSS	Solid State Sintering
t	Layer Thickness
UV	Ultra-Violet
v	Laser Scanning Speed
VP	Vat Photopolymerization
VED	Volumetric Energy Density
YAG	Ytterbium-Aluminum-Garnet

REFERENCES

- [1] Esmaeilian, B., Behdad, S., and Wang, B, 2016, The evolution and future of manufacturing: a review. *J. of Manuf. Sys.* **39**, 79-100.
- [2] Wohlers, T., and Gornet, T., 2014, History of additive manufacturing, *Wohlers Associates*, Annual worldwide progress report. Additional materials at wohlersassociates.com.
- [3] Kodama, H., 1981, Automatic method for fabricating a three dimensional plastic model with photo hardening polymer. *Rev. Sci. Instrum.* **52** (11), 1770-1773.
- [4] Bartolo, P., J., 2011, Stereolithography: materials, processes and applications, Chap. 2, Springer New York Dordrecht Heidelberg London, pp. 37-56.
- [5] Srivatsan, T. and S., Sudarshan, T., S., 2016, Additive manufacturing, innovations, advances, and applications, Chap. 1, Taylor & Francis Group, USA, pp. 1-48.
- [6] Shellabear, M. and Nyrhila, O., 2004, DMLS-Development history and state of the art. *Proc. LANE 2004 conference (LANE 2004)*, Erlangen, Germany, September 21-24, pp. 1-12.
- [7] American Society for Testing and Materials ASTM, 2009, Standards for additive manufacturing, ASTM-F42, Pennsylvania.
- [8] Wirth, M. and Thiesse, F., 2014, Shapeways and the 3D printing evolution. *Twenty second European conference on Information Systems*, Tel Aviv, Israel, June 9-11, pp. 1-14.
- [9] Wohlers, T., and Gornet, T., 2016, History of additive manufacturing, *Wohlers Associates*, Annual worldwide progress report. Additional materials at wohlersassociates.com.
- [10] ASTM International, "F2792-12a - Standard Terminology for Additive Manufacturing Technologies," Rapid Manuf. Assoc., 2013.
- [11] Gibson, I., Rosen, D. and Stucker, B., 2014, Additive manufacturing technologies: 3D printing, rapid prototyping, and direct digital manufacturing, Chap. 1, Springer, New York, pp. 1-18.
- [12] Heynick, M. and Stotz, I., 2013, 3D CAD, CAM, and rapid prototyping. *LAPA Digital Technology Seminar*, Workshop 1. May 10 & 11, Version 1, EPFL.
- [13] Enamul Hoque, M., 2011, Advance applications of rapid prototyping technology in modern engineering, Janeza Trdine, Rijeka, Croatia.
- [14] Muthu, S. S. and Savalani, M. M., 2016, Handbook of sustainability in additive manufacturing, Vol. 1, Chap. 1, Springer, Singapore, pp. 1-5.
- [15] Gibson, I., Rosen, D. and Stucker, B., 2014, Additive manufacturing technologies: 3D printing, rapid prototyping, and direct digital manufacturing, Chap. 3, Springer, New York, pp. 43-61.
- [16] Gu, D., 2015, Laser additive manufacturing of high performance materials, Chap. 1-2, Springer, Verlag Berlin Heidelberg, pp. 1-13.

- [17] Brandt, M., 2017, Laser additive manufacturing: materials, design, technologies and applications, Chap. 1, Woodhead Publishing Series in Electronic and Optical Materials (88), Elsevier, pp. 1-18.
- [18] Bandyopadhyay, A., Gualtieri, T., and Bose, S., 2016, Additive Manufacturing, Chap. 1, Taylor & Francis Group, Florida, USA, pp.1-16.
- [19] Manfredi, D., Calignano, F., Krishnan, M., Canali, R., Ambrosio, E., Biamino, S., Ugues, D., Pavese, M. and Fino, P., 2014, Light metal alloys applications, Chap. 1, InTech, pp. 3-34.
- [20] Gibson, I., Rosen, D. and Stucker, B., 2014, Additive manufacturing technologies: 3D printing, rapid prototyping, and direct digital manufacturing, Chap. 2, Springer, New York, pp. 19-42.
- [21] Turner, B., Strong, R., Gold, S., 2014, A review of melt extrusion additive manufacturing processes: I. Process design and modeling. *Rap. Protot. J.*, 192-204.
- [22] www.custompartnet.com/wu/fused-deposition-modeling.
- [23] Gibson, I., Rosen, D. and Stucker, B., 2014, Additive manufacturing technologies: 3D printing, rapid prototyping, and direct digital manufacturing, Chap. 4, Springer, New York, pp. 63-107.
- [24] www.custompartnet.com/wu/stereolithography.
- [25] Gibson, I., Rosen, D. and Stucker, B., 2014, Additive manufacturing technologies: 3D printing, rapid prototyping, and direct digital manufacturing, Chap. 7, Springer, New York, pp. 175-204.
- [26] www.utwente.nl/en (University of Twente-Additive Manufacturing).
- [27] Gibson, I., Rosen, D. and Stucker, B., 2014, Additive manufacturing technologies: 3D printing, rapid prototyping, and direct digital manufacturing, Chap. 8, Springer, New York, pp. 205-218.
- [28] www.custompartnet.com/wu/3d-printing.
- [29] Gibson, I., Rosen, D. and Stucker, B., 2014, Additive manufacturing technologies: 3D printing, rapid prototyping, and direct digital manufacturing, Chap. 9, Springer, New York, pp. 219-244.
- [30] <http://www.custompartnet.com/wu/laminated-object-manufacturing>.
- [31] Gibson, I., Rosen, D. and Stucker, B., 2014, Additive manufacturing technologies: 3D printing, rapid prototyping, and direct digital manufacturing, Chap. 10, Springer, New York, pp. 245-268.
- [32] Bhavar, V., Kattire, p., Patil, V., Khot, S., Gujar, K., Singh, J., 2014, A review of powder bed fusion technology of metal additive manufacturing. *Presented at 4th International conference and exhibition on Additive Manufacturing Technologies-AM*, Bangalore, India, September 1-2.
- [33] Gibson, I., Rosen, D. and Stucker, B., 2014, Additive manufacturing technologies: 3D printing, rapid prototyping, and direct digital manufacturing, Chap. 5, Springer, New York, pp. 107-146.

- [34] <http://www.popular3dprinters.com/electron-beam-melting-ebm>.
- [35] Srivatsan, T. and S., Sudarshan, T., S., 2016, Additive manufacturing, innovations, advances, and applications, Chap. 3, Taylor & Francis Group, USA, pp. 69-100.
- [36] <https://www.empa.ch/web/coating-competence-center/selective-laser-melting>.
- [37] Bandyopadhyay, A., Gualtieri, T., and Bose, S., 2016, Additive Manufacturing, Chap. 4, Taylor & Francis Group, Florida, USA, pp. 97-142.
- [38] Kruth, J., P., Mercelis, P., Froyen, L., Rombouts, M., 2005, Binding mechanisms in selective laser sintering and selective laser melting. *Rap. Protot. J.*, **11** (1), 26-36.
- [39] Gu, D., 2015, Laser additive manufacturing of high performance materials, Chap. 2, Springer, Verlag Berlin Heidelberg, pp. 15-72.
- [40] Mower, T. M., Long, M. J., 2016, Mechanical behavior of additive manufactured, powder-bed laser-fused materials. *Mater. Sci. & Eng. A*, **651**, 198-213.
- [41] Aboulkhair, N., T., Everitt, N., M., Ashcroft, I. and Tuck, C., 2014, Reducing porosity in AlSi10Mg parts processed by selective laser melting. *Addit. Manuf.*, **1-4**, 77-86.
- [42] Cheng, B., Shrestha, S. and Chou, K., 2016, Stress and deformation evaluations of scanning strategy effect in selective laser melting. *Addit. Manuf.*, **12**, 240-251.
- [43] Brandt, M., 2017, Laser additive manufacturing: materials, design, technologies and applications, Chap. 2, Woodhead Publishing Series in Electronic and Optical Materials (88), Elsevier, pp. 55-77.
- [44] Yadroitsev, I. and Smurov, I., 2010, Selective laser melting technology: from the single laser melted track stability to 3D parts of complex shape. *Phys. Proc.*, **5**, 551-560.
- [45] Li, R., Liu, J., Shi, Y., Wang, L. and Jiang, W., 2012, Balling behavior of stainless steel and nickel powder during selective laser melting process. *Int. J. Adv. Manuf. Tech.*, **59**, 1025-1035.
- [46] Liu, Y., Yang, Y., Mai, S., Wang, D. and Song, C., 2015, Investigation into spatter behavior during selective laser melting of AISI 316L stainless steel powder. *Mater. And desi.* **87**, 797-806.
- [47] Olakanmi, E. O., Cochrane, R. F. and Dalgarno, K. W., 2015, A review on selective laser sintering/melting (SLS/SLM) of aluminum alloy powders: Processing, microstructure, and properties. *Prog. In Mater. Sci.*, **74**, 401-477.
- [48] Sercombe, T. B. and Li, X., 2016, Selective laser melting of aluminum and aluminum metal matrix composites: review. *Mater. Tech.*, **31:2**, 77-85,
- [49] Olakanmi, E. O., 2013, Selective laser sintering/melting (SLS/SLM) of pure Al, Al-Mg, and Al-Si powders: Effect of processing conditions and powder properties. *J. Mater. Proc. Tech.*, **213**, 1387-1405.
- [50] Buchbinder, D., Schleifenbaum, H., Heidrich, S., Meiners, W. and Bültmann, J., 2011, High Power Selective Laser Melting (HP SLM) of aluminum parts. *Phys. Proc.*, **12**, 271-278.
- [51] Louvis, E., Fox, P. and Sutcliffe, C. J., 2011, Selective laser melting of aluminum components. *J. Mater. Proc. Tech.*, **211**, 275-284.

- [52] Aboulkhaira, N., Maskeryb, I., Ashcroftb, I., Tuckb, C. and Everitt, N. (2015), The role of powder properties on the processability of Aluminum alloys in selective laser melting. *Laser World of Photonics Congress 2015: Lasers in Manufacturing conference, WLT*, Munich, Germany.
- [53] Jhabvalaa, J., Boillata, E., Antignac, T. and Glardon, R., 2010, On the effect of scanning strategies in the selective laser melting process. *Virt. and Phys. Protot.*, **5** (2), 99-109.
- [54] Read, N., Wang, W., Essa, K. and Attallah, M., 2015, Selective laser melting of AlSi10Mg alloy: Process optimization and mechanical properties development. *Mater. And Desig.*, **65**, 417-424.
- [55] Kempen, K., Thijs, L., Van Humbeeck, J. and Kruth, J. P., 2012, Mechanical properties of AlSi10Mg produced by Selective Laser Melting. *Phys. Proc.*, **39**, 439-446.
- [56] Herzog, D., Seyda, V., Wycisk, E. and Emmelmann, C., 2016, Additive manufacturing of metals. *Acta Mater.*, **117**, 371-392.
- [57] SIMONELLI, M., TUCK, C., ABOULKHAIR, N. T., MASKERY, I., ASHCROFT, I., WILDMAN, R. and HAGUE, R., 2015, A Study on the Laser Spatter and the Oxidation Reactions During Selective Laser Melting of 316L Stainless Steel, Al-Si10-Mg, and Ti-6Al-4V. *The Miner., Metals & Mater. Soci. and ASM Int.*, **46A**, 3842-3851.
- [58] Lorusso, M., Aversa, A., Manfredi, D., Calignano, F., Ambrosio, E., Ugues, D. and Pavese, M., 2016, Tribological Behavior of Aluminum Alloy AlSi10Mg-TiB2 Composites Produced by Direct Metal Laser Sintering (DMLS). *J. of Mater. Eng. And Perform.*, **25** (8), 3152-3160.
- [59] Manfredi, D., Calignano, F., Krishnan, M., Canali, R., Ambrosio, E., Biamino, S., Ugues, D., Pavese, M. and Fino, P., 2014, Additive Manufacturing of Al Alloys and Aluminum Matrix Composites (AMCs), Light Metal Alloys Applications, Chap. 1, InTech.
- [60] Chen, M., Li, X., Ji, G., Wu, Y., Chen, Z., Baekelant, W., Vanmeensel, K., Wang, H. and Kruth, J. P., 2017, Novel Composite Powders with Uniform TiB2 Nano-Particle Distribution for 3D Printing. *Appl. Sci.*, **7** (250), 1-9.
- [61] Li, X., Ji, G., Chen, Z., Addad, A., Wu, Y., Wang, H., Vleugels, J., Van Humbeeck, J. and Kruth, J. P., 2017, Selective laser melting of nano-TiB2 decorated AlSi10Mg alloy with high fracture strength and ductility. *Acta Mater.*, **129**, 183-193.
- [62] Childs, T. H. C., Hauser, C. and Badrossamay, M., 2004, Mapping and Modelling Single Scan Track Formation in Direct Metal Selective Laser Melting. *CIRP Annals-Manufacturing Technology*, **53** (1), 191-194.
- [63] Hauser, C., Childs, T. H. C. and Badrossamay, M., 2004, Further developments in process mapping and modelling in direct metal selective laser melting. *15th Solid Free Form Fabrication Proceedings*, Austin-Texas, USA.
- [64] Wang, D., Yang, Y., Su, X. and Chen Y., 2012, Study on energy input and its influences on single-track, multi-track, and multi-layer in SLM. *Int. J Adv. Manuf. Technol.*, **58**, 1189-1199.
- [65] Ciurana, J., Hernandez, L. and Delgado, J., 2013, Energy density analysis on single tracks formed by selective laser melting with CoCrMo powder material. *Int. J Adv. Manuf. Technol.*, **68**, 1103-1110.

- [66] Gu, D. and Shen, Y., 2009, Balling phenomena in direct laser sintering of stainless steel powder: Metallurgical mechanisms and control methods. *Mater. And Desig.*, **30**, 2903-2910.
- [67] Beal, V. E., Erasenthiran, P., Hopkinson, N., Dickens, P. and Ahrens, C. H., 2006, The effect of scanning strategy on laser fusion of functionally graded H13/Cu materials. *Int. J. Adv. Manuf. Technol.*, **30**, 844-852.
- [68] Yadroitsev, I., Gusarov, A., Yadroitseva, I. and Smurov, I., 2010, Single track formation in selective laser melting of metal powders. *J. Mater. Proc. Tech.*, **210**, 1624-1631.
- [69] Yadroitsev, I. and Smurov, I., 2011, Surface Morphology in Selective Laser Melting of Metal Powders. *Phys. Proc.*, **12**, 264-270.
- [70] Yadroitsev, I., Yadroitsev, I., Bertrand, P. and Smurov, I., 2012, Factor analysis of selective laser melting process parameters and geometrical characteristics of synthesized single tracks. *Rap. Protot. J.*, **18** (3), 201-208.
- [71] Yadroitsev, I., Krakhmalev, P., Yadroitsev, I., Johansson, S., and Smurov, I., 2013, Energy input effect on morphology and microstructure of selective laser melting single track from metallic powder. *J. Mater. Proc. Tech.*, **213**, 606-613.
- [72] Rao, H., Giet, S., Yamg, K., Wu, X. and Davies, C.H.J., 2016, The influence of processing parameters on aluminium alloy A357 manufactured by Selective Laser Melting. *Mater. And Desi.*, **109**, 334-346.
- [73] <https://commons.wikimedia.org>
- [74] Moshiri, M., 2016, Messa a punto di una procedura di caratterizzazione per lo studio dell'interazione laser-polvere nei sistemi AM. *Master of Science Thesis*, Politecnico di Torino.
- [75] King, W., Barth, H., Castillo, V., Gallegos, G., Gibbs, J., Hahn, D., Kamath, C. and Rubenchik, A., 2014, Observation of keyhole-mode laser melting in laser powder-bed fusion additive manufacturing. *J. Mater. Proc. Tech.*, **214**, 2915-2925.

APPENDICES

I. Numerical Values of On Top Width (SSTs)

Table I.1 On Top width and standard deviation of measurements, case of A357

Type of Sample	Power [W]	Speed [mm/s]	P/V [J/mm]	Average Width [μm]	Standard Deviation
Not Enough	60	1200	0.05	0	0
Not Enough	60	1900	0.03	0	0
Not Enough	60	3000	0.02	0	0
Not Enough	60	5000	0.01	0	0
Not Enough	100	1900	0.05	0	0
Not Enough	100	3000	0.03	0	0
Not Enough	100	5000	0.02	0	0
Not Enough	130	1900	0.07	15.87	16.9
Not Enough	130	3000	0.04	10.81	11.56
Not Enough	130	5000	0.03	0	0
Not Enough	160	1900	0.08	0	0
Not Enough	160	3000	0.05	17.37	18.6
Not Enough	160	5000	0.03	0	0
Not Enough	180	1900	0.09	62.37	24.45
Not Enough	180	3000	0.06	22.18	18.08
Not Enough	180	5000	0.04	0	0
Not Enough	195	1900	0.1	72.49	39.01
Not Enough	195	3000	0.07	14.26	22.54
Not Enough	195	5000	0.04	0	0
Balling	60	300	0.2	74.51	23.88
Balling	60	800	0.08	20.73	21.88
Balling	100	300	0.33	115.93	13.98
Balling	100	800	0.13	66.71	32.17
Balling	100	1200	0.08	48.55	31.43
Balling	130	800	0.16	127.37	24.34

Balling	130	1200	0.11	127.37	24.34
Balling	160	800	0.2	85.38	37.22
Balling	160	1200	0.13	80.32	38.41
Balling	180	1200	0.15	102.33	13.98
Thin & Stable	160	300	0.53	156.9	9.62
Thin & Stable	180	300	0.6	164.69	6.97
Thin & Stable	180	800	0.23	140.17	5.16
Thin & Stable	195	300	0.65	172.38	9.57
Thin & Stable	195	800	0.24	134.08	3.76
Thin & Stable	195	1200	0.16	118.46	4.99
Irregular	60	50	1.2	98.24	45.1
Irregular	100	50	2	164.77	37.69
Irregular	130	50	2.6	232.92	39.12
Irregular	130	300	0.43	124.4	30.53
Irregular	160	50	3.2	180.66	22.98
Too Thick	180	50	3.6	348.45	5.32
Too Thick	195	50	3.9	382.48	6.53

Table I.2 On Top width and standard deviation of measurements, case of AlSi10Mg

Type of Sample	Power [W]	Speed [mm/s]	P/V [J/mm]	Average Width [μ m]	Standard Deviation
Not Enough	60	1200	0.05	0	0
Not Enough	60	1900	0.03	0	0
Not Enough	60	3000	0.02	0	0
Not Enough	100	3000	0.03	13.81	14.56
Not Enough	130	3000	0.04	0	0
Balling	60	800	0.08	30.72	24.8
Balling	100	1200	0.08	68.48	27.38
Balling	100	1900	0.05	57.27	30.32
Balling	130	1900	0.07	83.56	36.33
Balling	160	1900	0.08	92.35	10.53
Balling	160	3000	0.05	46.92	25.35
Balling	180	1900	0.09	44.45	30.62

Balling	180	3000	0.06	71.65	15.05
Balling	195	1900	0.1	111.44	33.79
Balling	195	3000	0.07	62.5	22.49
Thin& Stab	100	300	0.33	117.85	3.94
Thin& Stab	100	800	0.13	110.96	14.02
Thin& Stab	130	300	0.43	113.29	3.89
Thin& Stab	130	800	0.16	100.76	3.79
Thin& Stab	130	1200	0.11	103.22	3.12
Thin& Stab	160	300	0.53	132.84	2.86
Thin& Stab	160	800	0.2	126.99	6.59
Thin& Stab	160	1200	0.13	115.4	7.44
Thin& Stab	180	300	0.6	143.51	2.49
Thin& Stab	180	800	0.23	128.55	3.37
Thin& Stab	180	1200	0.15	118.64	3.6
Thin& Stab	195	300	0.65	235.02	14.13
Thin& Stab	195	800	0.24	135.89	6.91
Thin& Stab	195	1200	0.16	121.22	4.06
Irregular	60	50	1.2	108.81	36.35
Irregular	60	300	0.2	86.5	15.13
Irregular	100	50	2	153.58	27.32
Irregular	130	50	2.6	169.61	26.47
Irregular	160	50	3.2	254.77	29.6
Too Thick	180	50	3.6	433.92	5.05
Too Thick	195	50	3.9	516.57	15.74

Table I.3 On Top width and standard deviation of measurements, case of AlSi10Mg+nTiB₂

Type of Sample	Power [W]	Speed [mm/s]	P/V [J/mm]	Average Width [μm]	Standard Deviation
Not Enough	60	1900	0.03	0	0
Not Enough	60	3000	0.02	0	0
Not Enough	60	5000	0.01	0	0
Not Enough	100	3000	0.03	0	0
Not Enough	100	5000	0.02	0	0

Not Enough	130	3000	0.04	27.73	22.5
Not Enough	130	5000	0.03	0	0
Not Enough	160	3000	0.05	0	0
Not Enough	160	5000	0.03	0	0
Not Enough	180	5000	0.04	0	0
Not Enough	195	5000	0.04	0	0
Balling	60	800	0.08	60.35	22.04
Balling	60	1200	0.05	36.61	23.7
Balling	100	1200	0.08	39.45	26.13
Balling	100	1900	0.05	32.8	26.57
Balling	130	1900	0.07	74.93	18.95
Balling	160	1900	0.08	39.85	32.13
Balling	180	3000	0.06	52.84	24.86
Balling	195	3000	0.07	60.55	28.49
Thin & Stable	100	800	0.13	105.43	10.47
Thin & Stable	130	300	0.43	136.77	2.85
Thin & Stable	130	800	0.16	116.85	1.93
Thin & Stable	130	1200	0.11	110.83	4.12
Thin & Stable	160	300	0.53	146.33	2.73
Thin & Stable	160	800	0.2	134.72	4.67
Thin & Stable	160	1200	0.13	128.5	5.91
Thin & Stable	180	800	0.23	151.31	7.59
Thin & Stable	180	1200	0.15	141.02	5.87
Thin & Stable	180	1900	0.09	113.1	9.21
Thin & Stable	195	800	0.24	157.54	11.28
Thin & Stable	195	1200	0.16	135.84	4.41
Thin & Stable	195	1900	0.1	103.91	7.44
Irregular	60	50	1.2	94.34	34.98
Irregular	60	300	0.2	114.15	16.22
Irregular	100	50	2	147.73	28.94
Irregular	100	300	0.33	126.96	19.33
Irregular	130	50	2.6	166.23	20.27
Irregular	160	50	3.2	178.68	11.41
Too Thick	180	50	3.6	388.02	2.83

Too Thick	180	300	0.6	260.82	3.51
Too Thick	195	50	3.9	467.79	2.38
Too Thick	195	300	0.65	285.55	3.18

II. Numerical Values of Cross Sectional Parameters (SSTs)

Table II.1 Geometrical parameters of cross section for A357

Type	P [W]	v [mm/s]	P/v [J/mm]	Total depth [μm]	Width [μm]	Growth [μm]	Depth [μm]	Angle [$^\circ$]	Area [μm^2]
N. E.	60	1200	0.05	0	0	0	0	0	0
N. E.	60	1900	0.03	0	0	0	0	0	0
N. E.	60	3000	0.02	0	0	0	0	0	0
N. E.	60	5000	0.01	0	0	0	0	0	0
N. E.	100	1900	0.05	24.93	75.85	11.97	12.97	147.64	1502.52
N. E.	100	3000	0.03	12.25	22.96	10.41	1.84	44.81	467.6
N. E.	100	5000	0.02	0	0	0	0	0	0
N. E.	130	1900	0.07	35.8	70.64	23.12	12.69	121.92	1674.29
N. E.	130	3000	0.04	37.89	27.73	31.34	6.54	25.94	2053.13
N. E.	130	5000	0.03	0	0	0	0	0	0
N. E.	160	1900	0.08	45.83	58.75	32.79	13.04	110.6	2076.1
N. E.	160	3000	0.05	63.66	69.63	57.06	6.6	74.92	3573.45
N. E.	160	5000	0.03	0	0	0	0	0	0
N. E.	180	1900	0.09	101.42	69.84	92.45	8.98	51.87	8466.1
N. E.	180	3000	0.06	0	0	0	0	0	0
N. E.	180	5000	0.04	0	0	0	0	0	0
N. E.	195	1900	0.1	90.02	64.86	81.11	8.92	75.88	7420.11
N. E.	195	3000	0.07	0	0	0	0	0	0
N. E.	195	5000	0.04	0	0	0	0	0	0
B.	60	300	0.2	72.56	87.41	60.16	12.4	90.14	6104.57
B.	60	800	0.08	8.57	30.64	3.29	5.28	80.71	397.24
B.	100	300	0.33	117.51	109.73	91.08	26.43	82.72	11373.01
B.	100	800	0.13	100.44	81.29	88.55	11.9	62.2	8987.84

B.	100	1200	0.08	71.5	64.79	60.08	11.42	110.33	4810.43
B.	130	800	0.16	117.15	67.07	105.51	11.63	86.86	11420.09
B.	130	1200	0.11	64.3	66.5	49.46	14.84	96.44	4008.63
B.	160	800	0.2	153.27	71.53	143.86	9.42	30.49	18887.38
B.	160	1200	0.13	103.56	68.28	93.27	10.29	47.52	8913.13
B.	180	1200	0.15	66.13	112.47	44.88	21.26	128.4	5245.5
T.&St.	160	300	0.53	104.38	164.43	67.06	37.32	116.35	12742.03
T.&St.	180	300	0.6	129.59	160.77	80.88	48.71	107.1	14816.49
T.&St.	180	800	0.23	76.96	129.74	44.19	32.77	126.28	6767.79
T.&St.	195	300	0.65	126.02	206.22	32.78	93.24	140.56	18639.6
T.&St.	195	800	0.24	90.32	146.93	46.08	44.24	129.36	9649.05
T.&St.	195	1200	0.16	76.92	112.77	49.06	27.86	119.62	6018.7
Ir.	60	50	1.2	172.43	139.25	143.67	28.76	55.32	21117.18
Ir.	100	50	2	134.8	142.16	109.07	25.72	65.14	17182.77
Ir.	130	50	2.6	128.47	175.72	90.05	38.42	110.84	18021.58
Ir.	130	300	0.43	107.1	147.2	76.12	30.99	111.03	12519.47
Ir.	160	50	3.2	134.45	157.91	92.31	42.14	101.77	15738.53
T.T	180	50	3.6	247	357.04	56.52	190.48	153.53	57411.87
T.T	195	50	3.9	272.65	408.66	33.78	238.86	161.71	72560.47

Table II.2 Geometrical parameters of cross section for AlSi10Mg

Type	P [W]	v [mm/s]	P/v [J/mm]	Total depth [μm]	Width [μm]	Growth [μm]	Depth [μm]	Angle [°]	Area [μm ²]
N. E.	60	1200	0.050	0	0	0	0	0	0
N. E.	60	1900	0.032	0	0	0	0	0	0
N. E.	60	3000	0.020	0	0	0	0	0	0
N. E.	100	3000	0.033	11	38	4	7	547	145
N. E.	130	3000	0.043	10	59	1	7	506	172
B.	60	800	0.075	74	41	74	1	7151	71
B.	100	1200	0.083	85	73	73	12	6987	95
B.	100	1900	0.053	98	56	96	2	9329	64
B.	130	1900	0.068	72	67	69	4	5634	93

B.	160	1900	0.084	86	70	70	15	6088	73
B.	160	3000	0.053	43	102	33	9	3254	128
B.	180	1900	0.095	76	57	58	7	4950	76
B.	180	3000	0.060	48	71	33	21	2817	123
B.	195	1900	0.103	137	16	137	0	16121	25
B.	195	3000	0.065	32	68	16	16	1519	142
T.&ST.	100	300	0.333	94	105	77	17	8259	85
T.&ST.	100	800	0.125	59	80	44	15	3758	102
T.&ST.	130	300	0.433	87	148	57	30	9892	115
T.&ST.	130	800	0.163	82	134	54	28	8046	112
T.&ST.	130	1200	0.108	82	106	55	27	6526	108
T.&ST.	160	300	0.533	92	160	50	42	10387	132
T.&ST.	160	800	0.200	72	138	38	32	7476	129
T.&ST.	160	1200	0.133	75	123	43	32	6827	124
T.&ST.	180	300	0.600	91	169	45	44	11298	131
T.&ST.	180	800	0.225	125	162	60	59	14446	131
T.&ST.	180	1200	0.150	78	140	45	32	7938	131
T.&ST.	195	300	0.650	136	227	47	102	24898	146
T.&ST.	195	800	0.244	105	157	54	53	12578	118
T.&ST.	195	1200	0.163	78	144	47	42	9538	129
Ir.	60	50	1.200	103	106	91	13	13138	95
Ir.	60	300	0.200	91	88	77	14	7399	83
Ir.	100	50	2.000	107	131	75	32	11167	88
Ir.	130	50	2.600	145	165	108	38	20971	69
Ir.	160	50	3.200	184	295	41	144	38403	153
T.T	180	50	3.600	273	381	47	227	68285	156
T.T.	195	50	3.900	355	492	77	294	114672	150

Table II.3 Geometrical parameters of cross section for AlSi10Mg+nTiB₂

Type	P [W]	v [mm/s]	P/v [J/mm]	Total depth [μm]	Width [μm]	Growth [μm]	Depth [μm]	Angle [°]	Area [μm ²]
N. E.	60	1900	0.03	0	0	0	0	0	0
N. E.	60	3000	0.02	0	0	0	0	0	0

N. E.	60	5000	0.01	0	0	0	0	0	0
N. E.	100	3000	0.03	0	0	0	0	0	0
N. E.	100	5000	0.02	0	0	0	0	0	0
N. E.	130	3000	0.04	0	0	0	0	0	0
N. E.	130	5000	0.03	0	0	0	0	0	0
N. E.	160	3000	0.05	50	74.62	32.88	17.13	117.23	2818.5
N. E.	160	5000	0.03	0	0	0	0	0	0
N. E.	180	5000	0.04	0	0	0	0	0	0
N. E.	195	5000	0.04	28.75	56.12	18.81	9.94	131.72	1201.9
B.	60	800	0.08	78.9	66.82	70.83	8.07	68.81	5445.8
B.	60	1200	0.05	0	0	0	0	0	0
B.	100	1200	0.08	54.01	53.68	39.46	14.56	120.72	2825.3
B.	100	1900	0.05	96.33	38.26	93.43	2.91	38.44	7753
B.	130	1900	0.07	56.93	75	45.19	11.73	86.39	3567.4
B.	160	1900	0.08	79.19	32.12	75.01	4.17	43.33	5411.3
B.	180	3000	0.06	72.79	51.07	62.7	10.09	89.95	4104.1
B.	195	3000	0.07	35.63	45.88	27.84	7.79	94.56	1455.3
T.&St.	100	800	0.13	96.1	87.2	77.76	18.35	59.2	9274
T.&St.	130	300	0.43	53.42	132.89	29.21	24.21	135.37	5019.8
T.&St.	130	800	0.16	55.42	111.17	21.68	33.74	138.09	4592.7
T.&St.	130	1200	0.11	62.47	101.16	39.93	22.54	122.13	4534.2
T.&St.	160	300	0.53	83.49	142.21	41.06	42.43	124.96	8747.2
T.&St.	160	800	0.2	68.13	123.03	38.15	29.97	134.31	5870.6
T.&St.	160	1200	0.13	91.92	102.6	67.69	24.23	95.79	7675.2
T.&St.	180	800	0.23	74.01	124.78	18.66	55.36	150.86	6821.1
T.&St.	180	1200	0.15	112.23	129.54	71.87	40.37	101.75	10915
T.&St.	180	1900	0.09	89.91	102.83	67.6	22.31	86.71	6684.1
T.&St.	195	800	0.24	81.35	165.79	40.07	41.28	137.91	9020
T.&St.	195	1200	0.16	79.83	121.11	39.62	40.22	116.83	7007.7
T.&St.	195	1900	0.1	104.15	101.39	86.55	17.6	88.17	9274.7
Ir.	60	50	1.2	100.46	76	81.35	19.12	76.92	7635
Ir.	60	300	0.2	45.28	97.11	25.69	19.59	142.17	2627.8
Ir.	100	50	2	155.98	119.02	120.49	35.49	78.11	19340
Ir.	100	300	0.33	81.68	113.67	55.86	25.82	98.06	8120.3

Ir.	130	50	2.6	110.78	138.77	65.14	45.64	94.12	11554
Ir.	160	50	3.2	98.2	175.47	47.71	50.5	124.05	12042
T.T.	180	50	3.6	280.51	398.63	67.43	213.08	141.07	146208
T.T.	180	300	0.6	175.87	247.1	47.72	128.15	143.49	29056
T.T.	195	50	3.9	340.98	439.01	50.92	290.06	153.71	97952
T.T.	195	300	0.65	212.28	270.04	24.78	187.5	159.25	37646

III. Numerical Values of total Depth (MSTs)

Table III.1 Total depth of Multi Scan Track Samples of A357

Power [W]	Speed [mm/s]	Hatch [mm]	VED [J/mm ³]	Depth [μm]	Standard Deviation
195	800	0.07	69.6429	49.85	5.41
195	800	0.12	40.625	47.1	3.42
195	800	0.17	28.6765	60.44	6.35
195	800	0.22	22.1591	77.2	7.13
195	1200	0.07	46.4286	50.47	4.14
195	1200	0.12	27.0833	46.95	3.91
195	1200	0.17	19.1176	63.08	8.28
195	1200	0.22	14.7727	91.36	18.98
180	300	0.07	171.429	64.77	3.11
180	300	0.12	100	77.91	2.75
180	300	0.17	70.5882	69.53	2.86
180	300	0.22	54.5455	83.32	5.95

Table III.2 Total depth of Multi Scan Track Samples of AlSi10Mg

Power [W]	Speed [mm/s]	Hatch [mm]	VED [J/mm ³]	Depth [μm]	Standard Deviation
195	800	0.07	69.6429	51.06	4.59
195	800	0.12	40.625	56.29	4.71
195	800	0.17	28.6765	62.17	4.93
195	800	0.22	22.1591	64.04	4.42

195	1200	0.07	46.4286	48.07	2.29
195	1200	0.12	27.0833	50.03	3.81
195	1200	0.17	19.1176	61.84	4.63
195	1200	0.22	14.7727	77.43	2.22
180	300	0.07	171.429	62.72	3.66
180	300	0.12	100	64.95	6.3
180	300	0.17	70.5882	70.65	3.78
180	300	0.22	54.5455	87.98	4.74

Table III.3 Total depth of Multi Scan Track Samples of AlSi10Mg+nTiB₂

Power [W]	Speed [mm/s]	Hatch [mm]	VED [J/mm³]	Depth [μm]	Standard Deviation
195	800	0.07	69.6429	51.06	4.59
195	800	0.12	40.625	56.29	4.71
195	800	0.17	28.6765	62.17	4.93
195	800	0.22	22.1591	64.04	4.42
195	1200	0.07	46.4286	48.07	2.29
195	1200	0.12	27.0833	50.03	3.81
195	1200	0.17	19.1176	61.84	4.63
195	1200	0.22	14.7727	77.43	2.22
180	300	0.07	171.429	62.72	3.66
180	300	0.12	100	64.95	6.3
180	300	0.17	70.5882	70.65	3.78
180	300	0.22	54.5455	87.98	4.74

IV. Numerical Values of Cubic Samples

Table IV.1 Archimedean and Geometrical Density of cubic Samples, case of AlSi10Mg

P [W]	v [mm/s]	VED [J/mm³]	W Air [g]	W in Water [g]	W Wet [g]	Archimedean [g/cm³]	Geometrical [g/cm³]
195	300	76.47	0.84	0.53	0.85	2.67	2.66
195	1200	19.12	0.83	0.5	0.83	2.56	2.55
130	1200	12.75	0.74	0.45	0.79	2.54	2.15

100	300	39.22	0.91	0.55	0.92	2.53	2.5
195	50	458.82	0.91	0.56	0.91	2.64	2.64
100	50	235.29	0.84	0.51	0.84	2.55	2.55
160	50	376.47	0.88	0.55	0.88	2.65	2.65
100	1200	9.8	0.64	0.39	0.71	2.58	2.01
100	1900	6.19	0.95	0.57	1.13	2.52	1.7
195	3000	7.65	0.64	0.38	0.71	2.49	1.93
60	1900	3.72	0	0	0	0	0

Table IV.2 Porosity measurements of cubic samples, case of AlSi10Mg

P [W]	v [mm/s]	VED [J/mm³]	Open Porosity%	Close Porosity %	Total Porosity %	Porosity Image analysis %
195	300	76.47	0.19	1.25	1.44	0.354
195	1200	19.12	0.28	5.32	5.59	8.50325
130	1200	12.75	15.25	5.13	20.38	23.3
100	300	39.22	1.31	6.17	7.48	8.323
195	50	458.82	0.15	2.09	2.23	3.063
100	50	235.29	0.36	5.35	5.72	7.8112
160	50	376.47	0	1.98	1.98	1.9094
100	1200	9.8	21.95	3.46	25.41	30.3329241
100	1900	6.19	32.52	4.43	36.95	42.84
195	3000	7.65	22.53	6.02	28.55	34.0662
60	1900	3.72	0	0	0	100

Table IV.3 Archimedean and Geometrical Density of cubic Samples, case of AlSi10Mg+nTiB₂

P [w]	v [mm/s]	Hatch [mm]	VED [J/mm³]	W Air [g]	W in Water [g]	W Wet [g]	Archimedean [g/cm³]	Geometrical [g/cm³]
160	300	0.12	148.15	1.857	1.16	1.86	2.646	2.633
160	800	0.12	55.56	1.6728	1.03	1.68	2.617	2.599
160	1200	0.15	29.63	1.4983	0.90	1.53	2.498	2.366
180	300	0.15	133.33	1.7361	1.07	1.74	2.614	2.595
180	800	0.15	50.00	1.6826	1.04	1.69	2.606	2.578
180	1200	0.12	41.67	1.5857	0.96	1.59	2.537	2.514
195	300	0.17	127.45	1.6611	1.008	1.66	2.545	2.536

195	800	0.17	47.79	1.632	1.004	1.63	2.602	2.588
195	1200	0.1	54.17	1.5379	0.95	1.54	2.612	2.591
195	800	0.1	81.25	1.5676	0.97	1.57	2.640	2.613
195	800	0.17	47.79	1.6112	0.99	1.62	2.589	2.573

Table IV.4 Porosity measurements of cubic samples, case of AlSi10Mg+nTiB₂

P [w]	v [mm/s]	Hatch [mm]	VED [J/mm³]	Open Porosity %	Close Porosity %	Total Porosity %
160	300	0.12	148.15	0.5	0.9	1.4
160	800	0.12	55.56	0.7	2.0	2.7
160	1200	0.15	29.63	5.3	6.1	11.4
180	300	0.15	133.33	0.8	2.1	2.9
180	800	0.15	50.00	1.1	2.4	3.5
180	1200	0.12	41.67	0.9	5.0	5.9
195	300	0.17	127.45	0.4	4.7	5.0
195	800	0.17	47.79	0.5	2.6	3.1
195	1200	0.1	54.17	0.8	2.2	3.0
195	800	0.1	81.25	1.0	1.2	2.2
195	800	0.17	47.79	0.6	3.0	3.7

ACKNOWLEDGEMENTS

I would like to thank professor Matteo Pavese who more than supervision, was a supportive friend during all activities of the thesis. I would also like to thank Alberta Aversa who always was in touch to help me develop this thesis in all aspects, from sample preparation, to analysis of results and discussions. Special thanks goes to professor Mario Guagliano for his supportive role. A great thanks goes to Hamed Saboori who helped me in some technical issues of sample preparation. I would also like to thank Giulio Marchese and Luca Lavagna for their help in working with laboratory equipment. A great thanks goes to IIT members at Politecnico Di Torino who provided us with SLM machine for sample preparation, and welcomed us during our footwork at the center. And finally, I thank and acknowledge all the members and staffs of DISAT and its laboratory members who coordinated, helped, and provided a friendly environment to work.